Ph.D. Thesis
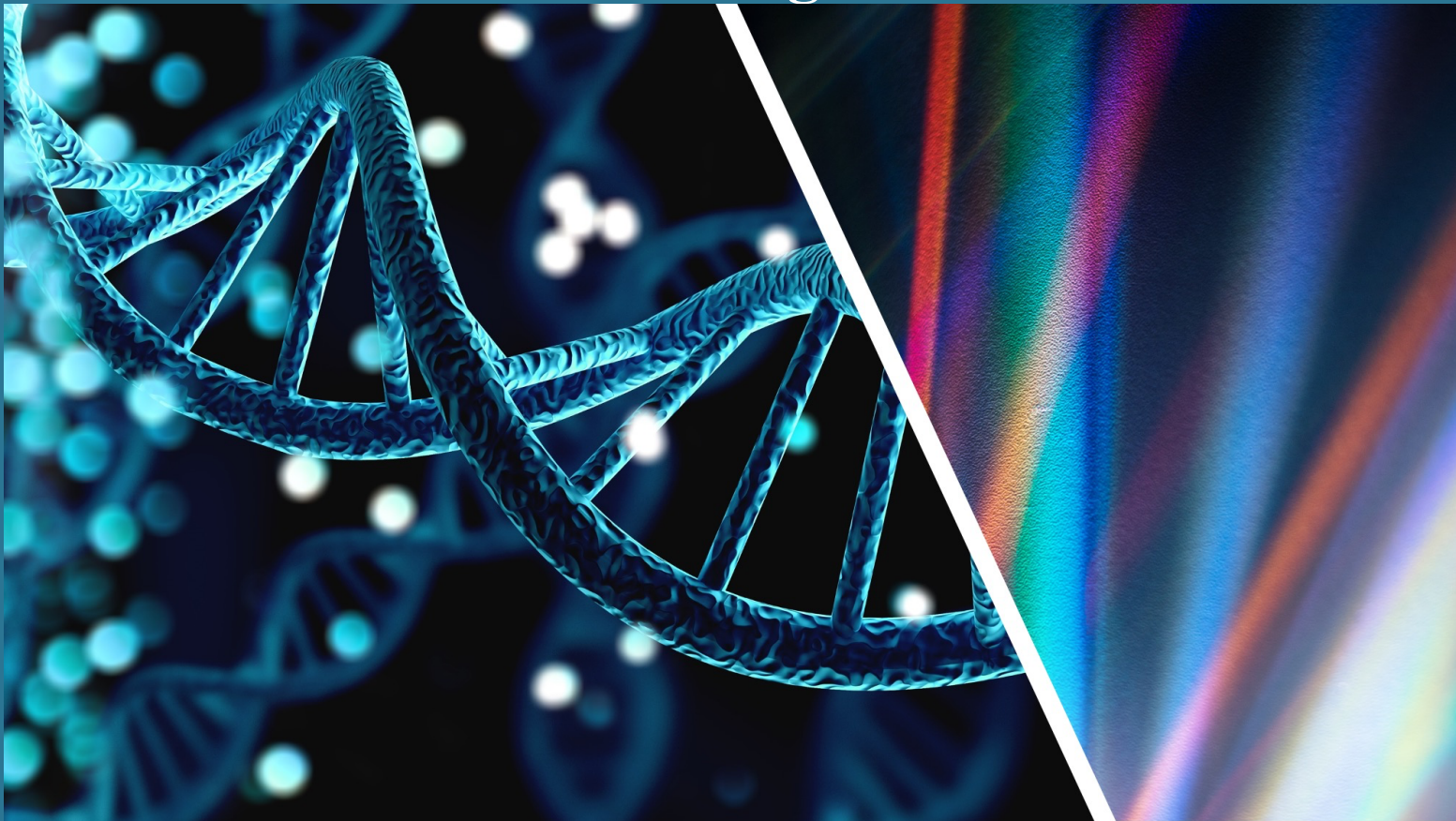
Holographic biosensors made of DNA-functionalised hydrogels for *in vitro* diagnostic

Paola Zezza

UNIVERSITAT POLITÈCNICA DE VALÈNCIA

Ph.D. Supervisors:
Prof. Dr. Ángel Maquieira Catalá
Prof. Dr. María-José Bañuls Polo

Date of submissions: Valencia, 21/11/2023

UNIVERSITAT POLITÈCNICA DE VALÈNCIA

DEPARTAMENT DE QUÍMICA

Holographic biosensors made of DNA-functionalised hydrogels for *in vitro* diagnostic

Ph.D. Thesis

submitted by

Paola Zezza

Doctoral Programme in
Experimental Techniques in Chemistry

Instituto Interuniversitario de Investigación para el Reconocimiento
Molecular y el Desarrollo Tecnológico (IDM)

Acknowledgements

Abstract

This PhD thesis, entitled "Holographic biosensors made of DNA-functionalised hydrogels for *in vitro* diagnostics", focuses on the development of an analyte-sensitive hydrogel, functionalised with oligonucletide probes, with a diffractive structure as an optical transducer for *in vitro* diagnostic applications. The first chapter includes an overview of the different concepts related to biosensing, recent developments in the *in vitro* diagnostics market and, in particular, DNA biosensors. In addition, the synthesis and characterization of hydrogels, their role as a support matrix in biosensing, and immobilization strategies are presented. Finally, the basic concepts of holography as a new detection strategy and the role of different diffraction gratings for biosensing are explained.

Next, in Chapter 2, the objectives of this project are discussed. The aim of this research is to design, fabricate and study experimentally hydrogel-based diffractive gratings created by holographic techniques for biosensing applications. The focus was on developing bioresponsive hydrogels incorporating specific oligonucleotide probes and endowing them with a diffractive structure to act as optical transducer for *in vitro* diagnostic applications. Two types of diffractive structures are considered: surface relief holographic gratings (SRGs) and volume transmission holographic gratings (VTGs). The initial phase of this work was focus on hydrogel optimization, by adjusting their composition to act as holographic biosensors. This implies obtaining hydrogels that show excellent optical transparency, good porosity and good mechanical properties. Acrylamide and bisacrylamide were selected as monomer and crosslinker respectively, for hydrogel preparation by means of free radical polymerization reaction (FRP). In addition, to introduce analyte response in the 3D hydrogel network, different bioreceptor immobilization strategies had to be investigated and tuned.

In Chapter 3, DNA probes are covalently incorporated into an acrylamide-based hydrogel. The optimized strategy consists of directly incorporating acrydite-modified DNA probes via copolymerisation with acrylamide monomers during hydrogel formation. In this case, the covalent bonding reaction is a vinyl addition polymerization, activated both photochemically and thermally. DNA-functionalized hydrogels were characterized by fluorescence imaging and their versatility was explored through microarrays fabrication. Finally, the optimized analyte-sensitive hydrogel was used a platform for the preparation of surface relief gratings.

Chapter 4 describes another approach which was adopted for the functionalisation of the hydrogel with DNA probes. Propargyl acrylate co-monomer was added to the acrylamide hydrogel, in order to introduce the presence of alkynic residues and facilitate greater incorporation of the DNA probes. The DNA probes used had thiol terminal groups and were incorporated via thiol-ene/thiol-yne *click* chemistry, due to the presence of double and triple C-C bonds. With this strategy, two approaches of DNA probe immobilisation were demonstrated: during and after hydrogel synthesis. Consequently, the bioreceptors immobilisation could be performed both before and after the transducer fabrication. Surface relief gratings (SRGs) were fabricated on the hydrogel surface through the combination of Direct laser interference patterning (DLIP) and replica molding (REM). Preliminary results showed that SRGs have potential to directly detect hybridization of oligonucleotide in a label-free format.

In Chapter 5, the recording process of unslanted volume transmission gratings (VTGs) in hydrogel layers was optimized in order to improve the transducer performance and consequently the biosensor sensitivity. After careful evaluation of the holographic recording parameters, incubation solution compositions and incubation times, the VTG structures were recorded with good reproducibility, achieving an excellent diffraction efficiency of over 80%. In addition, their stability in water for bioassays was studied. Finally, it was observed that VTGs, modified with oligonucleotides, responded selectively by hybridising only with the complementary target while retaining their diffraction properties.

The research work demonstrated the feasibility of using holographic diffractive gratings (SRG and VTG) recorded in hydrogel layers as label-free biosensors, capable of detecting short oligonucleotide DNA probes, complementary to the immobilised sequence, in an aqueous environment.

Finally, the general conclusions from this PhD Thesis are presented in Chapter 6. The performance and applicability of the different approaches studied are comparatively analysed, and future outlook of nucleic acid hydrogels for holographic sensing is discussed.

Resumen

Esta tesis doctoral, titulada "Biosensores holográficos de hidrogeles funcionalizados con ADN para diagnóstico *in vitro*", se centra en el desarrollo de un hidrogel sensible a analitos, funcionalizado con sondas de oligonucleótidos, con una estructura difractiva como transductor óptico para aplicaciones de diagnóstico *in vitro*. El primer capítulo incluye una visión general de los diferentes conceptos relacionados con el biosensado, los desarrollos recientes en el mercado del diagnóstio *in vitro* y, en particular, los biosensores de ADN. Además, se presenta la síntesis y caracterización de hidrogeles, su papel como matriz de soporte en biosensado y las estrategias de inmovilización. Por último, se explican los conceptos básicos de la holografía como nueva estrategia de detección y el papel de las diferentes redes de difracción en el biosensado.

A continuación, en el Capítulo 2, se discuten los objetivos de este proyecto. El objetivo de esta investigación es diseñar, fabricar y estudiar experimentalmente redes difractivas basadas en hidrogeles creadas mediante técnicas holográficas para aplicaciones de biodetección. La atención se centró en desarrollar hidrogeles biorreactivos que incorporasen sondas oligonucleotídicas específicas y dotarlos de una estructura difractiva para que actuasen como transductores ópticos en aplicaciones de diagnóstico *in vitro*. Se consideran dos tipos de estructuras difractivas: redes holográficas de relieve superficial (SRGs) y redes holográficas de transmisión volumétrica (VTGs). La fase inicial de este trabajo se ha centrado en la optimización de hidrogeles, ajustando su composición para que actúen como biosensores holográficos. Esto implica la obtención de hidrogeles que presenten una excelente transparencia óptica, buena porosidad y buenas propiedades mecánicas. Se seleccionaron acrilamida y bisacrilamida como monómero y reticulante respectivamente, para la preparación del hidrogel mediante reacción de polimerización por radicales libres (FRP). Además, para introducir la respuesta del analito en la red de hidrogeles tridimensionales, hubo que investigar y poner a punto diferentes estrategias de inmovilización del biorreceptor.

En el capítulo 3, se incorporan covalentemente sondas de ADN en un hidrogel basado en acrilamida. La estrategia optimizada consiste en incorporar directamente sondas de ADN modificadas con acrilamida mediante copolimerización con monómeros de acrilamida durante la formación del hidrogel.

En este caso, la reacción de unión covalente es una polimerización por adición de vinilo, activada tanto fotoquímicamente como térmicamente. Los hidrogeles funcionalizados con ADN se caracterizaron mediante imágenes de fluorescencia y se exploró su versatilidad mediante la fabricación de microarrays. Por último, el hidrogel optimizado sensible a los analitos se utilizó como plataforma para la preparación de redes de relieve superficial.

El capítulo 4 describe otro enfoque adoptado para la funcionalización del hidrogel con sondas de ADN. Se añadió un comonómero de acrilato de propargilo al hidrogel de acrilamida, con el fin de introducir la presencia de residuos alquínicos y facilitar una mayor incorporación de las sondas de ADN. Las sondas de ADN utilizadas tenían grupos terminales tiol y se incorporaron mediante química *click* tiol-eno/tiol-ino, debido a la presencia de enlaces C-C dobles y triples. Con esta estrategia, se demostraron dos enfoques de inmovilización de las sondas de ADN: durante y después de la síntesis del hidrogel. En consecuencia, la inmovilización de los bioreceptores pudo realizarse tanto antes como después de la fabricación del transductor. Se fabricaron redes de relieve superficial (SRG) en la superficie del hidrogel mediante la combinación del patrón de interferencia láser directo (DLIP) y el moldeo de réplicas (REM). Los resultados preliminares mostraron que las SRGs tienen potencial para detectar directamente la hibridación de oligonucleótidos en un formato libre de etiquetas.

En el capítulo 5, se optimizó el proceso de grabación de rejillas de transmisión de volumen no inclinadas (VTG) en capas de hidrogel con el fin de mejorar el rendimiento del transductor y, en consecuencia, la sensibilidad del biosensor. Tras una cuidadosa evaluación de los parámetros de grabación holográfica, las composiciones de las soluciones de incubación y los tiempos de incubación, las estructuras VTG se grabaron con una buena reproducibilidad, alcanzando una excelente eficiencia de difracción de más del 80%. Además, se estudió su estabilidad en agua para bioensayos. Por último, se observó que los VTG, modificados con oligonucleótidos, respondían selectivamente hibridándose sólo con la diana complementaria, al tiempo que conservaban sus propiedades de difracción.

El trabajo de investigación demostró la viabilidad del uso de redes difractivas holográficas (SRG y VTG) grabadas en hidrogeles como biosensores libres de etiquetas, capaces de detectar sondas cortas de ADN oligonucleótido, complementarias a la secuencia inmovilizada, en un medio acuoso.

Por último, en el capítulo 6 se presentan las conclusiones generales de esta tesis doctoral. Se analizan comparativamente el rendimiento y la aplicabilidad de los distintos enfoques estudiados, y se discuten las perspectivas futuras de los hidrogeles de ácido nucleico para la detección holográfica.

Resum

Esta tesi doctoral, titulada "Biosensores hologràfics d'hidrogels funcionalitzats amb ADN per a diagnòstic *in vitro*", se centra en el desenvolupament d'un hidrogel sensible a anàlits, funcionalitzat amb sondes de oligonucleótidos, amb una estructura difractiva com a transductor òptic per a aplicacions de diagnòstic in vitro. El primer capítol inclou una visió general dels diferents conceptes relacionats amb el biosensado, els desenvolupaments recents en el mercat del diagnóstio *in vitro* i, en particular, els biosensores d'ADN. A més, es presenta la síntesi i caracterització d'hidrogels, el seu paper com a matriu de suport en biosensado i les estratègies d'immobilització. Finalment, s'expliquen els conceptes bàsics de l'holografia com a nova estratègia de detecció i el paper de les diferents xarxes de difracció en el biosensado.

A continuació, en el Capítol 2, es discuteixen els objectius d'este projecte. L'objectiu d'esta investigació és dissenyar, fabricar i estudiar experimentalment xarxes difractivas basades en hidrogels creades mitjançant tècniques hologràfiques per a aplicacions de biodetección. L'atenció es va centrar en desenvolupar hidrogels biorreactivos que incorporaren sondes oligonucleotídicas específiques i dotar-los d'una estructura difractiva perquè actuaren com a transductors òptics en aplicacions de diagnòstic in vitro. Es consideren dos tipus d'estructures difractivas: xarxes hologràfiques de relleu superficial (SRGs) i xarxes hologràfiques de transmissió volumètrica (VTGs). La fase inicial d'este treball s'ha centrat en l'optimització d'hidrogels, ajustant la seua composició perquè actuen com biosensores hologràfics. Això implica l'obtenció d'hidrogels que presenten una excel·lent transparència òptica, bona porositat i bones propietats mecàniques. Es van seleccionar acrilamida i bisacrilamida com a monòmer i reticulante respectivament, per a la preparació de l'hidrogel mitjançant reacció de polimerització per radicals lliures (FRP). A més, per a introduir la resposta de l'anàlit en la xarxa d'hidrogels tridimensionals, va caldre investigar i posar a punt diferents estratègies d'immobilització del biorreceptor.

En el capítol 3, s'incorporen covalentemente sondes d'ADN en un hidrogel basat en acrilamida. L'estratègia optimitzada consisteix a incorporar directament sondes d'ADN modificades amb acrilamida mitjançant copolimerización amb monòmers d'acrilamida durant la formació de l'hidrogel.

En este cas, la reacció d'unió covalent és una polimerització per addició de vinil, activada tant fotoquímicament com tèrmicament. Els hidrogels funcionalitzats amb ADN es van caracteritzar mitjançant imatges de fluorescència i es va explorar la seua versatilitat mitjançant la fabricació de bioxips. Finalment, l'hidrogel optimitzat sensible als anàlits es va utilitzar com a plataforma per a la preparació de xarxes de relleu superficial.

El capítol 4 descriu un altre enfocament adoptat per a la funcionalització de l'hidrogel amb sondes d'ADN. Es va afegir un comonómero de acrilato de propargilo a l'hidrogel d'acrilamida, amb la finalitat d'introduir la presència de residus alquínicos i facilitar una major incorporació de les sondes d'ADN. Les sondes d'ADN utilitzades tenien grups terminals tiol i es van incorporar mitjançant química clic tiol-eno/tiol-ino, a causa de la presència d'enllaços C-C dobles i triples. Amb esta estratègia, es van demostrar dos enfocaments d'immobilització de les sondes d'ADN: durant i després de la síntesi de l'hidrogel. En conseqüència, la immobilització dels bioreceptores va poder realitzar-se tant abans com després de la fabricació del transductor. Es van fabricar xarxes de relleu superficial (SRG) en la superfície de l'hidrogel mitjançant la combinació del patró d'interferència làser directe (DLIP) i l'emotlament de rèpliques (REM). Els resultats preliminars van mostrar que les SRGs tenen potencial per a detectar directament la hibridació de oligonucleótidos en un format lliure d'etiquetes.

En el capítol 5, es va optimitzar el procés de gravació de reixetes de transmissió de volum no inclinades (VTG) en capes d'hidrogel amb la finalitat de millorar el rendiment del transductor i, en conseqüència, la sensibilitat del biosensor. Després d'una acurada avaluació dels paràmetres de gravació hologràfica, les composicions de les solucions d'incubació i els temps d'incubació, les estructures VTG es van gravar amb una bona reproducibilidad, aconseguint una excel·lent eficiència de difracció de més del 80%. A més, es va estudiar la seua estabilitat en aigua per a bioensayos. Finalment, es va observar que els VTG, modificats amb oligonucleótidos, responien selectivament hibridant-se només amb la diana complementària, al mateix temps que conservaven les seues propietats de difracció.

El treball de recerca va demostrar la viabilitat de l'ús de xarxes difractivas hologràfiques (SRG i VTG) gravades en hidrogels com biosensores lliures d'etiquetes, capaces de detectar sondes curtes d'ADN oligonucleótido, complementàries a la seqüència immobilitzada, en un medi aquós.

Finalment, en el capítol 6 es presenten les conclusions generals d'esta tesi doctoral. S'analitzen comparativament el rendiment i l'aplicabilitat dels diferents enfocaments estudiats, i es discuteixen les perspectives futures dels hidrogels d'àcid nucleic per a la detecció hologràfica.

LIST OF PUBBLICATIONS

1- <u>Zezza, P.</u>, Lucío M.I., Maquieíra Catalá A., Bañuls Polo M.J., DNA-based hydrogel for high-performance optical biosensing applications, Talanta, (2022).

2- Berramdane, K., Ramírez, M.G., Zezza, P., Lucío M.I., Bañuls Polo M.J., Maquieíra Catalá A., Morales-Vidal, M., Beléndez A., Pascual, I., Processing of holographic hydrogels in liquid media: a study by high-performance liquid chromatography and diffraction efficiency, Polymers, (2022)

3- Berramdane, K., Ramírez, M.G., Zezza, P., Lucío M.I., Bañuls Polo M.J., Maquieíra Catalá A., Morales-Vidal, M., Beléndez A., Pascual, I., Bending in the holograms stored in hydrogel matrices, Proceedings of SPIE, (2022).

4- <u>Zezza, P.</u>, Lucío M.I., Fernández M.E., Maquieíra Catalá A., Bañuls Polo M.J., Surface micro-patterned biofunctionalized hydrogel for direct nucleic acid hybridization detection, Biosensors, (2023).

5- <u>Zezza, P.</u>, Lucío M.I., Naydenova, I., Bañuls Polo M.J., Maquieíra Catalá A., Holographic recording of unslanted volume transmission gratings in acrylamide/propargyl acrylate hydrogel layers: towards nucleic acid biosensing, Gels, (2023).

Communications in conferences:

1- <u>Zezza, P.</u>, Lucío M.I., Bañuls Polo M.J., Maquieíra Catalá A., Novel (poly)rotaxane-based hydrogel for biomolecular sensing, XIV International Workshop on Sensors and Molecular Recognition (IWOSMOR 2021).

2- <u>Zezza, P.</u>, Lucío M.I., Bañuls Polo M.J., Maquieíra Catalá A., Nucleic acid-functionalized hydrogels for diffraction-based label-free biosensing, XIV International Workshop on Sensors and Molecular Recognition (IWOSMOR 2021)

3- <u>Zezza, P.</u>, Lucío M.I., Bañuls Polo M.J., Maquieíra Catalá A., Designing surface diffractive gratings in a DNA-functionalized hydrogel for specific biomolecular recognition, XV International Workshop on Sensors and Molecular Recognition (IWOSMOR 2022).

4- <u>Zezza, P.</u>, Lucío M.I., Maquieíra Catalá A., Bañuls Polo M.J., Versatile DNA-based hydrogels for high-performance microarray and potential optical biosensing application, Global Meet on Sensors and Sensing Technology (GMSST 2022).

5- <u>Zezza, P.</u>, Lucío M.I., Bañuls Polo M.J., Maquieíra Catalá A., DNA-based hydrogels for high-performance optical biosensing application, 2nd Workshop for Young Researchers in Chemistry (YRChem 2022).

6- Lucío M.I., Cubelles-Gómez, A., <u>Zezza, P.,</u> Bañuls Polo M.J., Maquieíra Catalá A., Label-free detection of analytes using bioresponsive hydrogel-based surface relief diffraction gratings, Symposium of the Spanish Royal Society of Chemistry (2021).

7- Bañuls Polo M.J., Lucío M.I., <u>Zezza, P.,</u> Cubelles-Gómez, A., Maquieíra Catalá A., Bioresponsive hydrogels for holographic biosensing, XXXVIII Reunión Bienal de la Real Sociedad Española de Química (RSEQ 2022).

8- Cubelles-Gómez, A., Lucío M.I., <u>Zezza, P.,</u> Maquieíra Catalá A., Bañuls Polo M.J., Surface diffraction gratings made of protein hydrogels for label-free biosensing, XXXVIII Reunión Bienal de la Real Sociedad Española de Química (RSEQ 2022).

9- Lucío M.I., Cubelles-Gómez, A., <u>Zezza, P.,</u> Hernández-Montoto, A., Fernández-Sánchez M.E., Bañuls Polo M.J., Maquieíra Catalá A., Engineering hydrogels for label-free biosensing: form chemical formulation to transducer fabrication, X International Congress on Analytical Nanoscience and Nanotechnology (NyNA 2022).

10- Lucío M.I., Cubelles-Gómez, A., <u>Zezza, P.,</u> Hernández-Montoto, A., Fernández-Sánchez M.E., Bañuls Polo M.J., Maquieíra Catalá A., Diffraction gratings of smart hydrogels as transducers for the label-free detection of biomolecules, Analytical Research Forum 2022 (ARF 2022).

LIST OF ABBREVIATIONS

AuNPs	Gold nanoparticles
β-LG	β-lacto globulin
CHA	Catalyzed hairpin assembly
CCD	Charged-coupled device
CRP	C-reactive protein
DNA	Deoxyribonucleic acid
dsDNA	Double stranded DNA
DI	Deionized water
DLIP	Direct Laser Interference Patterning
FDA	Food and Drug Administration
FRP	Free-radical polymerization
GAH-IgG	Goat-anti-human IgG
GMA	Glycidyl methacrylate
HEMA	Hydroxyethyl methacrylate
HRC	Hybridisation chain reaction
H-IgG	Human immunoglobulin G
IVD	In vitro diagnostics
ITO/PET	Indium tin oxide/polyethylene terephthalate
LOD	Limit of detection
MB	Molecular beacon
NA	Nucleic acids
Nd:YVO$_4$	Neodymium-doped Yttrium orthovanadate
PCR	Polymerase chain reaction
POC	Point-of-care
PC	Polycarbonate
PMMA	Polymethylmethacrylate
PEGDA	Poly(ethylene glycol) diacrylate
PGM	Portable glucose meter
PVA	Poly(vinyl alcohol)
PEG	Polyethylene glycol
PBA	Phenylboronic acid
PET	Polyethylene terephthalate

PNIPAM	Poly(N-isopropylacrylamide)
QCM	Quartz crystal microbalance
RCA	Rolling circle amplification
REM	Replica moulding
RI	Refractive index
ssDNA	Single stranded DNA
SPR	Surface plasmon resonance
SRGs	Surface relief gratings
VHGs	Volume holographic gratings
WHO	World Health Organisation

CONTENTS

4- Chapter 4

Surface Micro-Patterned Biofunctionalized Hydrogel for Direct Nucleic Acid Hybridization Detection

5- Chapter 5

Holographic recording of unslanted volume transmission gratings in Acrylamide/Propargyl acrylate hydrogel layers

6- Chapter 6
CONCLUSIONS AND PERSPECTIVES

LIST OF FIGURES

Figures of Chapter 1

Figure 15. Hybrid DNA-hydrogels as biosensing platforms based on different strategies. A DNA-functionalized hydrogel for visual detection of the DNA target labelled with AuNPs, reprinted with permission from Ref. [83]. B Polyacrylamide DNA hydrogels of glucosamine-boronate esters and G-quadruplexes synergistically cross-linked in the presence of K+/crown ethers undergoing cyclic hydrogel-solution transition. Reproduced with permission from Ref.

Figures of Chapter 3

Figures of Chapter 4

Figures of Chapter 5

LIST OF TABLES

1- Chapter 1

INTRODUCTION

1.1 BIOSENSORS

1.1.1 Biosensor definition and classification

Sensors are analytical tools used to examine the presence of a target analyte in a sample. Three categories of sensors can be distinguished: (a) *physical sensors* for measuring distance, mass, temperature, pressure, etc., (b) *chemical sensors* which analyze chemical substances by chemical or physical response, and (c) *biosensors* which measure substances, by using a biological sensing element. All of these devices have to be connected to a transducer of some sort, so that a measurable response occurs. Thus, a **biosensor** can be defined as a device incorporating a biological sensing element connected to a transducer [1]. The term biosensor began to appear in the scientific literature around 1970s. Nevertheless, the basic concept of biosensors and even their introduction to the market preceded that. The biosensor concept was first described by Clark and Lyons in the early 1960s, marking the beginning of the biosensor research [2]. Thereafter, the development and use of biosensors in various fields of analytical chemistry continued to grow. Examples of biosensors that every human being possesses are the nose and tongue, which are extremely sensitive and selective and difficult to imitate artificially (electronic tongue and nose) [3]. They can distinguish between many different substances qualitatively and can give an idea of the quantity. The brain acts as a transducer, translating the response into sensations such as smell or taste. In general, the function of a biosensor is to provide fast, real-time, accurate and reliable information on the target analyte. Biosensor research is multidisciplinary and requires different scientific and technological knowledge, including chemistry, biochemistry, physics, and engineering among others.
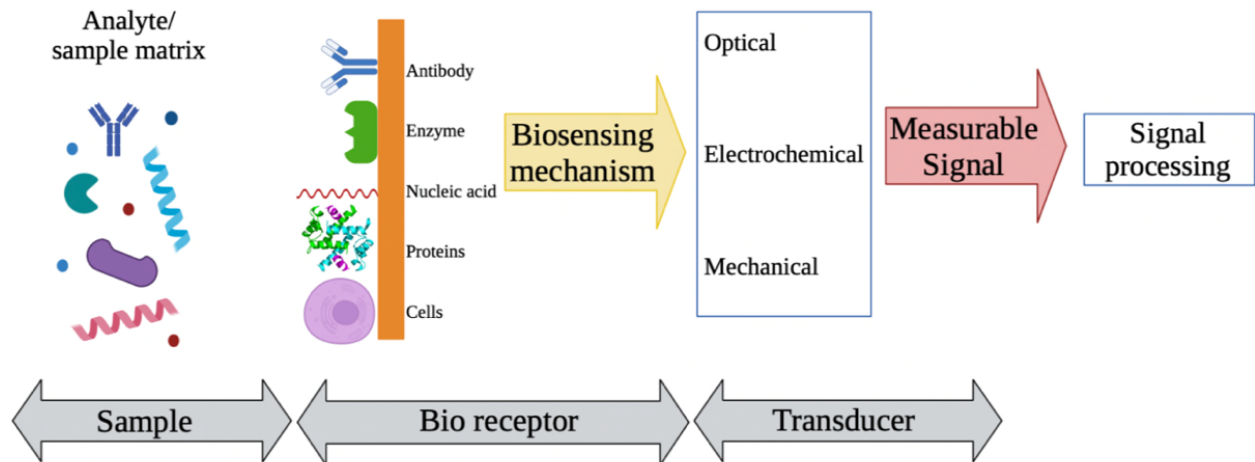
Fig. 1. Schematic representation of biosensor components.

Normally, biosensors are composed of three main elements (Fig. 1.):

◊ **Biorecognition element**

◊ **Transducer**

◊ **Signal processing system**

Biorecognition elements are key components of the biosensor device. They provide the selectivity necessary for the biosensor to react only to a certain analyte, preventing interference from other chemicals. The most common biorecognition elements include enzymes, antibodies, oligonucleotides, aptamers, receptors, cells and tissues . The change generated by the bioreceptor-analyte interaction is known as the biosensing mechanism. The signal produced through this interaction is then transformed into a measurable and quantifiable electrical signal through the transducer [4]. The transducer is essentially the detector of the biosensor. Therefore, the fabrication of a biosensor requires the biorecognition elements to be properly connected to the transducer surface (solid surface, e.g., glass, metal, microbeads, hydrogels) [5] [6] [7]. This process is known as (bio)immobilisation or biofunctionalization.

Usually, immobilisation methods are based on adsorption, entrapment or by covalent attachment [8]. Further details about the immobilisation methods will be discussed in Section 1.2.4. Biosensors can be distinguished according to the transducer element or the biological receptors used (Fig.2.). Thus, they can be classified based on the physicochemical principle (transduction) used to generate output signals, including magnetic [9], optical [10], plasmonic [11], gravimetric [12], piezoelectric [13], and others. On the other hand, they can be further classified depending on the bioreceptors and their specific interactions involving antibodies/antigen [14], nucleic acids/DNA [15], enzymes [16] and cellular structure/cells [17]. Consequently, the development of materials that improve molecular recognition and transduction processes is crucial to design biosensors with higher sensitivity, higher selectivity, rapid response and low detection limits.
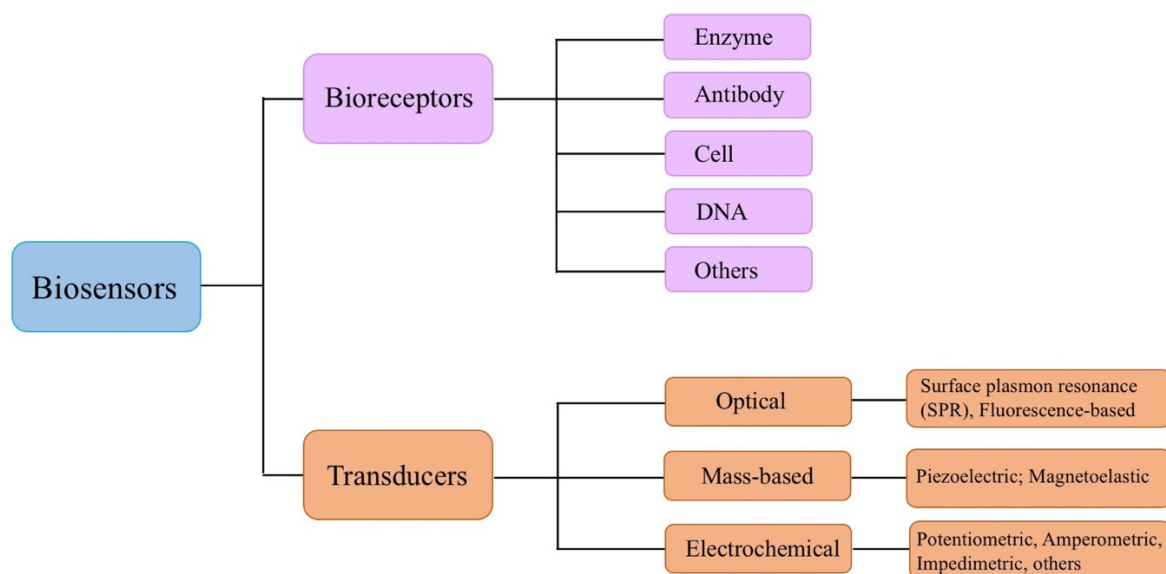
Fig. 2. Classification of biosensor based on the bioreceptors and transducers employed.

There are several factors that define the performance of a biosensor [18] [19]: (i) *Selectivity* refers to the ability to discriminate between different substances. This behavior is principally a function of the recognition element, although the operation of the transducer also contributes. (ii) *Sensitivity* is defined as the ratio between the change in analyte concentration and the signal intensity generated by the transducer. The sensitivity rate is generally measured by the **limit of detection (LOD)**. Typically, a lower LOD value indicates a highly sensitive biosensor. There are a number of approaches which can be used to evaluate the LOD [20]. The LOD can be calculated directly from the calibration, according to the formula:

$$LOD = S_{blank} + 3\ \sigma_{blank} \tag{1}$$

where S_{blank} is the mean value of the signal for the reagent blank measured multiple times and σ_{blank} is the standard deviation of the signal for the reagent blank.

(iii) *Reproducibility* refers to the ability of the biosensor device to generate consistent output signals across multiple experimental runs. (iv) *Reusability* is defined as the ability of a biosensor to be reused multiple times. Although much progress has been made in the field of biosensors, making a biosensor that meets all of these characteristics still remains a challenge. In recent years, biosensors have gained interest as portable devices, being simple and allowing rapid measurement for a wide range of biologically relevant analytes. Indeed, in the wake of the Covid-19 pandemic, a new awareness of the potential societal impact of this research has arisen [21], and biosensors have become one of the most studied technologies for label-free and real-time detection applications. To date, numerous improvements have been made to the sensitivity, selectivity, and multiplexing capability of biosensors. Ultimately, portable biosensors, and point of care or point of need, play a significant analytical role in various fields, such as disease detection [22], food safety [23], environmental monitoring [24] and many more.

1.1.2 Advances in *in vitro* diagnostic testing

Generally, diagnostic tests must be sensitive, selective, and accurate to be validated for their commercial use in clinical diagnostics. In addition, they should meet the **ASSURED** criteria set by The World Health Organisation (WHO) which translate into Affordable, Sensitive, Specific, User-friendly, Rapid and Robust, Equipment free or Environmentally friendly, and Deliverable to end-users (Table 1) [25] [26]. Recently, the criteria were updated with the acronym **REASSURED**, which also include Real-time connectivity and Ease of specimen collection. However, it is difficult for any diagnostic device to incorporate all of these features and compromises are often made in one or more aspects to achieve others. Another interesting advantage of an analytical test is the possibility of multiplexing, which is the simultaneous detection or identification of several biomarkers in a single diagnostic test [27]. Diagnostic tests can be conducted *in vitro* or *in vivo*. *In vivo* tests, conducted in the organism itself (i.e., wearable devices), are potentially continuous and can be used for real-time monitoring. *In vitro* tests are typically conducted outside the body, in test tubes or similar equipment.

Table 1. The REASSURED guidelines that indicate the features that should be designed into all diagnostic devices.

R: Real-time connectivity
E: Ease of specimen collection
A: Affordable - Low cost
S: Sensitive - Low false negatives
S: Specific - Low false positives
U: User friendly - Skilled personnel is not required
R: Rapid and Robust - Short turnaround time and easy handling and storage
E: Equipment free - Complex instrumentation is not required
D: Delivered - Available to end users

Currently in medical diagnostics, the monitoring of many diseases by traditional laboratory and hospital tests is perceived as invasive, time-consuming, expensive and requires skilled personnel. In order to improve the healthcare system efficiency and counter the emergence of new diseases and their spread, the *in vitro* diagnostics (IVD) market and research is increasingly orientated towards personalised medicine (Fig. 3.) [28] [29]. This current trend in the IVD market is characterised by the minimisation of the size of instruments and procedures and the increasing use of new technologies. Hence, there is a growing interest for rapid and easy-to-use diagnostics to facilitate testing outside the laboratory. Indeed, with the emergence of coronavirus disease 2019 (COVID-19), diagnostic testing has supported containment efforts to mitigate the outbreak. The severity of this crisis and the increasing capacity issues associated with polymerase chain reaction (PCR)-based testing have sped up the development of new diagnostic solutions to meet the demand for mass testing. Therefore, the development of highly sensitive, specific, portable and inexpensive analytical test is in high demand because it contributes to accurate diagnosis and personalised medicine. Today, a number of diagnostic tests that fulfil the ASSURED and/or REASSURED criteria are available on the market.

Point-of-care (**POC**) testing, also known as near-patient testing, refers to any analytical test performed outside the laboratory [30]. Notably, in the case of point-of-care tests, in addition to meeting the above-mentioned requirements (Table 1), they must also reduce the cost and complexity of testing. POC tests can give either quantitative or qualitative/semiquantitative results. POC technologies can be split into two categories (Fig. 3.). The first one, are **bench-top devices** which are essentially laboratory instruments which have been reduced in both size and complexity. The second category consists of **handheld devices** that can determine an increasing number of analytes qualitatively or quantitatively. Early examples of POC handheld tests include strip-based urine testing such as pregnancy tests, antigen tests for Covid, and blood glucose tests. Furthermore, it is essential to develop POC tests using easy accessible (non-invasive or minimally invasive sampling) and easy-to-prepare samples, without the need for additional purification or amplification steps [31]. Samples for these sensors include urine, sweat, saliva, interstitial fluid, blood or wound fluids, tear fluid, or breath samples.

Strip tests (dipsticks) or lateral-flow tests are the most established handheld POC tests widely used to measure the concentration or detect the presence of various target analytes [32] [33] [34] [35]. They are lightweight and compact and provide qualitative or semiquantitative results without external instrumentation. Such tests are used for urinalysis, immunoassays, veterinary screening, food quality testing, environmental monitoring and drug abuse screening [36] [37].
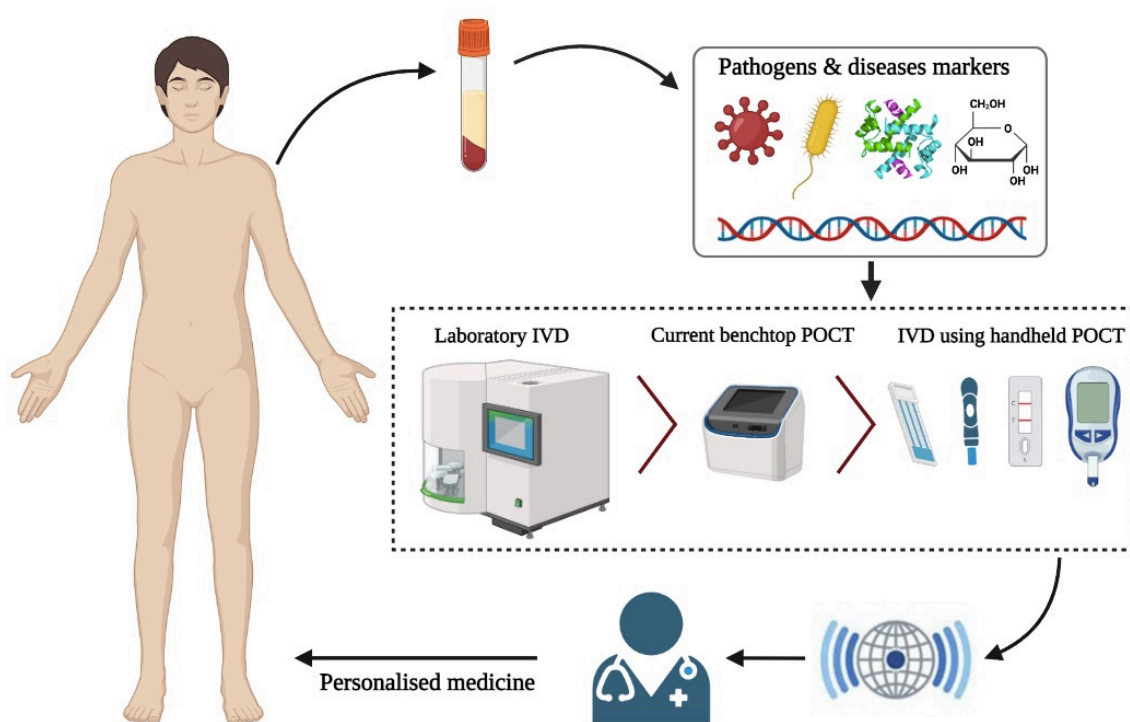
Fig. 3. Trend of *in vitro* diagnostics towards miniaturization: from laboratory analysis to personalized medicine with point-of-care tests.

It is clear that the use of POC testing shortens the time between sample acquisition and analysis. Of particular interest among new POC approaches are those that operate in a **label-free** format and **wearable devices** that enable **real-time monitoring** [38]. Some innovative examples are smart contact lenses [39] [40] or skin patches [41] [42] for diabetics, which can track the sugar level of the user in real-time. The most successful commercial POC tests developed so far are glucose biosensors, which are used for home testing by people with diabetes [43] [44]. In 2014, a breakthrough in the wearable commercial market came with Google contact lens for monitoring blood glucose in tears [45]. However, due to the poor results in the correlation between blood and tear glucose levels, the glucose contact lens project was discontinued. Later, in 2017, another wearable device that monitors glucose in a minimally invasive manner appeared on the market, namely Freestyle Libre (Abbott Inc.), which received FDA approval [46], it constitutes the gold standard of POC label-free biosensor. However, POC technology is still under development and represents a promising approach for direct monitoring in order to reduce the cost, time and complexity of analysis and, in addition, to enable patient diagnosis at home. Examples of emerging technologies that look promising for the future (Fig. 4.) are contact lens sensors [47], tattoo-based sensors [48] and smart holograms [49], all of which are very patient-centered in their configuration.
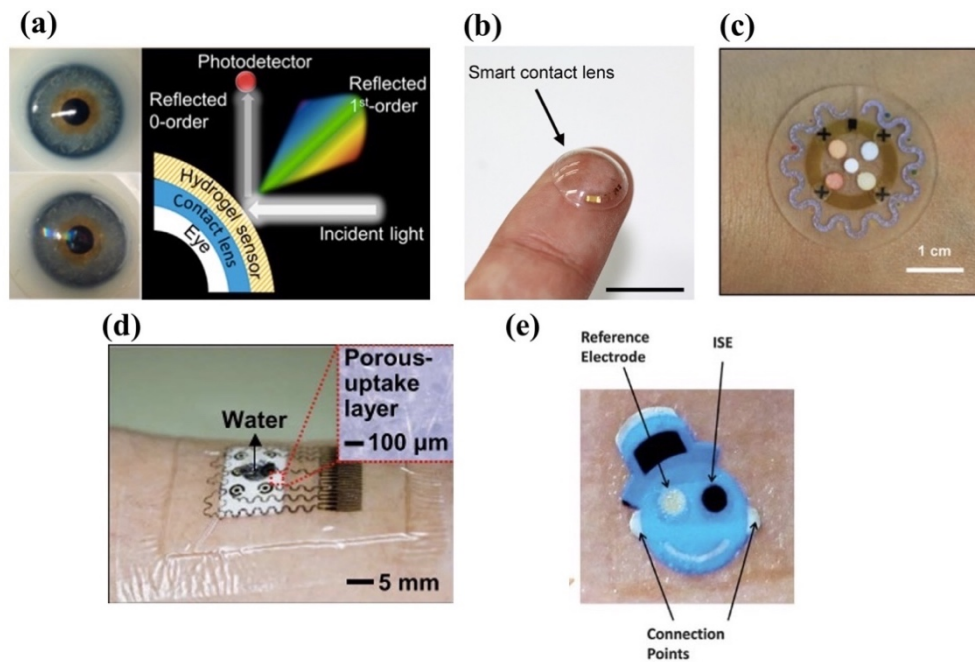
Fig. 4. Recent developed wearable devices for real-time monitoring: **(a)** Smart contact lens reproduced with permission from Ref. [39]; **(b)** Smart contact lenses with integrations of wireless circuits reproduced with permission from Ref. [40]; **(c)** Wearable microfluidic patch for sweat monitoring reproduced with permission from Ref. [41]; **(d)** Wearable sweat-based glucose monitoring device reproduced with permission from Ref. [42]; **(e)** Novel tattoo-based ion-selective electrodes (ISEs) for non-invasive potentiometric monitoring of epidermal pH levels, reproduced with permission from Ref. [48].

1.1.3 DNA-based biosensors

It is known that DNA and its assembly structures can detect specific targets, such as nucleic acids, and proteins, metal ions, and other small biological molecules as well. Therefore, DNA biosensors (or genosensors) find many fields of application, such as gene analysis, human diagnostics and environmental monitoring.

The main DNA-based diagnostic method is the polymerase chain reaction (PCR) technique, developed by Kary Mullis in the 1980s [50]. The method isolates, amplifies and quantifies a short DNA sequence from a complex pool of DNA using a specific primer pair and DNA polymerase as the enzyme. In recent years, interest in developing new deoxyribonucleic acid (DNA)-based diagnostic tests has grown due to DNA biocompatibility, thermal stability and easy modification [51]. Nucleic acid recognition layers, unlike enzymes or antibodies, can be easily synthesised and regenerated for multiple uses. Moreover, compared to commonly used molecular probes, DNA has long-lasting biological activity, remarkable addressability and adjustable rigidity which make it a promising candidate for intelligent biosensing. Therefore, DNA biosensors are developing rapidly with the aim of quick, simple and inexpensive testing for genetic and infectious diseases and the detection of DNA damage and interactions. DNA biosensors are based on nucleic acid recognition processes and they usually consist of immobilised DNA strands to detect the complementary sequences by DNA-DNA hybridisation (Fig. 5.). In other words, the formation of the well-known double helix (dsDNA) between two totally complementary single DNA strands (ssDNA) occurs, which is one of the most selective and strongest interactions between biomolecules [52]. Nucleic acids hybridisation is stronger and more specific when the degree of complementarity between two DNA chains increases. In fact, binding specificity and stability reach a maximum (100% hybridization efficiency) in the case of full complementarity [53]. In the case of few mismatches between the chains, non-specific binding may occur between the immobilised DNA capture probes and other DNA strands present in the sample matrix.
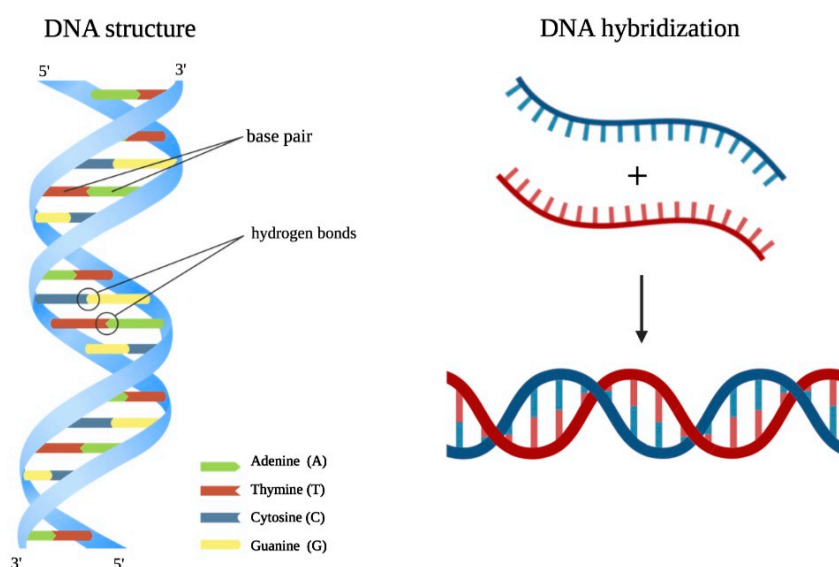
Fig. 5. Schematic representation of doble helix DNA (dsDNA) general structure and DNA hybridization reaction between two single DNA strands (ssDNA).

In a typical configuration, single-stranded DNA sequences are immobilised within the recognition layer, where base pairing interactions recruit the target DNA, generating the recognition signal (Fig. 6.). Common transduction elements for DNA sensors are optical, electrochemical or mass-sensitive devices, which generate light, current or frequency signals, respectively [54]. The immobilisation of DNA probes, as biorecognition elements, takes place directly in the transducer layer. Various immobilisation methods can be used to develop DNA biosensors (section 1.2.4), depending on the substrate used. The specificity of the hybridisation reaction depends on the biorecognition properties of the capture oligonucleotide and thus on the immobilisation method employed [55].
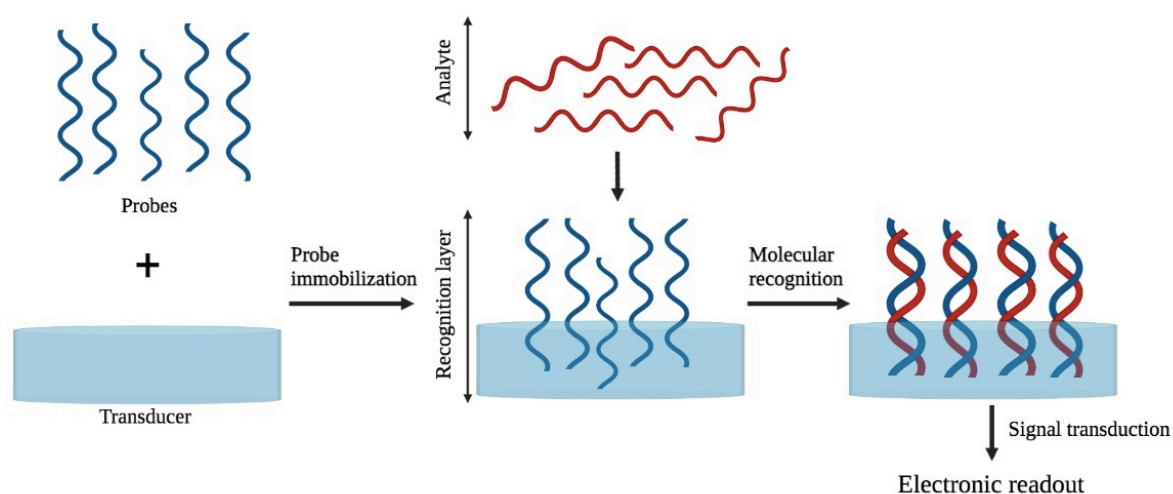
Fig. 6. DNA-based biosensor design and working principle.

Consequently, achieving high sensitivity and selectivity of the biosensor requires the stability of the immobilised biomolecules and minimisation of non-specific adsorption. A high-performance biosensor should be able to discriminate even a single base pair mismatch between different target DNA strains. In addition, experimental variables affecting the efficiency of the hybridisation reaction include: the composition of buffers (ionic strength) used during hybridisation for and post-hybridisation washing, pH and reaction temperature [56].

In this thesis work, single-stranded DNA (ssDNA) probes were immobilised, as receptors, directly within the transducer layer for the construction of a DNA biosensor. Specifically, this research focused on the design and development of a new hydrogel-based DNA biosensor type based on holography.

1.1.3.1 DNA nanotechnology-based biosensors

To date, DNA-based analytical technique that are most established, sensitive, qualitative, quantitative, and that allow for accurate DNA detection, are based on real time polymerase chain reactions (PCR). However, the demand of more accessible and compact detection analysis through employing biosensors system has increased, and research is focused on ways of producing portable devices that would allow fast and accurate detection. One of the strategies for improving the biosensor sensitivity is signal amplification. Starting with the polymerase chain reaction (PCR), scientists developed a number of strategies for DNA amplification [57]. Thus, it is now possible to design detection platforms using different DNA amplification methods, including (i) enzyme-dependent and (ii) enzyme-free methods. However, due to a high cost of enzymatic techniques which often lack reproducibility and robustness, the development of enzyme-free methods is of growing interest in industry and academia. DNA amplification strategies are interesting and powerful for providing a sensitive signal and improving the performance of DNA-based biosensors, but some scientists insist that they are overly elaborate, time-consuming, expensive and sometimes lose specificity. In recent years, it has been demonstrated that biosensors with fast and sensitive results can be also developed without any DNA amplification process. Currently, with the development of DNA nanotechnology, nucleic acids have become a powerful building block for bottom-up assembly of complex 3D nanostructures, often called DNA "nanomachines" or DNA "nanodevices" [58]. DNA nanostructures devices have attracted considerable attention and have been extensively used in various fields including nanomachines, gene editing, targeted medication delivery, and biosensing [59].

DNA nanotechnology-based biosensors can be divided into: (1) Functional DNA strand-based biosensors, (2) DNA hybridization-based biosensors and (3) DNA template-based biosensors [60] (Fig. 7).

(1) **Functional DNA strand-based biosensors** refer to biosensors that use functional DNA strands to recognise certain targets. Examples of these biosensors include DNA aptamer biosensors and DNAzyme biosensors (Figure 7 (1)). DNA aptamer biosensors are based on the use of aptamers (short, single-stranded nucleic acids) that can specifically bind non-nucleotidic targets by forming stable tertiary structures. DNAzymes consist of a loop-shaped catalytic domain coupled to two substrate recognition domains; the most commonly used method based on this principle is called a molecular beacon. A good example of DNA aptamer biosensors are those using graphene that targets β-globulin for milk allergen detection [61]. The aptamer that binds to the milk allergen β-lacto globulin (β-LG) is integrated into graphene exploiting the conformational change of the aptamer sequence upon binding with the β-LG protein, which results in the release of the aptamer from the graphene surface reaching a detection limit of 20 pg /mL. A work based on a DNA enzyme biosensor, combines a catalytic and molecular beacon (MB) for the amplified detection of Pb^{2+} with a LOD of 600 pM [62]. The DNA enzyme substrate is incorporated in the loop of the MB to form a complex structure. The addition of the metal ions splits the MB in two and cleaves the substrate, causing stem dehybridisation and an improved fluorescence signal.
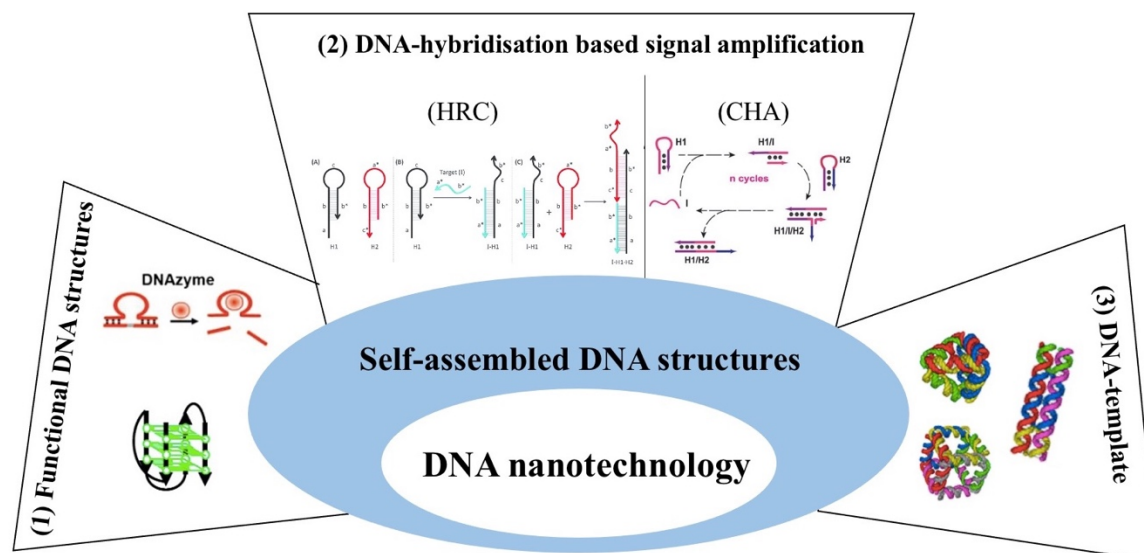
Fig. 7. Schematic representation of self-assembled DNA nanostructures.

(2) **DNA hybridisation-based biosensors** refer to biosensors that use enzyme-free nucleic acid amplification strategies to enhance their response, such as DNA hairpin-based biosensors, the hybridisation chain reaction (HRC) and catalyzed hairpin assembly (CHA). DNA hairpins-based biosensors, due to the highly specific hybridisation between the hairpin and the target nucleic acid, a conformation change of the hairpin itself occurs, which can be easily converted into an electrochemical or fluorescent signal change. HRC and CHA biosensors both use the detection target to stimulate the DNA hairpin amplification process. Hybridization Chain Reaction (HCR) is a self-assembly strategy in which the target nucleic acid sequence triggers the formation of DNA nanostructures, this process can be coupled to different signal transduction schemes [63]. Catalyzed hairpin assembly (CHA) is another enzyme-free signal amplification method achieved by DNA hybridization (self-assembling and disassembling) rather than HCR (Figure 7 (2)). Li et al. proposed a DNA-based electronic sensor for nucleic acid analysis, immobilizing the hairpin-like DNA on the surface of a gold electrode [64]. In this paper, a dual-thiol modified hairpin DNA was used as capture probe by forming a Y-shaped DNA duplex upon target binding.

(3) **DNA template** is the third category of DNA biosensors, such as biosensors based on DNA tetrahedron and DNA origami (Figure 7 (3)). The DNA origami technique takes advantage of nucleic acids' capacity for self-assembly to create a variety of nanoscale systems. Wang et al. reported a DNA origami-based nanowalker device for sensitive detection of target nucleic acids [65]. After that the DNA target binds the DNA origami, it can release the fluorescence of many molecules by acting as the catalyst of an enzymatic reaction.

1.1.4 NA microarray

An interesting analytical approach based on nucleic acids that has proved to be very useful is Nucleic acids (NA) microarrays. NA microarray assays allows massively parallel analysis on a high-density single device, the so-called DNA chip or DNA microarray. This technology is based on detecting molecular interactions so providing useful information for massive diagnostic research [66]. Basically, the microarray consist of numerous oligonucleotide probes deposited on a solid support [67]. The DNA chip consists of a solid substrate where specific oligonucleotides (DNA probes) are immobilized to detect complementary DNA sequences (target DNA) through hybridisation reactions. Since the binding is highly stable and selective, it allows identifying and quantifying the target present in the sample, separating it from the other components. Its advantages include multiplexing since several targets can be analysed simultaneously in a short time and at reduced cost. Indeed, its small size and simplicity facilitate miniaturization of assay devices with high selectivity using small sample volumes and different detection modes. On one single DNA microarray, tens of thousands of hybridisations can be performed simultaneously. Besides, this is a technology that supports the development of biosensors, as, for example, it enables the evaluation of the best ways to immobilise probes and their bioavailability using a high-throughput platform.

The process to build a DNA microarray can be divided in (1) select and prepare the substrate material to attach different probes at different positions, (2) hybridisation by the exposure of the probes to the sample solution containing the targets, (3) scanning to detect the molecular interactions, and (4) data analysis (Fig. 8.) [68].

After hybridization, several washing steps must be performed. The microarray is then scanned to obtain the complete hybridisation pattern generated by the binding of immobilised probes with the target DNA sequence. The most common reading technique in microarray technology is based on fluorescence imaging [69]. Overall, factors influencing the fabrication of DNA microarrays are the platform used, the immobilisation chemistry, the spotting buffer and the probe concentration [70]. The type of material where the probe-target interaction occurs play a key role, as the chemical and physical properties of the platform determine the performance of the microarray assay. Indeed, the surface properties of the solid support influence the probe immobilization density and its bioavailability.

Various surface materials such as glass, silicon, metal, carbon or plastic substrates have been tested for the fabrication of oligonucleotide-based biochips [71]. Of these, glass has remained the most commonly used in the form of microscopic slides due to its unique advantages: (i) it can be easily activated for covalent attachment of oligonucleotide probes, (ii) it has excellent chemical resistance to solvents and can withstand high temperatures (iii) it has flat, non-porous characteristics that help keep the hybridisation volume to a minimum, and (iv) its low background fluorescence does not interfere during the scanning process. Synthetic polymers or plastics are another interesting group of solid supports for microarray fabrication [72]. Among different polymers, polycarbonate (PC), polymethylmethacrylate (PMMA), nylon, and polystyrene have been extensively used. Due to its interesting physical properties and low cost, several microarray strategies have been developed on PC substrates [73].

As already mentioned, the first step of microarray fabrication involves sample preparation and its deposition on a surface. Sample patterning techniques can be divided in two broad groups: *in-situ* or *ex-situ* (spotting).

- In *in-situ* microarray fabrication, oligonucleotides are synthetised base by base on the array surface [74].
- *Ex-situ* or robotic spotting techniques are based on atomised delivery of pre-synthesised probe to specific locations on microarrays [75].
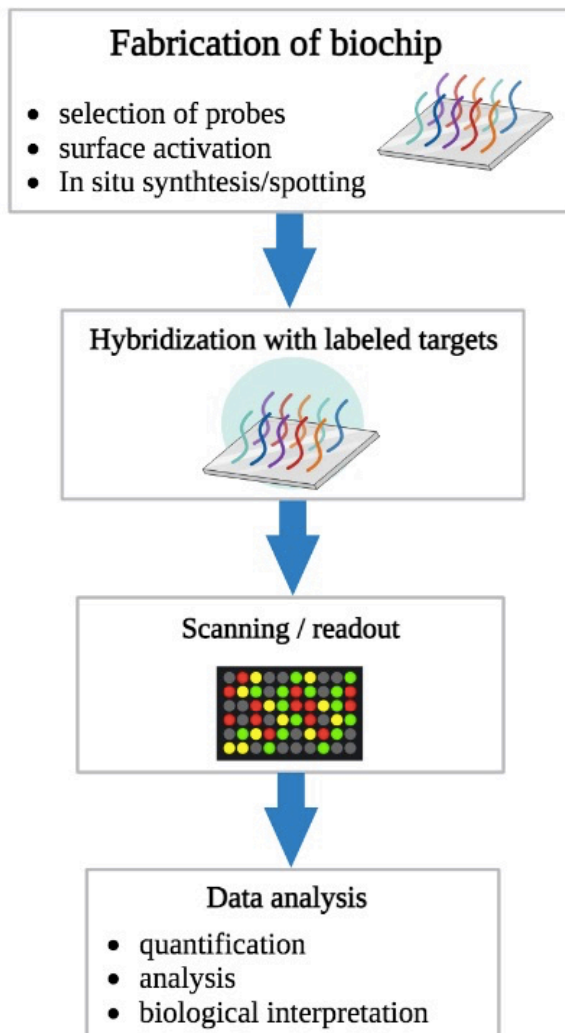
Fig. 8. Schematic representation of steps involved in construction of biochips.

The *ex-situ* spotting techniques is more accessible and commonly used for microarray fabrication, especially in research settings. There is no limit on probe sequence length, and it is cheaper than *in-situ* techniques. Within *ex-situ* techniques, two procedures for probe deposition are available: contact and non-contact procedure. Contact methods require direct contact between the platform and the deposition device. Although this method is very simple, it can lead to contamination and damage of the deposition device or platform. The non-contact method, on the other hand, reduces contamination and damage.

Once the substrates are patterned, different strategies can be applied to immobilise probes on the surface (discussed in section 1.2.4). At this point, the properties of the surface and the probe come into play, in order to achieve strong, oriented immobilisation without loss of activity.

Among the ways to increase the sensitivity of microarrays has recently emerged to use hydrogels as a support for probe immobilisation. The advantages of this approach over direct immobilization on flat substrates are higher loading, better accessibility and a 3D liquid-like environment that is more suitable for maintaining activity and enabling biological interactions. The conventional approach to fabricate hydrogel-based DNA microarrays consists of depositing a homogeneous layer of hydrogel on a substrate followed by probe immobilisation or, alternatively, directly synthesising in situ hydrogels spots containing oligonucleotide probes. For example, M. Pikula et al. developed a simple approach for the fabrication of hydrogel-based DNA microarrays where the product of rolling circle amplification (RCA) was physically trapped in hydrazone crosslinked poly(oligoethylene glycol methacrylate) hydrogel during in situ gelation [76]. Whereas, Yuan Qi et al. used a glycidyl methacrylate (GMA)-poly(ethylene glycol) diacrylate (PEGDA) hydrogel that was fixed on modified slides by photopolymerisation and the hybridisation assay demonstrated a high microarray sensitivity with a LOD of 30.5 pmol L^{-1} [77].

1.2 HYDROGELS

1.2.1 DNA Hydrogels in biosensing

Hydrogels exhibit numerous attractive features such as ease of synthesis and modification, high biocompatibility, and flexibility, making them extremely promising for bioanalytical detection. Numerous studies have been carried out on **bioresponsive hydrogels**, which undergo swelling/shrinkage or sol-gel transitions following the application of different triggering factors [78]. In particular, DNA-based hydrogels have attracted great interest for the exploration of smart hydrogels, whose properties can change in response to various external stimuli [79]. In terms of composition, DNA hydrogels can be divided into two categories (Fig. 9.): 1) **hybrid DNA hydrogels** and 2) **pure DNA hydrogels** [80].
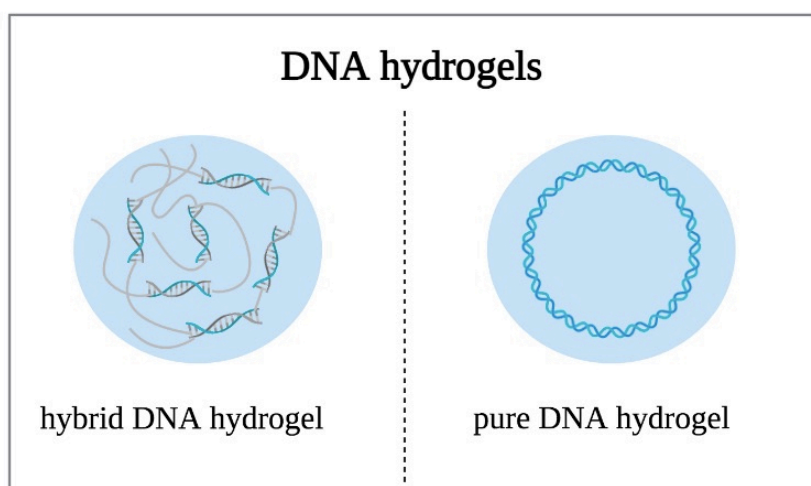
Fig. 9. Schematic representation of DNA hydrogels: 1) hybrid DNA hydrogels and 2) pure DNA hydrogels.

1) A **hybrid DNA hydrogel**, specifically, is a gel material that is not composed entirely of DNA and may refer to the binding of DNA strands to different polymers and/or nanoparticles. Usually, they are obtained by binding functional nucleic acids to synthetic or natural polymers. These polymer/DNA hybrid hydrogels have been widely investigated since Nagahara and Matsuda reported the first copolymer-DNA hybrid hydrogel [81]. Some recent examples were developed in 2013 by Yan and colleagues, who reported a polyacrylamide/DNA hydrogel for quantitative detection of non-glucose targets combined with a portable personal glucose meter (PGM) [82]. In this strategy, two short DNA sequences, grafted onto polyacrylamide polymers, hybridise with an aptamer sequence to produce a three-stranded complex. This results in a 3D hydrogel with glucoamylase stably trapped inside. When target molecules are introduced, the aptamers bind them in a specific and preferential way, causing the hydrogel to break down and release of glucoamylase, which in turns produces a large amount of glucose for quantitative detection by the PGM. Another example, developed by J. Liu, is based on a DNA-functionalised hydrogel for colourimetric detection of DNA [83]. In this study, two probe DNAs were used: one modified with acrydite to achieve covalent binding to the hydrogel matrix and the second containing a thiol modification to bind to gold nanoparticles (AuNPs). In the presence of the target DNA, the AuNPs bind to the surface of the hydrogel producing a colour change from transparent gel to red. More recently, based on the same principle, Y. Ma et al. proposed a target responsive DNA hydrogel as rapid and portable biosensor for visual detection of glucose [84].

2) The second category involves **pure DNA hydrogels**, constructed exclusively from DNA molecules and assembled by enzymatic ligation, polymerisation, hybridisation and specific binding of DNA building blocks [85]. Pure DNA hydrogels are also often used in drug delivery applications as they are biocompatible and biodegradable. Moreover, they could potentially be used as implantable sensors for *in vivo* diagnostics. In 2004, DNA pure hydrogels were firstly obtained by controlled assembly of dendrimer-like DNA [86].

A few years later, Luo and coworkers designed three types of branched DNA monomers, namely X-DNA, Y-DNA, and T-DNA and first reported the construction of a hydrogel consisting entirely of branched DNA by means of an enzymatic reaction [87]. The last developed approach uses well-designed DNA sequences that possess complementary ends. In this way, they are able to self-assemble through hybridisation and mutual binding via the reaction catalyzed by T4 DNA ligase, resulting in 3D hydrogel structures.

As recent examples in biosensing applications, Mao et al. synthesised a pure DNA hydrogel using an induced surface primer induction to immobilise it on the surface of a solid electrode. The immobilised DNA function as a 3D scaffold for enveloping enzymes, and direct electrochemical and colorimetric detection of hydrogen peroxide and bilirubin has been demonstrated [88]. In another work, a responsive pure DNA hydrogel was developed by one-step preparation to realise a new label-free strategy for Pb^{2+} biosensing. The presence of Pb^{2+} in the sample activates the enzyme filament in the hydrogel and triggers the cleavage of the hydrogel structure. DNA fragments released from the collapsed hydrogel are measured as an output signal to quantify Pb^{2+} concentrations with a minimum detection limit of 7.7 nM [89]. Due to the cost and the unavoidable accumulated errors associated with DNA self-assembly, the preparation of pure DNA hydrogels by nucleic acid amplification has gained significant attention [90]. Tian et al. developed a rolling cycle amplification (RCA) method for an automated production of pure DNA hydrogel [91]. Glucose oxidase was incorporated into the hydrogel to be used for accurate and sensitive glucose detection.

Table 2. Stimuli-responsive DNA hydrogels.

Output signal	Type of DNA hydrogel	Target	Sensitivity (LOD)	Detection time	Ref
Electrochemical	Hybrid DNA	Cocaine	3.8 μM	1 h	[79]
Colorimetry	Hybrid DNA	Target DNA	1 pM	2 h	[80]
Colorimetry	Hybrid DNA	Glucose	0.44 mM	1.5 h	[81]
Colorimetry	Pure DNA	Hydrogen peroxide	22 nM	N/A	[85]
Electrochemical	Pure DNA	Hydrogen peroxide	13 nM	N/A	[85]
Colorimetry	Pure DNA	Bilirubin oxidase	32 nM	N/A	[85]
Fluorescence	Pure DNA	Lead ion	7.7 nM	N/A	[86]
Colorimetry	Pure DNA	Glucose	3.2 μM	N/A	[88]

In conclusion, stimuli responsive DNA hydrogels have been widely investigated as portable and low-cost biosensor platform (Table 2). To date, several DNA hydrogels have been constructed as an excellent biosensing substrate for detecting a wide range of stimuli [92]. Considering recent advances, DNA hydrogel sensors offer great potential in different fields. Compared to hybrid DNA hydrogels, obtaining pure DNA hydrogels still has some limitations. The intrinsic properties of DNA impose high synthesis costs and a highly negative net charge, in addition to the few functionalities available in the DNA molecule, limiting further modifications and reducing versatility. Consequently, more and more researchers are focusing their studies on the use of hybrid DNA hydrogels.

In this thesis, we have focused on hybrid DNA hydrogels for the development of biosensors, as they offer synergic properties from the combination of two materials with different characteristics and are affordable for large-scale production. In the following sections, the synthesis, characterisation and properties of these hydrogels is described.

1.2.2 Hydrogels: synthesis and characterization

Hydrogels are three-dimensional networks of hydrophilic polymers capable of storing a large amount of water, a property that distinguishes them from other polymers [93]. When they are in a dehydrated state, or xerogel, are glassy, while in the presence of water they absorb a significant amount of water, forming soft and elastic gels. Their insolubility and shape stability are the result of the presence of a 3D crosslinked network. The high-water content, which can exceed the 95% by weight ratio, mimics the functions of biological tissues. The hydrophilic groups, such as -COOH, -OH, -NH$_2$, -CONH-, -CONH$_2$, and -SO$_3$H, present in the network of hydrogels are responsible for water absorption. Hydrogels include natural polymers or synthetic polymers, examples are given in Table 3 [94]. Natural polymers are suitable for biomedical applications as they are biocompatible and biodegradable, but often lack good mechanical properties. In contrast, synthetic polymers are increasingly used because they can be designed to achieve the desired mechanical and other favorable properties [95]. The diversity of hydrogels, natural and synthetic, with different polymer topologies and chemical compositions, makes them highly adaptive to a vast array of applications (Fig. 10). Established applications of functional hydrogels include tissue engineering [96], wound dressing [97], contact lenses [98], drug delivery [99], soft robotics [100] and sensing [101].

Table 3. The most common synthetic and natural polymers used for the preparation of hydrogels.

Monomers used for synthetic polymers	Natural polymers
Acrylamide (AM)	Chitosan
Hydroxyethyl methacrylate (HEMA)	Alginate
Hydroxyethoxyethyl methacrylate (HEEMA)	Collagen
Hydroxydiethoxyethyl methacrylate (HDEEMA)	Dextran
Methoxyethyl methacrylate (MEMA)	Cellulose
Methoxyethoxyethyl methacrylate (MEEMA)	Hyaluronic acid
Methoxydiethoxyethyl methacrylate (MDEEMA)	DNA
Ethylene glycol dimethacrylate (EGDMA)	Chitin
N-vinyl-2-pyrrolidone (NVP)	Gelatin
N-isopropyl AAm (NIPAAm)	Fibrin
Vinyl acetate (VAc)	
Acrylic acid (AA)	
N-(2-hydroxypopyl) methacrylamide (HPMA)	
Ethylene glycol (EG)	
Vinyl alcohol (VA)	
EG acrylate	
EG methacrylate	
EG diacrylate	
EG dimethacrylate	
Methacrylic acid (MA)	

Fig. 10. Established hydrogel applications in industrial and research fields.

In addition, they have a key role in many applications as coating materials for improving the biocompatibility of materials that will interact with living tissues, e.g., *in vivo* sensing devices or implantable medical devices. Hydrogels, known hydrophilic materials, can substantially enhance the hydrophilicity of the coated surface by exhibiting anti-biofouling properties [102]. For hydrophilic surfaces, resistance to the adhesion of soiling agents is attributed to the hydration layer that forms between the coating and its surroundings. This hydration layer acts as a physical barrier to resist the adhesion of fouling agents. Hydrogels commonly used as anti-biofouling coatings include poly (vinyl alcohol) (PVA), polyethylene glycol (PEG) and natural polysaccharides, such as chitosan and dextran [103] [104] [105]. Another category of anti-biofouling hydrogel is zwitterionic hydrogels which are neutral but have an equal number of positive and negative charges along the polymer network [106].

The synthesis and composition of the hydrogel play an important role, as they influence the final properties of the material. The formation of hydrogels, called gelation, involves a **crosslinking process** of polymer chains. Based on different mechanisms, the polymerisation can take place either by **self-assembly** (physical crosslinking) or by **addition polymerization** (chemical crosslinking) of polymer chains [107].

In the case of physically crosslinked hydrogels the formation of hydrogel network results from various weak intermolecular interactions between the polymer chains (e.g., hydrogen bond, electrostatic interactions, hydrophobic interactions, etc.).

In the case of chemically crosslinked hydrogels, polymer chains are covalently bonded (between monomers or between monomers and crosslinkers). The monomer is the main building block of the hydrogel structure, while the crosslinker is defined as the molecular entity in which three or more chains can join to form a crosslinking point and transform the polymer into a 3D network. The hydrogel polymerisation reaction can be initiated: (i) catalytically, (ii) thermally or (iii) photochemically, using an appropriate initiator. The speed of polymerization depends on the concentration of the initiators and the reaction conditions. Addition polymerisation, to obtain chemical hydrogels, is a chain reaction that converts olefin monomers into polymers by stimulating the opening of the double bond with a free radical or ionic initiator (Fig. 11.(A)) [108]. Typically, for addition polymerisation the polymer formed has the same chemical composition as the monomer, as there is no elimination of molecules during the reaction. The **Free Radical Polymerization** (FRP) is the conventional reaction commonly used for the preparation of hydrogels. This method follows the typical steps of addition polymerisation in the sequence of initiation, propagation and termination (Fig. 11.(B)) [109]. This mechanism of polymer formation is characterised by three reactions in sequence: the first is the initiation reaction in which an active centre is produced, thanks to the presence of an initiator or catalyst of polymerisation, which can be a radical, a cation or an anion; subsequently, the second reaction known as the addition or propagation reaction takes place, in which the monomer species is added to this active centre, leading to the simultaneous formation of a similar active centre on the added unit.

This reaction in the polymerisation process allows the subsequent addition of several monomer units and thus the formation of the polymer chain. Finally, there is the termination reaction that leads to the interruption of the chain propagation, and thus to the production of the final polymer chain, i.e., no longer capable of adding monomer units. The polymerisation initiator or catalyst is generally a free radical, which is able to add itself to a monomer molecule, through the breaking of the double bond, with the simultaneous formation of another radical and so on.
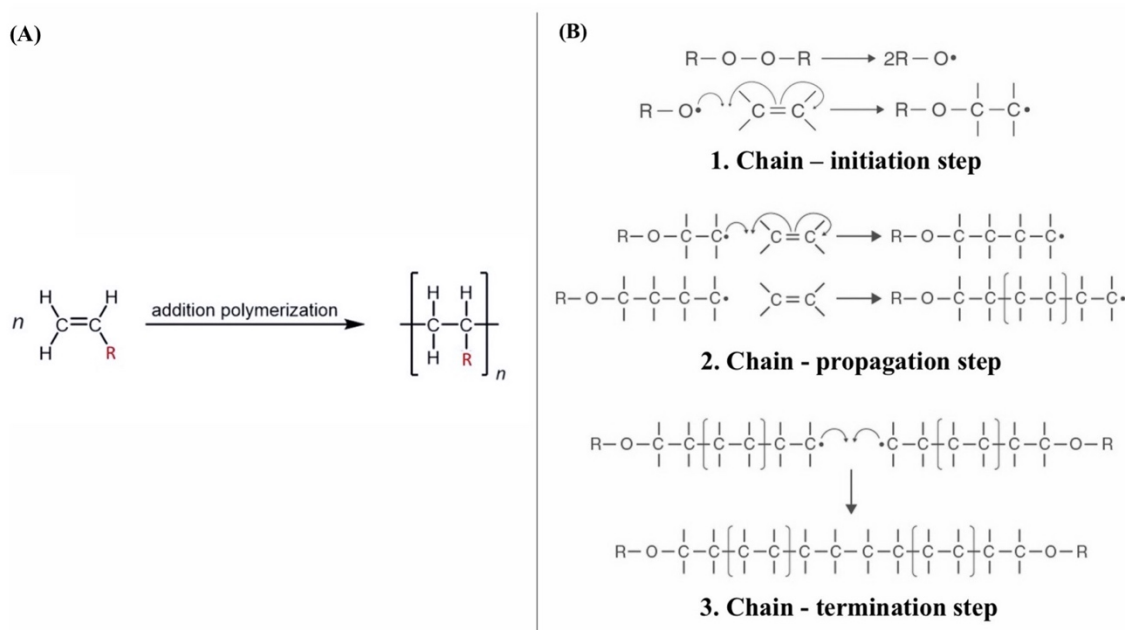
Fig. 11. (A) General scheme of addition polymerisation reaction. (B) Typical steps of addition polymerisation.

The conversion efficiency of hydrogel monomers to a hydrogel network does not reach 100%, which leaves unreacted monomers and initiators that are toxic and that can leak from the hydrogel matrix. Prior to use, it is crucial to remove these leftover small molecules, especially in biomedical applications.

The common procedure for removing these unwanted small molecules is to incubate the polymerised hydrogel in an excess of deionized water (DI) for several hours or days, with regular refilling of the DI water [110].

There are various ways to classify hydrogels according to different parameters (Fig. 12.) [111]. Based on the monomer employed in the synthesis, hydrogels are classified into homopolymers (one type of monomer), copolymers (two types of monomers) and multipolymers (three or more monomers). They can be also classified according to the types of bonds existing between the polymer chains, into physically crosslinked gels (non-covalent bonds) or chemically crosslinked gels (covalent bonds) or a combination of the two.
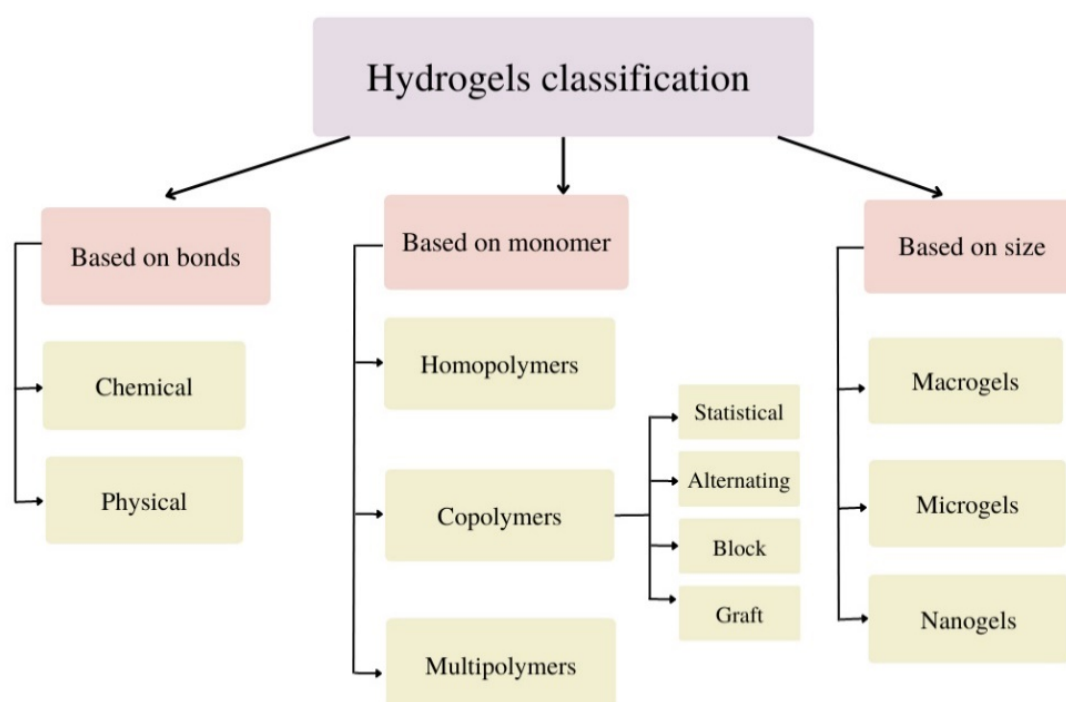
Fig. 12. Classification of hydrogels based on different parameters.

Moreover, they can be obtained in almost any shape and size (macrogels, microgels, nanogels). Copolymers prepared from bifunctional monomers can be subdivided further into four main categories: i) Statistical copolymers in which the distribution of the two monomers in the chain is random, ii) Alternating copolymers with a regular placement along the chain; iii) Block copolymers comprised of substantial sequences of each; and iv) Graft copolymers in which blocks of one monomer are grafted on to a backbone of the other branches [108].

The process of absorbing large amounts of water (Fig. 13.) is known as swelling of the hydrogel [112]. The swelling percentage, which is an important performance of synthesised hydrogels, can be calculated with the following equation:

$$Swelling \ (\%) = \frac{Ws-Wi}{Wi} \cdot 100 \tag{2}$$

Where Ws is the weight of the hydrogel in its fully swollen state and Wi is the weight of the fully dry hydrogel.
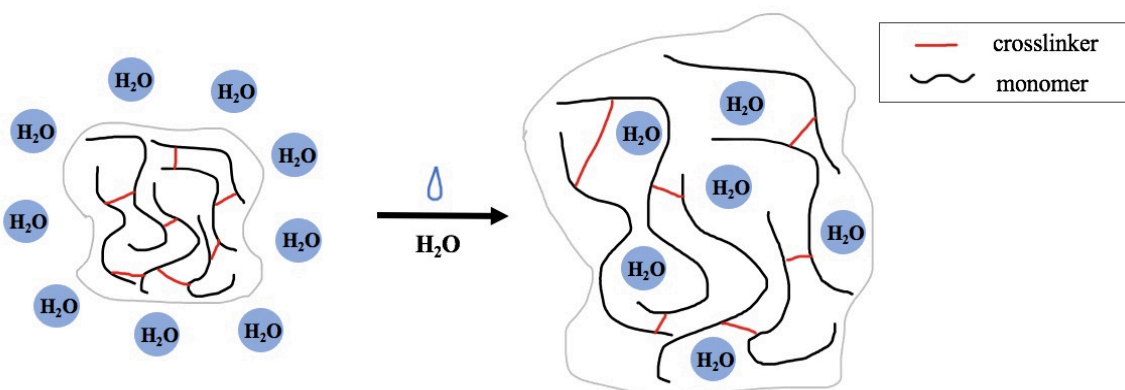
Fig. 13. Representation of the hydrogel swelling process.

It is also possible to obtain the swelling kinetics of the hydrogel over time. This is achieved by starting with the hydrogel completely dry and measuring its weight after successive immersions in water. The swelling capacity of hydrogels is determined by the monomer nature (e.g., hydrophilicity) and the degree of crosslinking, and is one of the most important properties, as it influences permeability, mechanical, surface and other properties [113]. Further, it is interesting to note that stimuli-responsive hydrogels, known as smart hydrogels, which are able to respond to external stimuli including pH, temperature, solvent composition, enzymes and electric fields, are gaining popularity for a wide range of applications [114] [115] [116].
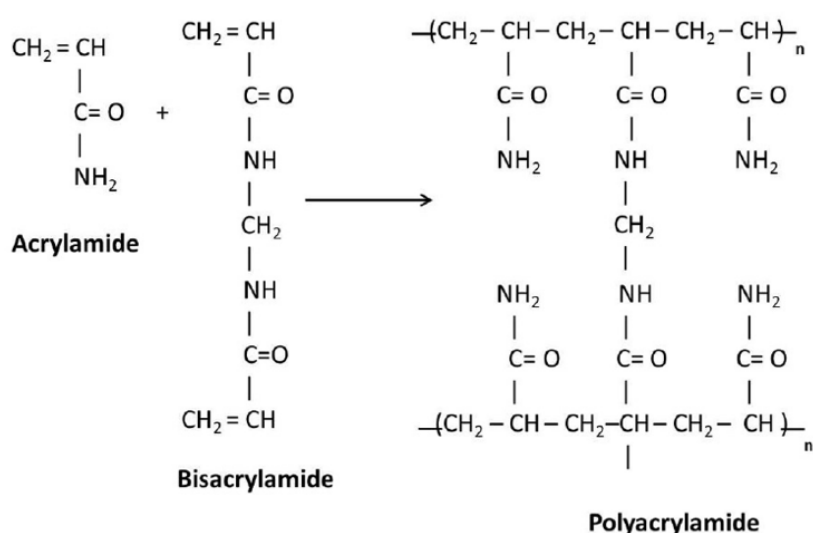
Fig. 14. Chemical crosslinking of poly(acrylamide) hydrogel, reaction between Acrylamide as monomer and Bis-acrylamide as crosslinker.

In this Thesis, a chemically crosslinked Acrylamide-based hydrogel was selected as 3D support for the covalent incorporation of DNA probes (Fig. 14.). Acrylamide (C_3H_5NO) is an organic compound derived from acrylic acid, whose hydroxyl group (-OH) has been replaced by an amine group (-NH2).

At room temperature, it presents itself as a colourless or slightly white crystalline solid, soluble in water with a strongly endothermic reaction, having a non-perceptible odour. Acrylamide, being a neurotoxin, in powder form can be easily inhaled with potentially very dangerous effects, but once it has gelled it loses its dangerousness [117].

1.2.3 Hydrogel as support matrix for DNA biosensors

In general, polymer matrices are used as 3D supports in numerous fields of biotechnology, including molecular diagnostics, drug delivery and tissue engineering [118] [119] [120] [121] [122]. However, the idea of **DNA-functionalised hydrogels** is a relatively new field, and most developments have only occurred in the last ten years [123] [124] [125]. The water contained in hydrogels provides a medium for the transport of water-soluble species. Indeed, due to their significant water content and relatively soft consistency, they closely resemble natural tissues, providing an optimal environment for biological interactions [126]. The use of hydrogels as immobilisation matrices for biosensing applications has several advantages. Firstly, compared to 2D planar surfaces, they have much higher loading capacity because immobilisation takes place in 3D [127]. Secondly, the high-water absorption and porous morphology provide an optimal environment for biomolecular interactions. Another characteristic feature of hydrogels as immobilisation matrices is the significant decrease of nonspecific binding, due to the hydrophilicity of polymer used in hydrogels [128] [129]. Therefore, the combination of the high loading capacity and the low non-specific adsorption in the hydrogel lead to increased sensitivity. Finally, the internal pore structure of the hydrogel can be adjusted to make diffusion faster and thus improve the sensing performance. The sensing principle relies on the analyte recognition which triggers the response of DNA hydrogels biosensor and leads to changes in the physicochemical properties of the gel matrix (such as changes in crosslinking density, volume, mechanical or optical behavior, etc.) which can be further transduced into a detectable signal [130]. Some recent approaches of hybrid DNA hydrogels employed as biosensing platforms are given in Fig. 15.
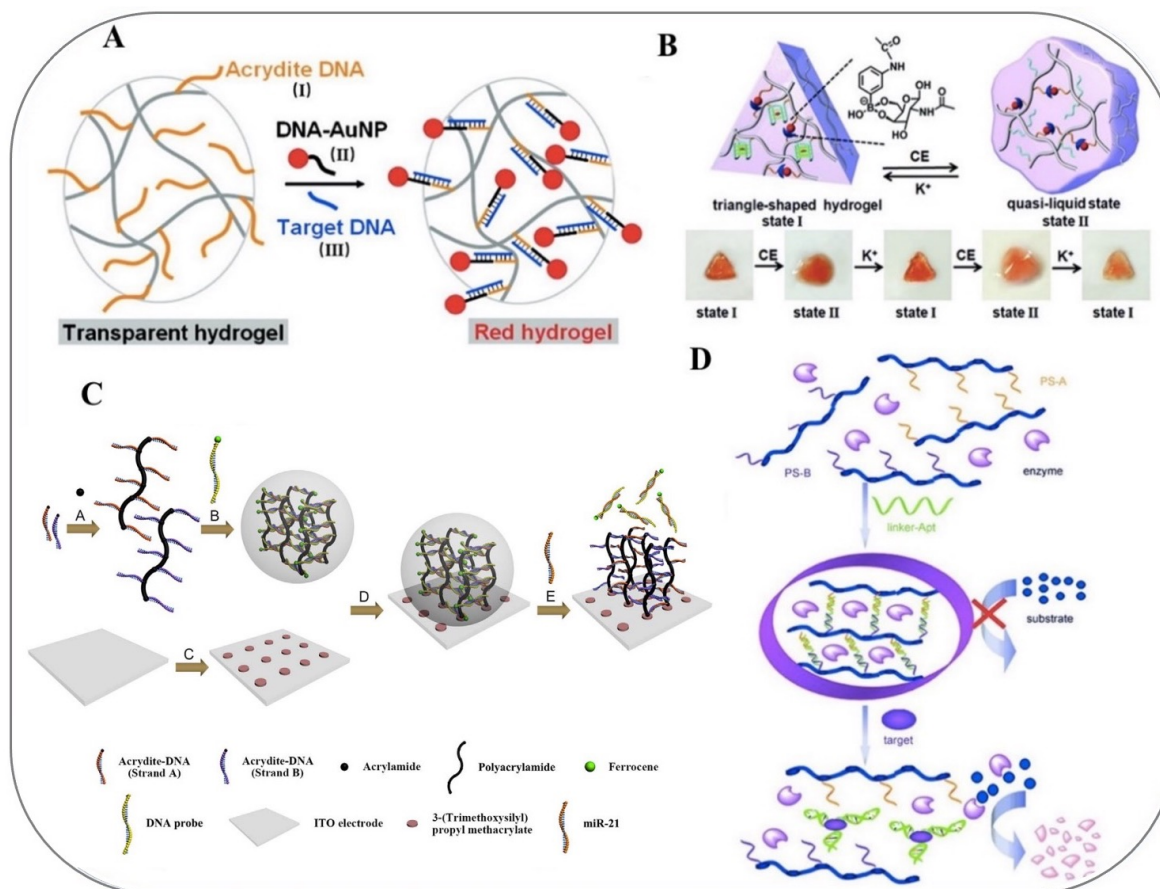
Fig. 15. Hybrid DNA-hydrogels as biosensing platforms based on different strategies. **A** DNA-functionalized hydrogel for visual detection of the DNA target labelled with AuNPs, reprinted with permission from Ref. [83]. **B** Polyacrylamide DNA hydrogels of glucosamine-boronate esters and G-quadruplexes synergistically cross-linked in the presence of K^+/crown ethers undergoing cyclic hydrogel-solution transition. Reproduced with permission from Ref. [131]. **C** The self-assembly DNA hydrogel is fixed on ITO electrode and miR-21 can cause the dissociation of it through recognizing with probe. Reproduced with permission from Ref. [132]. **D** Enzyme trapped hydrogel for signal amplification and visual detection. Reproduced with permission from Ref. [133].

In the first approach (Fig 15.A), a DNA-functionalised polyacrylamide hydrogel was obtained by co-polymerization with acrydite DNA probes. The hybrid DNA hydrogel was employed for the colorimetric detection of the DNA target labelled with AuNPs, achieving a LOD of 1 pM.

The second reported DNA-based hydrogel (Fig. 15.B), was crosslinked by glucosamine-boronate ester bridges and by K^+-ion-stabilized G-quadruplex units [131]. The dissociation of the K^+-ion-stabilized G-quadruplex crosslinkers occurred in the presence of 18-crown-6-ether and led to the sol-gel transition of the hydrogel into a soft, quasi-liquid matrix. In Fig 15.C, a self-assembled DNA hydrogel was immobilised on indium tin oxide/polyethylene terephthalate (ITO/PET) electrode for the detection of lung cancer-specific microRNA, miR-21 [132]. When the recognition probe was hybridised with the target miR-21, the hydrogel dissolved, producing a loss of ferrocene tags and a reduction in current. The biosensor demonstrated a detecting capability with a LOD of 5 nM. Finally, the last example (Fig 15.D) is based on agent-caging hydrogel as colorimetric detection platform [133]. Two DNA strands are grafted onto linear polyacrylamide to form polymer strand A and polymer strand B. The sequence of DNA strand A and B are complementary to an area of a DNA aptamer sequence. Therefore, the addition of the aptamer linker initiates the hybridisation, thus crosslinking the linear polyacrylamide polymers. If an enzyme is added prior to the addition of the aptamer linker, it will be trapped inside the 3D hydrogel network. Upon introduction of the target, the aptamer will bind with it, and the gel will be dissolved as a result of the competitive target-aptamer binding. The enzyme is consequently released and can take part in its catalytic role for signal amplification. Binding to the target triggers an enzymatic reaction that changes the colour of the substrate, thus enabling visual detection. Normally, AuNPs are used as indicator reagents or signal amplification agents based on their unique optical properties and chemical stability. In this case, the AuNPs initially trapped inside the hydrogel (red gel) are then released due to molecular recognition leading to the dissolution of the gel, thus observing a colour change from a dark red gel to a less intense red solution.

Although many different approaches have been developed, to date there are no commercial biosensors based on hydrogels. Extensive investigations on sensitivity, specificity, response time, reproducibility and durability have yet to be performed. Hydrogels, in particular for point-of-care diagnostics, could be crucial because they boost the readout signal and give the option to incorporate the visualization agent into the sensing network.

1.2.4 Immobilisation strategies

The process of immobilising bioreceptors consists of introducing the bioreceptor elements into 2D or, in the case of polymers, 3D substrates. The use of a reliable strategy for the immobilisation of the bioreceptors is one of the most important and critical steps in biosensor design [134]. In general, the physical-chemical characteristics of the support matrix and the bioreceptor molecule dictate the immobilisation technique to be used. To obtain a DNA biosensor with good performance, an immobilisation strategy is required in which the probes within the substrate can maintain their affinity for the target DNA [135]. Therefore, the amine groups of the DNA nucleotides (Adenine, Guanine, Cytosine, Tyrosine) must remain free and fully functional after immobilisation. Depending on the nature of the support matrix, various methods can be used to anchor DNA probes (Fig. 16.). Typically, DNA probes can be immobilised by: 1) **Physical adsorption**, 2) **Entrapment**, 3) **Affinity coupling** or 4) **Covalent bonding** [136] [66].

An **adsorptive immobilisation**, in general, is a noncovalent coupling method on solid supports that is based on electrostatic, van der Waals interactions, hydrogen bonds and hydrophobic interactions [136]. This technique does not involve any functionalisation of the support or the probes, so it generally does not affect the activity of the receptor probes. Moreover, because the bonds between the bioreceptors and the substrate are not very strong, changes in temperature, pH, and ionic strength can lead to desorption of the probes. Normally, the negatively charged phosphate backbone of the DNA probe is used to couple it to a wide variety of supports, such as charged gels, carbon surfaces, polymers and various metal surfaces. As an example, Bo et al. demonstrated the successful immobilization of DNA probes on a chitosan-coated graphene paste electrode utilizing electrostatic adsorption [122].

In **entrapment**, large quantities of probes are irreversibly retained within a 3D polymeric network [137]. As many biomolecular interactions occur within a three-dimensional space, a 3D matrix for trapping nucleic acid probes is sometimes favourable as functional elements can be locally charged at a high concentration, allowing an increase in the overall sensitivity of the assay, especially when the matrix consist of a hydrogel. For the direct immobilisation of DNA in polymeric matrices, the pre-polymer solution is prepared by adding bioreceptor elements that are trapped in the matrix during polymerisation. There are several reports on the trapping of biomolecules in hydrogels, particularly on enzymes, as hydrogels have been found to preserve the native conformation of proteins and thus enhance enzyme activity [138]. However, this method present diffusion problems producing many non-specific signals. In summary, physical adsorption and matrix entrapment are simple methods as they no require reagents, matrix activation, or modified DNA. However, the limitations of these two methods are basically the poor reproducibility and accessibility.
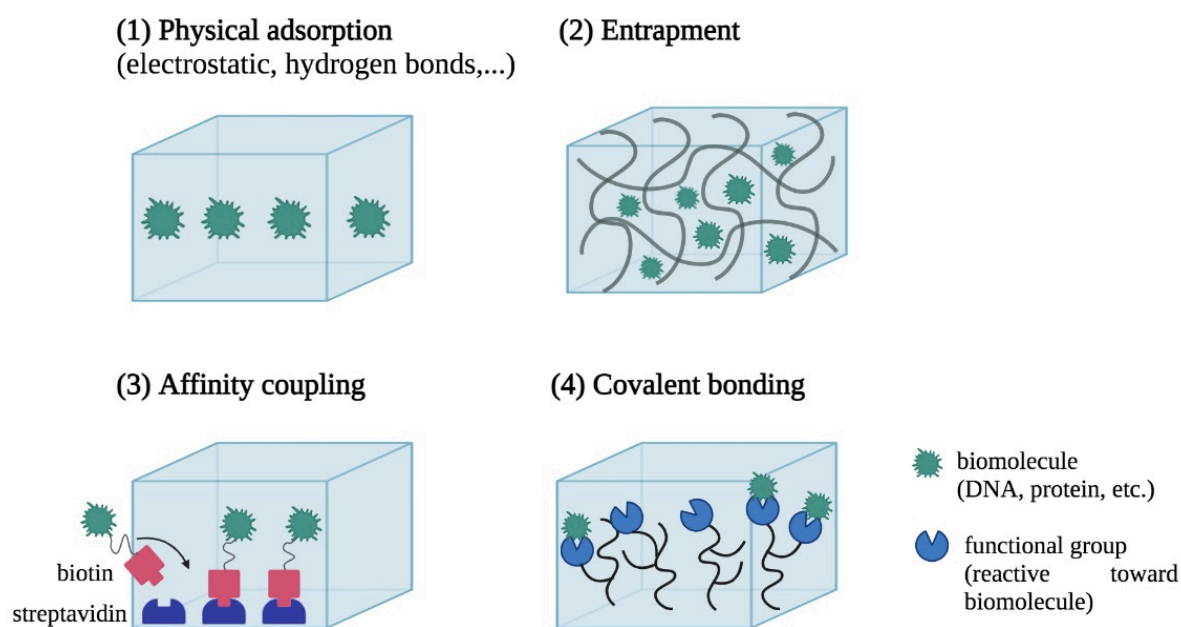
Fig. 16. Representation of possible immobilization methods of biomolecules onto a support gel matrix.

Affinity immobilisation methods take advantage of the specific interaction between a pair of complementary biomolecules that form a strong complex due to the high affinity constants, resulting in high selectivity [139]. The most common form of nucleic acid affinity binding onto several different surfaces involves the use of biotin–avidin/streptavidin linkages, a system known to form one of the strongest non-covalent bonds [140].

A very common method for probe immobilization is **covalent bonding**. Due to the stability of covalent bonds, this method is preferred to avoid probe desorption from the sensing matrix, allowing irreversible binding of biomolecules. Moreover, these covalent chemical bonds can be made in an ordered way to achieve an oriented anchoring with a more selective response. This approach involves a carefully designed bond between a functional group of the bioreceptor element and the substrate. Due to the versatility of nucleic acid synthesis, DNA probes can be modified at either the 3'- or 5'-end with many functional groups such as amino ($-NH_2$), acrydite ($-C=C$), thiol ($-SH$), hydroxyl ($-OH$), carboxyl ($-COOH$), etc. [141].

In this approach, the matrix needs to bear appropriate functional groups to allow the covalent bond formation. So far, many methods of covalent immobilisation in 2D and 3D supports have been reported [142] [143] [144]. In the case of polymeric 3D networks, functionalisation with the desired DNA sequences can be achieved both during and after the formation of the 3D network. During the 3D network formation, immobilisation by covalent bonding can occur by copolymerization between previously modified DNA probes and the polymer matrix. In other instances, the polymer matrix is first activated by introducing reactive functional groups, such as comonomers, which are then reacted with the functional groups of the bioreceptors.

Among the pool of covalent immobilisation strategies, photoinduced reactions show very interesting properties. Photochemical immobilisation reactions are performed using radicals generated by irradiation at a certain wavelength in the presence of photosensitive reagents. Since these chemical reactions avoid the use of harsh conditions and can be used on all organic materials, being fast, efficient and performed in a single step, they are of particular interest for surface probe immobilisation and for the design of hybrid materials [145].

An interesting group of these reactions is known as photo-***click* chemistry**. The *click* chemistry concept was introduced by K.B. Sharpless and co-workers in 2001 [146]. These reactions are stereospecific, easy to perform, high-yielding, without by-products, and solvent-free or with non-aggressive solvents. When they are activated by light, photoclick coupling occurs, where the main advantage is that they can be activated by irradiation at a wavelength close to visible light (365 nm) which make them interesting reactions for probe immobilization. In fact, irradiation does not cause significant damage to biomolecules and, as a result, photoimmobilised biomolecules maintain their biological activity once anchored; such reactions are usually applied to the fabrication of microarrays. Example include thiol-alkene or thiol-alkyne coupling reactions [147] [143]. These are based on the use of UV light as a radical initiator of the reaction, presenting advantages such as short working times, reduction of reaction steps, simplification of the processes, etc. [144]. As an example, our group worked on covalent immobilization of biomolecules on an acrylate phosphorylcholine hydrogel, by thiol-acrylate *click* chemistry for the preparation of DNA glass microarrays [148]. Such is the importance and broad utility of this kind of reactions that, in 2022, K.B. Sharpless, C. R. Bertozzi and M. Meldal received the Nobel Prize in Chemistry for their contributions in this field. The prize recognised the significant impact that click chemistry and bio-orthogonal chemistry have had in both biology and medicine [149]. The methodological approach developed by K.B. Sharpless and M. Meldal, allows small units to be linked in a simple and effective manner for the synthesis of more advanced chemical compounds through the copper catalysed azide-alkyne cycloaddition. C.R. Bertozzi has applied this strategy to the development of click reactions that work inside living organisms. The bioorthogonal reactions take place without disrupting the normal chemistry of the cell. Today, people all over the world use these reactions to investigate cells and monitor biological processes. Researchers have enhanced the targeting of cancer pharmaceuticals using bioorthogonal reactions, which are currently being tested in clinical trials. Thus, such reactions are an appealing tool for the optimal probe immobilization, also in hydrogel materials.

1.3 NOVEL DETECTION STRATEGIES

1.3.1 Transduction mechanisms

Once the target DNA has been captured in the biosensor substrate, various approaches can be used to transduce the biodetection event. Transduction mechanisms in the field of DNA biosensors are mainly based on electrochemical, gravimetric or optical detection (Fig. 17.) [51] [66]. In **electrochemical biosensors**, a single DNA chain is immobilised on an electrically active surface (electrode) and changes in electrical parameters (e.g., current, potential, conductance, impedance and capacitance) caused by the hybridisation reaction are measured. These approaches are inexpensive, fast, and easily miniaturized, so they have been used in multiple works based on the oxidation of DNA bases or in charge transport reactions. Although their lifetime is limited because electrochemical species may be easily reduced or oxidized due to their low stability.

Gravimetric biosensors are mass-based biosensors which measure mass change induced by the formation of the bioreceptor-target binding, producing a measurable signal. Their main advantage is that they allow direct detection without labeling with high sensitivity. However, the multiplexing capacity is limited [150]. For example, in the case of quartz crystal microbalance (QCM), DNA hybridisation is revealed by the correlation between the resonance frequency of the crystal and the increase in mass generated by target recognition [151].

In **optical biosensors**, on the other hand, the transduction process induces a change in an optical property (absorption/transmission, reflection, refraction, phase/amplitude, frequency or polarisation of light) in response to physical or chemical changes created by the biorecognition. Optical transduction for biosensors has certain advantages over the other two transduction mechanisms mentioned above. As for electrochemical methods, despite their good resolution and accuracy, their weakness is due to the short duration and the ease with which they are affected by temperature variations and electromagnetic interferences. Gravimetric methods, on the other hand, although very sensitive, are mechanically unstable and fragile devices.

The most commonly ways to optically detect DNA hybridisation are based on (a) fluorescence, (b) colorimetry, (c) Surface plasmon resonance (SPR) and (d) interferometry.

Fluorescence-based biosensors are widely used for their high selectivity, sensitivity and short response time [152]. When the DNA target is labelled with a fluorophore, its hybridisation with a probe can be easily measured with a fluorescence imaging device (i.e., a charged-coupled device (CCD) camera). Long used as fluorescent markers to visualize DNA, DNA intercalators are fluorophores that bind between adjacent base pairs of dsDNA. However, intercalators are known to disrupt the structure and mechanical properties of DNA. Although ethidium bromide was the most common labelling agent in the past, other dyes such as the cyanine group have been exploited for the detection of nucleic acids [153]. In fact, cyanine dyes, such as SYBR Green I (SG), which does not pose the same exposure risks for humans and has a brighter fluorescence, has largely replaced ethidium bromide. Other fluorophores for labelling include the cyanines Cy3 (λexc = 550 nm; λem = 570 nm), and Cy5 (λexc = 650 nm; λem = 670 nm), and AlexaFluor 647 dye.

Biosensors based on colorimetry have many advantages, such as ease of operation, cost-effectiveness, fast response time, portability and above all, they provide a direct visual signal that can be read by the naked eye and quantified with inexpensive equipment [154]. One of the most used procedures is based on an additional detection biomolecule which recognises the hybridised product and is usually labeled with enzymes or gold nanoparticles. These abovementioned methods involve molecule labelling.

Alternatively, label-free formats such as SPR or interferometry can be also used. Surface plasmon resonance (SPR) is a label-free, real-time analytical method that enables high sensitive detection [155]. Surface plasmonic waves are used by SPR-based biosensors to identify refractive index changes caused by molecular interaction on metal surfaces. In more detail, SPR is observed when an electromagnetic field strikes a metal film under conditions of total internal reflection. An element of the electromagnetic field of incident radiation, known as an evanescent wave, propagates up to a certain distance in the medium with a lower refractive index at the interface between two media with different refractive indices (such as glass and air).
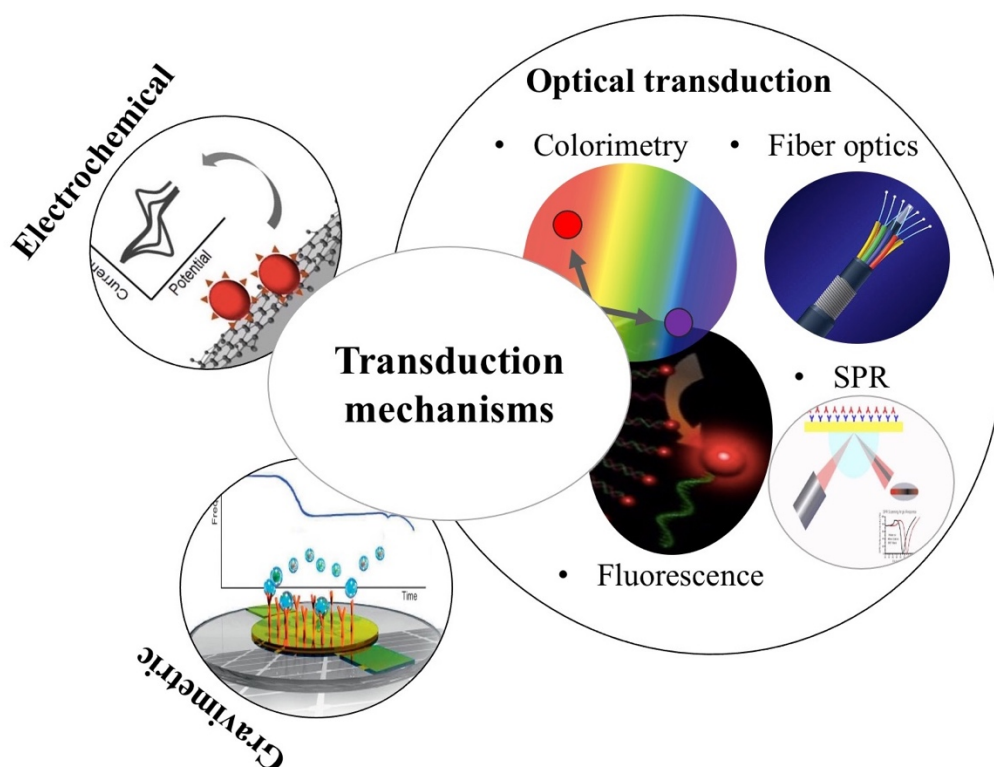
Fig. 17. Most common transduction mechanism for DNA biosensors.

If there is a thin metal layer at the interface between the two media and the light is monochromatic and polarised, the evanescent wave interacts with the free electrons of the metal to produce a plasmonic wave on the surface of the metal layer. The plasma, consisting of the mobile electrons on the metal surface, has a high electron density and oscillates in a direction parallel to the metal-electron interface. Surface plasmons are the term used to describe moving plasma waves. Resonance conditions occur when, at a specific angle, the wave vector of incident light couples with the vector of moving electrons (plasmons). This coupling of the incident light with the surface plasmons leads to a loss of energy, as the energy of the photons is transmitted to the plasmons. Therefore, at the angle at which resonance occurs, a minimum in the intensity of the reflected radiation is observed.

Thus, when mass accumulates on the surface of the sensor, the change in the refractive index on the surface produces a change in the evanescent field that shifts the position of the minimum of the reflected intensity. This shift is quantitatively related to the amount of mass accumulated on the surface.

Finally, interferometry-based biosensor systems such as optical fibers use the same principle as surface plasmon resonance to quantify biological species. In fact, an evanescent wave is produced at the sample interface when light passes through an optical fiber or waveguide as a result of total internal reflection [156]. When a bioconjugation event occurs and the propagating light beam passes through the volume in which the binding event occurred, a change in the refractive index can be observed. To measure this variation, a reference propagation beam is used. This reference beam is usually adjacent to the detection beam but does not encounter the binding event. The reference is combined with the detection beam to create an interference pattern of alternating dark and light fringes. Whenever a chemical or physical change occurs in the sensing arm, the interference pattern shifts.

According to the transduction mechanism, optical biosensors can be divided in **label-free** (direct) and **label-based** (indirect) (Fig. 18.) [157]. In the label-free format, the analytical signal is produced directly by the interaction of the analyte with the transducer. In contrast, in label-based detection, the signal is generated indirectly via a label. Even though the labelling step improves the sensitivity and even selectivity of biosensors, it also could increase the time, complexity and cost of the measurement.

Of the other techniques, optical transduction is the most attractive due to their high selectivity and specificity, multiplexing potential, low sample volume and noise background and the additional possibility of label-free or real-time detection [158] [159]. For this reason, the research and technological development of optical biosensors has grown exponentially over the last decade, especially for biosensors based on direct (label-free) optical signal transduction due to molecular recognition events. Thus, they are good candidates for next generation technologies for bioanalysis as they offer real-time observation of molecular binding; multiplexed detection and they reduce the operational complexity and cost.
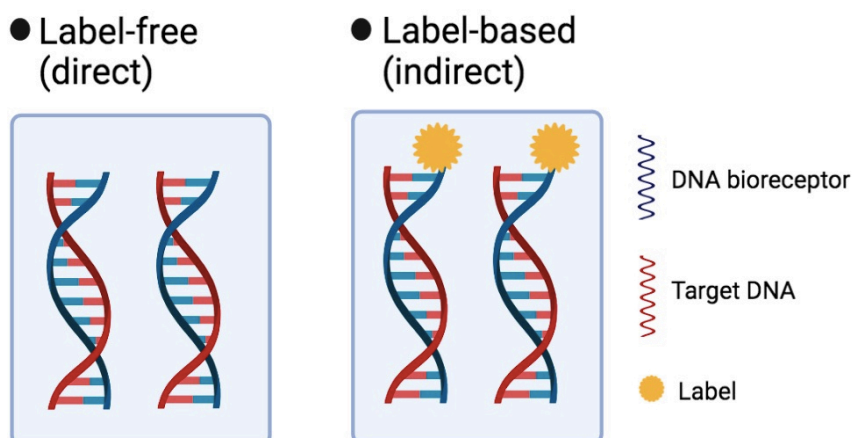
Fig. 18. Schematic representation of direct versus indirect transduction.

Recently, holographic gratings have emerged as label-free optical transducers for the development of chemical and physical sensors and biosensors [160]. Holograms offers a new direct transduction method with great advantages such as simplicity, rapidity, relatively low cost and suitability for the development of portable devices.

The motivation behind this project is the development of a hydrogel-based biosensor with potential application for holographic label-free detection of DNA hybridization [161]. Therefore, fluorescence microscopy was employed in combination with the use of holographic gratings to study the performance of the designed DNA biosensor.

1.3.1.1 Label-free optical transducers

Most label-free optical sensing techniques belong to the category of evanescent wave sensors, in which the optical field decays exponentially in the medium surrounding the structure tens or hundreds of nm from the solid surface of the sensor. The electromagnetic field interacts directly with molecules that bind to the sensor surface. The sensing mechanism of most of these devices is based on refractive index (RI) changes induced by molecular interaction with the evanescent electromagnetic field. The optical refractive index (RI) of most biological molecules is higher than that of water (1.45-1.55 versus 1.33 Refractive Index Units (RIU), respectively). Label-free optical biosensors are designed to sensitively monitor changes in RI, which not only makes it possible to use the molecules in their native form, but also to characterise bio-molecular interactions in real-time, thus obtaining information on the kinetic constants of reactions. The sensing method based on evanescent fields has been applied to various material platforms and device geometries. The main configurations of label-free optical biosensors are the surface plasmon sensors[162], interferometry sensors[163], fiber-optic sensors[164], waveguides[165], photonic crystal sensors[166][167] and ring resonators [168] which have been proposed in the literature on various materials and for a number of specific applications. So far, plasmonic biosensing is the most established and successful technology. In fact, for DNA detection, high-performance SPR biosensors have been obtained with LOD at nM or 100 pM levels. For instance, Milkani *et al.* presented a DNA monolayer immobilised on a gold surface which detected, by surface plasmon resonance (SPR), hybridisation events at a LOD of 20pM[169]. An extension of SPR, called localised plasmon resonance (LPR), refers to the occurrence of SPR confined to the surface of noble metal nanoparticles. A study by Piliarik *et al.* on an LPR biosensor based on an array of gold nanorods achieved a LOD of 100 pM for the detection of DNA hybridization [170]. Nevertheless, despite the proven success of plasmonic optical biosensing and its application in many fields, this technology remains an unused research tool in hospitals or homes. Furthermore, conventional SPR technology is less flexible in construction for miniaturisation and multiplexing purposes. Among interferometry-based biosensors a recent work on a label-free DNA biosensor uses a microstructured exposed-core optical fiber capable of detecting DNA with a LOD of 0.31 nM[171].

Leung *et al.* reported on a label-free technique using ssDNA immobilized on a gold-coated tapered optical fiber [172]. The system works in a flow mode and can detect target DNA in 750 fM to 7.5 nM concentrations. Another study developed an optical diagnostic platform based on a silicon photonic microring sensor coupled to the asymmetric isothermal amplification technique, achieving a LOD of 5 fg/µL for *M. tuberculosis* ssDNA in a test time of 3-6 minutes, so that the sensor can quickly and efficiently detect the probe-target hybridisation events [173]. Another approximation is based on a colloidal photonic crystal structure embedded in hydrogel microspheres functionalised with DNA probe strands[174]. The utility of this label-free detection approach was demonstrated through the detection of a target sequence of the DNA binding domain of the tumour suppressor protein p53. The binding of the complementary target filaments caused the variation of the distance between the beads and the shift of their Bragg diffraction peak, due to the increased concentration of immobilised negative charges within the hydrogel, enabling the detection of picomole concentrations of the p53 target sequence.

Table 4. Limits of detection obtained by different label-free optical bioanalytical methods for ssDNA detection

Label-free method	Analyte	LOD	Ref.
Surface plasmon resonance (SPR)	ssDNA	20 pM	[169]
localised plasmon resonance (LPR)	ssDNA	100 pM	[170]
Interferometry	ssDNA;	0.31 nM;	[171]
(optical fibre, ring resonators, photonic	ssDNA;	750 fM-7.5 nM	[172]
crystal)	*M.tuberculosis* ssDNA;	5 fg·µL;	[173]
	ssDNA	25 pmol-50 nmol	[174]
Grating-based	hgDNA584	0.2 to 2.4 ng/µl	[175]

Although the reported studies offer excellent results in terms of analytical performance, they present some limitations for the development of portable biosensors due to their complexity, the need for expensive facilities, time-consuming operations and small-scale production. In recent years, there has been a large research effort aimed at developing new label-free optical sensing methods with the goal of obtaining portable devices. Label-free optical detection based on the use of holographic gratings has recently emerged as an attractive and cost-effective alternative to the previously discussed methods. For example, Kun Chen et al. fabricated an array of silicon oxide nanopillars as two-dimensional raised periodic gratings (2DPRGs) on Si surfaces functionalised with thiolated oligonucleotides to detect human genomic DNA (hgDNA584) from a biological sample [175]. Hybridization with hgDNA584 leads to a drastic change in the scale of the pillars, resulting in a colour change from pure blue to red within 5 minutes. The diffraction peak shift occurs in the concentration range of hgDNA584 between 0.2 to 2.4 ng/μl. Exploiting diffraction to transduce biodetection events is an attractive and powerful way to design innovative, compact and miniaturised biosensing systems. Because gratings are internally referenced, they have the benefit of attenuating signal drift caused by changes in temperature, the material's refractive index, the light source's emission wavelength, and mechanical disturbances. Compared to the other types of label-free optical transducers discussed, gratings offer significant potential as wearable biosensors for continuous monitoring of biomolecule concentrations.

1.3.2 Holography

Holography is a technique that allows recording three-dimensional images of an object or digital information through the use of a photosensitive material and laser light. The term hologram is originally derived from Greek, where *holos* means "whole" and *gramma* means "to write". The theoretical foundations needed to understand and develop holography date back to the 19th century. In fact, it was the scientist D. Gabor who elaborated the basic principle of holography and his contribution was recognised by the 1971 Nobel Prize in Physics [176].

However, obtaining holograms on an experimental level had to wait for the development of laser technology that allowed the use of coherent monochromatic light sources. In 1962, in the USA, E. Leith and J. Upatnieks recorded the first holograms [177]. Meanwhile, in Russia, another scientist, Y. Denisyuk experimented with an optical configuration different from Gabor's and successfully created a hologram that could be reconstructed using a white light source [178]. Thereafter, holography began to develop rapidly. A hologram is a recording of the interaction of two coherent light beams in the form of an interference fringe pattern. The recording layer is a photosensitive material capable of capturing and storing information from light. In a typical holography optical set-up (Fig. 19. (a)), a coherent light source (laser beam) is split into two beams. The first beam illuminates the object (object wave) and the scattered light hits the recording layer. A second beam (reference wave) irradiates the recording layer directly. The object and reference waves interfere with each other, producing constructive (antinodes) and destructive (nodes) interferences (Fig. 19. (b)) on the recording layer, producing a characteristic interference pattern [179].
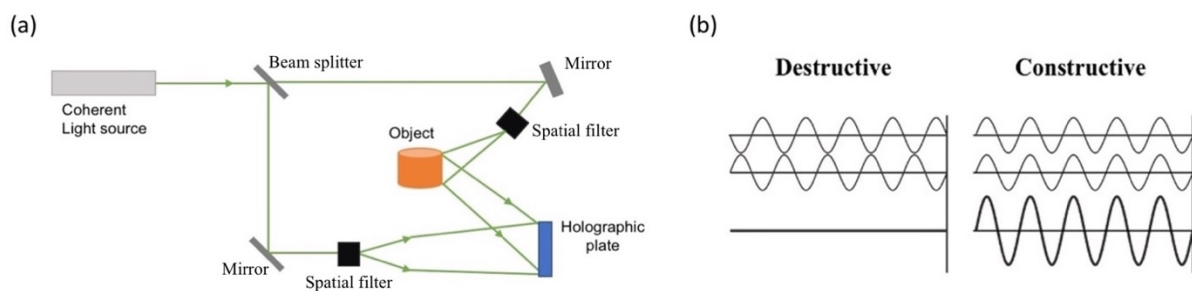
Fig. 19. (a) Hologram recording set-up showing the interference between object wave and reference wave; (b) the interference produced can be constructive or destructive.

The recording interference pattern generated by the superposition of the object beam and the reference beam yields a **hologram**. As a result, the complete phase and amplitude information of the light scattered by an object and its intensity distribution are recorded.

The optical characteristics of the recording medium are altered during holographic recording. After hologram developing, the image recorded can be reconstructed when the interference pattern is illuminated by the reference wave. The wavelength of the laser light used and the angle between the two recording beams are what determine the narrowband spectral peak formed by the diffracted light from the **periodic gratings**.

The holographic diffraction is governed by the **Bragg's law**:

$$\lambda_{peak} = 2\, n_o\, \Lambda\, sin\theta_{Bragg} \tag{3}$$

Where, λ_{peak} is the wavelength of the first order diffracted light at the maximum intensity *in vacuo*, n_o is the effective index of refraction of the recording medium, Λ is the line spacing of the formed fringes in the photosensitive material and θ_{Bragg} is the Bragg angle determined by the recording geometry.

Although holography has origins in the chemistry utilized in photography, there are significant differences between the two processes' applications and potential future applications. In fact, photography images are the recording of a wavefront reflected from an object, while holographic images depend on the recording of the interference pattern of the beam reflected from the object and a reference beam. **Silver halides** were the first materials used in the development of holograms [180]. An emulsion of gelatin and silver halide crystals, also referred to as a photographic emulsion, serves as the foundation for a silver halide recording photographic material. There are three types of silver halides: silver chloride ($AgCl$), silver bromide ($AgBr$) and silver iodide (AgI), which are all sensitive to light. Practically, a solution of silver nitrate is mixed with another solution containing gelatin and an alkali halide (e.g., potassium bromide). In this way, solid crystals are formed from the solution by precipitation. The final emulsion can have different particle sizes depending on the mixing method and gelatin concentration. However, the production of silver halide emulsions is a laborious, complicated and multi-step process, which is not recommended for use in typical holographic applications [181].

Over the last two decades, many kinds of materials, such as dichromate gelatin emulsions, photopolymers, thermal recording materials and many hybrid materials have been used for this purpose [182]. Photopolymers are currently the most widely used materials as they have excellent holographic properties, such as large refractive index modulation, real-time recording, low cost, etc. These materials respond differently depending on factors such as the intensity of the incident beam, monomer concentration, polymerisation speed, humidity, temperature, sample thickness, etc. In addition, the spectral sensitivity of these materials can be easily modified if the photopolymers are mixed with dyes.

Holography has various applications ranging from scientific to industrial fields, such as chemical [183], biological [184] and physical sensors [185], data storage [186] and optical security devices [187] (Fig.20.). Moreover, holography allows fabrication of different **diffractive gratings**, i.e., fringes patterns, which can be used as label-free optical transducers. They are therefore suitable for development of disposable sensors that are lightweight for miniaturization and multiplexing purposes.
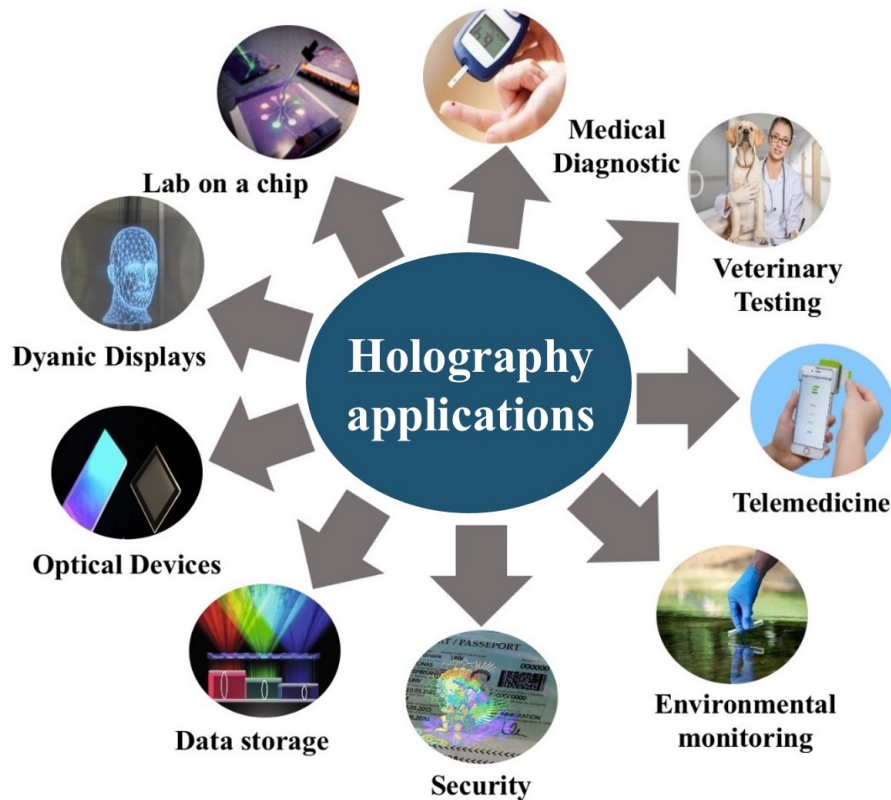
Fig. 20. Applications of holography in various fields.

1.3.3 Holographic sensing

As explained before, holography is a technique that enables a wavefront to be recorded and later re-constructed [188]. The simplest hologram is a diffraction grating of specific periodicity fabricated by the interference of two laser beams. **Holographic diffractive gratings** are obtained by optical interference on the surface or the entire volume of the recording layer or micro/nano patterning techniques. When illuminated with a laser or a white light, they produce a signal that is dependent on many factors such as the wavelength of the probe beam, the periodicity of the grating, the modulation of the refractive index and the layer thickness.

If we create such holographic pattern in a polymeric responsive film, we will have a **holographic sensor**, where the holographic gratings can transduce the analyte presence into a diffraction signal change due to analyte-induced polymer structural modification (i.e., size or refractive index (RI) change). Thus, a holographic sensor is a device comprising a diffractive grating embedded in a responsive material that diffracts light for application in the detection and quantification of analytes and/or physical parameters. Any physical or chemical stimulant that change the fringe spacing (Λ) or the refractive index (n) of the film cause observable changes in the wavelength (λ peak) or its profile (colour distribution), or the intensity (brightness) of the hologram. The diffraction grating act as optical transducer, whose properties are determined by the changes in the polymer matrix. One is the change in the diffraction efficiency due to a change in the refractive index modulation of the hologram, as a result of the chemical interaction with the analyte (Fig. 21. (b)). Alternatively, the analyte may cause a change in the fringe spacing due to a volume change in the hydrogels after analyte recognition (Fig. 21. (a)). Furthermore, the inclusion of functional groups in the polymer is a way to improve the chemical and physical interactions with the analytes, thus conferring greater sensitivity and selectivity. The sensitive material, used during the recording, is capable of changing its optical characteristics when it is exposed to a target analyte [189] [190]. Analyte-sensitive materials incorporating optical structures have emerged as sensing platforms for point-of-care diagnostics [39]. In addition, due to the holographic sensing mechanism, utilizing reversible binding of analytes allows continuous monitoring. As a transducer, a diffractive grating is recorded in the sensing layer, which consists of a periodic structure with alternating strips, which diffracts light.

In general, the interaction between a light source and a diffractive grating, with a constant spatial period, will produce a diffraction pattern consisting of various diffraction orders. The grating **diffraction efficiency** ($\eta(\%)$) is defined as +1 diffracted order intensity and incident beam intensity ratio expressed as percentage, as it is represented in equation (4).

$$\eta(\%) = \frac{I1}{Ii} \cdot 100 \tag{4}$$

Where I_1 is the first (+1) diffracted order intensity and I_i the incident beam intensity. It is a quantitative measure of the brightness of the hologram.
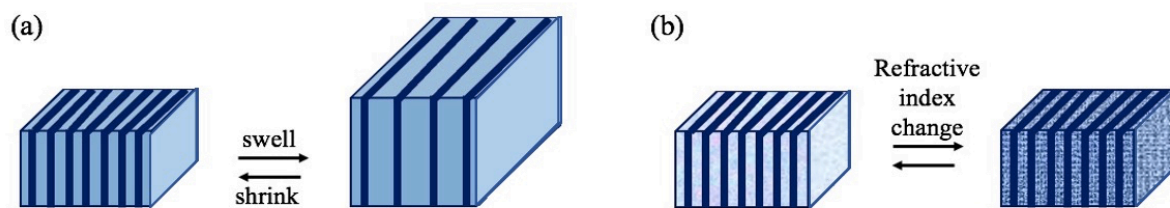
Fig. 21. The working principle of a holographic biosensor is based on a change in the holographic gratings properties due to (a) dimensional change or (b) change in the optical properties of the layer.

After the holographic recording, the polymer matrix, which is permeable to the target analyte, produces a change in the diffractive pattern under analyte recognition. The sensitivity of the holographic grating will depend largely on the extent to which the refractive index of the material changes, and on the ability of the material to undergo dimensional changes by shrinking/swelling.

The applications of holographic sensors have been clearly demonstrated in the literature for a variety of analytes that can be identified using diffraction gratings as transducers, including ions, glucose, temperature and illicit drugs (Fig. 22.). However holographic sensors, and biosensors in particular, are still at an early stage of development. Most common applications focus on physical and chemical sensing (humidity, pH, gases and solvents) [191].

A holographic protease sensor was first proposed by Lowe's group [192]. Since then, several applications of holographic hydrogel-based sensors have been reported in the literature. Most have used holographic systems as sensors for pH [193], humidity and temperature [194] and certain cations [195], but very few employ them for biosensing. Published results in the field of biosensing are scarce and so far, the main focus has been on glucose detection, thus indicating that holographic biosensing is a new research area with a promising potential.
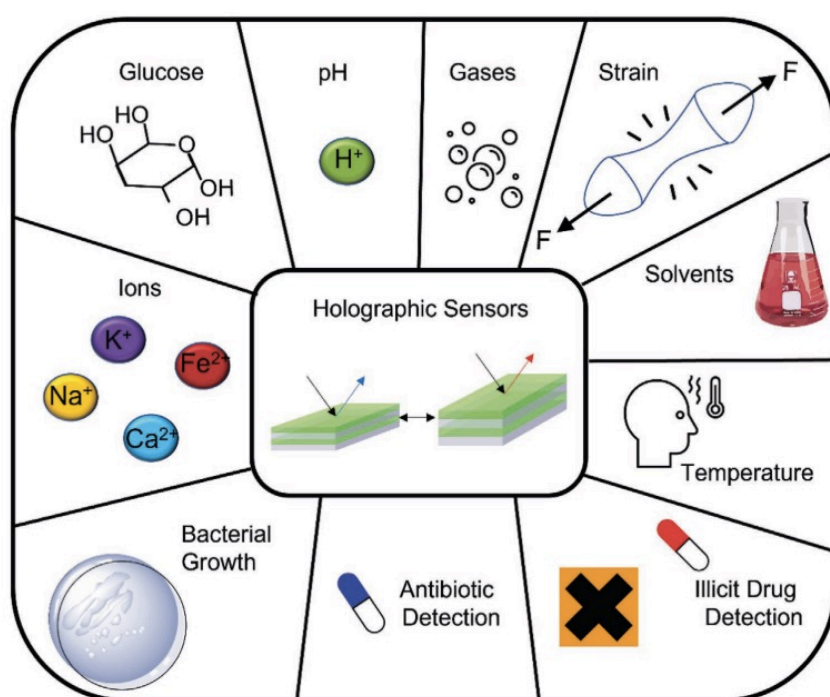
Fig. 22. Various analytes detected by holographic sensors. Reproduced with permission from Ref. [191].

For example, holographic pH sensors consist of pendant carboxyl groups that are introduced to the polymer matrix. Thus, a pH sensor was fabricated in the form of 1D slanted optical crystal flakes [196]. The pH response of the sensor is based on ionization of the carboxylic acid groups in the hydrogel matrix as the pH increases. As they ionize, the Donnan osmotic pressure increases, resulting in water uptake into the hydrogel matrix, increasing fringes lattice spacing, shifting the Bragg peak into longer wavelengths. The volumetric change caused by change in pH was found to be reversible, giving the sensor the potential for reusability.

Also, the formation of composite materials allows for greater functionalisation of sensors with alternative functionalities [197]. As an example, Naydenova *et al.* have demonstrated the use of the hydrophilic and hydrophobic properties of zeolite nanocrystals in the inkjet printing of alcohol sensitive holographic gratings [198]. For sensing metal ions, on the other hand, holographic sensors have been functionalized with crown ethers. To incorporate crown ethers in polymer matrixes, methacrylated derivatives were synthesized [199]. These derivatives consisted of methacrylated 12/15/18-crown-4/5/6, which were copolymerized with hydroxyethyl methacrylate (HEMA) to form a pHEMA matrix with pendant crown ethers. After the diffraction gratings were formed by silver halide chemistry, the holograms were tested with a range of metal ions. The hologram was found to be sensitive to K^+ ions. Indeed, the Bragg peak of the hologram shifted around 200 nm in the presence of 30 mM K^+ ions. Recently, holographic sensors were functionalized with 8-hydroxyquinoline for divalent metal ion sensing [200]. The sensor was used to quantitatively measure Pb^{2+} and Cu^{2+} ions (0.1–10.0 mM) with limits of detection of 11.4 and 18.6 µM, respectively. In any case, main efforts in this field have been focused on holographic sensors to detect glucose. Thus, Wang pioneered the first demonstration of a glucose sensor through a diffraction grating of a hydrogel [201] and few other examples can be found [39] [202] [203]. The hydrogel is functionalised with 3-(acrylamido)-phenylboronic acid (PBA) which can forms reversible covalent bonds with *cis*-diol moieties of glucose, lactate, fructose and other carbohydrates [204]. Boronic acid (pKa = ~8.8) at low pH values is in an uncharged and trigonal planar configuration, while at higher pH values (pH > pKa) the trigonal form can react with OH^- to form the more stable negatively charged tetrahedral state, which can bind to cis-diol groups more readily. Following the production of charged groups, the osmotic Donnan pressure of the polymer increases, causing the hydrogel to absorb more water. As a result, the hydrogel swells, and its Bragg peak shifts to longer wavelengths. While this mechanism showed promising results, several aspects of holographic glucose sensors need improvement. A limitation of the developed holographic glucose sensors is the low selectivity because the polymer matrix also responds to other carbohydrates such as fructose and lactate. Another aspect that requires to be improved is the assay time, which takes from 30 min to 1 hour for the sensor to saturate.

To our knowledge, there are no holographic biosensors for the detection of oligonucleotide probes. The novelty of this thesis work is the use of acrylamide-based hydrogels to optically detect target DNA. Detection is realised by monitoring the variation of **diffraction efficiency** ($\eta(\%)$) or the **grating period** (Λ) using two different types of holographic gratings as transducers.

1.3.4 Types of diffractive gratings

Depending on the recording geometry and the optical properties of the material that are changed during holographic recording, different diffractive gratings can be produced: **transmission** or **reflection gratings**, and **phase** or **amplitude gratings** (Table 5) [205]. Additionally, depending on whether the diffraction grating is recorded in the volume or on the surface of the recording layer, they can be divided in **surface relief gratings** (SRGs) or **volume holographic gratings** (VHGs) [160].

Table 5. Classification of holograms.
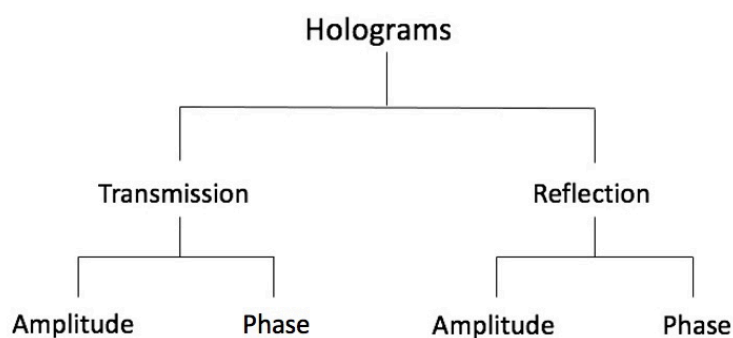
One of the main factors used to distinguish holograms is the geometry used for recording, which is the main difference between reflection and transmission holograms [206].

In **transmission** mode, the two recording beams are incident from the same side on the recording material and the interference fringes created are perpendicular to the surface of the recording material (Fig. 23. (1)).

In a **reflection** recording mode, the two coherent beams are incident from the opposite sides on the recording material (Fig. 23. (2)). Therefore, the recorded lines are parallel to the surface of the material. The interference fringes generated are equidistant and the line spacing depends on the angle between the two incident beams.
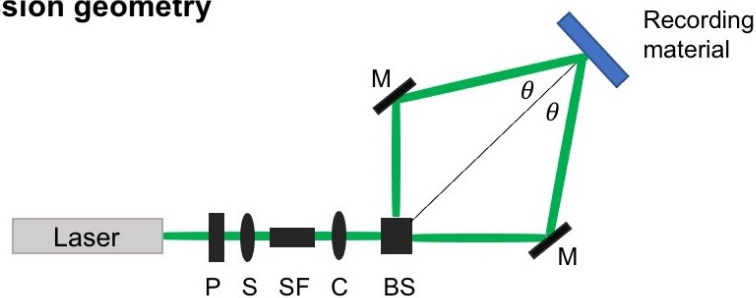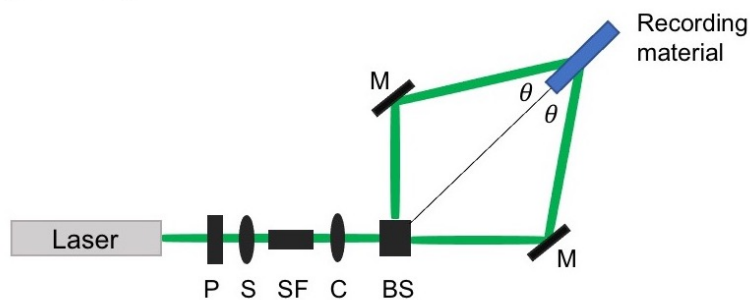
Fig. 23. Experimental set-up for recording: 1) Transmission gratings, 2) Reflection gratings. P polarizer, S shutter, SF spatial filter, C collimator, BS beam splitter, M mirror.

A simplified geometry for recording reflection holograms is the 'Denisyuk' configuration (Fig. 24). The Denisyuk technique makes it possible to record single colour reflection holograms using a single beam configuration. The laser beam is transmitted through the recording material and reflected by a mirror positioned behind the object.

2) Denisyuk geometry
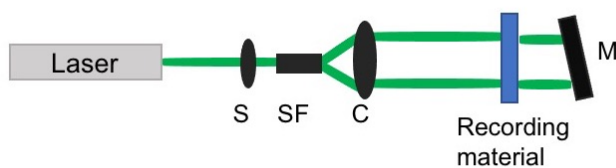
Fig. 24. Denisyuk configuration for reflection holograms.

The main consequence of these recording geometries is that when a transmission grating is reconstructed, it produces a **diffracted transmitted wave** (Fig. 25. (a)). Conversely, when a reflection grating is reconstructed, it produces a **diffracted reflected wave** (Fig. 25. (b)).
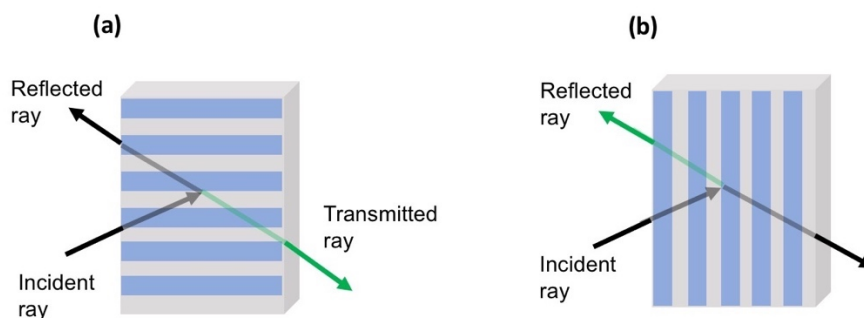
Fig. 25. Diffraction gratings recorded in (a) Transmission mode and (b) Reflection mode and how the grating orientation affects the interaction with light.

When a transmission diffraction grating is illuminated with a white light source, the rainbow effect is produced, that is, the white light is scattered into its component colors (Fig. 26.(B)). While, in the case of reflection gratings, a single color is observed after white light illumination (Fig. 26.(D)). Accordingly, reflection holograms do not require an additional readout method to interpret the response, whereas holograms based on the transmission mode require a spectrometer or optical power meter for reading. For example, "Denisyuk" reflection holograms can be used as colorimetric indicators as they can diffract light when they are illuminated with a white light source. In either case, the maximum diffraction efficiency occurs at a wavelength that satisfies Eq. (3).
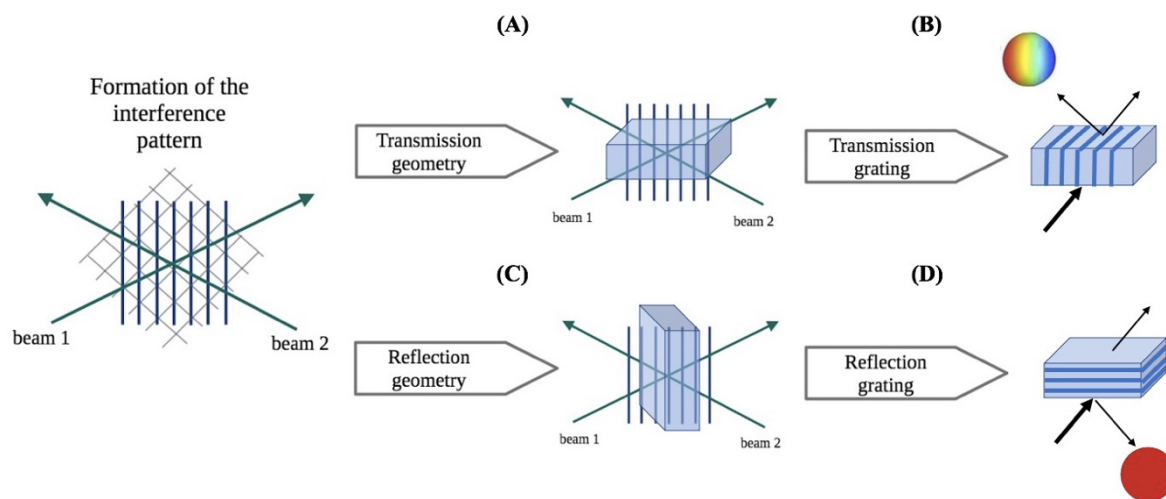
Fig. 26. Holograms recorded in the volume of the layer: recording (A) and reconstruction (B) of transmission holograms; recording (C) and reconstruction (D) of reflection holograms.

A hologram is classified as a phase hologram or amplitude hologram, depending on the parameter modulated during recording [207]. In **phase holograms**, the holographic recording results in a spatial modulation of the **refractive index** (RI) of the material. In **amplitude holograms**, on the other hand, holographic recording results in a spatial modulation of the material's **absorption coefficient**. Both amplitude and phase holograms can be recorded using either transmission or reflection geometries (Table 2).

Although, amplitude holograms have a limited diffraction efficiency (<8%), which is why most holographic sensor platforms employed in research are built on phase holograms [205]. As mentioned at the start, another categorisation of holograms depends on whether the diffraction grating is recorded in the volume or on the surface of the analyte-sensitive layer. Holograms can operate in different regimes depending on the thickness: **thin** and **thick holograms**. The Q-factor of a hologram is one method of determining what regime one is working in:

$$Q = \frac{2\pi\lambda d}{n_0\Lambda^2}$$
(5)

where λ is the recording wavelength, d is the thickness, n_o is the refractive index and Λ is the fringe spacing. If the distance between the fringes created during the interference of the laser beams is larger than the thickness of the recording material, a thin hologram is generated. In the opposite situation, a thick hologram is produced [207]. In general Q values greater than 10 are considered to be in the thick regime while values less than 1 are considered thin. Considering in which of the two regimes the sensor will operate is important because it determines the dynamic range of the sensor and its sensitivity [208]. Thin holograms have a maximum diffraction efficiency of 33% for sinusoidal modulation of the refractive index and produce multiple diffracted waves at almost any angle of incidence of the probe beam. Thick holograms are usually referred to as 'volume' holograms in the literature, and this is related to their operating regime and not just the fact that they are recorded in the layer volume. These holograms can theoretically reach 100% diffraction efficiency and produce a single diffracted wave only at the Bragg angle of incidence. Two theories used to describe the behaviour of thin and thick gratings, which are widely accepted in the optics community, are **Raman-Nath's theory** [209] and **Kogelnik's coupled-wave theory** [210], respectively. Thin phase gratings, where Λ is large relative to d, exhibit Raman–Nath behavior and produce several diffracted waves.

The diffraction efficiency (η) for **thin phase gratings** is given by:

$$\eta = J_m^2 \left(\frac{\varphi}{2}\right) = \frac{Id}{Io} \tag{6}$$

where φ is the grating phase and *m* is the diffraction order. J_m is the Bessel function of the order m. The incident beam is diffracted into several orders, with the diffracted amplitude in the m_{th} order proportial to the value of the Bessel function. φ is defined as:

$$\varphi = \frac{2\pi \, \Delta n \, d}{\lambda r \, cos \, \theta B} \tag{7}$$

where θ_B is the Bragg angle and λ_r is the reconstruction wavelenght.

Thick phase gratings exhibit Bragg behavior and produce only one diffracted beam. A maximum η is obtained when the reconstruction beam is incident on the grating at a particular angle of incidence θ_B following the Bragg equation. For thick holographic transmission gratings, η is defined by Kogelnik's coupled wave theory as:

$$\eta = sin^2 \left(\frac{\varphi}{2}\right) = sin^2 \left(\frac{\pi \, \Delta n \, d}{\lambda r \, cos \, \theta B}\right) \tag{8}$$

1.3.4.1 Surface relief grating (SRGs)

Surface relief gratings can be fabricated using various approaches such as laser ablation and photolithography [211] [212]. They can be formed upon exposure of a photoresist to a patterned light (holographically or with a mask) [213], or by direct inscription in self-processing photopolymers [214]. Thus, another method of surface hologram fabrication consists of holographic patterning of a material using a high power laser which ablates locally material from the surface [199] [215]. This technique is a flexible one-step patterning method that can be applied to a range of materials and it is more suitable for large scale production. In this project, this last approach was used, called **Direct Laser Interference Patterning** (DLIP). The DLIP patterning method exploits the interference generated by the coherent superposition of two or more laser beams, thus producing a periodic modulation of the laser intensity.

The shape of the interference pattern is transferred directly to the material surfaces. In this way, different materials can be ablated locally at the positions of the interference maxima, allowing the desired surface microstructure to be created [216]. The structuring process was performed with a two-beam laser configuration (Fig. 27.(a)); therefore, the laser beam was split into two beams of equal intensity by a beam splitter and a periodic line pattern was produced (Fig. 27.(b));. The period and amplitude of the surface relief grating are controlled by the holographic recording conditions used.

The **grating period** (Λ) is controlled by the angle between the laser beams, θ_{Bragg}, and the laser wavelength, λ, of the laser light according to the following equation:

$$\Lambda = \frac{\lambda}{2\sin\theta_{Bragg}} \tag{9}$$

In addition, when the surface periodic structures are illuminated with white light, an angle-dependent colour spectrum can be observed (Fig. 27.(c)).
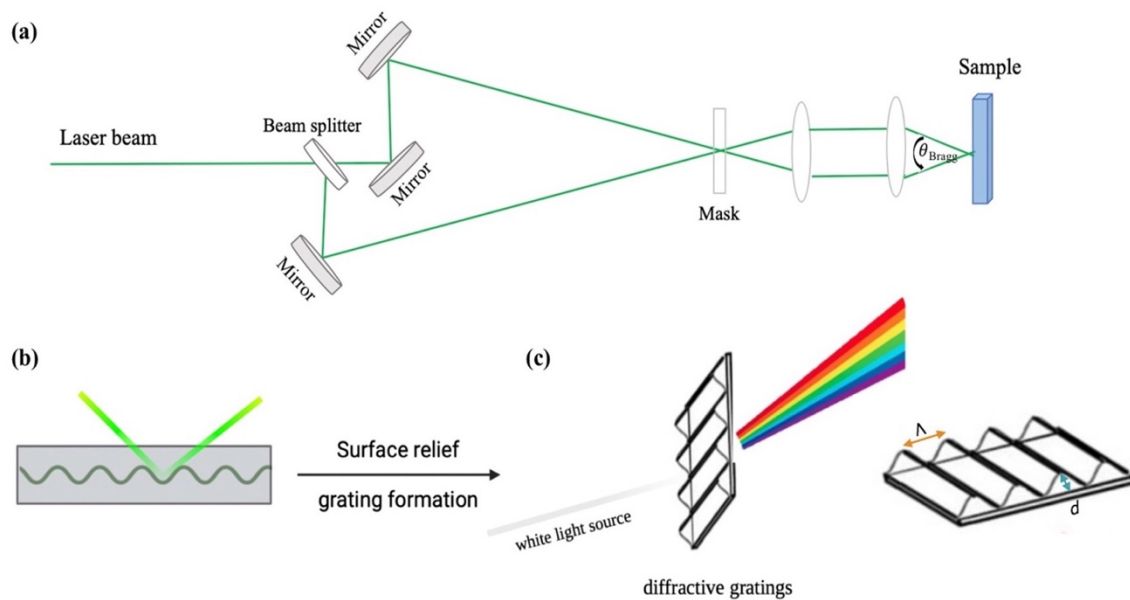
Fig. 27. (a) Schematic representation of the DLIP two-beam interference configuration set-up; (b) surface relief grating (SRG) recording by laser ablation on the layer surface, the two recording beams interfere from the same side; (c) rainbow reflection of SRG when shined with white light, and its structural parameters such as surface relief amplitude (d) to the grating period (Λ).

SRG structures are defined by the aspect ratio, which is the ratio of the surface relief amplitude (d) to the grating period (Λ) (Fig. 27.(c)). After the fabrication of an SRG master, the diffractive grating can be transferred to the surface of a material by means of **replica moulding** (REM), a soft lithography technique [217] [161]. **Soft lithography** is a well-known method for preparing various patterned microstructures [218]. Combining surface relief gratings (SRGs) with soft lithography can be an effective way to prepare numerous SRGs, which can be used as optical transducers for sensing application [219]. The surface patterning technique has certain advantages, such as the ability to create large-scale micro-patterns and the ease and inexpensiveness of fabrication. In this thesis, the DLIP was performed at the Fraunhofer Institute for Material and Beam Technology (IWS) in Dresden, on polyethylene terephthalate (PET) substrates which were used as masters [220].

To date, biosensing with hydrogel-based surface relief gratings has been reported by Wang et al. for the detection of glucose using a hydrogel bearing phenylboronic acid groups [201]. The approach used by this group, combine the fabrication of SRG on azo polymer films with soft-lithographic methods to prepare hydrogel diffractive gratings. The reaction of phenylboronic groups with glucose causes an increase in the borate anion fraction and consequently swelling of the hydrogel occurs. After being exposed to the solution of glucose for 10 min, the trough depth of the grating increased, resulting in an increase in diffraction efficiency. This approach showed a proper sensitivity to glucose with a limit of detection (LOD) of 0.023 mmol/L and, additionally, glucose detection with this system can be repeated several times. A few years later, the same group developed a thrombin-reactive hydrogel [221]. The hydrogel was functionalised with the aptamer and its complementary sequence used as physical crosslinking points, in addition to the typical covalent crosslinking points. When the hydrogel was exposed to human thrombin solution, the aptamer tends to bind to the human thrombin and the physical crosslinks are broken, causing the hydrogel to swell due to the decrease in crosslinking density. Consequently, the diffraction efficiency increased in accordance with the thrombin concentration. Recently, Zhao et al. developed a smart diffraction grating immunosensor based on antigen-reactive hydrogels with analyte-induced volume changes for highly selective and sensitive detection of human immunoglobulin G (H-IgG) with a LOD of 1.3×10^{-8} M [222].

The hydrogel grating contains poly(N-isopropylacrylamide) (PNIPAM) backbones that is dynamically cross-linked via reversible complexation between the pendent goat-anti-human IgG (GAH-IgG) and pendent H-IgG. The pendent GAH-IgG units in GAH-IgG/H-IgG complexes can specifically recognize free H-IgG in the sample solution because the binding constant of GAH-IgG to free H-IgG is much larger than that of GAH-IgG to the pendent and denatured H-IgG and result in decomplexation of GAH-IgG/H-IgG complex as well as the swelling of hydrogel grating. Additionally, the PNIPAM backbones with thermo-responsive volume changes enable enhancement of the H-IgG-induced swelling via temperature regulation. Furthermore, a hydrogel based SRG with incorporated phosphocholine groups, capable of specifically recognising C-reactive protein (CRP) was newly developed in our group [223]. This work demonstrated that the biosensing system allows the selective label-free detection of CRP in human serum with a LOD of 1.07 mg L^{-1}. Amplification techniques were also used to increase sensitivity, broaden the linear range, and produce a better LOD of 0.30 mg L^{-1}. For the detection of nucleic acids, examples reported in the literature are mainly based on the use of complementary strands as crosslinking junctions, which break when the target is added as it recognises one of these strands with a higher specific complementarity. The sensing mechanism is based on a competitive substitution. For hydrogels with dissociative crosslinks, a sol-gel transition is observed, whereas in the case of non-dissociative (covalent) crosslinks, swelling or shrinkage of the hydrogel is observed. Based on this strategy, a portable POCT platform for miRNA detection was recently developed by introducing a DNA-AuNP hybrid hydrogel film that can specifically recognise the target miRNA and initiate dissociation of the hybrid hydrogel film resulting in the release of AuNPs for colorimetric detection [224]. Another example is based on DNA-acrylamide hydrogel microcapsules in which a competitive displacement of the sequence of the target miR-141 with the bridging DNA in the microcapsule shell leads to the unblocking of the hydrogel microcapsules and the release of the incapsulated quantum dots [225]. However, the signal transduction mechanism for these two miRNA biosensors is based on colorimetric and fluorescent detection respectively. Accordingly, direct detection of oligonucleotides by holographic sensing is still lacking in literature. This means that no biosensors based on this technology capable of detecting DNA or RNA targets have yet been developed.

1.3.4.2 Volume holographic gratings (VHGs)

The fabrication method of volume holographic gratings (VHGs) consists of combining the recording layer with a light-absorbing material and exposing it to high-intensity lasers. Optical recording in light-sensitive materials is based on the process of **photoinduced polymerization** [226]. Normally, a mixture of monomers, crosslinker, photoinitiator and a photosensitive dye are required for the registration of volume holographic gratings in photopolymers. The role of the dye photosensitiser is to absorb the light and transfer the absorbed energy to directly convert the monomers in free radicals so that polymerization can begin. Indeed, when light is absorbed, the monomers undergo free radical photopolymerisation. Hence, the components of the recording material are spatially redistributed when illuminated by an optical interference pattern, resulting in a holographic volume grating. Hologram formation involves a spatial variation of the polymer layer density due to concentration-driven diffusion of monomer molecule from dark to illuminated areas [227]. As explained above, in volume phase holograms, the spatial variation of the intensity of the interference pattern is recorded as a change in the **refractive index**. Due to the internal diffusion of unpolymerized monomers in a holographic film, areas of high and low refractive index are formed during irradiation with an interference pattern (Fig. 28) [205].
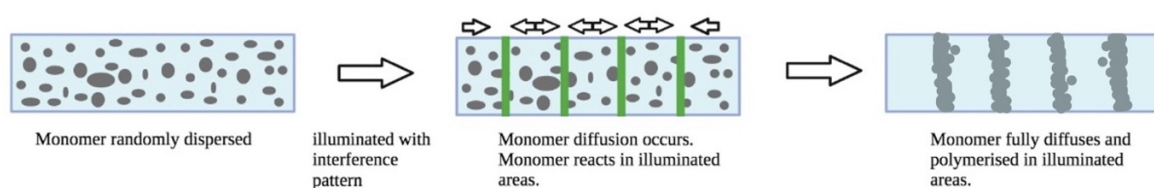
Fig. 28. Representation of holographic recording process within the volume of the layer.

The overall refractive index is higher in the polymerised region than in the unpolymerized region due to the higher density. The diffraction efficiency of the recorded hologram depends on many factors: the recording parameters used (exposure time, laser intensity), the recording layer composition and thickness, and from all of them will depend the refractive index modulation achieved. A typical optical set-up, represented in Fig. 29, consist of a Neodymium-doped yttrium orthovanadate (Nd:YVO$_4$) laser (532 nm) for recording and a helium-neon (He-Ne) laser (633 nm) for reading [228].
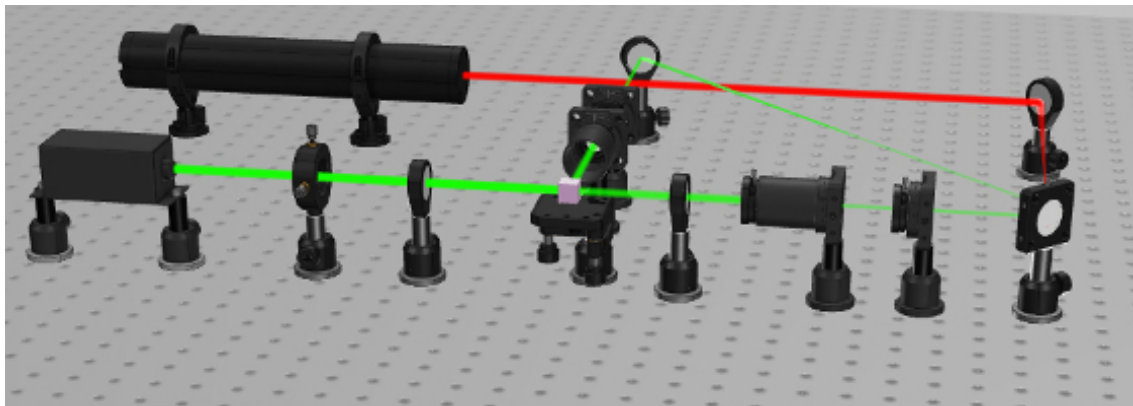
Fig. 29. Typical optical set-up employed for the study of volume holograms: red laser for reading, green laser for recording.

In addition, transmission holographic gratings can be recorded in *unslanted* or *slanted* mode [229]. They are *unslanted* gratings when the two recording beams have the angles of incidence equal and opposite, this means that there is no inclination of the recorded fringes respect to the layer surface. On the other hand, in *slanted* grating the two recording beams incident with unequal angles to the surface layer, thus leading to an inclination of the recorded fringes [194]. Of the two, the slanted configuration is more sensitive, but more difficult to record, especially in materials that undergo severe shrinkage during recording such as photopolymers or hydrogels. In order to fabricate holograms in hydrogel layers, the thin films are first polymerised and then immersed in an incubation solution, after they are exposed to interference beams that generate a second polymerisation process in the exposed areas.

Photopolymers, on the other hand, are directly synthesised with all the necessary components for holographic recording. Normally, the incubation solutions contain an aqueous mixture of monomers and crosslinker, a polymerization initiator and a sensitive dye. The reaction between the dye and the initiator, after light absorption, produces free radicals that react with the monomers to initiate polymerisation. The correct choice and concentration of the dye are important to ensure optimum sensitivity to the wavelength of the recording beam and to obtain efficient polymerization. The principle of detection of VTGs is based on the alteration of the diffraction efficiency when interaction with the target DNA occurs. Alternatively, a change in the period of the recorded grating can occur due to shrinkage or swelling of the material leading to a change in the angular position of the Bragg peak.

Bianco et al. demonstrated metal detection in bathing waters using a VHG recorded in a photopolymer based on a functionalised sol-gel matrix [230]. The ability of VHG to detect heavy metals in water was demonstrated by measuring a first-order diffraction angular shift of the grating of approximately 3° when exposed to a solution of water and lead. In addition, VHG were fabricated by embedding holographic fringes of silver within thin-polymer films and used as transduction systems to monitor pH changes associated with specific enzymatic reactions to build prototype biosensors sensitive to urea and penicillin [231]. Urease or penicillinase were immobilized onto the gratings, generating reflection holograms whose replay color was dependent on the concentration of substrate in the test media. However, the response was very dependent on the ionic strength and buffering capacity of the medium, which hinders its application to real samples. Recently, Naydenova et al. reported a temperature-sensitive VHG hologram, based on Denisyuk reflection gratings, recorded in poly(N-isopropylacrylamide) photopolymer [232]. The temperature dependence of the characteristics of poly-NIPA-based gratings was strongly related to water desorption/absorption by the photopolymer layer. The temperature effect on the VHG was observed as color change from green to blue. An interesting approach, demonstrated by Yestisen et el., is based on self-processing holographic photopolymers and consisted of a holographic reflection Bragg mirror made of poly-HEMA and containing porphyrin units [199]. Its reversible colour response to changing concentrations of organic solvents and metal cations has been demonstrated.

A more specific system was proposed by the same group, which used a polyacrylamide-carboxylic acid matrix and slanted Bragg gratings recorded with silver nanocrystals [200]. The volume hologram specifically detected Pb^{2+} and Cu^{2+} due to the presence of 8-hydroxyquinoline units.

In conclusion, the detection of DNA oligonucleotide probes using holographic volumetric structures has not yet been reported in the literature. Therefore, studying the performance and potential of holographic hydrogels for nucleic acid detection is still an unexplored topic. This PhD thesis aims to open up new analytical solutions to reduce the complexity and cost of detection, exploring innovative principles of optical transduction and offering interesting avenues for the future of biosensors.

1.4 REFERENCES

[1] C. Karunakaran, R. Rajkumar, K. Bhargava, Introduction to Biosensors, Elsevier Inc., 2015. https://doi.org/10.1016/B978-0-12-803100-1.00001-3.

[2] and C.L. Leland C. Clark, Jr., Electrode systems for continuous monitoring in cardiovascular surgery, (1962).

[3] M.I. Svechtarova, I. Buzzacchera, B.J. Toebes, J. Lauko, N. Anton, C.J. Wilson, Sensor Devices Inspired by the Five Senses: A Review, Electroanalysis. 28 (2016) 1201–1241. https://doi.org/10.1002/elan.201600047.

[4] V. Naresh, N. Lee, A review on biosensors and recent development of nanostructured materials-enabled biosensors, Sensors (Switzerland). 21 (2021) 1–35. https://doi.org/10.3390/s21041109.

[5] S.M. George, S. Tandon, B. Kandasubramanian, Advancements in Hydrogel-Functionalized Immunosensing Platforms, ACS Omega. 5 (2020) 2060–2068. https://doi.org/10.1021/acsomega.9b03816.

[6] H. Filik, A.A. Avan, Electrochemical immunosensors for the detection of cytokine tumor necrosis factor alpha: A review, Talanta. 211 (2020) 120758. https://doi.org/10.1016/j.talanta.2020.120758.

[7] G.S. Kassahun, S. Griveau, S. Juillard, J. Champavert, A. Ringuedé, B. Bresson, Y. Tran, F. Bedioui, C. Slim, Hydrogel Matrix-Grafted Impedimetric Aptasensors for the Detection of Diclofenac, Langmuir. 36 (2020) 827–836. https://doi.org/10.1021/acs.langmuir.9b02031.

[8] M. Asal, Ö. Özen, M. Şahinler, H.T. Baysal, İ. Polatoğlu, An overview of biomolecules, immobilization methods and support materials of biosensors, Sens. Rev. 39 (2019) 377–386. https://doi.org/10.1108/SR-04-2018-0084.

[9] K.M. Koo, N. Soda, M.J.A. Shiddiky, Magnetic nanomaterial–based electrochemical biosensors for the detection of diverse circulating cancer biomarkers, Curr. Opin. Electrochem. 25 (2021) 100645. https://doi.org/10.1016/j.coelec.2020.100645.

[10] R.G. Mahmudunnabi, F.Z. Farhana, N. Kashaninejad, S.H. Firoz, Y.B. Shim, M.J.A. Shiddiky, Nanozyme-based electrochemical biosensors for disease biomarker detection, Analyst. 145 (2020) 4398–4420. https://doi.org/10.1039/d0an00558d.

[11]   E. Mauriz, L.M. Lechuga, Plasmonic biosensors for single-molecule biomedical analysis, Biosensors. 11 (2021). https://doi.org/10.3390/bios11040123.

[12]   T. Mirea, J. Olivares, M. Clement, E. Iborra, Impact of FBAR design on its sensitivity as in-liquid gravimetric sensor, Sensors Actuators, A Phys. 289 (2019) 87–93. https://doi.org/10.1016/j.sna.2019.02.012.

[13]   G. Ji, Z. Chen, H. Li, D.E. Awuye, M. Guan, Y. Zhu, Electrospinning-Based Biosensors for Health Monitoring, Biosensors. 12 (2022). https://doi.org/10.3390/bios12100876.

[14]   A. Gupta, S.K. Bhardwaj, A.L. Sharma, K.H. Kim, A. Deep, Development of an advanced electrochemical biosensing platform for E. coli using hybrid metal-organic framework/polyaniline composite, Environ. Res. 171 (2019) 395–402. https://doi.org/10.1016/j.envres.2019.01.049.

[15]   Y. Chen, C. Qian, C. Liu, H. Shen, Z. Wang, J. Ping, J. Wu, H. Chen, Nucleic acid amplification free biosensors for pathogen detection, Biosens. Bioelectron. 153 (2020) 112049. https://doi.org/10.1016/j.bios.2020.112049.

[16]   J. Kaur, P.K. Singh, Enzyme-based optical biosensors for organophosphate class of pesticide detection, Phys. Chem. Chem. Phys. 22 (2020) 15105–15119. https://doi.org/10.1039/d0cp01647k.

[17]   Y. Fang, Label-free cell-based assays with optical biosensors in drug discovery, Assay Drug Dev. Technol. 4 (2006) 583–595. https://doi.org/10.1089/adt.2006.4.583.

[18]   P.M.S. Phumlani Tetyana, and Z. Njengele-Tetyana, Biosensors: Design, Development and Applications, n.d.

[19]   A.A. Hamzah, S. Nadzirah, Biosensor Development, Elsevier, 2023. https://doi.org/10.1016/b978-0-12-822548-6.00112-6.

[20]   P. Araujo, Key aspects of analytical method validation and linearity evaluation, J. Chromatogr. B Anal. Technol. Biomed. Life Sci. 877 (2009) 2224–2234. https://doi.org/10.1016/j.jchromb.2008.09.030.

[21]   E. Morales-Narváez, C. Dincer, The impact of biosensing in a pandemic outbreak: COVID-19, Biosens. Bioelectron. 163 (2020). https://doi.org/10.1016/j.bios.2020.112274.

[22]   A. Tricoli, N. Nasiri, S. De, Wearable and Miniaturized Sensor Technologies for Personalized and Preventive Medicine, Adv. Funct. Mater. 27 (2017). https://doi.org/10.1002/adfm.201605271.

[23] V. Velusamy, K. Arshak, O. Korostynska, K. Oliwa, C. Adley, An overview of foodborne pathogen detection: In the perspective of biosensors, Biotechnol. Adv. 28 (2010) 232–254. https://doi.org/10.1016/j.biotechadv.2009.12.004.

[24] P. Ramnani, N.M. Saucedo, A. Mulchandani, Carbon nanomaterial-based electrochemical biosensors for label-free sensing of environmental pollutants, Chemosphere. 143 (2016) 85–98. https://doi.org/10.1016/j.chemosphere.2015.04.063.

[25] J.A. Otoo, T.S. Schlappi, REASSURED Multiplex Diagnostics: A Critical Review and Forecast, Biosensors. 12 (2022). https://doi.org/10.3390/bios12020124.

[26] D.C. Christodouleas, B. Kaur, P. Chorti, From Point-of-Care Testing to eHealth Diagnostic Devices (eDiagnostics), ACS Cent. Sci. 4 (2018) 1600–1616. https://doi.org/10.1021/acscentsci.8b00625.

[27] C. Dincer, R. Bruch, A. Kling, P.S. Dittrich, G.A. Urban, Multiplexed Point-of-Care Testing – xPOCT, Trends Biotechnol. 35 (2017) 728–742. https://doi.org/10.1016/j.tibtech.2017.03.013.

[28] A. Poschenrieder, M. Thaler, R. Junker, P.B. Luppa, Recent advances in immunodiagnostics based on biosensor technologies—from central laboratory to the point of care, Anal. Bioanal. Chem. 411 (2019) 7607–7621. https://doi.org/10.1007/s00216-019-01915-x.

[29] A.P.F. Turner, Biosensors: Sense and sensibility, Chem. Soc. Rev. 42 (2013) 3184–3196. https://doi.org/10.1039/c3cs35528d.

[30] J.H. Nichols, Point-of-care testing, INC, 2020. https://doi.org/10.1016/B978-0-12-815499-1.00019-3.

[31] J. Shin, S. Chakravarty, W. Choi, K. Lee, D. Han, H. Hwang, J. Choi, H. Il Jung, Mobile diagnostics: Next-generation technologies for: In vitro diagnostics, Analyst. 143 (2018) 1515–1525. https://doi.org/10.1039/c7an01945a.

[32] K. Mahato, A. Srivastava, P. Chandra, Paper based diagnostics for personalized health care: Emerging technologies and commercial aspects, Biosens. Bioelectron. 96 (2017) 246–259. https://doi.org/10.1016/j.bios.2017.05.001.

[33] P. Singh, P. Nath, R.K. Arun, S. Mandal, N. Chanda, Novel synthesis of a mixed Cu/CuO-reduced graphene oxide nanocomposite with enhanced peroxidase-like catalytic activity for easy detection of glutathione in solution and using a paper strip, RSC Adv. 6 (2016) 92729–92738. https://doi.org/10.1039/c6ra20882g.

[34] P. Yager, G.J. Domingo, J. Gerdes, Point-of-care diagnostics for global health, Annu. Rev. Biomed. Eng. 10 (2008) 107–144. https://doi.org/10.1146/annurev.bioeng.10.061807.160524.

[35] N. Jiang, R. Ahmed, M. Damayantharan, B. Ünal, H. Butt, A.K. Yetisen, Lateral and Vertical Flow Assays for Point-of-Care Diagnostics, Adv. Healthc. Mater. 8 (2019) 1–19. https://doi.org/10.1002/adhm.201900244.

[36] M. Zarei, Portable biosensing devices for point-of-care diagnostics: Recent developments and applications, TrAC - Trends Anal. Chem. 91 (2017) 26–41. https://doi.org/10.1016/j.trac.2017.04.001.

[37] B.M. Cummins, F.S. Ligler, G.M. Walker, Point-of-care diagnostics for niche applications, Biotechnol. Adv. 34 (2016) 161–176. https://doi.org/10.1016/j.biotechadv.2016.01.005.

[38] D. Rodrigues, A.I. Barbosa, R. Rebelo, I.K. Kwon, R.L. Reis, V.M. Correlo, Skin-integrated wearable systems and implantable biosensors: A comprehensive review, Biosensors. 10 (2020). https://doi.org/10.3390/BIOS10070079.

[39] M. Elsherif, M.U. Hassan, A.K. Yetisen, H. Butt, Wearable Contact Lens Biosensors for Continuous Glucose Monitoring Using Smartphones, ACS Nano. 12 (2018) 5452–5462. https://doi.org/10.1021/acsnano.8b00829.

[40] J. Park, J. Kim, S.-Y. Kim, W.H. Cheong, J. Jang, Y.-G. Park, K. Na, Y.-T. Kim, J.H. Heo, C.Y. Lee, J.H. Lee, F. Bien, † Jang-Ung Park, Soft, smart contact lenses with integrations of wireless circuits, glucose sensors, and displays, Sci. Adv. (2018) 1–12. http://advances.sciencemag.org/.

[41] R.M.P. et al. Ahyeon Koh, Daeshik Kang, Yeguang Xue, Seungmin Lee, A Soft, Wearable Microfluidic Device for the Capture, Storage, and Colorimetric Sensing of Sweat, Physiol. Behav. 176 (2017) 139–148. https://doi.org/10.1126/scitranslmed.aaf2593.A.

[42] H. Lee, C. Song, Y.S. Hong, M.S. Kim, H.R. Cho, T. Kang, K. Shin, S.H. Choi, T. Hyeon, D.H. Kim, Wearable/disposable sweat-based glucose monitoring device with multistage transdermal drug delivery module, Sci. Adv. 3 (2017) 1–9. https://doi.org/10.1126/sciadv.1601314.

[43] J.D. Newman, A.P.F. Turner, Home blood glucose biosensors: A commercial perspective, Biosens. Bioelectron. 20 (2005) 2435–2453. https://doi.org/10.1016/j.bios.2004.11.012.

[44] J. Wang, Glucose biosensors: 40 Years of advances and challenges, Electroanalysis. 13 (2001) 983–988. https://doi.org/10.1002/1521-4109(200108)13:12<983::aid-elan983>3.0.co;2-%23.

[45] S.M. Herald, How Google's smart contact lens works, (2014).

[46] Abbott, The FreeStyle Libre Sensor, (2017). https://www.freestyle.abbott/ie-en/products/freestyle-libre.html.

[47] X. Ma, S. Ahadian, S. Liu, J. Zhang, S. Liu, T. Cao, W. Lin, D. Wu, N.R. de Barros, M.R. Zare, S.E. Diltemiz, V. Jucaud, Y. Zhu, S. Zhang, E. Banton, Y. Gu, K. Nan, S. Xu, M.R. Dokmeci, A. Khademhosseini, Smart Contact Lenses for Biosensing Applications, Adv. Intell. Syst. 3 (2021) 2000263. https://doi.org/10.1002/aisy.202000263.

[48] A.J. Bandodkar, V.W.S. Hung, W. Jia, G. Valdés-Ramírez, J.R. Windmiller, A.G. Martinez, J. Ramírez, G. Chan, K. Kerman, J. Wang, Tattoo-based potentiometric ion-selective sensors for epidermal pH monitoring, Analyst. 138 (2013) 123–128. https://doi.org/10.1039/c2an36422k.

[49] S. Kabilan, A.J. Marshall, A. Horgan, C.D. Creasey, S.J. Kew, K.E.S. Dean, S.F. Terrell, L.J. Affleck, "Smart" holograms - A novel diagnostics platform, 2006 NSTI Nanotechnol. Conf. Trade Show - NSTI Nanotech 2006 Tech. Proc. 3 (2006) 467–470.

[50] R.K. Saik, D.H. Gelfand, S. Stoffel, S.J. Scharf, R. Higuchi, G.T. Horn, K.B. Mullis, H.A. Erlich, Primer-directed enzymatic amplifincation of DNA with a thermostable DNA polymerase, Science (80-.). 239 (1987) 487–491. https://doi.org/10.1126/science.2448875.

[51] F.R.R. Teles, L.P. Fonseca, Trends in DNA biosensors, Talanta. 77 (2008) 606–623. https://doi.org/10.1016/j.talanta.2008.07.024.

[52] A. Manz, P. Dittrich, N. Pamme, D. Iossifidis, Bioanalytical Chemistry (2nd edition), 2015. https://doi.org/10.1142/P1000.

[53] B. Juskowiak, Nucleic acid-based fluorescent probes and their analytical potential, Anal. Bioanal. Chem. 399 (2011) 3157–3176. https://doi.org/10.1007/s00216-010-4304-5.

[54] S. Lee, S. Godhulayyagari, S.T. Nguyen, J.K. Lu, S.B. Ebrahimi, D. Samanta, Signal Transduction Strategies for Analyte Detection Using DNA-Based Nanostructures, Angew. Chemie. 134 (2022). https://doi.org/10.1002/ange.202202211.

[55] S. Bi, S. Yue, S. Zhang, Hybridization chain reaction: A versatile molecular tool for biosensing, bioimaging, and biomedicine, Chem. Soc. Rev. 46 (2017) 4281–4298. https://doi.org/10.1039/c7cs00055c.

[56] R.E. Farrell, Practical Nucleic Acid Hybridization, RNA Methodol. (2010) 283–299. https://doi.org/10.1016/b978-0-12-374727-3.00013-9.

[57] K. Mullis, F. Faloona, S. Scharf, R. Saiki, G. Horn, H. Erlich, Specific enzymatic amplification of DNA in vitro: the polymerase chain reaction. 1986., Biotechnology. 24 (1992) 17–27.

[58] N.C. Seeman, Nanomaterials based on DNA, Annu. Rev. Biochem. 79 (2010) 65–87. https://doi.org/10.1146/annurev-biochem-060308-102244.

[59] Y. Krishnan, F.C. Simmel, Nucleic acid based molecular devices, Angew. Chemie - Int. Ed. 50 (2011) 3124–3156. https://doi.org/10.1002/anie.200907223.

[60] Y. Hua, J. Ma, D. Li, R. Wang, DNA-Based Biosensors for the Biochemical Analysis: A Review, Biosensors. 12 (2022). https://doi.org/10.3390/bios12030183.

[61] S. Eissa, M. Zourob, In vitro selection of DNA aptamers targeting β-lactoglobulin and their integration in graphene-based biosensor for the detection of milk allergen, Biosens. Bioelectron. 91 (2017) 169–174. https://doi.org/10.1016/j.bios.2016.12.020.

[62] X.B. Zhang, Z. Wang, H. Xing, Y. Xiang, Y. Lu, Catalytic and molecular beacons for amplified detection of metal ions and organic molecules with high sensitivity, Anal. Chem. 82 (2010) 5005–5011. https://doi.org/10.1021/ac1009047.

[63] F.M. Spiga, A. Bonyár, B. Ring, M. Onofri, A. Vinelli, H. Sántha, C. Guiducci, G. Zuccheri, Hybridization chain reaction performed on a metal surface as a means of signal amplification in SPR and electrochemical biosensors, Biosens. Bioelectron. 54 (2014) 102–108. https://doi.org/10.1016/j.bios.2013.10.036.

[64] C. Li, D. Wu, X. Hu, Y. Xiang, Y. Shu, G. Li, One-Step Modification of Electrode Surface for Ultrasensitive and Highly Selective Detection of Nucleic Acids with Practical Applications, Anal. Chem. 88 (2016) 7583–7590. https://doi.org/10.1021/acs.analchem.6b01250.

[65] D. Wang, C. Vietz, T. Schröder, G. Acuna, B. Lalkens, P. Tinnefeld, A DNA Walker as a Fluorescence Signal Amplifier, Nano Lett. 17 (2017) 5368–5374. https://doi.org/10.1021/acs.nanolett.7b01829.

[66] A. Sassolas, B.D. Leca-Bouvier, L.J. Blum, DNA biosensors and microarrays, Chem. Rev. 108 (2008) 109–139. https://doi.org/10.1021/cr0684467.

[67] S.B. Nimse, K. Song, M.D. Sonawane, D.R. Sayyed, T. Kim, Immobilization techniques for microarray: Challenges and applications, Sensors (Switzerland). 14 (2014) 22208–22229. https://doi.org/10.3390/s141222208.

[68] J. Escorihuela, M.J. Bañuls, R. Puchades, Á. Maquieira, Development of oligonucleotide microarrays onto Si-based surfaces via thioether linkage mediated by UV irradiation, Bioconjug. Chem. 23 (2012) 2121–2128. https://doi.org/10.1021/bc300333a.

[69] M. Bally, M. Halter, J. Vörös, H.M. Grandin, Optical microarray biosensing techniques, Surf. Interface Anal. 38 (2006) 1442–1458. https://doi.org/10.1002/sia.2375.

[70] I. Barbulovic-Nad, M. Lucente, Y. Sun, M. Zhang, A.R. Wheeler, M. Bussmann, Bio-microarray fabrication techniques - A review, Crit. Rev. Biotechnol. 26 (2006) 237–259. https://doi.org/10.1080/07388550600978358.

[71] M.J. Heller, DNA microarray technology: Devices, systems, and applications, Annu. Rev. Biomed. Eng. 4 (2002) 129–153. https://doi.org/10.1146/annurev.bioeng.4.020702.153438.

[72] L.A.T.-G. and Á.M. María-José Bañuls , Sergi B. Morais, Microarray development on plastic substrates, Microarray, New York, 2016.

[73] S. Morais, R. Puchades, Á. Maquieira, Disc-based microarrays: principles and analytical applications, Anal. Bioanal. Chem. 408 (2016) 4523–4534. https://doi.org/10.1007/s00216-016-9423-1.

[74] Affymetrix, n.d. http://www.affymetrix.com.

[75] D. González-Lucas, M.J. Bañuls, R. Puchades, Á. Maquieira, Versatile and Easy Fabrication of Advanced Surfaces for High Performance DNA Microarrays, Adv. Mater. Interfaces. 3 (2016) 4–7. https://doi.org/10.1002/admi.201500850.

[76] M. Pikula, M.M. Ali, C. Filipe, T. Hoare, Single-step printable hydrogel microarray integrating long-chain DNA for the discriminative and size-specific sensing of nucleic acids, ACS Appl. Mater. Interfaces. 13 (2021) 2360–2370. https://doi.org/10.1021/acsami.0c21061.

[77] Y. Qi, K. Li, C. Zhao, Y. Ma, W. Yang, Preparation of a poly (PEGDA-co-GMA) thin hydrogel matrix for oligonucleotide microarray applications, J. Chem. Technol. Biotechnol. 96 (2021) 1902–1908. https://doi.org/10.1002/jctb.6709.

[78] J. Bae, J. Park, S. Kim, H. Cho, H.J. Kim, S. Park, D.S. Shin, Tailored hydrogels for biosensor applications, J. Ind. Eng. Chem. 89 (2020) 1–12. https://doi.org/10.1016/j.jiec.2020.05.001.

[79] M. Chen, Y. Wang, J. Zhang, Y. Peng, S. Li, D. Han, S. Ren, K. Qin, S. Li, Z. Gao, Stimuli-responsive DNA-based hydrogels for biosensing applications, J. Nanobiotechnology. 20 (2022) 1–22. https://doi.org/10.1186/s12951-022-01242-x.

[80] L. Zhou, X. Jiao, S. Liu, M. Hao, S. Cheng, P. Zhang, Y. Wen, Functional DNA-based hydrogel intelligent materials for biomedical applications, J. Mater. Chem. B. 8 (2020) 1991–2009. https://doi.org/10.1039/c9tb02716e.

[81] S. Nagahara, T. Matsuda, Hydrogel formation via hybridization of oligonucleotides derivatized in water-soluble vinyl polymers, Polym. Gels Networks. 4 (1996) 111–127. https://doi.org/10.1016/0966-7822(96)00001-9.

[82] L. Yan, Z. Zhu, Y. Zou, Y. Huang, D. Liu, S. Jia, D. Xu, M. Wu, Y. Zhou, S. Zhou, C.J. Yang, Target-responsive "sweet" hydrogel with glucometer readout for portable and quantitative detection of non-glucose targets, J. Am. Chem. Soc. 135 (2013) 3748–3751. https://doi.org/10.1021/ja3114714.

[83] A. Baeissa, N. Dave, B.D. Smith, J. Liu, DNA-functionalized monolithic hydrogels and gold nanoparticles for colorimetric DNA detection, ACS Appl. Mater. Interfaces. 2 (2010) 3594–3600. https://doi.org/10.1021/am100780d.

[84] Y. Ma, Y. Mao, Y. An, T. Tian, H. Zhang, J. Yan, Z. Zhu, C.J. Yang, Target-responsive DNA hydrogel for non-enzymatic and visual detection of glucose, Analyst. 143 (2018) 1679–1684. https://doi.org/10.1039/c8an00010g.

[85] S. Khajouei, H. Ravan, A. Ebrahimi, DNA hydrogel-empowered biosensing, Adv. Colloid Interface Sci. 275 (2020) 102060. https://doi.org/10.1016/j.cis.2019.102060.

[86] L.I. Yougen, Y.D. Tseng, S.Y. Kwon, L. D'Espaux, J.S. Bunch, P.L. McEuen, D. Luo, Controlled assembly of dendrimer-like DNA, Nat. Mater. 3 (2004) 38–42. https://doi.org/10.1038/nmat1045.

[87] S.H. Um, J.B. Lee, N. Park, S.Y. Kwon, C.C. Umbach, D. Luo, Enzyme-catalysed assembly of DNA hydrogel, Nat. Mater. 5 (2006) 797–801. https://doi.org/10.1038/nmat1741.

[88] X. Mao, G. Chen, Z. Wang, Y. Zhang, X. Zhu, G. Li, Surface-immobilized and self-shaped DNA hydrogels and their application in biosensing, Chem. Sci. 9 (2018) 811–818. https://doi.org/10.1039/c7sc03716c.

[89] J. Chu, C. Chen, X. Li, L. Yu, W. Li, M. Cheng, W. Tang, Z. Xiong, A responsive pure DNA hydrogel for label-free detection of lead ion, Anal. Chim. Acta. 1157 (2021) 338400. https://doi.org/10.1016/j.aca.2021.338400.

[90] J.B. Lee, S. Peng, D. Yang, Y.H. Roh, H. Funabashi, N. Park, E.J. Rice, L. Chen, R. Long, M. Wu, D. Luo, A mechanical metamaterial made from a DNA hydrogel, Nat. Nanotechnol. 7 (2012) 816–820. https://doi.org/10.1038/nnano.2012.211.

[91] Y. Huang, W. Xu, G. Liu, L. Tian, A pure DNA hydrogel with stable catalytic ability produced by one-step rolling circle amplification, Chem. Commun. 53 (2017) 3038–3041. https://doi.org/10.1039/C7CC00636E.

[92] N. Yang, D. You, J. Wang, L. Ge, Progress in DNA-based hydrogels for biosensing, Mater. Technol. 37 (2022) 798–813. https://doi.org/10.1080/10667857.2021.1885228.

[93] S. Khan, A. Ullah, K. Ullah, N.U. Rehman, Insight into hydrogels, Des. Monomers Polym. 19 (2016) 456–478. https://doi.org/10.1080/15685551.2016.1169380.

[94] X. Sun, S. Agate, K.S. Salem, L. Lucia, L. Pal, Hydrogel-Based Sensor Networks: Compositions, Properties, and Applications - A Review, ACS Appl. Bio Mater. 4 (2021) 140–162. https://doi.org/10.1021/acsabm.0c01011.

[95] U.S.K. Madduma-Bandarage, S. V. Madihally, Synthetic hydrogels: Synthesis, novel trends, and applications, J. Appl. Polym. Sci. 138 (2021) 1–23. https://doi.org/10.1002/app.50376.

[96] K.Y. Lee, D.J. Mooney, Hydrogels for tissue engineering, Chem. Rev. 101 (2001) 1869–1879. https://doi.org/10.1021/cr000108x.

[97] G.M.E. JOSHUA S. BOATENG, KERR H. MATTHEWS, HOWARD N.E. STEVENS, Wound Healing Dressings and Drug Delivery Systems: A Review, J. Pharm. Sci. 97 (2008) 2893–2923. https://doi.org/10.1002/jps.

[98] J. Kopeĉek, Hydrogels: From soft contact lenses and implants to self-assembled nanomaterials, J. Polym. Sci. Part A Polym. Chem. 47 (2009) 5929–5946. https://doi.org/10.1002/pola.23607.

[99] J. Li, D.J. Mooney, Designing hydrogels for controlled drug delivery, Nat. Rev. Mater. 1 (2016) 1–18. https://doi.org/10.1038/natrevmats.2016.71.

[100] X. Yang, C. An, S. Liu, T. Cheng, V. Bunpetch, Y. Liu, S. Dong, S. Li, X. Zou, T. Li, H. Ouyang, Z. Wu, W. Yang, Soft Artificial Bladder Detrusor, Adv. Healthc. Mater. 7 (1969) 1–9. https://doi.org/10.1002/adhm.201701014.

[101] J.Y. Sun, C. Keplinger, G.M. Whitesides, Z. Suo, Ionic skin, Adv. Mater. 26 (2014) 7608–7614. https://doi.org/10.1002/adma.201403441.

[102] D. Chan, J.C. Chien, E. Axpe, L. Blankemeier, S.W. Baker, S. Swaminathan, V.A. Piunova, D.Y. Zubarev, C.L. Maikawa, A.K. Grosskopf, J.L. Mann, H.T. Soh, E.A. Appel, Combinatorial Polyacrylamide Hydrogels for Preventing Biofouling on Implantable Biosensors, Adv. Mater. 34 (2022). https://doi.org/10.1002/adma.202109764.

[103] B. Yu, C. Wang, Y.M. Ju, L. West, J. Harmon, Y. Moussy, F. Moussy, Use of hydrogel coating to improve the performance of implanted glucose sensors, Biosens. Bioelectron. 23 (2008) 1278–1284. https://doi.org/10.1016/j.bios.2007.11.010.

[104] L. Rao, H. Zhou, T. Li, C. Li, Y.Y. Duan, Polyethylene glycol-containing polyurethane hydrogel coatings for improving the biocompatibility of neural electrodes, Acta Biomater. 8 (2012) 2233–2242. https://doi.org/10.1016/j.actbio.2012.03.001.

[105] Y. Lu, D. Wang, T. Li, X. Zhao, Y. Cao, H. Yang, Y.Y. Duan, Poly(vinyl alcohol)/poly(acrylic acid) hydrogel coatings for improving electrode-neural tissue interface, Biomaterials. 30 (2009) 4143–4151. https://doi.org/10.1016/j.biomaterials.2009.04.030.

[106] Y.N. Chou, F. Sun, H.C. Hung, P. Jain, A. Sinclair, P. Zhang, T. Bai, Y. Chang, T.C. Wen, Q. Yu, S. Jiang, Ultra-low fouling and high antibody loading zwitterionic hydrogel coatings for sensing and detection in complex media, Acta Biomater. 40 (2016) 31–37. https://doi.org/10.1016/j.actbio.2016.04.023.

[107] W. Wang, R. Narain, H. Zeng, Hydrogels, Elsevier Inc., 2020. https://doi.org/10.1016/B978-0-12-816806-6.00010-8.

[108] V.A. J.M.G. Cowie, Polymers: chemistry and physics of modern materials, third edit, 2008.

[109] S. Mantha, S. Pillai, P. Khayambashi, A. Upadhyay, Y. Zhang, Smart Hydrogels in Tissue Engineering and, Materials (Basel). 12 (2019) 33. https://www.ncbi.nlm.nih.gov/pmc/articles/PMC68/.

[110] C.A.-L. Fernando Yanez, Anuj Chauhan, Angel Concheiro, Timolol-Imprinted Soft Contact Lenses: Influence of the Template: Functional Monomer Ratio and the Hydrogel Thickness, J. Appl. Polym. Sci. 122 (2011) 1333–1340. https://doi.org/10.1002/app.

[111] M. Mahinroosta, Z. Jomeh Farsangi, A. Allahverdi, Z. Shakoori, Hydrogels as intelligent materials: A brief review of synthesis, properties and applications, Mater. Today Chem. 8 (2018) 42–55. https://doi.org/10.1016/j.mtchem.2018.02.004.

[112] F. Ganji, S. Vasheghani-Farahani, E. Vasheghani-Farahani, Theoretical description of hydrogel swelling: A review, Iran. Polym. J. (English Ed. 19 (2010) 375–398.

[113] D. Calvet, J.Y. Wong, S. Giasson, Rheological monitoring of polyacrylamide gelation: Importance of cross-link density and temperature, Macromolecules. 37 (2004) 7762–7771. https://doi.org/10.1021/ma049072r.

[114] W.H. Chen, W.C. Liao, Y.S. Sohn, M. Fadeev, A. Cecconello, R. Nechushtai, I. Willner, Stimuli-Responsive Nucleic Acid-Based Polyacrylamide Hydrogel-Coated Metal–Organic Framework Nanoparticles for Controlled Drug Release, Adv. Funct. Mater. 28 (2018) 1–9. https://doi.org/10.1002/adfm.201705137.

[115] Y. Hu, C.H. Lu, W. Guo, M.A. Aleman-Garcia, J. Ren, I. Willner, A Shape Memory Acrylamide/DNA Hydrogel Exhibiting Switchable Dual pH-Responsiveness, Adv. Funct. Mater. 25 (2015) 6867–6874. https://doi.org/10.1002/adfm.201503134.

[116] D. Roy, J.N. Cambre, B.S. Sumerlin, Future perspectives and recent advances in stimuli-responsive materials, Prog. Polym. Sci. 35 (2010) 278–301. https://doi.org/10.1016/j.progpolymsci.2009.10.008.

[117] A.A. Gafar, M.E. Khayat, M.B.H.A. Rahim, M.Y. Shukor, Acrylamide toxicity and its biodegradation, Bioremediation Sci. Technol. Res. 5 (2017) 8–12. https://doi.org/10.54987/bstr.v5i2.357.

[118] A. Herrmann, R. Haag, U. Schedler, Hydrogels and Their Role in Biosensing Applications, Adv. Healthc. Mater. 10 (2021) 1–25. https://doi.org/10.1002/adhm.202100062.

[119] M.L. Davies, C.J. Hamilton, S.M. Murphy, B.J. Tighe, Polymer membranes in clinical sensor applications. I. An overview of membrane function, Biomaterials. 13 (1992) 971–978. https://doi.org/10.1016/0142-9612(92)90147-G.

[120] J. Gačanin, C. V. Synatschke, T. Weil, Biomedical Applications of DNA-Based Hydrogels, Adv. Funct. Mater. 30 (2020). https://doi.org/10.1002/adfm.201906253.

[121] A. Pattammattel, B.S. Stromer, C. Baveghems, K. Benson, C. V. Kumar, Stimuli-responsive, protein hydrogels for potential applications in enzymology and drug delivery §, J. Chem. Sci. 130 (2018) 1–11. https://doi.org/10.1007/s12039-018-1538-9.

[122] I.Y. Jung, J.S. Kim, B.R. Choi, K. Lee, H. Lee, Hydrogel Based Biosensors for In Vitro Diagnostics of Biochemicals, Proteins, and Genes, Adv. Healthc. Mater. 6 (2017) 1–19. https://doi.org/10.1002/adhm.201601475.

[123] J. Liu, Oligonucleotide-functionalized hydrogels as stimuli responsive materials and biosensors, Soft Matter. 7 (2011) 6757–6767. https://doi.org/10.1039/c1sm05284e.

[124] F. Li, J. Tang, J. Geng, D. Luo, D. Yang, Polymeric DNA hydrogel: Design, synthesis and applications, Prog. Polym. Sci. 98 (2019) 101163. https://doi.org/10.1016/j.progpolymsci.2019.101163.

[125] D. Buenger, F. Topuz, J. Groll, Hydrogels in sensing applications, Prog. Polym. Sci. 37 (2012) 1678–1719. https://doi.org/10.1016/j.progpolymsci.2012.09.001.

[126] J.L. Drury, D.J. Mooney, Hydrogels for tissue engineering: Scaffold design variables and applications, Biomaterials. 24 (2003) 4337–4351. https://doi.org/10.1016/S0142-9612(03)00340-5.

[127] J. Tavakoli, Y. Tang, Hydrogel based sensors for biomedical applications: An updated review, Polymers (Basel). 9 (2017) 1–25. https://doi.org/10.3390/polym9080364.

[128] V.I. Dyukova, E.I. Dementieva, D.A. Zubtsov, O.E. Galanina, N. V. Bovin, A.Y. Rubina, Hydrogel glycan microarrays, Anal. Biochem. 347 (2005) 94–105. https://doi.org/10.1016/j.ab.2005.09.009.

[129] P. Arenkov, A. Kukhtin, A. Gemmell, S. Voloshchuk, V. Chupeeva, A. Mirzabekov, Protein microchips: Use for immunoassay and enzymatic reactions, Anal. Biochem. 278 (2000) 123–131. https://doi.org/10.1006/abio.1999.4363.

[130] F. Li, D. Lyu, S. Liu, W. Guo, DNA Hydrogels and Microgels for Biosensing and Biomedical Applications, Adv. Mater. 32 (2020) 1–9. https://doi.org/10.1002/adma.201806538.

[131] X. Liu, J. Zhang, M. Fadeev, Z. Li, V. Wulf, H. Tian, I. Willner, Chemical and photochemical DNA "gears" reversibly control stiffness, shape-memory, self-healing and controlled release properties of polyacrylamide hydrogels, Chem. Sci. 10 (2019) 1008–1016. https://doi.org/10.1039/c8sc04292f.

[132] S. Liu, W. Su, Y. Li, L. Zhang, X. Ding, Manufacturing of an electrochemical biosensing platform based on hybrid DNA hydrogel: Taking lung cancer-specific miR-21 as an example, Biosens. Bioelectron. 103 (2018) 1–5. https://doi.org/10.1016/j.bios.2017.12.021.

[133] Z. Zhu, C. Wu, H. Liu, Y. Zou, X. Zhang, H. Kang, C.J. Yang, W. Tan, An aptamer cross-linked hydrogel as a colorimetric platform for visual detection, Angew. Chemie - Int. Ed. 49 (2010) 1052–1056. https://doi.org/10.1002/anie.200905570.

[134] J. Wang, From DNA biosensors to gene chips, Nucleic Acids Res. 28 (2000) 3011–3016.

[135] K. Kahn, K.W. Plaxco, Principles of biomolecular recognition, 2010. https://doi.org/10.1007/978-1-4419-0919-0_1.

[136] A.S. Hoffman, J.A. Hubbell, Surface-Immobilized Biomolecules, Third Edit, Elsevier, 2013. https://doi.org/10.1016/B978-0-08-087780-8.00032-2.

[137] F. Kong, Y.F. Hu, Biomolecule immobilization techniques for bioactive paper fabrication, Anal. Bioanal. Chem. 403 (2012) 7–13. https://doi.org/10.1007/s00216-012-5821-1.

[138] P. Dey, M. Adamovski, S. Friebe, A. Badalyan, R.C. Mutihac, F. Paulus, S. Leimkühler, U. Wollenberger, R. Haag, Dendritic polyglycerol-poly(ethylene glycol)-based polymer networks for biosensing application, ACS Appl. Mater. Interfaces. 6 (2014) 8937–8941. https://doi.org/10.1021/am502018x.

[139] B. Prieto-Simon, M. Campas, J.-L. Marty, Biomolecule Immobilization in Biosensor Development: Tailored Strategies Based on Affinity Interactions, Protein Pept. Lett. 15 (2008) 757–763. https://doi.org/10.2174/092986608785203791.

[140] H. Orelma, L.S. Johansson, I. Filpponen, O.J. Rojas, J. Laine, Generic method for attaching biomolecules via avidin-biotin complexes immobilized on films of regenerated and nanofibrillar cellulose, Biomacromolecules. 13 (2012) 2802–2810. https://doi.org/10.1021/bm300781k.

[141] E.J. Devor, D. Ph, M. a Behlke, Strategies for Attaching Oligonucleotides to Solid Supports, Bioinformatics. 1 (2005) 1–24. http://citeseerx.ist.psu.edu/viewdoc/download?doi=10.1.1.93.1787&rep=rep1&type=pdf.

[142] M. Rendl, A. Bönisch, A. Mader, K. Schuh, O. Prucker, T. Brandstetter, J. Rühe, Simple one-step process for immobilization of biomolecules on polymer substrates based on surface-attached polymer networks, Langmuir. 27 (2011) 6116–6123. https://doi.org/10.1021/la1050833.

[143] M.J. Bañuls, M.Á. González-Martínez, J. Sabek, J. García-Rupérez, Á. Maquieira, Thiol-click photochemistry for surface functionalization applied to optical biosensing, Anal. Chim. Acta. 1060 (2019) 103–113. https://doi.org/10.1016/j.aca.2019.01.055.

[144] J. Escorihuela, M.J. Bañuls, S. Grijalvo, R. Eritja, R. Puchades, Á. Maquieira, Direct covalent attachment of DNA microarrays by rapid thiol-ene "click" chemistry, Bioconjug. Chem. 25 (2014) 618–627. https://doi.org/10.1021/bc500033d.

[145] G. Kaur, G. Singh, J. Singh, Photochemical tuning of materials: A click chemistry perspective, Mater. Today Chem. 8 (2018) 56–84. https://doi.org/10.1016/j.mtchem.2018.03.002.

[146] H.C. Kolb, M.G. Finn, K.B. Sharpless, Click Chemistry: Diverse Chemical Function from a Few Good Reactions, Angew. Chemie - Int. Ed. 40 (2001) 2004–2021. https://doi.org/10.1002/1521-3773(20010601)40:11<2004::AID-ANIE2004>3.0.CO;2-5.

[147] J. Escorihuela, A.T.M. Marcelis, H. Zuilhof, Metal-Free Click Chemistry Reactions on Surfaces, Adv. Mater. Interfaces. 2 (2015) 1–42. https://doi.org/10.1002/admi.201500135.

[148] Z. Díaz-Betancor, M.J. Bañuls, F.J. Sanza, R. Casquel, M.F. Laguna, M. Holgado, R. Puchades, Á. Maquieira, Phosphorylcholine-based hydrogel for immobilization of biomolecules. Application to fluorometric microarrays for use in hybridization assays and immunoassays, and nanophotonic biosensing, Microchim. Acta. 186 (2019). https://doi.org/10.1007/s00604-019-3691-3.

[149] J. Zaia, The 2022 Nobel Prize in Chemistry for the development of click chemistry and bioorthogonal chemistry, Anal. Bioanal. Chem. 415 (2023) 527–532. https://doi.org/10.1007/s00216-022-04483-9.

[150] D. Sadighbayan, K. Sadighbayan, M.R. Tohid-kia, A.Y. Khosroushahi, M. Hasanzadeh, Development of electrochemical biosensors for tumor marker determination towards cancer diagnosis: Recent progress, TrAC - Trends Anal. Chem. 118 (2019) 73–88. https://doi.org/10.1016/j.trac.2019.05.014.

[151] H. Yoshimine, K. Sasaki, H. Furusawa, Pocketable Biosensor Based on Quartz-Crystal Microbalance and Its Application to DNA Detection, Sensors. 23 (2023). https://doi.org/10.3390/s23010281.

[152] C. Li, H. Li, J. Ge, G. Jie, Versatile fluorescence detection of microRNA based on novel DNA hydrogel-amplified signal probes coupled with DNA walker amplification, Chem. Commun. 55 (2019) 3919–3922. https://doi.org/10.1039/c9cc00565j.

[153] H. Hilal, J.A. Taylor, Cyanine dyes for the detection of double stranded DNA., J. Biochem. Biophys. Methods. 70 (2008) 1104–1108. https://doi.org/10.1016/j.jprot.2007.12.008.

[154] Z. Zhu, C. Wu, H. Liu, Y. Zou, X. Zhang, H. Kang, C.J. Yang, W. Tan, An Aptamer Cross-Linked Hydrogel as a Colorimetric Platform for Visual Detection, Angew. Chemie. 122 (2010) 1070–1074. https://doi.org/10.1002/ange.200905570.

[155] B. Guo, B. Wen, W. Cheng, X. Zhou, X. Duan, M. Zhao, Q. Xia, S. Ding, An enzyme-free and label-free surface plasmon resonance biosensor for ultrasensitive detection of fusion gene based on DNA self-assembly hydrogel with streptavidin encapsulation, Biosens. Bioelectron. 112 (2018) 120–126. https://doi.org/10.1016/j.bios.2018.04.027.

[156] M.J. Yin, C. Wu, L.Y. Shao, W.K.E. Chan, A.P. Zhang, C. Lu, H.Y. Tam, Label-free, disposable fiber-optic biosensors for DNA hybridization detection, Analyst. 138 (2013) 1988–1994. https://doi.org/10.1039/c3an36791f.

[157] P. Damborský, J. Švitel, J. Katrlík, Optical biosensors, Essays Biochem. 60 (2016) 91–100. https://doi.org/10.1042/EBC20150010.

[158] N. Khansili, G. Rattu, P.M. Krishna, Label-free optical biosensors for food and biological sensor applications, Sensors Actuators, B Chem. 265 (2018) 35–49. https://doi.org/10.1016/j.snb.2018.03.004.

[159] Y.T. Chen, Y.C. Lee, Y.H. Lai, J.C. Lim, N.T. Huang, C.T. Lin, J.J. Huang, Review of Integrated Optical Biosensors for Point-of-Care Applications, Biosensors. 10 (2020) 1–22. https://doi.org/10.3390/BIOS10120209.

[160] M.I. Lucío, A. Cubells-Gómez, Á. Maquieira, M.J. Bañuls, Hydrogel-based holographic sensors and biosensors: past, present, and future, Anal. Bioanal. Chem. 414 (2022) 993–1014. https://doi.org/10.1007/s00216-021-03746-1.

[161] P. Zezza, E. Fern, Á. Maquieira, Surface Micro-Patterned Biofunctionalized Hydrogel for Direct Nucleic Acid Hybridization Detection, (2023).

[162] J.N. Anker, W.P. Hall, O. Lyandres, N.C. Shah, J. Zhao, R.P. Van Duyne, Biosensing with plasmonic nanosensors, Nat. Mater. 7 (2008) 8–10.

[163] G. Gauglitz, A. Brecht, G. Kraus, W. Mahm, Chemical and biochemical sensors based on interferometry at thin (multi-) layers, Sensors Actuators B. Chem. 11 (1993) 21–27. https://doi.org/10.1016/0925-4005(93)85234-2.

[164] X. Wang, O.S. Wolfbeis, X. Wang, O.S. Wolfbeis, Fiber-Optic Chemical Sensors and Biosensors, (2012).

[165] C. Stamm, W. Lukosz, Integrated optical difference interferometer as immunosensor, Sensors Actuators, B Chem. 31 (1996) 203–207. https://doi.org/10.1016/0925-4005(96)80067-0.

[166] A.K. Yetisen, H. Butt, L.R. Volpatti, I. Pavlichenko, M. Humar, S.J.J. Kwok, H. Koo, K.S. Kim, I. Naydenova, A. Khademhosseini, S.K. Hahn, S.H. Yun, Photonic hydrogel sensors, Biotechnol. Adv. 34 (2016) 250–271. https://doi.org/10.1016/j.biotechadv.2015.10.005.

[167] C. Fenzl, T. Hirsch, O.S. Wolfbeis, Photonic crystals for chemical sensing and biosensing, Angew. Chemie - Int. Ed. 53 (2014) 3318–3335. https://doi.org/10.1002/anie.201307828.

[168] Y. Sun, X. Fan, Optical ring resonators for biochemical and chemical sensing, Anal. Bioanal. Chem. 399 (2011) 205–211. https://doi.org/10.1007/s00216-010-4237-z.

[169] E. Milkani, S. Morais, C.R. Lambert, W.G. McGimpsey, Detection of oligonucleotide systematic mismatches with a surface plasmon resonance sensor, Biosens. Bioelectron. 25 (2010) 1217–1220. https://doi.org/10.1016/j.bios.2009.09.010.

[170] M. Piliarik, H. Šípová, P. Kvasnička, N. Galler, J.R. Krenn, J. Homola, High-resolution biosensor based on localized surface plasmons, Opt. Express. 20 (2012) 672. https://doi.org/10.1364/oe.20.000672.

[171] X. Li, N. Chen, X. Zhou, Y. Zhang, Y. Zhao, L.V. Nguyen, H. Ebendorff-Heidepriem, S.C. Warren-Smith, In-situ DNA detection with an interferometric-type optical sensor based on tapered exposed core microstructured optical fiber, Sensors Actuators B Chem. 351 (2022) 130942. https://doi.org/10.1016/j.snb.2021.130942.

[172] A. Leung, P.M. Shankar, R. Mutharasan, Label-free detection of DNA hybridization using gold-coated tapered fiber optic biosensors (TFOBS) in a flow cell at 1310 nm and 1550 nm, Sensors Actuators, B Chem. 131 (2008) 640–645. https://doi.org/10.1016/j.snb.2007.12.058.

[173] Q. Liu, B.K.L. Lim, S.Y. Lim, W.Y. Tang, Z. Gu, J. Chung, M.K. Park, T. Barkham, Label-free, real-time and multiplex detection of Mycobacterium tuberculosis based on silicon photonic microring sensors and asymmetric isothermal amplification technique (SPMS-AIA), Sensors Actuators, B Chem. 255 (2018) 1595–1603. https://doi.org/10.1016/j.snb.2017.08.181.

[174] K.I. MacConaghy, D.M. Chadly, M.P. Stoykovich, J.L. Kaar, Label-free detection of missense mutations and methylation differences in the p53 gene using optically diffracting hydrogels, Analyst. 140 (2015) 6354–6362. https://doi.org/10.1039/c5an01191d.

[175] J.K. Chen, G.Y. Zhou, C.J. Chang, A.W. Lee, F.C. Chang, Label-free DNA detection using two-dimensional periodic relief grating as a visualized platform for diagnosis of breast cancer recurrence after surgery, Biosens. Bioelectron. 54 (2014) 35–41. https://doi.org/10.1016/j.bios.2013.10.032.

[176] M icroscopy by reconstructed wave-fronts, (1949).

[177] E.N. Leith, J. Upatnieks, Reconstructed Wavefronts and Communication Theory*, J. Opt. Soc. Am. 52 (1962) 1123. https://doi.org/10.1364/josa.52.001123.

[178] S.F. Johnston, Yuri Denisyuk: an appreciation, (2006). http://eprints.gla.ac.uk/57256/.

[179] U. Schnars, C. Falldorf, J. Watson, W. Jüptner, Digital holography and wavefront sensing: Principles, techniques and applications, 2015. https://doi.org/10.1007/978-3-662-44693-5.

[180] J. Blyth, R.B. Millington, A.G. Mayes, E.R. Frears, C.R. Lowe, Holographic sensor for water in solvents, Anal. Chem. 68 (1996) 1089–1094. https://doi.org/10.1021/ac9509115.

[181] A.K. Yetisen, Holographic Sensors (2015).pdf, 2015.

[182] P.A. Blanche, Holographic recording media and devices, Encycl. Mod. Opt. 1–5 (2018) 87–101. https://doi.org/10.1016/B978-0-12-803581-8.09610-7.

[183] A.G. Mayes, J. Blyth, R.B. Millington, C.R. Lowe, Metal Ion-Sensitive Holographic Sensors, 74 (2002) 3649–3657.

[184] F.K. Sartain, X. Yang, C.R. Lowe, Holographic Lactate Sensor monitor exercise performance in sports medicine . This, Anal. Chem. 78 (2006) 5664–5670. http://pubs.acs.org/doi/pdfplus/10.1021/ac060416g.

[185] I. Naydenova, R. Jallapuram, V. Toal, S. Martin, A visual indication of environmental humidity using a color changing hologram recorded in a self-developing photopolymer, Appl. Phys. Lett. 92 (2008) 1–4. https://doi.org/10.1063/1.2837454.

[186] F.K. Bruder, R. Hagen, T. Rölle, M.S. Weiser, T. Fäcke, From the surface to volume: Concepts for the next generation of optical-holographic data-storage materials, Angew. Chemie - Int. Ed. 50 (2011) 4552–4573. https://doi.org/10.1002/anie.201002085.

[187] K.T.P. Lim, H. Liu, Y. Liu, J.K.W. Yang, Holographic colour prints for enhanced optical security by combined phase and amplitude control, Nat. Commun. 10 (2019) 1–8. https://doi.org/10.1038/s41467-018-07808-4.

[188] G. Saxby, Practical holography, second edi, 1994.

[189] A.K. Yetisen, I. Naydenova, F. Da Cruz Vasconcellos, J. Blyth, C.R. Lowe, Holographic sensors: Three-dimensional analyte-sensitive nanostructures and their applications, Chem. Rev. 114 (2014) 10654–10696. https://doi.org/10.1021/cr500116a.

[190] E. Mihaylova, D. Cody, I. Naydenova, S. Martin, V. Toal, Research on Holographic Sensors and Novel Photopolymers at the Centre for Industrial and Engineering Optics, Hologr. - Basic Princ. Contemp. Appl. (2013). https://doi.org/10.5772/56061.

[191] S. Davies, Y. Hu, N. Jiang, J. Blyth, M. Kaminska, Y. Liu, A.K. Yetisen, Holographic Sensors in Biotechnology, Adv. Funct. Mater. 31 (2021). https://doi.org/10.1002/adfm.202105645.

[192] R.B. Millington, A.G. Mayes, J. Blyth, C.R. Lowe, A Holographic Sensor for Proteases, Anal. Chem. 67 (1995) 4229–4233. https://doi.org/10.1021/ac00119a004.

[193] A.J. Marshall, J. Blyth, C.A.B. Davidson, C.R. Lowe, pH-sensitive holographic sensors, Anal. Chem. 75 (2003) 4423–4431. https://doi.org/10.1021/ac020730k.

[194] T. Mikulchyk, J. Walshe, D. Cody, S. Martin, I. Naydenova, Humidity and temperature induced changes in the diffraction efficiency and the Bragg angle of slanted photopolymer-based holographic gratings, Sensors Actuators, B Chem. 239 (2017) 776–785. https://doi.org/10.1016/j.snb.2016.08.052.

[195] S. e. Gul, D. Cody, A. Kharchenko, S. Martin, S. Mintova, J. Cassidy, I. Naydenova, LTL type nanozeolites utilized in surface photonics structures for environmental sensors, Microporous Mesoporous Mater. 261 (2018) 268–274. https://doi.org/10.1016/j.micromeso.2017.11.019.

[196] A.K. Yetisen, Y. Montelongo, H. Butt, Rewritable three-dimensional holographic data storage via optical forces, Appl. Phys. Lett. 109 (2016). https://doi.org/10.1063/1.4960710.

[197] Z. Gong, S. Karandikar, X. Zhang, V. Kotipalli, Y. Lvov, L. Que, Composite nanomaterial thin film-based biosensors, Proc. IEEE Sensors. (2010) 29–32. https://doi.org/10.1109/ICSENS.2010.5690979.

[198] I. Naydenova, J. Grand, T. Mikulchyk, S. Martin, V. Toal, V. Georgieva, S. Thomas, S. Mintova, Hybrid Sensors Fabricated by Inkjet Printing and Holographic Patterning, Chem. Mater. 27 (2015) 6097–6101. https://doi.org/10.1021/acs.chemmater.5b02629.

[199] A.K. Yetisen, M.M. Qasim, S. Nosheen, T.D. Wilkinson, C.R. Lowe, Pulsed laser writing of holographic nanosensors, J. Mater. Chem. C. 2 (2014) 3569–3576. https://doi.org/10.1039/c3tc32507e.

[200] A.K. Yetisen, Y. Montelongo, M.M. Qasim, H. Butt, T.D. Wilkinson, M.J. Monteiro, S.H. Yun, Photonic nanosensor for colorimetric detection of metal ions, Anal. Chem. 87 (2015) 5101–5108. https://doi.org/10.1021/ac504274q.

[201] G. Ye, X. Wang, Glucose sensing through diffraction grating of hydrogel bearing phenylboronic acid groups, Biosens. Bioelectron. 26 (2010) 772–777. https://doi.org/10.1016/j.bios.2010.06.029.

[202] S. Kabilan, J. Blyth, M.C. Lee, A.J. Marshall, A. Hussain, X.P. Yang, C.R. Lowe, Glucose-sensitive holographic sensors, J. Mol. Recognit. 17 (2004) 162–166. https://doi.org/10.1002/jmr.663.

[203] G. Khalili Moghaddam, H. Margerison, J. Suzuki, J. Blyth, C.R. Lowe, A transparent glucose-sensitive double polymerised holographic sensor, Sensors Actuators, B Chem. 267 (2018) 1–4. https://doi.org/10.1016/j.snb.2018.04.009.

[204] S. Kabilan, A.J. Marshall, F.K. Sartain, M.C. Lee, A. Hussain, X. Yang, J. Blyth, N. Karangu, K. James, J. Zeng, D. Smith, A. Domschke, C.R. Lowe, Holographic glucose sensors, Biosens. Bioelectron. 20 (2005) 1602–1610. https://doi.org/10.1016/j.bios.2004.07.005.

[205] I. Naydenova, Holographic sensors, Elsevier Inc., 2019. https://doi.org/10.1016/B978-0-12-815467-0.00007-4.

[206] T. Mikulchyk, S. Martin, I. Naydenova, N-isopropylacrylamide-based photopolymer for holographic recording of thermosensitive transmission and reflection gratings, Appl. Opt. 56 (2017) 6348. https://doi.org/10.1364/ao.56.006348.

[207] V. Toal, Introduction to holography, 2011. https://doi.org/https://doi.org/10.1201/b11706.

[208] D. Cody, I. Naydenova, Theoretical modeling and design of photonic structures in zeolite nanocomposites for gas sensing Part II: volume gratings, J. Opt. Soc. Am. A. 35 (2018) 12. https://doi.org/10.1364/josaa.35.000012.

[209] F.W. Sears, P. Biquard, The diffraction of light by high frequency sound waves: Part 1, Indian Acad. Sci. 32 (1935) 406–412. https://doi.org/10.1007/BF03035840.

[210] H. Kogelnik, Coupled Wave Theory for Thick hologram Gratings, Bell Syst. Tech. J. 48(9) (1969) 2909–47.

[211] M. Zawadzka, I. Naydenova, Surface holograms for sensing application, J. Phys. Conf. Ser. 961 (2018). https://doi.org/10.1088/1742-6596/961/1/012002.

[212] Q. Li, Azobenzene Polymers as Photoactive Materials for Shape Changes of Micro / Nano - objects Why Azobenzene - Based Photoactive, (2019).

[213] O.T. Picot, R. Alcalá, C. Sánchez, M. Dai, N.F. Hughes-Brittain, D.J. Broer, T. Peijs, C.W.M. Bastiaansen, Manufacturing of surface relief structures in moving substrates using photoembossing and pulsed-interference holography, Macromol. Mater. Eng. 298 (2013) 33–37. https://doi.org/10.1002/mame.201100433.

[214] I. Naydenova, E. Mihaylova, S. Martin, V. Toal, Holographic patterning of acrylamide-based photopolymer surface, Opt. Express. 13 (2005) 4878. https://doi.org/10.1364/opex.13.004878.

[215] D.W. Müller, T. Fox, P.G. Grützmacher, S. Suarez, F. Mücklich, Applying Ultrashort Pulsed Direct Laser Interference Patterning for Functional Surfaces, Sci. Rep. 10 (2020) 1–14. https://doi.org/10.1038/s41598-020-60592-4.

[216] A.F. Lasagni, C. Gachot, K.E. Trinh, M. Hans, A. Rosenkranz, T. Roch, S. Eckhardt, T. Kunze, M. Bieda, D. Günther, V. Lang, F. Mücklich, Direct laser interference patterning, 20 years of development: from the basics to industrial applications, Laser-Based Micro- Nanoprocessing XI. 10092 (2017) 1009211. https://doi.org/10.1117/12.2252595.

[217] P. Zezza, M.I. Lucío, Á. Maquieira, M.J. Bañuls, DNA -based hydrogels for high-performance optical biosensing application, Talanta. 244 (2022). https://doi.org/10.1016/j.talanta.2022.123427.

[218] D. Qin, Y. Xia, G.M. Whitesides, Soft lithography for micro- and nanoscale patterning, Nat. Protoc. 5 (2010) 491–502. https://doi.org/10.1038/nprot.2009.234.

[219] G. Ye, X. Wang, Polymer diffraction gratings on stimuli-responsive hydrogel surfaces: Soft-lithographic fabrication and optical sensing properties, Sensors Actuators, B Chem. 147 (2010) 707–713. https://doi.org/10.1016/j.snb.2010.03.052.

[220] T. Kunze, A.F. Lasagni, Direct laser interference patterning : from fundamentals to industrial applications, (2017).

[221] X. Wang, X. Wang, Aptamer-functionalized hydrogel diffraction gratings for the human thrombin detection, Chem. Commun. 49 (2013) 5957–5959. https://doi.org/10.1039/c3cc41827h.

[222] J.J. Zhao, W. Wang, W. Wang, F. Wang, Y. Zhao, Q.W. Cai, R. Xie, R. Xie, X.J. Ju, X.J. Ju, Z. Liu, Z. Liu, Y. Faraj, Y. Faraj, L.Y. Chu, Smart Hydrogel Grating Immunosensors for Highly Selective and Sensitive Detection of Human-IgG, Ind. Eng. Chem. Res. 59 (2020) 10469–10475. https://doi.org/10.1021/acs.iecr.0c00780.

[223] M.I. Lucío, A.H. Montoto, E. Fernández, S. Alamri, T. Kunze, M.J. Bañuls, Á. Maquieira, Label-free detection of C-Reactive protein using bioresponsive hydrogel-based surface relief diffraction gratings, Biosens. Bioelectron. 193 (2021). https://doi.org/10.1016/j.bios.2021.113561.

[224] C. Wang, Y. Zhang, C. Liu, S. Gou, S. Hu, W. Guo, A portable colorimetric point-of-care testing platform for MicroRNA detection based on programmable entropy-driven dynamic DNA network modulated DNA-gold nanoparticle hybrid hydrogel film, Biosens. Bioelectron. 225 (2023) 115073. https://doi.org/10.1016/j.bios.2023.115073.

[225] W.H. Chang, Y.F. Lee, Y.W. Liu, I. Willner, W.C. Liao, Stimuli-responsive hydrogel microcapsules for the amplified detection of microRNAs, Nanoscale. 13 (2021) 16799–16808. https://doi.org/10.1039/d1nr05170a.

[226] K. Berramdane, M.G. Ramírez, P. Zezza, M.I. Lucío, M.J. Bañuls, Á. Maquieira, M. Morales-Vidal, A. Beléndez, I. Pascual, Processing of Holographic Hydrogels in Liquid Media: A Study by High-Performance Liquid Chromatography and Diffraction Efficiency, Polymers (Basel). 14 (2022). https://doi.org/10.3390/polym14102089.

[227] I. Naydenova, R. Jallapuram, R. Howard, S. Martin, V. Toal, Investigation of the diffusion processes in a self-processing acrylamide-based photopolymer system, Appl. Opt. 43 (2004) 2900–2905. https://doi.org/10.1364/AO.43.002900.

[228] M. Moothanchery, I. Naydenova, V. Toal, Study of the shrinkage caused by holographic grating formation in acrylamide based photopolymer film, Opt. Express. 19 (2011) 13395. https://doi.org/10.1364/oe.19.013395.

[229] I. Naydenova, R. Jallapuram, S. Martin, V. Toal, Holographic humidity sensors, (2011).

[230] G. Bianco, M.A. Ferrara, F. Borbone, F. Zuppardi, A. Roviello, V. Striano, G. Coppola, Volume holographic gratings as optical sensor for heavy metal in bathing waters, Opt. Sensors 2015. 9506 (2015) 95062B. https://doi.org/10.1117/12.2179171.

[231] A.J. Marshall, D.S. Young, J. Blyth, S. Kabilan, C.R. Lowe, Metabolite-Sensitive Holographic Biosensors, Anal. Chem. 76 (2004) 1518–1523. https://doi.org/10.1021/ac030357w.

[232] M. Irfan, S. Martin, I. Naydenova, Temperature-Sensitive Holograms with Switchable Memory, Adv. Photonics Res. 2 (2021) 2100062. https://doi.org/10.1002/adpr.202100062.

AIM AND OBJECTIVES

2- Chapter 2

AIMS AND OBJECTIVES

The motivation behind this research was the synthesis and optimisation of biofunctionalised hydrogels for label-free holographic biosensing. This thesis work is part of the research involved in the Spanish project ADBHIOL - 'Towards Advanced Holographic Biosensing'. The aim of this project is to develop new diagnostic devices that can improve the accessibility of healthcare worldwide. Having rapid, self-monitoring tests that enable on-site detection is a global interest to avoid hospital crowding and the spread of contagious diseases. Undoubtedly, the development of portable devices for point-of-care testing (POCT), which allow rapid detection with an easily interpretable reading, is crucial for the future. In this context, holographic biosensors offer an attractive approach for label-free optical detection. The aim of this thesis is to investigate and develop new hydrogels that incorporate nucleic acids probes in a simple and efficient manner, with rapid procedures, that maintain the mechanical and optical properties of the hydrogel necessary to be applied as holographic biosensors. Thus, several strategies are to be explored in this thesis, whose particular objectives are:

1) Synthesis and optimisation of acrylamide/bisacrylamide hydrogels.
2) Incorporation of additional functional groups (co-monomers) to improve functionalisation with bioreceptors.
3) Characterisation of Physical and chemical properties of the synthesised functional materials.
4) Development of immobilisation strategies for the incorporation of bioreceptors (DNA probes) effectively into hydrogels.
5) Study of the oligonucleotide's immobilization and hybridization capabilities by fluorescence detection.
6) Application of the generated hydrogels in microarray format for read-out, performance studies.
7) Fabrication and optical characterisation of two types of diffraction gratings: 1) surface relief gratings (SRG) and 2) volume holographic gratings (VHG).
8) Assessment of their capabilities to act as holographic biosensors by diffraction efficiency monitoring.

EXPERIMENTAL SECTION AND RESULTS

3- Chapter 3

DNA-based hydrogel for high-performance optical biosensing applications

3- Chapter 3. DNA-based hydrogel for high-performance optical biosensing applications

In this chapter, a DNA-based hydrogel was designed and used as a sensing platform to perform the detection of a specific DNA target sequence. The novelty is the combination of a 3D hydrogel network as a support for functionalisation with DNA probes with a holographic diffraction grating on the surface of the hydrogel as a potential label-free optical transducer. Furthermore, the biosensing properties of the DNA-based hydrogel were also studied in the microarray format, demonstrating its versatility for multiplexing. The challenge was to obtain a hydrogel for sensitive and selective DNA detection, discriminating oligonucleotides with single mismatches, with good physical, optical and mechanical properties to develop a holographic transducer for future label-free detection.

In this study, the composition of the hydrogel was optimised and the best reaction conditions were identified to favour the formation in a single step of a hydrogel covalently functionalised with DNA, which retains the appropriate characteristics to be used as a holographic biosensor. Indeed, it has been demonstrated that the target DNA is efficiently recognised, enabling sensitive and selective detection. As a proof of concept for label-free detection, a surface relief grating with good reproducibility was produced and its optical properties in an aqueous environment, such as diffraction and grating period, were studied.
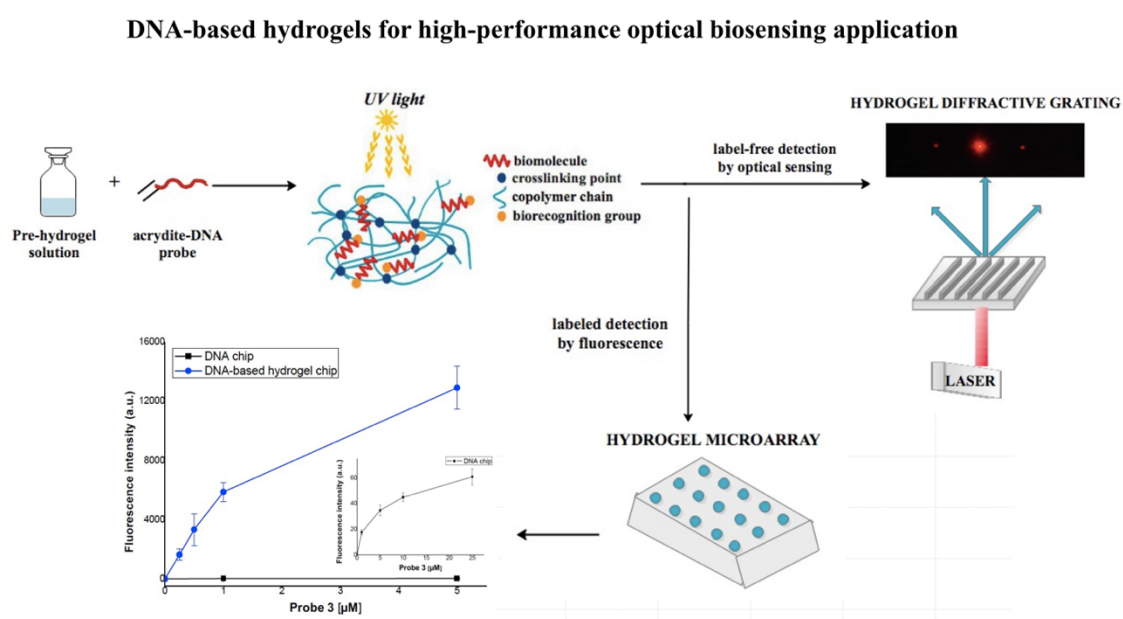
Summary figure. Overview chapter 3.

DNA-based hydrogels for high-performance optical biosensing application

Paola Zezza[1], María Isabel Lucío[1,2], Ángel Maquieira[1,2], María-José Bañuls*[1,2]

[1] Instituto Interuniversitario de Investigación de Reconocimiento Molecular y Desarrollo Tecnológico (IDM), Universitat Politécnica de Valéncia, Universitat de Valéncia, Camino de Vera s/n, 46022, Valencia, Spain. E-mail: mbpolo@upv.es
[2] Departamento de Quimica, Universitat Politécnica de Valéncia, Camino de Vera s/n, 46022, Valencia, Spain.

3.1 Abstract

Analyte-sensitive DNA-based hydrogels find multiple applications in the field of biosensors due to their adaptable nature. Here, the design of DNA-based hydrogel and its application as sensing platform for the detection of a specific target sequence are presented. DNA-functionalized hydrogel structures were formed via a free radical copolymerization process. A simple one-step probe immobilization procedure is reported: DNA probe molecules are added to the photoactive polymer mixture, dispensed onto a solid support, or a mold, and covalently attached while the hydrogel is formed through UV light exposure. Such hydrogels can be synthesized with desired recognition ability through the selection of a certain nucleotide sequence. Here we show the application of DNAbased hydrogel to detect the target with high performance in fluorescence microarray format and, additionally, to fabricate holographic surface relief gratings for label-free sensing assays.

3.2 Introduction

Hydrogels have found wide application in the biomedical field due to their versatile nature. They are three dimensional networks of polymers, characterized by the ability to retain a large amount of water being permeable. This feature makes them ideal for a variety of applications, such as biosensing [1], drug delivery [2], immunotherapy [3] and tissue engineering [4]. Furthermore, they are suitable for multiplexing, miniaturization and label-free systems. Hence, they are being increasingly used, thanks to their suitable properties both mechanical (porosity, sorption capacity, elasticity, strength) as well as optical (transparency), chemical (easy fabrication process, ability to be chemically derivatized) and biochemical (low nonspecific signals, biocompatibility, bio-specificity) [5–7]. The immobilization of nucleic acids on solid supports has been broadly employed in sensor technology for the detection of DNA and other biomolecules [8]. Microarrays are versatile tools in biomedical research, as they permit highly parallel analysis of various samples [9]. Immobilization strategies of biomolecules at the surfaces of the chips plays a decisive factor for the assay performance.

Three-dimensional (3-D) hydrogel matrixes offer significant advantages for catching probes over more conventional two dimensional (2-D) rigid substrates and, additionally, they provide a solution-mimicking environment that makes them attractive supports for bio-analysis [10–12]. Moreover, DNA can be modified with several functional groups including amino, biotin, acrydite, azide, and thiol to promote the covalent binding to the substrate [13]. DNA-based hydrogel chips were prepared by simple and fast procedure; in comparison to other multiple steps and thus time consuming procedures presented in literature [14]. Initially, in this work, the functionalization approach of acrylamide hydrogel was based on the polymerization with glycidyl methacrylate (GMA), as a co-monomer functional group, and the immobilization of thiol-modified DNA by thiol–epoxy coupling reaction. This immobilization procedure was performed by click photochemistry, during or after the polymerization. Secondly, acrydite-modified DNA were used to direct co-polymerize with acrylamide monomers during gel formation, as already reported in literature [15]. Compared to the already published method, our strategy for the immobilization in the 3D-hydrogel is based on the same chemical reaction but activated photochemically and/or thermally, thus avoiding the use of toxic catalyst for future biomedical applications and, moreover, obtaining better porosity. This last approach was used for the microarray fabrication in which acrylamide-based hydrogel were attached on a glass substrate, by UV irradiation, and simultaneously functionalized by co-polymerization with acrydite-modified DNA probes. In this method, the UV light plays a double role as it catalyzes both the co-polymerization of acrylamide monomers with DNA probes and the covalent attachment to the microarray substrate. Basically, a simple one-step immobilization process for hydrogel 3D-microarray fabrication is shown and its transfer in label-free biosensing was explored [16]. Towards future applications as label-free system, a diffraction grating has been produced on the hydrogel surface by replica molding (REM) and employed as optical transducer [17–20]. So far, very few hydrogel-based diffractive gratings have been developed for label-free biosensing applications, and none of them is for nucleic acid recognition [21–24]. Sensitive DNA-based hydrogels as label-free sensors are highly promising in disease diagnosis and healthcare monitoring applications.

3.3 Experimental

Material and methods

Acrylamide (AA), N, N′ -methylenebis (acrylamide) (MBA), Potassium persulfate (KPS), glycidyl methacrylate (GMA), 2-Hydroxy-4′ -(2- hydroxyethoxy)-2-methylpropiophenone (Irgacure 2959), toluene ≥99.5% and 3 (trimethoxysilyl)propylmethacrylate (TMSPMA) ≥98% were purchased from Sigma–Aldrich (Madrid, Spain). The employed oligonucleotides were supplied by Sumilab (Valencia, Spain), sequences used are listed in Table 1. Phosphate buffered saline solution with Tween 20 (PBS1x: 0.008 M disodium phosphate, 0.002 M monosodium phosphate, 0.137 M sodium chloride, 2.7 M potassium chloride, pH 7.5 with 0.05%Tween 20) and Saline-sodium citrate (SSC1x: 0.15 M sodium chloride and 0.015 M sodium citrate, pH 7) were prepared following the preparation procedures. Polydimethylsiloxane (PDMS) Sylgard 184 was purchased from Dow Corning (Wiesbaden, Germany). Glass microscope slides were provided from Labbox (Barcelona, Spain). Microarray printing was carried out with a low-volume noncontact dispensing system from Biodot (Irvine, CA, USA), model AD1500. Irradiation was carried out with a UV-ozone cleaning system (FHR, Ottendorf, Germany). Hydrogel fluorescence measurements are registered with a homemade surface fluorescence reader (SFR) having a high-sensitivity charge-coupled device camera [25]. Microarray fluorescence measurements were carried out with a fluorescence microarray analyzer SensoSpot (Radolfzell, Germany). For fluorescence image analysis and quantification, GenePix Pro 4.0 software from Molecular Devices, Inc. (Sunnyvale, CA, USA) was employed. Images were also analyzed with ImageJ software. Morphological characterization of hydrogel was carried out using scanning electron microscopy (SEM, Gemini SEM 500 system, Zeiss), and optical microscopy (OM, Leica microsystems, MZ APO). For SEM characterization hydrogels were completely swollen in distilled water and frozen at −20 °C. Then, they were lyophilized overnight in a Telstar Lyoquest freeze-drier to yield completely dry aerogel samples. Finally, dry samples were prepared by sputter coating with an Au layer of about 15 nm (BAL-TEC SCD 005 sputter coater, Leica microsystems).

Moreover, swelling behavior study was carried out with lyophilized hydrogel samples. Samples with a size of approximately 1 cm were immersed in PBS-T (10 mL) at room temperature. The weight of the swollen hydrogels was recorded at different times until they were totally swollen (reaching of a constant weight). Water excess on the surface of the hydrogel was removed with a filter paper before weighing. The swelling degree was calculated from equation (1), where Wt is the weight of the hydrogel after being immersed in water during time "t" and W0 is the weight of the lyophilized hydrogel before the immersion.

Table 1
Nucleotide sequence of probes and target used.

Name	Sequence (5′–3′)	5′ end	3′end
Probe 1	$(T)_{15}$ – CCCGATTGACCAGCTAGCATT	SH	Cy5
Probe 2	CCCGATTGACCAGCTAGCATT	acrydite	Cy5
Probe 3	CCCGATTGACCAGCTAGCATT	acrydite	none
Target	AATGCTAGCTGGTCAATCGGG	Cy5	none
control probe	CCCGATTGACCAGCTAGCATT	none	none

Hydrogel diffraction gratings, as surface relief gratings, have been fabricated through replica molding technique (REM) and characterized by a simple home-made optical set-up.

$$\% \, Swelling = \frac{Wt - Wo}{Wo} \, 100 \tag{1}$$

Optimization of hydrogel synthesis

AA/GMA hydrogels were prepared by free radical polymerization (FRP) thermally initiated at 60 °C. Synthesis optimization was reached varying the % of the monomers (AA and GMA) and the crosslinker (MBA) in 1 mL of distilled water, while the thermal initiator (KPS) was always kept at 1% w/v (supporting information). The prepared hydrogels were stored at 4 °C.

DNA-based hydrogels preparation and hybridization assay

Hyd10 and hyd11 compositions were finally used for DNA-based hydrogels preparation in milli-Q water. Firstly, DNA-based hydrogels solutions were prepared in 1 mL of milli-Q ultrapure water with 25% w/ v AA, 0.5 μM of 5′ -thiol oligonucleotide (Probe 1), 0.6% w/v MBA, 0.01% w/v GMA and 1% w/v of KPS. The free radical polymerization of AA/GMA hydrogel (hyd11) was initiated thermally at 60 ∘C. Secondly, for hyd10 preparation, DNA-based hydrogels solutions were prepared in 1 mL of milli-Q ultrapure water with 25% w/v acrylamide, 0.6% w/v MBA and 0.5 μM of 5′ -acrydite modified DNA (Probe 3). Hydrogel pregel solutions (hyd10) with DNA probes were stirred during 1h at RT and, after that, 1% w/v of the photo initiator (Irgacure 2959) was added in order to trigger the free-radical polymerization photochemically at 254 nm. Alternatively, the AA-hydrogel (hyd10) polymerization was thermally activated with KPS. To study the biosensing performance, hybridization of acrydite-functionalized hydrogel (hyd10-DNA) with the labelled anti-probe (Target) was carried out and compared with two reference systems: hyd10, without any probe, and hyd10-control probe (the same oligonucleotide sequence of probe 3 but without any modification). Labelled anti-probe solutions were prepared at growing concentrations (0.5, 0.1, 0.2, 0.3, 0.4, 0.5 μM) in SCC 1×. Hybridization was performed in triplicate by incubating hydrogels (0.5 × 0.5 cm) with the prepared anti-probe solutions for a duration of 2h at 37 °C. Subsequently, fabricated hydrogels were washed three times with PBS-T in order to eliminate the unbinding oligonucleotides probes. Fluorescent detection was performed before washing, after 2 h washing and after overnight washing with PBS-T.

Glass surface modification

In order to modify the glass slides surface with acrylate groups, firstly, they were washed with ethanol and dried. Next, surfaces were activated with a UV-ozone cleaner for 3 min and, immediately after, immersed in a toluene solution containing 3-(trimethoxysilyl)propylmethacrylate (TMSPMA) organosilane (2% w/v). After 2 h at room temperature, glass slides were washed with toluene and placed in the oven at 120 ∘C for 20 min.

Microarrays fabrication and hybridization assay

DNA-based hydrogel microarray was obtained by free radical polymerization (FRP) initiated by UV light. Hence, pre-polymeric solutions containing the DNA-probe (Probe 3) were prepared at different concentrations (5, 1, 0.5, 0.25 μM) in PBS 1×. As comparing system, conventional DNA-microarray were used. For that, DNA-probe (Probe 3) was solved in PBS 1× at different concentration (25, 10, 5, 1 μM) with 1% w/v of the photo initiator and directly immobilized on a glass slide. The prepared solutions were spotted on the microscope glass slides with a template of 5 rows, 3 spots per row (10 nL/spot), and 12 microarray replicas per glass slide. DNA-microarrays were irradiated by UV light at 254 nm (50 mW cm^{-2}) for 10 min, while 25 min were necessary in the case of DNA-based hydrogel microarrays. An extra row with the labeled DNA-probe (Probe 2) was included as a positive immobilization control (at 10 μM and 1 μM for simple DNA and DNA-based hydrogel microarrays, respectively). The 3 × 5 microarrays were spotted at 24 °C and with 80% of relative humidity. After UV irradiation, they were washed with PBS-T 10 ×, in order to eliminate the non-bonded oligonucleotides probes, and dried. Furthermore, 20 μL of the complementary oligonucleotide 5′ Cy5-labeled (Target) in SSC 1 × was dispensed and spread out with a coverslip and incubated in a dark and humidified chamber for 1h at 37 °C. The microarrays were then washed with PBS-T and dried. To study the immobilization density for the two microarray platforms, fluorescence images were measured at λ 650 nm with the fluorescence microarray analyzer SensoSpot and quantified by the GenePix 4.0 software.

Label-free format of DNA-based hydrogel

Holographic grating masters, employed as optical transducers, were fabricated using the Direct Laser Interference Patterning (DLIP) technology [26]. PET grating masters were supplied by Fraunhofer Institute (structuring parameters indicated in Table 2). Afterwards, hydrogel diffraction gratings were made by reproducing the grating of the master via replica molding (REM). REM is a soft lithography technique which consists of 3 steps: i) a line-like diffractive pattern was recorded by DLIP on a PET master; then ii) transferring the pattern on the master into PDMS, thus a negative copy of the pattern was obtained using PDMS as "ink"; iii) the original pattern is replicated on the hydrogel surface, during the curing process, by solidifying the prepolymer solution against the PDMS mold. In the last step, the prepolymer solution was poured into vials with the PDMS molder stuck to the base. In this case, DNA-based hydrogel polymerization had been triggered thermally at 60 °C for 2 h, adding to the prepolymer mixture only KPS as thermal initiator. Before solidifying the hydrogel with the PDMS mold in oven, vacuum was applied for about 15 min to remove any trapped air bubbles and to allow a greater adhesion to the mold. Afterwards, the diffraction of the grating fabricated within the hydrogel was observed through samples irradiation, with a laser beam (650 nm) incident from the bottom side of the hydrogel. The diffraction was projected on a white screen, placed at fixed distance where a digital camera captures the images.

3.4 Results and discussion

Poly(AA) hydrogels preparation

Polyacrylamide (PAA) hydrogels are biocompatible, low cost and ease to prepare. Usually, the preparation of PAA hydrogels by free radical polymerization (FRP) involves mixtures of acrylamide, bisacrylamide and catalysts for the polymerization such as tetramethylenediamine (TEMED) and ammonium persulfate (APS). In this work, PAA hydrogels were made both using ultraviolet (UV) photocrosslinking with Irgacure 2959 or through thermal crosslinking with KPS in the oven at 60 °C, thus avoiding the use of toxic catalysts.

Table 2

Structuring parameters of DILP fabrication process for PET masters.

Master by DILP	Period (μm)	P_{laser} (J/cm^2)	Spot overlap[a] p (μm)	hatch distance h (μm)
P6H–H	5.90	1.8	8	23.6
P4H–H	4.00	1.8	8	19.5
P3H–H	3.00	1.8	5	20.9

[a] During the holographic pattern registration, the spot overlap is the pulse separation distance that measures the overlap of two successive laser spots, when the pulsed laser moves vertically [27].

PAA hydrogel composition has been optimized varying the ratio of monomer (acrylamide) to crosslinker (bisacrylamide) in order to obtain the desired hydrogel properties. Moreover, hydrogel properties such as transparency, porosity, mechanical stability, and malleability have been optimized for applying them as label-free optical sensors. The optical and mouldability properties sought were observed for hyd10 and hyd11 compositions (Table S1, supporting information). From the swelling and morphology characterizations, hyd10 composition (Fig. 1.) was chosen for DNA-based hydrogel preparation both for microarray format and for surface relief gratings fabrication.

Hydrogel bio-functionalization

In order to provide the sensitivity and selectivity for the hydrogel-based sensors designed, they were functionalized with a DNA probe, as biorecognition group. Firstly, thiol-modified DNA were used to introduce the DNA functionality in AA/GMA hydrogels by thiol-epoxy covalent binding, triggered by UV light. Secondly, another approach for DNA-based hydrogel preparation, was to use an acrydite-modified DNA to directly co-polymerize with AAM monomers. Commercially available thiol and acrydite-modified oligonucleotides were used for the proposed approaches.

Initially, several AA/GMA hydrogel compositions were tested for the immobilization of thiolate probes (highlighted in red in Table S1, supporting information) which was carried out both before and after the curing process. Fluorescence was measured after irradiation and after washing with a homemade surface fluorescence reader (SFR). It was not possible to directly monitor the immobilization using the fluorophore-labeled probes, because both KPS initiation and prolonged UV irradiation cause fluorophore quenching. Therefore, in order to demonstrate that the immobilization occurs and how effective it is for the hydrogel, unlabeled probes were used and the hybridization assay performed with the targets marked with the fluorophore. Following various immobilization strategies being investigated, polyAA/GMA hydrogel with thiol-modified DNA did not provide a higher fluorescent signal compared to the negative control which did not bear the thiol group. Hence, it was possible to conclude that thiol-probes (Probe 1) were physically trapped in the 3D hydrogel network. Subsequent hybridization assays with the target did not show good selectivity. Thus, the hyd10 composition, without GMA co-monomer, was employed for the second approach. Hydrogels (hyd10) with 0.5 μM of the acrydite modified DNA were prepared by both thermal and photochemical activations. After the hybridization assay, in both cases, it was demonstrated that a chemical immobilization of the acrydite-modified DNA occurs. Acrydite modified oligonucleotides had a similar reactivity as free acrylamide monomers allowing high incorporation efficiency. The swelling of hyd10 with and without probe was measured and compared, hyd10 without probe had higher swelling capacity (550%) than hyd10 with the probe incorporated (200%), which supports the effective inclusion of the probe in the polymer (Fig. 2.). Indeed, after hybridization with the labeled target and overnight washing with SCC1x buffer, a significant difference was observed in the fluorescence signals between hyd10-DNA and its controls systems not bearing the acrydite termination (Fig. 3.). This result indicated that the covalent binding of acrydite modified oligonucleotides to the acrylamide chains occurs and, in addition, the DNA-based hydrogel specifically recognized its complementary DNA strand. The optimized DNA-hydrogel composition was applied to create fluorescence microarrays as well as for the fabrication of diffractive surface relief gratings, as examples of its versatile possibilities and applications.

DNA-hydrogels chips fabrication and hybridization assay

For the microarray fabrication, glass surfaces were functionalized with 3-(trimethoxysilyl)propylmethacrylate (2% in toluene). Hence, DNA-hydrogels chips were prepared by spotting the prepolymer solution with acrydite oligonucleotides, as well as with the crosslinker and the photo initiator, onto a modified glass slide.
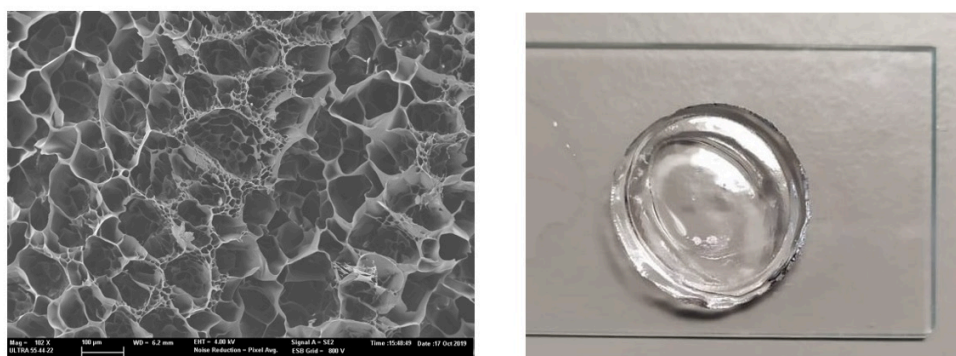
Fig. 1. On the left: SEM micrograph of lyophilized acrylamide hydrogel (hyd10) cross-section; on the right its digital photo.
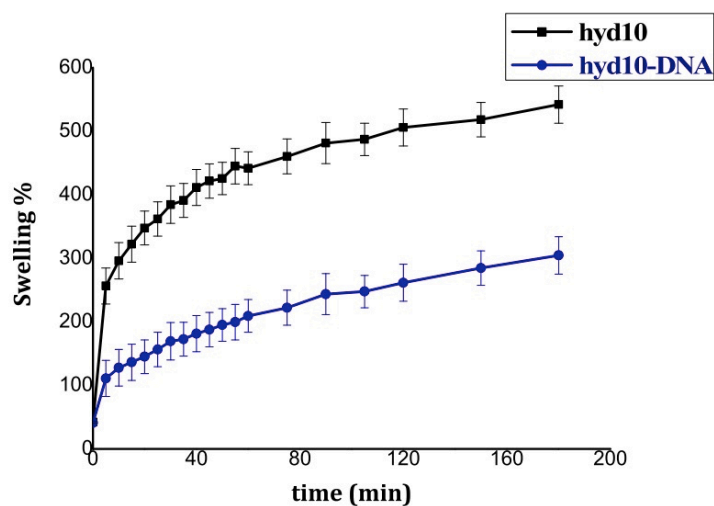
Fig. 2. Swelling kinetics of hyd10 and hyd10-DNA after immersion in PBS-T.

Whereas, to prepare DNAchips comparing system, dilutions of acrydite-modified probes with the photo initiator were directly spotted on modified glass slides. Subsequently, the anchoring of the spots to the surface was induced by irradiation at 254 nm. As mentioned above, it was not possible to quantify the amount of probe immobilized using the labeled probe due to the quenching of the fluorophore caused by the irradiation. Thus, after exposure and washing, the applicability of the proposed strategy to attach DNA probes onto the hydrogel network was assessed through hybridization assays with the target, establishing its sensitivity (Scheme 1). For that, Cy5-labeled complementary oligonucleotide in the hybridization buffer was dispensed, incubated for 1 h at 37 °C, and, after rinsing and drying, the fluorescence intensity was registered with a microarray surface reader SensoSpot. Results obtained demonstrated that the acrydite-probe was covalently immobilized into the 3D hydrogel network and, moreover, it specifically recognized the target. Further, an increased binding capacity of DNA in hydrogel spots compared to planar spots was observed. Thus, a calibration curve for Target (Fig. 4.) was measured by spotting increasing concentrations of Target (from 0 to 5 μM) and fluorescence obtained after hybridization was interpolated in the curve to determine the amount of target retained on the spot. For a probe concentration of 5 μM in the case of hyd-DNA 2.36 pmol cm^{-2} of target were quantified, while in the case of direct immobilization without hydrogel, for a probe concentration of 10 μM only 0.08 pmol cm^{-2} of Target resulted hybridized. Another advantage of these hydrogels was their transparency and consequently a very low signal background. It is well-known that three-dimensional (3D) volume immobilization in porous gels provides increased loading capacity, compared to two dimensional (2D) surfaces and, as a result, the sensitivity of the microarray was highly improved.

(A)

(B)
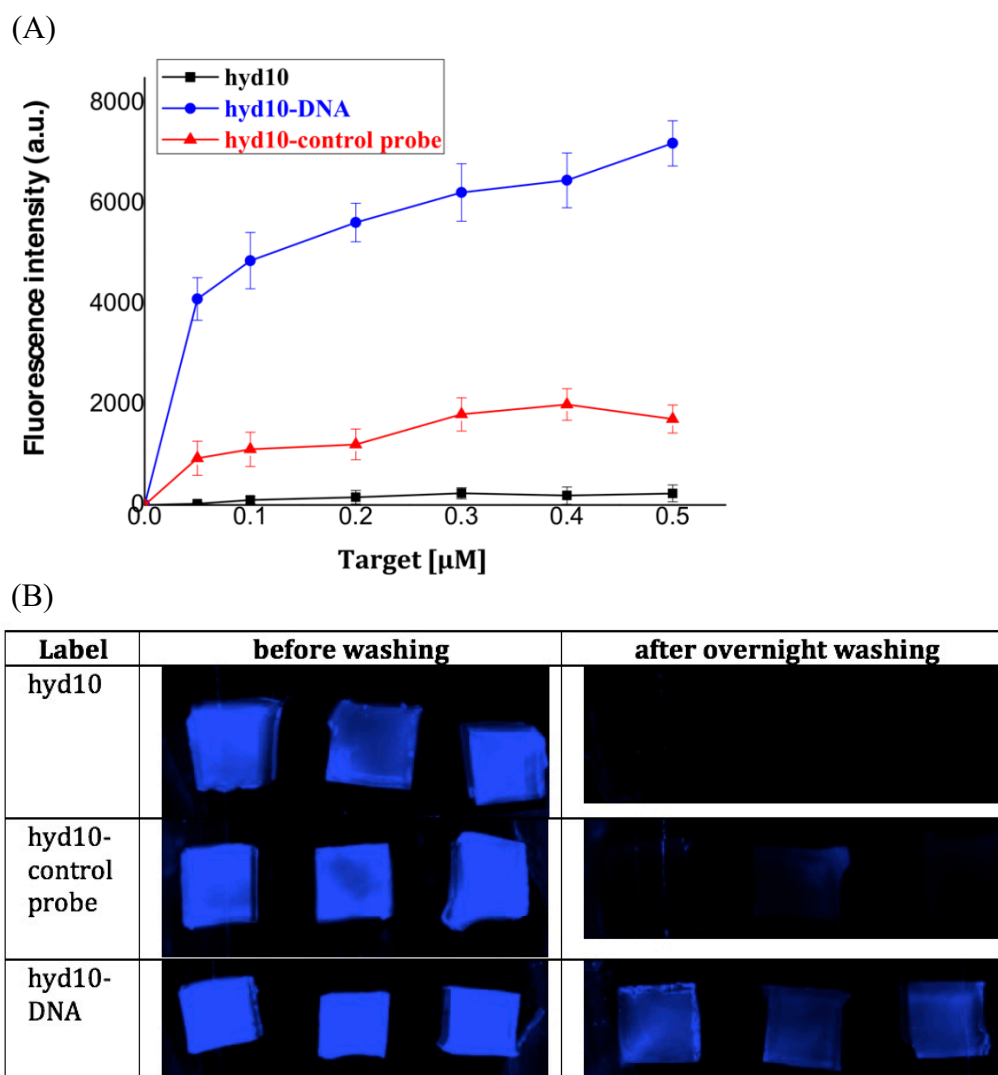
Fig. 3. (A) Hybridization assay curve of thermally obtained hyd10-DNA and its reference systems (hyd-without probe and hyd-control probe not bearing the acrydite tag) after washing overnight with SCC1x. (B) Images of hyd10-DNA and its controls obtained with a homemade surface fluorescence reader (SFR) after the hybridization with 0.2 µM of labeled Target (Table 1), before and after overnight washing.
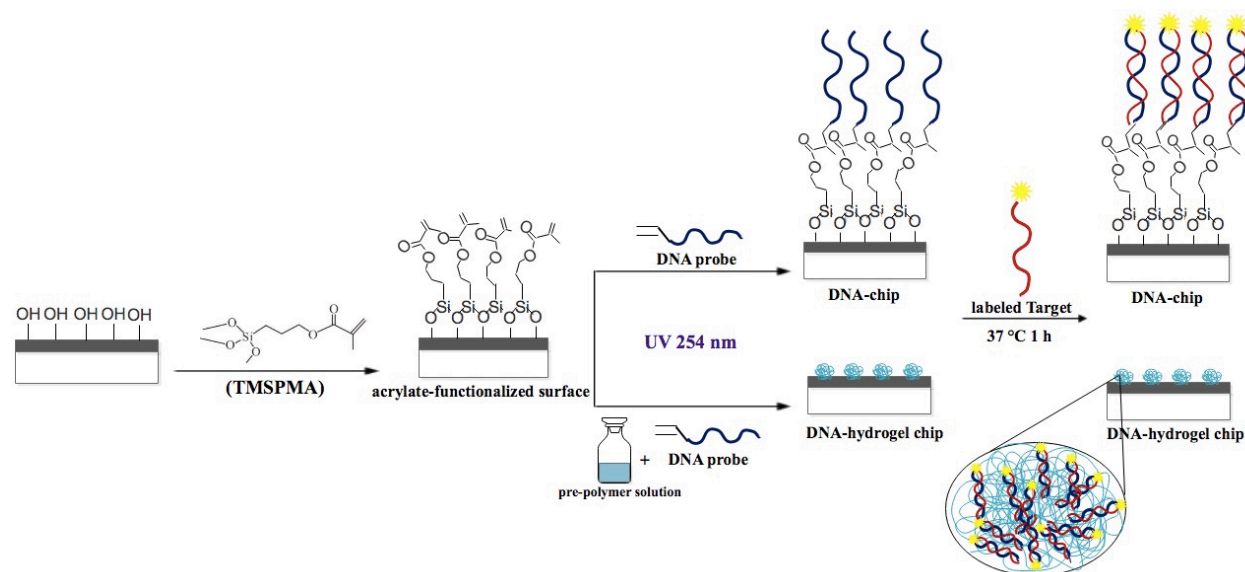
Scheme 1. Immobilization process of oligonucleotides for both 2D and 3D microarrays.

$y = 5652,8 \text{ x} - 418,15$

$R^2 = 0,9989$
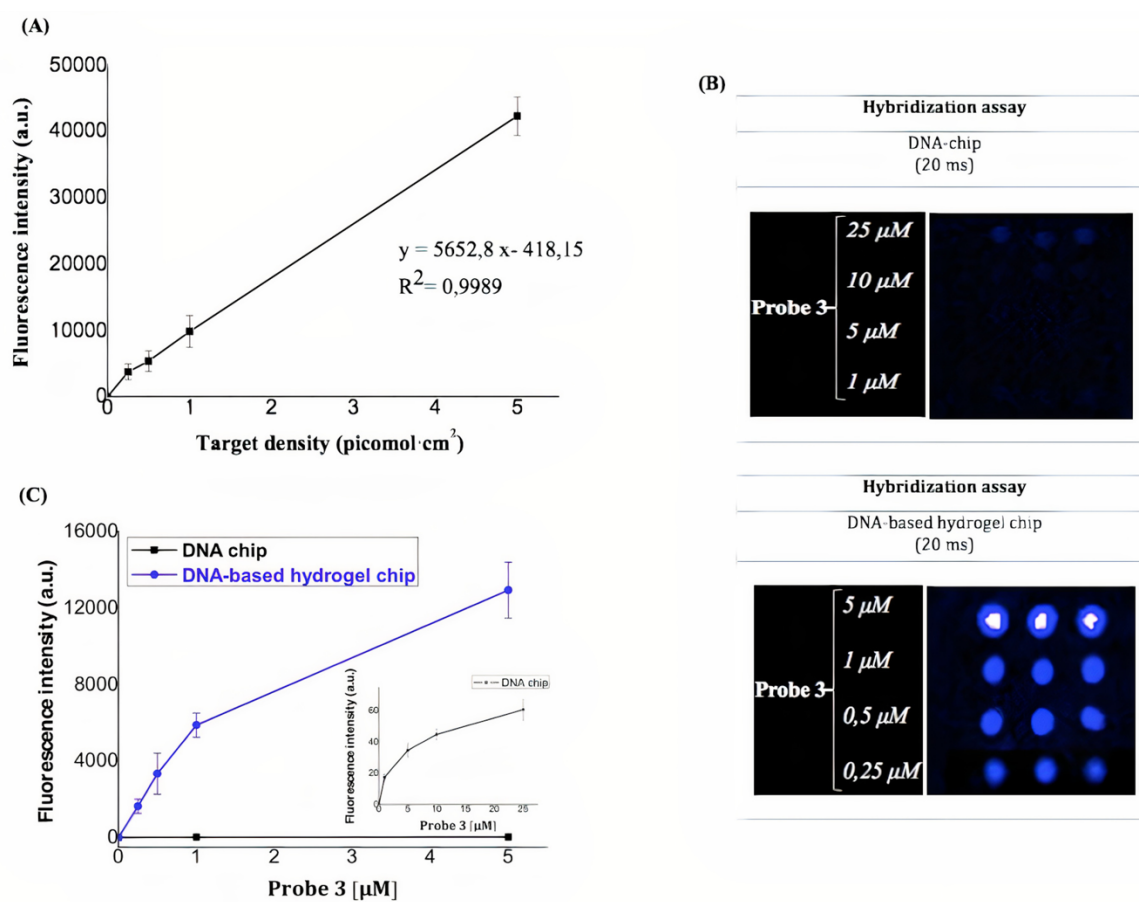
Fig. 4. (A) Calibration curve of the Target ranging from 0 to 5 mM. Spotted concentrations were transformed into picomol·cm^{-2} considering the spotted volume (10 nL) and the spot diameter (1000 mm). The regression equation and regression coefficient are shown in the plot. (B) Fluorescence images of DNA-based hydrogel chip and DNA-chip, after hybridization with the complementary labeled probe (Target at 5 µM), measurements at 20 ms are shown to appreciate the signal in the DNAchip microarray. (C) Hybridization assay curve (5 µM of the labeled target) obtained measuring at λ 650 nm, 5 ms for different probe concentrations. The inset in the plot is a close up of the hybridization curve for the DNA chip.
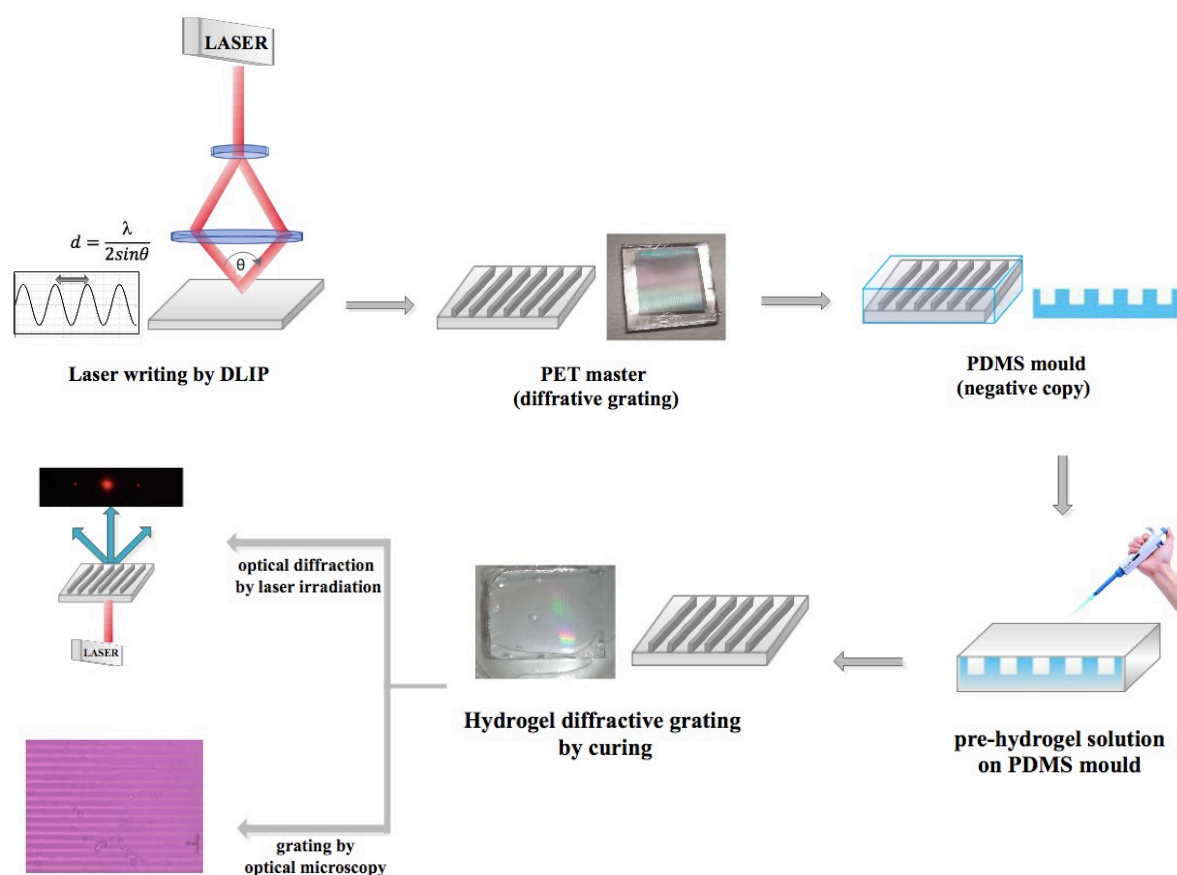
Fig. 5. Schematic representation of the sensor design process obtained by direct laser writing (DLIP) and replica molding technique (REM). REM consist of transferring the pattern on the master into PDMS stamps and finally transferring the pattern on the PDMS back into a replica of the original master by solidifying the prepolymer solution against the PDMS mold. After the fabrication, hydrogel diffractive gratings (rainbow diffraction when illuminated by white light), when hydrated, were optically characterized under laser illumination and by optical microscope (OM).

Towards label-free biosensing

Diffraction gratings can be employed to transduce biorecognition processes into measurable signals, with the aim of label-free detection of specific molecules. Thus, hydrogels (hyd10) diffraction gratings were fabricated by replica molding from holographic PET molds (see Materials Section). The tuned properties of the optimized material allowed the grating replication and the diffraction of the gratings was observed through a laser beam (660 nm) incident from the bottom side of the hydrogel (Fig. 5.). The diffraction pattern obtained on the hydrogel surface showed equally spaced diffraction spots, which indicated that a regular, periodic hydrogel grating was formed as it was possible to observe by laser irradiation and optical microscopy OM (Fig. S5, supporting information). Notably, the distance between the diffraction spots changed when the water content in the hydrogel raised. The grating period increased when the hydrogel swells owing to the absorption of water, but the straight shapes of the line structures were preserved, which demonstrated the optical tunability of the fabricated structure. Surface relief grating with good optical and physical properties were obtained, as resulted from the optical characterization. Diffraction efficiencies of PET masters, and DNA-hydrogels dry, fully hydrated, and after incubation with the complementary strand were measured, they varied between 2% and 11%. Distances in the diffraction first order were also measured. The data are provided in Table S2 in the supporting information. Typically, the binding of the analyte triggers a response of the hydrogel, such as changes in its swelling volume, mass, optical or mechanical properties. Our next step is the continuous monitoring of these changes for future application in label-free detection.

3.5 Conclusions

A rapid strategy for the covalent immobilization of DNA onto hydrogel network using the UV-initiated free radical polymerization has been developed to efficiently detect DNA. The DNA-hydrogel microarrays fabricated, thereby, allowed high and reproducible yields, increased stability of the attachment and low non-specific binding. The fabrication process was simple, consisting of one step and was very rapid.

Overall, it was possible to covalently incorporate the bioreceptor group in the hydrogel network and demonstrate the bio-sensing properties by DNA hybridization assays. Indeed, the resulting DNA-hydrogel microarrays exhibited a high density of bioavailable oligonucleotide probes. Furthermore, the hydrogel containing the DNA probe was easily fabricated into a diffractive grating and shown optimal diffractive properties thanks to its high optical transparency and mouldability. Accordingly, our future objective will be the combination of this highperformance biosensor with transductors that allow working in labelfree format. Hence, the developed strategy could be applied to the fabrication of point-of-care devices for biomolecular detection in medical diagnostics.

CRediT authorship contribution statement

Paola Zezza: Investigation, Writing – original draft. **María Isabel Lucío:** Methodology, Writing – review & editing. **Ángel Maquieira:** Writing – review & editing, Supervision, Funding acquisition. **María-José Bañuls:** Conceptualization, Methodology, Writing – original draft, Supervision, Funding acquisition.

Declaration of competing interest

The authors declare that they have no known competing financial interests or personal relationships that could have appeared to influence the work reported in this paper.

3.6 References

[1] I.Y. Jung, J.S. Kim, B.R. Choi, K. Lee, H. Lee, Hydrogel based biosensors for in vitro diagnostics of biochemicals, proteins, and genes, Adv. Healthc. Mater. 6 (2017) 1–19, https://doi.org/10.1002/adhm.201601475.

[2] A. Vashist, A. Vashist, Y.K. Gupta, S. Ahmad, Recent advances in hydrogel based drug delivery systems for the human body, J. Mater. Chem. B. 2 (2014) 147–166, https://doi.org/10.1039/c3tb21016b.

[3] N. Oliva, J. Conde, K. Wang, N. Artzi, Designing hydrogels for on-demand therapy, Acc. Chem. Res. 50 (2017) 669–679, https://doi.org/10.1021/acs. accounts.6b00536.

[4] J.L. Drury, D.J. Mooney, Hydrogels for tissue engineering: scaffold design variables and applications, Biomaterials 24 (2003) 4337–4351, https://doi.org/10.1016/ S0142-9612(03)00340-5.

[5] F. Ullah, M.B.H. Othman, F. Javed, Z. Ahmad, H.M. Akil, Classification, processing and application of hydrogels: a review, Mater. Sci. Eng. C 57 (2015) 414–433, https://doi.org/10.1016/j.msec.2015.07.053.

[6] Q. Chai, Y. Jiao, X. Yu, Hydrogels for biomedical applications: their characteristics and the mechanisms behind them, Gels (2017) 3, https://doi.org/10.3390/ gels3010006.

[7] K. Deligkaris, T.S. Tadele, W. Olthuis, A. van den Berg, Hydrogel-based devices for biomedical applications, Sensor. Actuator. B Chem. 147 (2010) 765–774, https:// doi.org/10.1016/j.snb.2010.03.083.

[8] J. Gaˇcanin, C.V. Synatschke, T. Weil, Biomedical applications of DNA-based hydrogels, Adv. Funct. Mater. 30 (2020), https://doi.org/10.1002/ adfm.201906253.

[9] I. Barbulovic-Nad, M. Lucente, Y. Sun, M. Zhang, A.R. Wheeler, M. Bussmann, Biomicroarray fabrication techniques - a review, Crit. Rev. Biotechnol. 26 (2006) 237–259, https://doi.org/10.1080/07388550600978358.

[10] S.J. Oh, B.J. Hong, K.Y. Choi, J.W. Park, Surface modification for DNA and protein microarrays, OMICS A J. Integr. Biol. 10 (2006) 327–343, https://doi.org/ 10.1089/omi.2006.10.327.
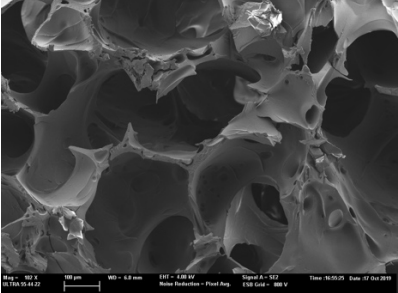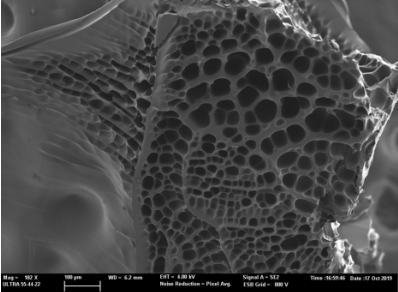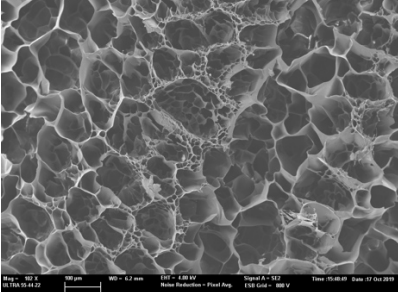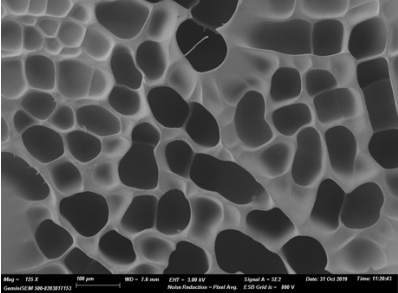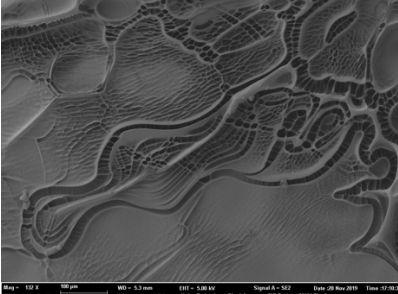
[11] A.Y. Rubina, S.V. Pan'kov, E.I. Dementieva, D.N. Pen'kov, A.V. Butygin, V. A. Vasiliskov, A.V. Chudinov, A.L. Mikheikin, V.M. Mikhailovich, A.D. Mirzabekov, Hydrogel drop microchips with immobilized DNA: properties and methods for large-scale production, Anal. Biochem. 325 (2004) 92–106, https://doi.org/ 10.1016/j.ab.2003.10.010.

[12] A.Y. Rubina, E.I. Dementieva, A.A. Stomakhin, E.L. Darii, S.V. Pan'kov, V. E. Barsky, S.M. Ivanov, E.V. Konovalova, A.D. Mirzabekov, Hydrogel-based protein microchips: manufacturing, properties, and applications, Biotechniques 34 (2003) 1008–1022, https://doi.org/10.2144/03345rr01.

[13] J. Liu, Oligonucleotide-functionalized hydrogels as stimuli responsive materials and biosensors, Soft Matter 7 (2011) 6757–6767, https://doi.org/10.1039/ c1sm05284e.

[14] N. Gupta, B.F. Lin, L.M. Campos, M.D. Dimitriou, S.T. Hikita, N.D. Treat, M. V. Tirrell, D.O. Clegg, E.J. Kramer, C.J. Hawker, A versatile approach to highthroughput microarrays using thiol-ene chemistry, Nat. Chem. 2 (2010) 138–145, https://doi.org/10.1038/nchem.478.

[15] F.N. Rehman, M. Audeh, E.S. Abrams, P.W. Hammond, M. Kenney, T.C. Boles, Immobilization of acrylamide-modified oligonucleotides by co-polymerization, Nucleic Acids Res. 27 (1999) 649–655, https://doi.org/10.1093/nar/27.2.649.

[16] K. Gawel, D. Barriet, M. Sletmoen, B.T. Stokke, Responsive Hydrogels for LabelFree signal transduction within biosensors, Sensors 10 (2010) 4381–4409, https:// doi.org/10.3390/s100504381.

[17] S. Kabilan, A.J. Marshall, A. Horgan, C.D. Creasey, S.J. Kew, K.E.S. Dean, S. F. Terrell, L.J. Affleck, "Smart" holograms - a novel diagnostics platform, 2006 NSTI Nanotechnol, Conf. Trade Show - NSTI Nanotech 2006 Tech. Proc. 3 (2006) 467–470.

[18] A.K. Yetisen, H. Butt, L.R. Volpatti, I. Pavlichenko, M. Humar, S.J.J. Kwok, H. Koo, K.S. Kim, I. Naydenova, A. Khademhosseini, S.K. Hahn, S.H. Yun, Photonic hydrogel sensors, Biotechnol. Adv. 34 (2016) 250–271, https://doi.org/10.1016/j. biotechadv.2015.10.005.

[19] A.K. Yetisen, I. Naydenova, F. Da Cruz Vasconcellos, J. Blyth, C.R. Lowe, Holographic sensors: three-dimensional analyte-sensitive nanostructures and their applications, Chem. Rev. 114 (2014) 10654–10696, https://doi.org/10.1021/ cr500116a.
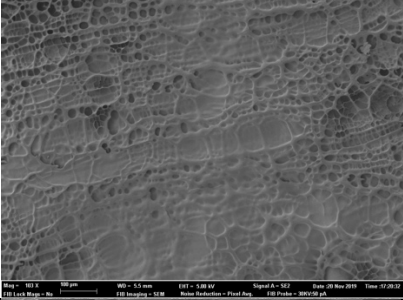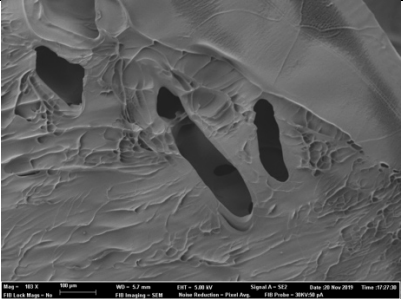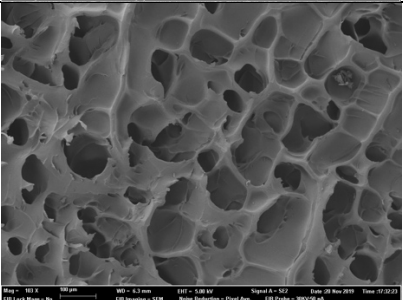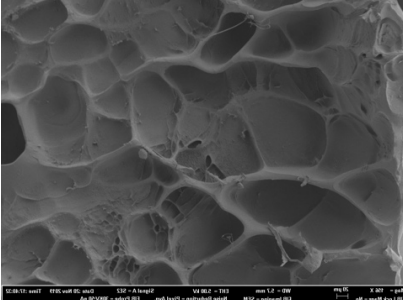
[20] G. Ye, X. Wang, Polymer diffraction gratings on stimuli-responsive hydrogel surfaces: soft-lithographic fabrication and optical sensing properties, Sensor. Actuator. B Chem. 147 (2010) 707–713, https://doi.org/10.1016/j. snb.2010.03.052.

[21] J.J. Zhao, W. Wang, W. Wang, F. Wang, Y. Zhao, Q.W. Cai, R. Xie, R. Xie, X.J. Ju, X. J. Ju, Z. Liu, Z. Liu, Y. Faraj, Y. Faraj, L.Y. Chu, Smart hydrogel grating immunosensors for highly selective and sensitive detection of human-IgG, Ind. Eng. Chem. Res. 59 (2020) 10469–10475, https://doi.org/10.1021/acs.iecr.0c00780.

[22] X. Wang, X. Wang, Aptamer-functionalized hydrogel diffraction gratings for the human thrombin detection, Chem. Commun. 49 (2013) 5957–5959, https://doi. org/10.1039/c3cc41827h.

[23] M.I. Lucío, A.H. Montoto, E. Fern´ andez, S. Alamri, T. Kunze, M.J. Banuls, A. Maquieira, Label-free detection of C-Reactive protein using bioresponsive hydrogel-based surface relief diffraction gratings, Biosens. Bioelectron. 193 (2021) 113561, https://doi.org/10.1016/j.bios.2021.113561.

[24] G. Ye, C. Yang, X. Wang, Sensing diffraction gratings of antigenresponsive hydrogel for human immunoglobulin-G detection, Macromol. Rapid Commun. 31 (2010) 1332–1336, https://doi.org/10.1002/marc.201000082.

[25] D. Mira, R. Llorente, S. Morais, R. Puchades, A. Maquieira, J. Marti, Highthroughput screening of surface-enhanced fluorescence on industrial standard digital recording media, Opt. Based Biol. Chem. Sens. Def. 5617 (2004) 364, https://doi.org/10.1117/12.578301.

[26] J. Diani, K. Gall, Finite Strain 3D Thermoviscoelastic Constitutive Model, Society, 2006, pp. 1–10, https://doi.org/10.1002/pen.

[27] A.I. Aguilar-Morales, S. Alamri, T. Kunze, A.F. Lasagni, Influence of processing parameters on surface texture homogeneity using Direct Laser Interference Patterning, Opt Laser. Technol. 107 (2018) 216–227, https://doi.org/10.1016/j. optlastec.2018.05.044.
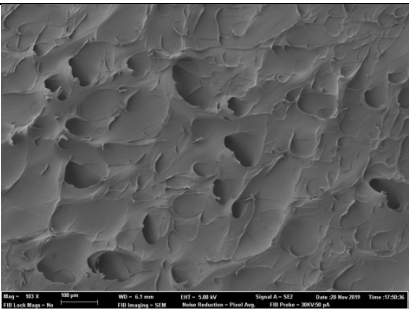
3.7 Supplementary information

Table S1. Experimental synthesis conditions for the AAM-based hydrogels. Other compositions with higher amounts of GMA (0.04 %w/v) were also prepared, but in all the cases the hydrogels lost the transparency. Therefore, hydrogel compositions with more than 0.02% *(w/v)* of GMA were not considered for the development of the optical biosensor.

Label	AAM %(w/v)	MBA %(w/v)	GMA %(w/v)	Notes	SEM images
hyd0	19	0.6	0	transparent	
hyd1	19	0.6	0.005	transparent	
hyd2	19	1.3	0.005	transparent, breakable	
hyd3	19	2.6	0.005	hard, transparent	
hyd4	19	0.6	0.01	soft and transparent	
hyd5	19	1.3	0.01	soft and transparent	

hyd6	19	2.6	0.01	surface wrinkles	
hyd7	19	0.6	0.02	soft and transparent	
hyd8	19	1.3	0.02	transparent, breakable	
hyd9	19	2.6	0.02	trasparent and hard	
hyd10	25	0.6	0	transparent, good mechanical properties	
hyd11	25	0.6	0.01	soft and trasparent	
hyd12	25	1.3	0.01	soft and trasparent	

hyd13	25	2.6	0.01	hard and transparent	
hyd14	25	3.9	0.01	hard and transparent	
hyd15	25	5.2	0.01	hard and transparent	
hyd16	25	6.5	0.01	hard and transparent	
hyd17	32	0.3	0.01	soft and trasparent	
hyd18	32	0.6	0.01	soft and trasparent	
hyd19	32	1.3	0.01		

				soft and trasparent	
hyd20	32	2.6	0.01	hard and transparent	
hyd21	32	3.9	0.01	hard and transparent, surface wrinkles	
hyd22	32	5.2	0.01	hard and white	
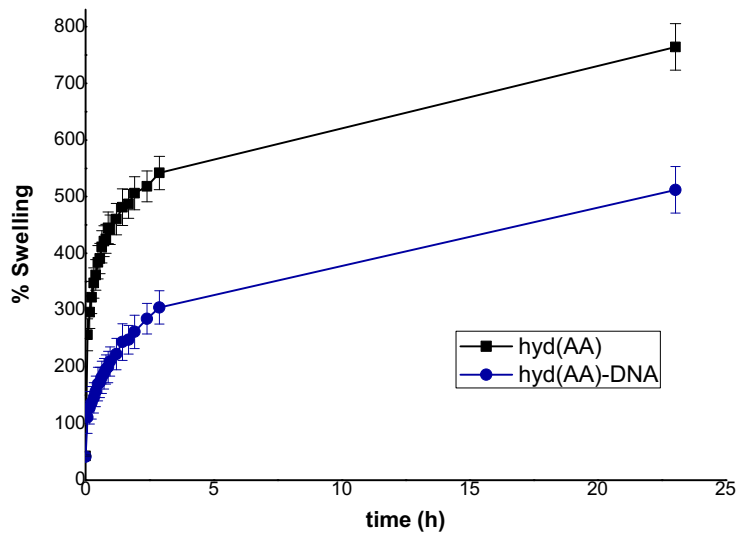
Fig S1. Swelling kinetics of hyd10 and hyd10-DNA until 24 hours after immersion in PBS-T.
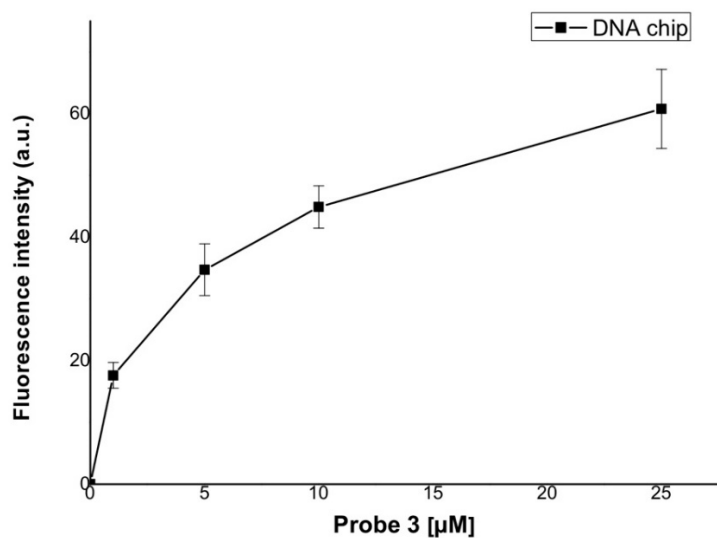
Fig S2. Hybridization curve with 5 μM of Target for a microarray with increasing concentration of Probe 3 covalently attached onto an acrylate-modified glass slide.
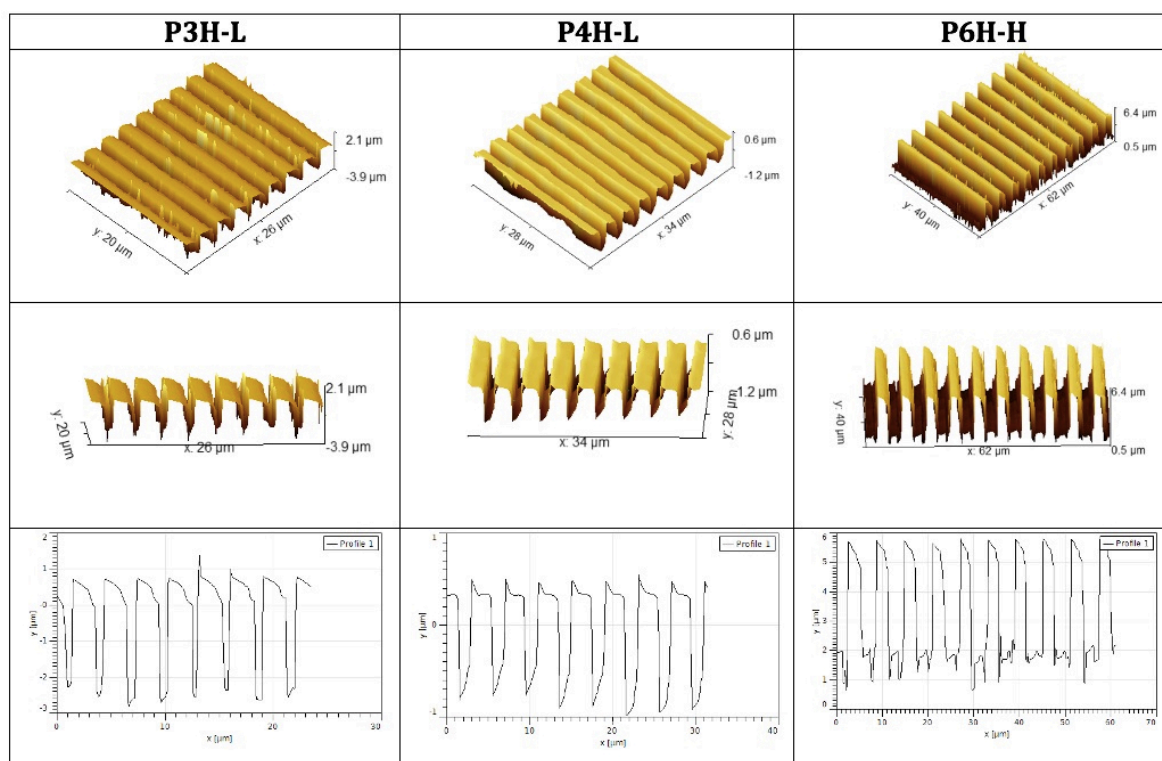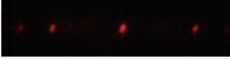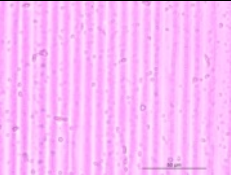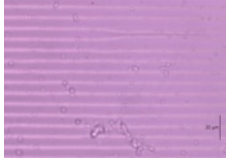
Fig S3. Atomic force microscopy (AFM) profiles of PET master P6H-H, P4H-L and P3H-L (the two last masters have a "low" depth, but the profile coincide with "high" depth ones. The reason why it was not possible to record the profile of the masters P4H-H and P3H-H is because it is more difficult due to the tip that has to go deeper.

Table S2. Diffraction efficiencies (DE%), distances in the first-order diffraction (d (mm)), and periods gratings calculated from the distances (d (mm)) for the PET masters, DNA-hydrogels dry, fully hydrated, and after hybridization with the complementary strand. The amount of probe and target used is indicated in the last columns.

	PET master	DNA-hydrogel (dry)	DNA-hydrogel (hydrated)	DNA-hydrogel after target hybridization (hydrated)	Probe (mM)	Target (mM)
P3H-H					0.5	2
d (mm)	420 ± 3	592 ± 3	311 ± 2	280 ± 3		
d (μm) = $2\lambda h/d1\text{-}1$	3.01	2.14	4.08	4.52		
DE %	11.5 %		5.7 %	5.9 %		
P4H-H					1	1
d(mm)	312.4 ± 0.4	470.4 ± 1.1	230 ± 12	247 ± 3		
d (μm) = $2\lambda h/d1\text{-}1$	4.05	2.69	5.40	5.12		
DE %	2.13 %		2.23 %	2.79 %		
P6H-H					1	2
d(mm)	212.2 ± 0.3	346.9 ± 1,3	156.4 ± 1.8	150.4 ± 0.7		
d (μm) = $2\lambda h/d1\text{-}1$	5.97	3.65	8.12	8.40		
DE %	5.36 %		3.31%	2.68%		

	PET master	DNA-hydrogel (dry)	DNA-hydrogel (hydrated)	DNA-hydrogel after target hybridization (hydrated)
P6H-H				
d(mm)	212.2 ± 0.3	346.9 ± 1.3	156.4 ± 1.8	150.4 ± 0.7
d (µm) = $2\lambda h/d_{1-1}$	5.97	3.65	8.12	8.40
DE %	5.36 %		3.31%	2.68%

Fig S4. Images of the diffraction spots measured for P6H-H grating with the optical setup employed to obtain the data in Table S2.

	Hydrated DNA-hydrogel (OM)
P3H-H	
P4H-H	
P6H-H	

Fig S5. Images by optical microscope (OM) of DNA-hydrogels, replicated using masters with different periods.

Surface Micro-Patterned Biofunctionalized Hydrogel for Direct Nucleic Acid Hybridization

4- Chapter 4. Surface Micro-Patterned Biofunctionalized Hydrogel for Direct Nucleic Acid Hybridization

In this chapter, a different strategy for hydrogels covalent biofunctionalization with DNA probes is addressed. The novelty lies in combining the main monomer with an alkyne-bearing co-monomer that allows for more effective immobilisation of the probes and, consequently, greater sensitivity towards the analyte to be detected. In particular, two different methods of immobilization were performed, during or after the formation of the hydrogel, endowing greater flexibility for the construction of the holographic transducer. The strategy developed is based on the use of photochemical *click* chemistry reactions between thiol-ene/thiol-yne groups.

Subsequently, surface micro-patterns were fabricated by a combination of Direct laser interference patterning (DLIP) and replica molding on the surface of the hydrogels to investigate label-free biosensing. The surface microstructures of the DNA-based hydrogels were incubated with the target probe and control probes in order to achieve selective hybridisation. The recognition products are optically detected by both fluorescence and holographic diffraction. The Surface relief grating (SRG) acts as a transducer that diffracts light, producing a measurable signal proportional to the probe–target interaction. The aim is to evaluate the analytical performance of this new technology based on a hydrogel as a DNA carrier and detector, in order to obtain a sensitive and specific low-cost POC device to detect the direct hybridisation of oligonucleotides.

Surface Micro-Patterned Biofunctionalized Hydrogel for Direct Nucleic Acid Hybridization Detection

Paola Zezza[1], María Isabel Lucío[1], Estrella Fernández[1], Ángel Maquieira[1,2], María-José Bañuls*[1,2]

[1] *Instituto Interuniversitario de Investigación de Reconocimiento Molecular y Desarrollo Tecnológico (IDM), Universitat Politécnica de València, Universitat de Valéncia, Camino de Vera s/n, 46022, Valencia, Spain. E-mail: mbpolo@upv.es*
[2] *Departamento de Quimica, Universitat Politécnica de Valéncia, Camino de Vera s/n, 46022, Valencia, Spain.*

4.1 Abstract

The present research is focused on the development of a biofunctionalized hydrogel with a surface diffractive micropattern as a label-free biosensing platform. The biosensors described in this paper were fabricated with a holographic recording of polyethylene terephthalate (PET) surface micro-structures, which were then transferred into a hydrogel material. Acrylamide-based hydrogels were obtained with free radical polymerization, and propargyl acrylate was added as a comonomer, which allowed for covalent immobilization of thiolated oligonucleotide probes into the hydrogel network, via thiol-yne photoclick chemistry. The comonomer was shown to significantly contribute to the immobilization of the probes based on fluorescence imaging. Two different immobilization approaches were demonstrated: during or after hydrogel synthesis. The second approach showed better loading capacity of the bioreceptor groups. Diffraction efficiency measurements of hydrogel gratings at 532 nm showed a selective response reaching a limit of detection in the complementary DNA strand of 2.47 µM. The label-free biosensor as designed could significantly contribute to direct and accurate analysis in medical diagnosis as it is cheap, easy to fabricate, and works without the need for further reagents.

4.2 Introduction

Nowadays, the interest in developing affordable and mass-producible clinical diagnostics devices is increasing to improve accessibility to healthcare worldwide. Having fast and self-monitoring tests that allow detection onsite is a global interest to avoid hospital crowding and the spreading of contagious diseases. Definitely, the development of portable devices for point-of-care testing (POCT), which allows fast analyte detection with an easily interpretable readout, is crucial for the future [1]. POCT is presently available for a variety of analyses, for example, pregnancy tests, infectious disease tests (such as respiratory infections and sexually transmitted diseases), glucose tests, and several other applications [2–6]. Among various types of sensors, optical biosensors present great advantages over conventional analytical techniques because they enable direct, real-time, and label-free detection of many biological and chemical substances [7–9].

Their advantages include high sensitivity, small size, light weight, cost-effectiveness, and the ability to provide multiplexed or distributed sensing. In this context, holographic biosensors offer an appealing approach for label-free optical biosensing. Holographic sensors are gratings, recorded with holographic techniques, of functionalized polymers capable of quantifying the concentration of the target analyte [10]. As a transducer, a holographic pattern is recorded in the sensitive polymer structure, which consists of a 3D periodic structure with alternating strips of differing refractive index (RI), and thus it diffracts the light. After the holographic recording, the polymer matrix, permeable to the target analyte, changes its physical and chemical characteristics, such as lattice spacing and/or refractive index based on its interaction with the target analyte, and produces a change in the diffraction pattern. So far, various hydrophilic and hydrophobic polymers have been used for the fabrication of holographic sensors including gelatin, poly(2-hydroxyethyl methacrylate) (pHEMA), poly(acrylamide) (pAAM), and polyvinyl alcohol (PVA). Their application includes humidity, temperature, and pressure sensors, as well as glucose, lactate, electrolytes, and pH chemical sensors [11]. However, there are very few examples using bioreceptors, mainly antibodies, to achieve holographic biosensing, with their use for nucleic acid hybridizations not being reported. In this work, an Acrylamide/Propargyl acrylate (AM/PA) hydrogel is used, simultaneously, as a matrix for the holographic pattern fabrication and for the functionalization with single strand thiolated oligonucleotides as a biorecognition element. Hydrogels are attractive platforms for bioanalysis thanks to their ability to retain large amounts of water, acting like biological tissues, optimal for biological interactions [12–16]. Hydrogel-based sensors found numerous applications in clinical diagnostics, biomedical research, environmental monitoring, and food testing [17–21]. Thus, because of their properties, hydrogels have been employed in POC systems for different purposes, which include cell and tissue immunostaining [22], localized photothermal heating [23], microneedle fabrication for drug delivery [24] or for interstitial fluid sampling [25], ion sensing [20], and cocaine, ochratoxin A [26], and glucose detection [27] as well as mRNA detection with hydrogel microparticles [28]. Here, a rapid, specific, and label-free detection system for nucleic acid hybridization based on surface relief holographic gratings was demonstrated.

To this aim, the surface of an oligonucleotide probe-functionalized hydrogel was micro-patterned [29]. Briefly, Acrylamide/Propargyl acrylate (AM/PA) hydrogels were obtained using the free radical polymerization (FRP) reaction, both thermally and photochemically activated. Using replica molding of holographic molds [30], a diffractive micropattern on the hydrogel surface was fabricated. It acts as a transducer that diffracts light, producing a measurable signal proportional to the probe–target interaction. The surface micropatterning technique that was used has some advantages: it is easy to manufacture, does not require expensive instrumentation, and allows the creation of patterns of micrometer size. To apply this surface micropatterned hydrogel in biosensing, DNA probes were incorporated into the network as bioreceptors for the target. In particular, covalent functionalization of thiolmodified ssDNA probes in acrylamide-based hydrogels was obtained using a photoclick thiol-ene reaction [31]. Hence, when hybridizing with the complementary strand, the hydrogel underwent changes that were monitored with optical diffraction measurements. The change in the diffraction efficiency of hydrogel gratings was specific for the complementary strand, given that this is the first time that holographic hydrogel gratings are used to detect the direct hybridization of oligonucleotides.

4.3 Materials and Methods

Chemicals

Acrylamide (AM), propargyl acrylate (PA), N, N' -methylenebis (acrylamide) (MBA), Potassium persulfate (KPS), 2,2-Dimethoxy-2-phenylacetophenone (DMPA) and Tetrahydrofuran (THF), sodium phosphate dibasic, potassium phosphate monobasic, sodium chloride, potassium chloride, sodium acetate, sodium citrate, ethylenediaminetetraacetic acid, and Tween-20 were purchased from Sigma–Aldrich (Madrid, Spain).

The acetate-Tris (2-carboxyethyl) phosphine buffer (Ac-TCEP, pH 4.5) consists of 25 mM of TCEP, 0.15 M sodium acetate, 0.1 M Ethylenediaminetetraacetic acid, and 0.1 M NaCl in DI water; the phosphate-buffered saline solution with 0.1% (v/v) of Tween 20 detergent (PBS-T, pH 7.4) consists of 137 mM NaCl, 2.7 mM KCl, 10 mM Na_2HPO_4, 1.8 mM KH_2PO_4; and the salinesodium citrate buffer (SSC1x, pH 7.4) consists of 0.15 M NaCl and 0.015 M sodium citrate. Polydimethylsiloxane (PDMS) Sylgard 184 was purchased from Dow Corning (Wiesbaden, Germany). The oligonucleotides were supplied by Sumilab (Valencia, Spain), and the sequences used are listed in Table S1.

Equipment

Hydrogel photopolymerization and bioreceptor immobilization with UV irradiation was carried out using a UV photoreactor LightOx PhotoReact 365 nm (13 mW/cm^2 light power) (Sigma–Aldrich, Madrid, Spain). Hydrogel fluorescence measurements were registered with a fluorescence microarray analyzer SensoSpot (Miltenyi Imaging GmbH, Radolfzell, Germany) (λex = 633 nm, λem = 670 nm). Fluorescence image data processing was performed with the GenePix Pro 4.0 software from Molecular Devices, Inc. (Sunnyvale, CA, USA).

The morphological characterization of hydrogels was carried out using scanning electron microscopy (SEM, Gemini SEM 500 system, Zeiss, Oxford Instruments, Oxford, UK). Hydrogels were completely swollen in distilled water and frozen at −20 °C. Then, they were lyophilized overnight (Telstar Lyoquest freeze-drier, Azbil Telstar Technologies, S. L. U., Terrasa, Spain) to yield completely dry aerogel samples. Finally, dry samples were prepared using sputter coating with an Au layer of about 15 nm (BAL-TEC SCD 005 sputter coater, Leica microsystems, Wetzlar, Germany). Fourier transform infrared (FT-IR) spectroscopy of lyophilized hydrogels was performed using a Tensor 27 FT-IR-spectrophotometer (Bruker, MA, USA). UV-Visible spectra of hydrogels immersed in H_2O were collected in an Agilent 8453 spectrophotometer (Santa Clara, CA, USA). For the analysis, hydrogels were polymerized inside an Eppendorf and, after washing, they were placed inside a 1 × 1 cm cuvette filled with H_2O.

Swelling behavior studies were carried out with lyophilized hydrogel samples. Samples with a size of approximately 1 cm^3 were immersed in PBS-T (10 mL) at room temperature. The weight of the swollen hydrogels was recorded at different times until they were totally swollen (reaching a constant weight). Buffer excess on the surface of the hydrogel was removed with filter paper before weighing. The swelling degree was calculated using Equation (1), where Wt is the weight of the hydrogel after being immersed in the buffer during time "t" and W0 is the weight of the lyophilized hydrogel before the immersion.

$$\% \ Swelling = \frac{Wt - Wo}{Wo} \ 100 \qquad (1)$$

Hydrogel Synthesis

Acrylamide/Propargyl acrylate (AM/PA) and acrylamide (AM) hydrogels were prepared using free radical polymerization (FRP) either with photochemical or thermal activation (Scheme S1). Different hydrogel compositions were optimized: AM(25)/PA, AM(8)/PA, AM(25), and AM(8). The AM(25)/PA hydrogel was prepared by mixing 25% (w/v) of AM monomer, 0.05% (w/v) of MBA crosslinker, and 15 µL of PA co-monomer in 1 mL of distilled water. The AM(8)/PA hydrogel was prepared by mixing 8% (w/v) of AM monomer, 0.25% (w/v) of MBA crosslinker, and 15 µL of PA co-monomer in 1 mL of distilled water. The control hydrogel AM(25) was prepared by mixing 25% (w/v) of AM monomer and 0.05% (w/v) of MBA crosslinker, while the control hydrogel AM(8) was prepared by mixing 8% (w/v) of AM monomer and 0.25% (w/v) of MBA crosslinker. For the synthesis of the hydrogel using thermal activation, potassium persulfate (KPS) at 1% (v/v) was added to the solution as a thermal initiator, and the reaction mixtures were placed in an oven at 60 °C for 90 min. For the synthesis of hydrogels with photochemical activation, 2,2-Dimethoxy-2-phenylacetophenone (DMPA) photoinitiator at 1% (w/v) was added to the reaction mixture and hydrogels were polymerized irradiating at 365 nm in a UV photoreactor (13 mW/cm^2) for 10 min. Once polymerized, the hydrogels were washed with immersion in distilled water for at least 2 h using three times fresh water to ensure that non-polymerized monomers were eliminated. The obtained hydrogels were stored completely swollen in distilled water at 4 °C.

Probe Immobilization and Hybridization Assay

For potential biosensing applications, AM/PA hydrogels and their control systems, AM hydrogels, were covalently functionalized with a thiol-modified oligonucleotide probe, and hybridization capacity was tested with a fluorescence-labeled target. All probes used are listed in Table S1. The bioreceptor immobilization was studied either during or after the hydrogel synthesis. In the first approach, after monomers and crosslinker homogenization in water, 1 μM of Probe 1 and 1% (w/v) of DMPA photoinitiator in water were added to the mixture, and the solution was irradiated at 365 nm (13 mW/cm^2) for 10 min. In this strategy, polymerization and bioreceptor immobilization were carried out simultaneously in one step. In the second approach, the already thermally synthesized hydrogels were cut into squares (0.5 × 0.5 cm) and immersed in 100 μL of 1 μM of Probe 1 and 1% (w/v) of DMPA photoinitiator in THF:Ac-TCEP 1:1. Then, the hydrogels were irradiated at 365 nm (13 mW/cm^2) for 30 min. In both approaches, after the immobilization step, the hydrogels were placed on an oscillator plate and washed overnight with PBS-T. For the hybridization assays, Probe 1-functionalized hydrogels of 0.5 × 0.5 cm were placed in a transparent ELISA (enzyme-linked immunosorbent assay) plate and equilibrated in 250 μL of SSC1x for 24 h. Then, SSC1x was discarded, and the hydrogels were incubated with 50 μL of Cy5-labeled, complementary strand Target 2, in SSC1x, at growing concentrations (0; 0.2; 0.4; 0.8; 1; 1.5; and 2 μM) for one hour at 37 °C. Fluorescence signals were collected immediately after the hybridization and after overnight washing with SSC1x. Control hydrogels having immobilized a non-complementary sequence (Probe 2) were also hybridized as described.

Surface Micropattern Fabrication

Surface microstructures made of Polyethylene terephthalate (PET) were fabricated using the direct laser interference patterning (DLIP) technique [32]. The DLIP system was equipped with a frequency quadrupled Q-switched laser head (TECH-263 Advanced Laserexport Co., Ltd., Moscow, Russia) with a maximum pulse energy of 50 μJ, operating at a wavelength of 263 nm and with a pulse duration shorter than 3 ns. A fluence of 0.09 J/cm^2 was used to obtain PET masters with a period of approximately 4 μm.

The structural features of the original PET master were characterized with a 3D optical profilometer (Sensofar, PLu neon, Terrasa, Spain). Hydrogel surface micropatterns were fabricated using the replica molding technique (REM) from the original PET master. The micropattern obtained on the hydrogel surface was observed with optical microscopy (OM, Leica microsystems, MZ APO, Wetzlar, Germany). Micropatterns were obtained in the hydrogel surface using replica molding (Scheme 1). Firstly, the original PET micropattern was copied onto PDMS. The PDMS solution was poured onto the PET surface, a vacuum was applied for 10 min to aid the solution-pattern adhesion, and then it was placed in the oven at 60 °C for 2 h. Secondly, the PDMS negative pattern was transferred onto the hydrogel surface. Initially, pre-polymeric solutions with monomers and crosslinkers of hydrogels AM(25)/PA, AM(25), AM(8)/PA, and AM(8) were stirred for 20 min until homogenization. Then, KPS was added, and the solution was sonicated for 2 min. The solutions were poured onto different PDMS micropatterned surfaces, a vacuum was applied for 10 min, and then they were placed in an oven at 60 °C for 1.5 h. Once polymerized, they were peeled off and washed with immersion in distilled water for at least 2 h using three times fresh water to ensure that non-polymerized monomers were eliminated. The micropatterned hydrogels were stored completely swollen in distilled water at 4 °C.
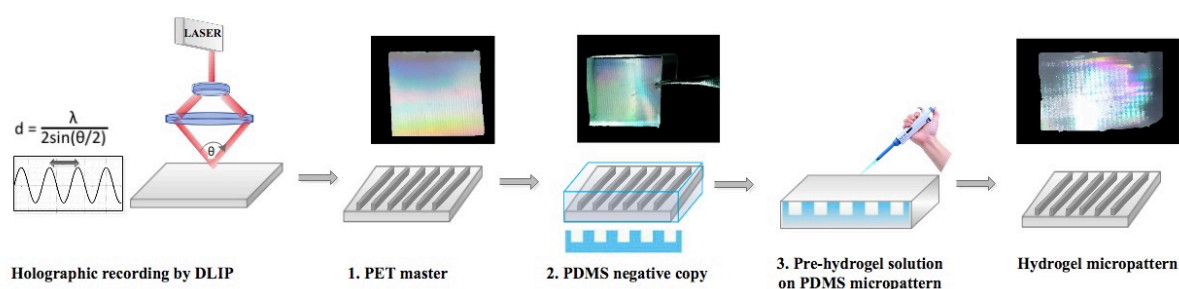

Scheme 1. Micropatterning process steps for hydrogel surface structures manufacturing.

The micropatterns obtained on the PDMS, and the swollen hydrogel surface were observed by Optical microscopy (OM, Leica microsystems, MZ APO). Surface pattern characterization was also carried out with an optical set-up as shown in Fig. 1. From the bottom, a continuous green laser beam (532 nm, 100 mW) is attenuated and orthogonally directed to the sample holder through a mirror. The sample holder is a 3D printed platform provided with a pinhole and patterned lanes that allow the x-y movement of a 96-well ELISA plate so the laser beam can be unequivocally directed towards every well. Then, movable silicon photodiodes are placed after the sample holder to register the to record the intensity of the different laser beams (incident or diffracted). A concave spherical lens (f = 30 mm) was placed on the top of the 96-well plate, to focus the diffracted beams produced by the hydrogel micropatterns.
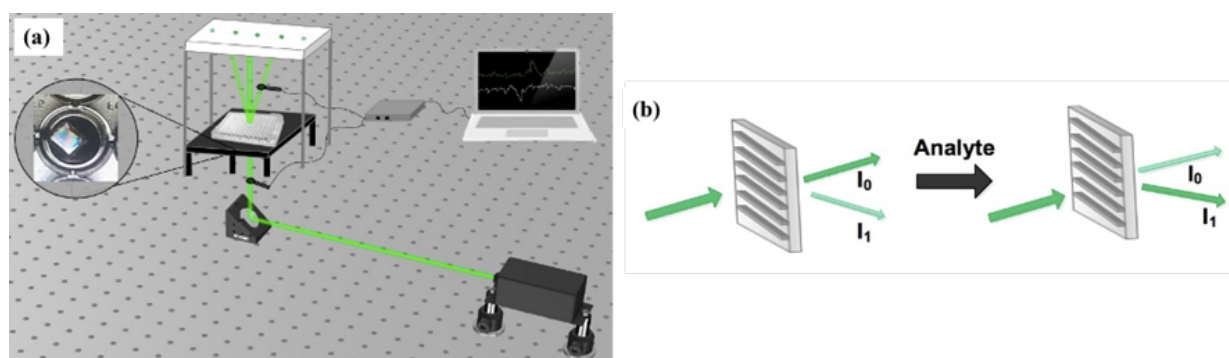
Figure 1. (a) Optical set-up employed for diffraction efficiency measurement. **(b)** Analyte sensing principle: after analyte biorecognition, the intensity of zero and first diffraction order changes, and thus the diffraction efficiency.

Diffraction efficiency (DE%) of the micropatterns was calculated with equation (2):

$$DE\ (\%) = \frac{I_1}{I_0}\ 100 \tag{2}$$

where I_0 was the intensity of the zero-diffraction order, and I_1 was the intensity of the first diffracted order.

Label-Free Hybridization Assay

Bioreceptor immobilization in micropatterned hydrogels was carried out in two steps. Firstly, thermally polymerized micropatterned hydrogel (AM(25)/PA) was functionalized with 5 µM of Probe 1. For that, micropatterned hydrogels were cut in squares (0.5x0.5cm) and treated with 100 µL of a 5 µM solution of Probe 1 and 1% (w/v) of DMPA photoinitiator in THF:Ac-TCEP 1:1. Then, hydrogels were irradiated at 365 nm (13 mW/cm^2) for 30 minutes. The functionalized micropatterned hydrogels were washed overnight with PBS-T to eliminate the non-covalently attached probes. For the label-free hybridization assays, the probe-functionalized micropatterned hydrogels were placed in separated wells of a transparent ELISA plate and equilibrated in 250 µL of SSC1x. The day after, SSC1x buffer solution was replaced with a fresh one and the initial diffraction efficiencies (DE$_i$) of the hydrogels were obtained using the optical set-up (Figure 1) and equation 2. Hybridization assay was performed by the incubation of the hydrogels with growing concentrations of Target 1 (0; 2; 5; 10; 25 µM) in 50 µL SSC1x for one hour at 37 °C. The hybridization experiment was also carried out with the AM(25)/PA hydrogel functionalized with a non-complementary, thiol-bearing oligonucleotide sequence (Probe 2), and hybridized at 10 and 25 µM of Target 1, as negative control. Then, hydrogels were washed overnight with SSC1x, to be sure that all the non-specifically bound targets were removed. The final diffraction efficiencies of hydrogels (DE$_f$) were obtained using the optical set-up (Fig. 1.) and equation (2).

The relative diffraction efficiency was used to characterize the response of the hydrogel to the target concentration, as described in equation (3):

$$\text{RDE}(\%) = \frac{\text{DE}_f - \text{DE}_i}{\text{DE}_i} \times 100 \qquad (3)$$

where RDE is the relative diffraction efficiency, DE$_i$ is the initial diffraction efficiency (after the equilibration step with SSC1x) and DE$_f$ is the final diffraction efficiency (after incubation and washing steps) for the first diffraction order. All experiments were repeated three times.

4.4 Results and Discussion

Optimized Hydrogel Compositions

First, hydrogel composition was optimized from both a physical and a chemical point of view. Polyacrylamide hydrogels are one of the most utilized materials in the synthesis of holographic and photonic hydrogel due, among other things, to their excellent optical properties [11], AM was chosen as the main monomer for the synthesis of the hydrogel networks and MBA as one the most common crosslinkers for polyacrylamide. PA co-monomer was incorporated to introduce the alkyne moiety, necessary for the further thiolated-probe covalent attachment through thiol-yne photo-click coupling chemistry [34]. Apart from reaching adequate physical and optical properties such as good porosity, transparency and low optical background, the chemical formulation was adapted to increase the immobilization density of the biorecognition Probe 1. For that, different ratios of monomer (AM), co-monomer (PA), and crosslinker (MBA) were assayed. All the assay compositions are shown in Table S2. As expected, all the hydrogels were transparent with almost zero absorbance at the working wavelength of our system (532 nm). Figure S1 shows the UV-Visible spectra of all hydrogels. However, not all the synthesized hydrogels showed the consistency required for part of our purposes: the fabrication of surface relief diffraction grating by replica molding. The requirements of hydrogels for potentially yielding suitable gratings include: they must adapt the form of the container used for the polymerization, they need to be manipulable, easy to cut, not brittle, and kept the macroscopical form after washing and swelling. The consistency of the different synthesized hydrogels polymerized by thermal activation is indicated in Table S2. In addition, Figure S2 shows photograph of hydrogels of different consistency. AM(25)/PA and AM(8)/PA showed the best consistency and potential to be used as surface relief gratings for DNA hybridization, so they, and their counterpart controls without PA, were selected for further optimization. The selected compositions are shown in Table 1 and photographs of the hydrogels are shown in Figure S3. As the activation process for the polymerization can affect the final properties of the hydrogel, i.e., porosity, swelling, etc., polymerization was carried out following two different activation processes, thermally and photochemically.

Table 1. Optimized hydrogel compositions.

Hydrogel	AM (% *w/v*)	MBA (% *w/v*)	PA (µL)	DI water (µL)
AM(25)	25	0.05	0	1000
AM(25)/PA	25	0.05	15	1000
AM(8)	8	0.25	0	1000
AM(8)/PA	8	0.25	15	1000

The morphology of the optimized hydrogel compositions that contain PA was comparatively observed for thermal and photochemical activation, as poor homogeneity has been previously reported in hydrogels polymerized by UV-light [35-37]. For that, lyophilized hydrogels were analyzed by SEM (Fig. 2 and Fig. S4). As it can be observed in the SEM micrographs, the thermal activation provided higher homogeneity and porosity to the hydrogel network for both AM(25)/PA and AM(8)/PA compositions, although both activation procedures resulted in adequate porosity level.
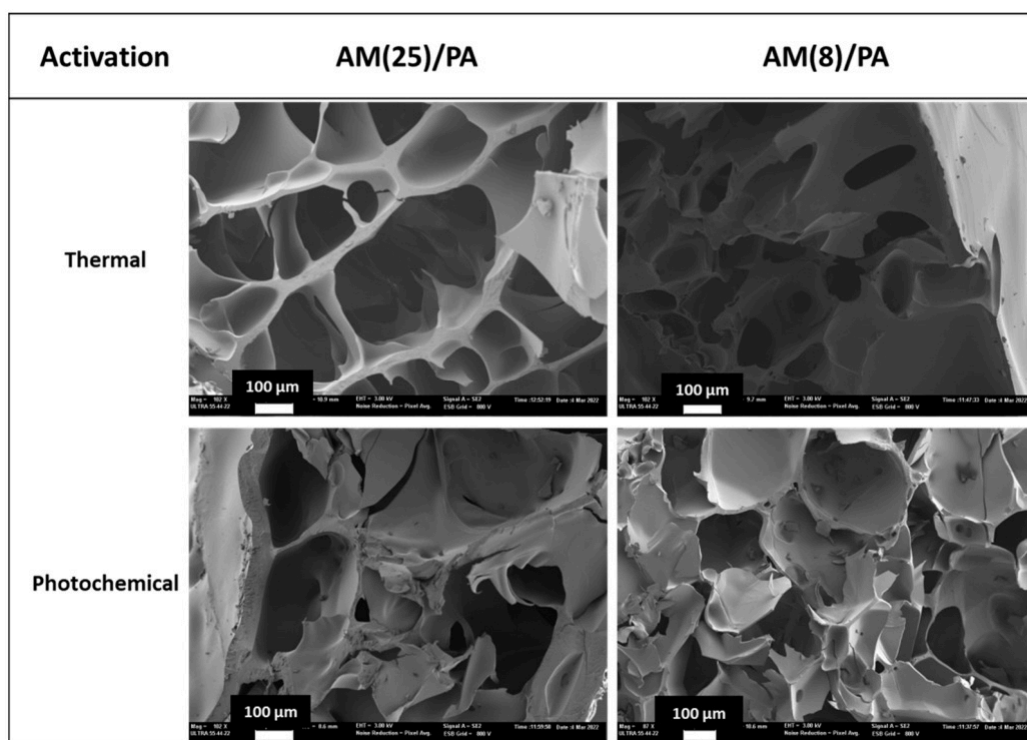
Figure 2. Porosity observed by SEM for selected hydrogel compositions (AM(25)/PA) and (AM(8)/PA) prepared by thermal and photochemical activation.

As the hydrogels obtained by thermal activation showed the best homogeneity by SEM, swelling behavior studies of these hydrogels were carried out to test the hydrogel buffer absorption capacity. In Figure S5 at the Supporting information, the swelling studies show how the chemical composition affects the hydrogel water uptakes. Hydrogels AM(8) demonstrated higher swelling degree than hydrogels AM(25). Probably, the larger quantity of monomer used in AM(25) hydrogels counteracts the higher crosslinker degree present in AM(8) hydrogels. Equally, the propargyl acrylate co-monomer contributed to the polymer swelling capacity. PA reduces the buffer absorption in AM(25)/PA and AM(8)/PA hydrogels in comparison to AM(25) and AM(8) reference systems, probably due to higher hydrophobicity of alkyne moiety. However, in both compositions, the swelling capacity was over 400%. Thus, the optimized compositions were tested for subsequent bioreceptor immobilization and surface micropatterning.

Probe Immobilization and Hybridization Assay

AM/PA hydrogels and their corresponding controls (without PA) were covalently functionalized with a thiol-bearing oligonucleotide probe for potential biosensing applications. The oligonucleotide probe acts as the specific biorecognition element for its complementary sequence (Target). In the hydrogel formulation, the propargyl acrylate (PA) co-monomer had a C-C triple bond that was expected to enhance the binding with thiol-probes, in comparison to the control system [38]. Thiolated probes incorporation was carried out through thiol-yne photoclick coupling reaction by UV irradiation at 365 nm (Scheme S2). Previous work of our group done in microarray format had demonstrated that these irradiation conditions did not affect the probes stability and bioavailability to hybridize with the complementary strands [39]. Firstly, the thermally polymerized AM(25)/PA and AM(8)/PA hydrogels were biofunctionalized as the thermal activation yielded hydrogels with higher homogeneity and porosity and, in addition, they showed high swelling degree. Hydrogels were functionalized with Probe 1, complementary to target, and, additionally, with Probe 2, which was a thiolated, non-complementary sequence.

In addition, hydrogels without PA, AM(25) and AM(8), were also submitted to functionalization with Probe 1 to assess the role of PA in the probe immobilization process. The immobilization was carried out in 1:1 THF:Ac-TCEP, TCEP was added to facilitate the reduction of disulfide bonds established between the thiolated probes. After probe immobilization, fluorescence labeled target sequence was employed for hybridization assays to verify the successful incorporation of the thiol probe and its bioavailability for the specific hybridization. Therefore, thermally activated, probe-biofuncionalized hydrogels AM(25)/PA, AM(25), AM(8)/PA, and AM (8) were hybridized with increasing concentrations of the Cy5-labeled target sequence (Target 2), for 1h at 37 °C, and the fluorescence was registered after washing overnight (Fig. 3a and 3b). As a control, fluorescence signal was also registered after hybridization in several cross-section pieces of the hydrogels AM(8)/PA and AM(25)/PA to demonstrate that the target 2 could reach the probe within 1h (Fig. S7). Fig. 3a and b show that significantly higher fluorescence signals (4-fold to 5-fold) were observed for AM(25)/PA and AM(8)/PA hydrogels, compared to their control systems AM(25) and AM(8) when they were functionalized with Probe 1, complementary to target. As expected, the introduction of the PA co-monomer allowed a much more effective probe immobilization, thanks to the thiol-yne coupling chemistry, increasing the probe loading in the hydrogels. Therefore, the immobilization strategy was successful for both AM(25)/PA and AM(8)/PA hydrogels. Moreover, a higher fluorescence signal was measured for the AM(25)/PA hydrogel in comparison to the AM(8)/PA hydrogel. In addition, almost no fluorescence was observed when AM(25)/PA and AM(8)/PA hydrogels were functionalized with Probe 2, having the non-complementary sequence, which demonstrated that specific hybridization was taking place, and non-specific binding was negligible inside the hydrogels supports. As polymerization could be also activated photochemically employing the same wavelength needed for the thiol-yne coupling reaction, a second strategy was assessed for the hydrogels biofunctionalization: a one-step process which consisted of the immobilization of the thiolated probe during hydrogel polymerization. In this strategy, the thiol-yne photoclick coupling reaction and acrylamide polymerization, using DMPA as a photoinitiator, were triggered with UV irradiation at the same time.

Therefore, pre-polymeric solutions of AM(25)/PA and AM(25) hydrogels were mixed with 1 µM of complementary Probe 1 and DMAP, and then irradiated at 365 nm for 30 minutes. Additionally, a control experiment was carried out with AM(25)/PA hydrogel and the non-complementary Probe 2. Once hydrogels were washed, and equilibrated with SSC1x, hybridization assays with the Cy5-labeled target sequence (Target 2) at increasing concentrations, as above, were carried out, and fluorescence was registered after washing (Fig. 3c). In this case, the highest fluorescence signal was also observed for hydrogels AM(25)/PA functionalized with Probe 1. However, the high fluorescence observed in the hybridization curve of hydrogel AM(25) showed that the thiolated probe resulted also immobilized without the presence of (PA) co-monomer. This is due to the thiol-acrylate coupling reaction which follows the same principle as thiol-yne photocoupling reaction [40]. Figure S6 shows the IR spectrum of a lyophilized AM(25) hydrogel which showed a spectral profile compatible to the presence of residual unreacted acrylamide groups. But, even in this case, the presence of PA increased the hydrogel probe immobilization capability. As before, AM(25)/PA hydrogels biofunctionalized with Probe 2 did not show significant fluorescence signal after hybridization, which reveals that non-specific binding is also avoided with the one-pot functionalization strategy. Comparing the two strategies for AM(25)/PA hydrogels functionalized with the Probe 1, complementary to Target 2, the ones biofunctionalized after polymerization (Fig. 3a) showed two-fold the fluorescence signal of the ones biofunctionalized during the polymerization (Fig. 3c). Probably, in the case of the biofunctionalization after the polymer synthesis, a larger number of bioreceptors are introduced and, in addition, these probes are more accessible to the target. Thus, thermally polymerized AM(25)/PA hydrogels biofuncionalized after their synthesis showed the best performance for the detection of the complementary target by fluorescence.
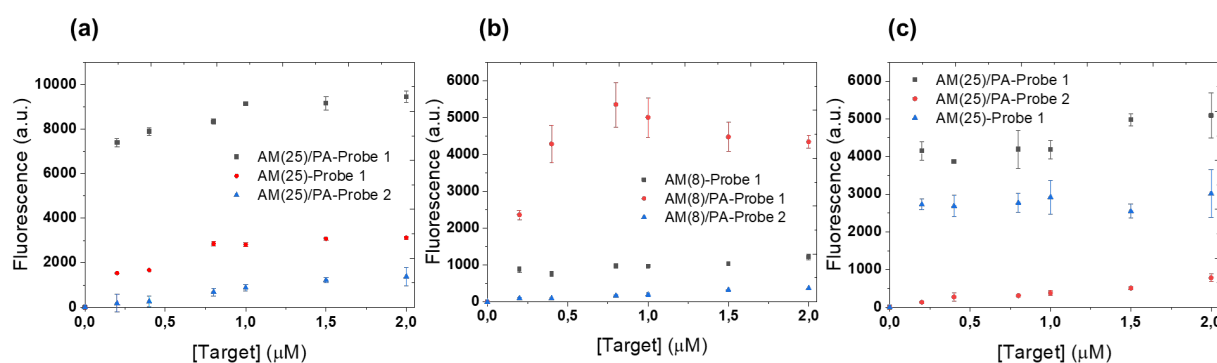
Figure 3. Fluorescence intensity measured after hybridization with increasing concentrations of labeled Target 2 **(a)** in AM(25)/PA and AM(25) hydrogels and **(b)** in AM(8)/PA and AM(8), biofunctionalized with Probe 1 or 2 after their polymerization; ; and **(c)** in AM(25)/PA and AM(25) hydrogels with Probe 1 or 2 covalently attached during the polymerization step. Probe 1 sequence was complementary to the Target 2, while Probe 2 sequence was non-complementary, both probes bear the thiol moiety needed for thiol-yne or thiol-ene coupling. Details of the obtained fluorescence signals are shown in section S-VI of the supporting information.

Surface Micropattern Fabrication and Characterization

For the surface micropatterning of hydrogels, PET masters were used to obtain a negative in PDMS which was in turn replicated with the above optimized hydrogel compositions. The fabricated PET master was characterized using confocal microscopy (Fig. 4a). The profile obtained from the confocal images shows that the gratings have a period of 4 µm and a depth of 2.1 µm (Fig. 4b). The PDMS negative copy was characterized by optical microscopy where, as expected, a period of 4 mm is observed, which confirms the correct replica of the PET master (Fig. 4c). In addition, the original PET master and its PDMS copies were irradiated with a continuous green laser at 532 nm using the optical set-up described in Materials and Methods section (Fig.1) and the diffraction efficiency (DE%) was calculated using the equation (2). Both fabricated microstructures showed good diffraction efficiency.
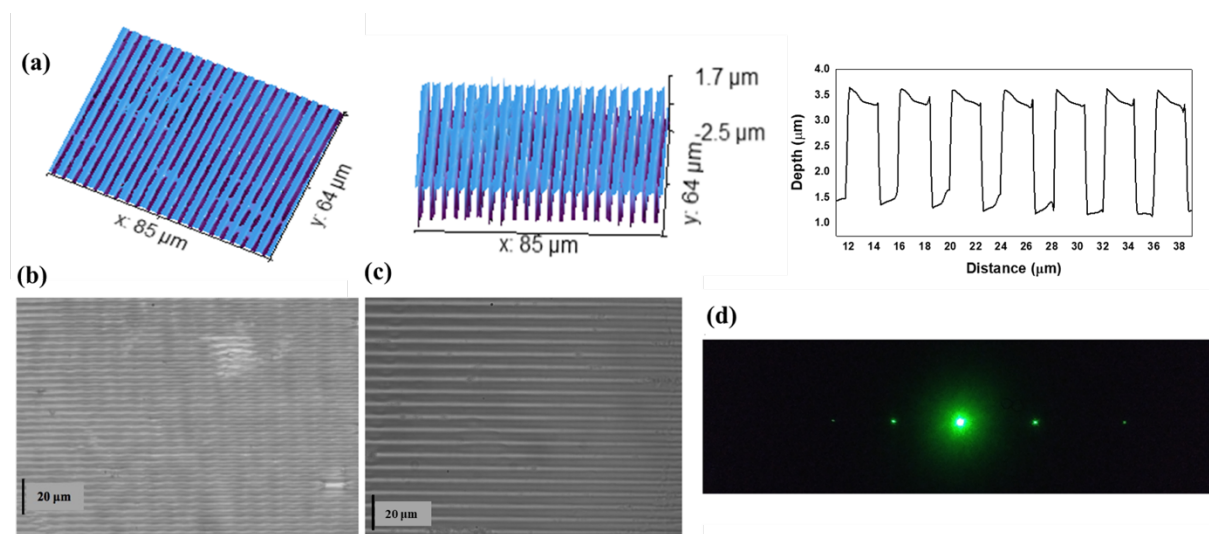
Figure 4. (a) Images and cross section profile of the microstructured PET master fabricated by Direct Laser Interference Patterning obtained using a 3D Optical Profilometer (Sensofar, Spain), Optical microscopy image of **(b)** the negative micropattern copied in PDMS by thermal curing, **(c)** the Surface Relief Grating (SRG) replicated in (AM(25)/PA) hydrogel from the PDMS micropattern; **(d)** Optical diffraction observed for the SRG, obtained in (c), measured with green laser irradiation (λ=532 nm) after complete swelling in distilled water.

Hydrogel surface micropatterning was realized, during the polymerization, for the optimized compositions by replica molding. The thermally activated curing process, for Acrylamide/Propargyl acrylate hydrogels, took place in 1.30 hours, supposedly a sufficient time for obtaining a good copy of the original PET microstructure. For AM(25)/PA and AM(25) compositions a good copy of the microstructure was obtained during the thermal curing. Fig. 4c shows the optical microscopy image of the AM(25)/PA hydrogel grating which correctly replicated the pattern. It should be noticed that a higher period is observed in the hydrogel compared to the PDMS master, as the first one is swollen in water. The diffraction of the AM(25)/PA hydrogel, thermally polymerized, was also evaluated after its irradiation with a continuous green laser at 532 nm using the optical set-up of Fig.1. Fig. 4d shows the diffraction pattern of AM(25)/PA hydrogel.

Zero, first and second diffractive orders are present and distinguishable, so it could be very useful for label-free biosensing based on diffractive measurements. The diffraction efficiency (DE%) was calculated for the first diffraction order using the equation (2), resulting 4.6 ± 0.5, 9.8 ± 0.5, and 1.1 ± 0.2, for PET, PDMS and AM(25)/PA gratings, respectively. Lower values were observed in comparison with the PET and PDMS master, which was expected as the hydrogel has a watery nature and the PET and PDMS are plastics. The replica of the microstructure by thermal activation was not possible for AM(8)/PA and AM(8) compositions. This was attributed to the amount of monomer used, which was too low for achieving the right viscosity for the replication process. On the other hand, trials of the grating replica molding using photochemical polymerization resulted unsuccessful, since the polymerization proceeded too fast to permit the correct molding. On the other hand, by varying UV photoreactor parameters individually for each hydrogel composition, such as UV light power and irradiation time, hydrogel surface micropatterns were successfully obtained for all the optimized hydrogel compositions. However, the peeling-off of the hydrogel surface pattern copied from the PDMS, by photochemical activation, was cumbersome, thus 20 µL of glycerol were added to promote the detach. For (AM(25)/PA), AM(25) and (AM(8)/PA) hydrogels, micro-patterned replicas were obtained employing 15 minutes of UV irradiation and 10 mW/cm^2 of light power. While for the AM(8) hydrogel, 10 minutes of UV irradiation and 0.6 mW/cm^2 of light power were used. Although it was possible to replicate the grating using both thermal and photochemical activation, it was concluded that better reproducibility in surface micropatterns copies was obtained for the AM(25)/PA hydrogel composition during thermal curing. Thus, the AM(25)/PA hydrogel composition showed the best results in terms of micropattern fabrication and biorecognition properties. Consequently, it was chosen for further label-free biosensing studies.

Label-Free Biorecognition

To evaluate the potential label-free sensing of surface relief gratings of probe-functionalized hydrogels, the hybridization assay was performed using unlabeled probes. Firstly, surface microstructures were obtained for AM(25)/PA hydrogels during the thermal curing as, according to previous results, this hydrogel composition and reaction conditions produced the hydrogel with the best properties for the selective detection of targets by fluorescent sensing, and, in addition, they yielded micropatterned hydrogels that were able to diffract correctly the light. Therefore, the same conditions were expected to produce hydrogels with the best properties for the label-free detection of targets. After the hydrogel synthesis, the AM(25)/PA hydrogel was functionalized with 5 μM of Probe 1. The functionalized hydrogel patterns were placed in a petri-dish and washed overnight with SSC1x buffer. The day after, they were cut into squares (0.5x0.5cm) and positioned in separated wells of a transparent ELISA plate with 250 μL of SSC1x. The size of the hydrogel was chosen to perfectly fit within the ELISA wells and, thus, avoid the crushing of their walls and their free flotation. Diffraction efficiencies (DE%) of the functionalized hydrogel patterns were registered using the optical set-up (Fig. 1) at controlled conditions (RH 45 ± 5% and 24 ± 1°C). Ambient conditions were reached with domestic air conditioning and humidifier systems. Figure S12 shows that signals were stable for at least 30 minutes. Therefore, the signal was not affected by the incidence of the focused laser beam and slight delays in the reading time would not affect the obtained results. After that, the hybridization assay was performed in triplicate. Hydrogels were incubated with growing concentration of Target 1 (0; 5; 10; 25 μM) in 50 μL of SSC1x for one hour at 37 °C. After overnight washing with SSC1x, DE were registered at 532 nm and RDE were calculated according to equation (3) to assess the direct detection of complementary DNA-sequence (Target 1) (Fig. 5). As a control experiment, AM(25)/PA hydrogel was also functionalized with a non-complementary DNA sequence (Probe 2) and hybridization assays were performed with Target 1 at 25 μM following exactly the same procedure.

A gradual decrease of the DE% with increasing concentration of the unlabelled target was observed for the (AM(25)/PA) hydrogel functionalized with Probe 1, while for the control system, having immobilized the non-complementary sequence Probe 2, no tendency was observed. The DE (%) data obtained with probe 1 can be best fitted by a Hill 1 correlation curve, obtaining a correlation coefficient of $R2 = 0.991$. The RDE (%) data obtained with Probe 1 can also be best fitted by a Hill 1 correlation curve, obtaining a correlation coefficient of $R^2 = 0.997$. The limit of detection (LOD) of 2.47 µM was calculated from the RDE (%) curve as the concentration associated with the mean signal of ten blank measurements plus three times their standard deviation. Thus, it was possible to detect the analyte in the range from 2.47 to 10 µM, using the micropatterned hydrogels as optical transducer.
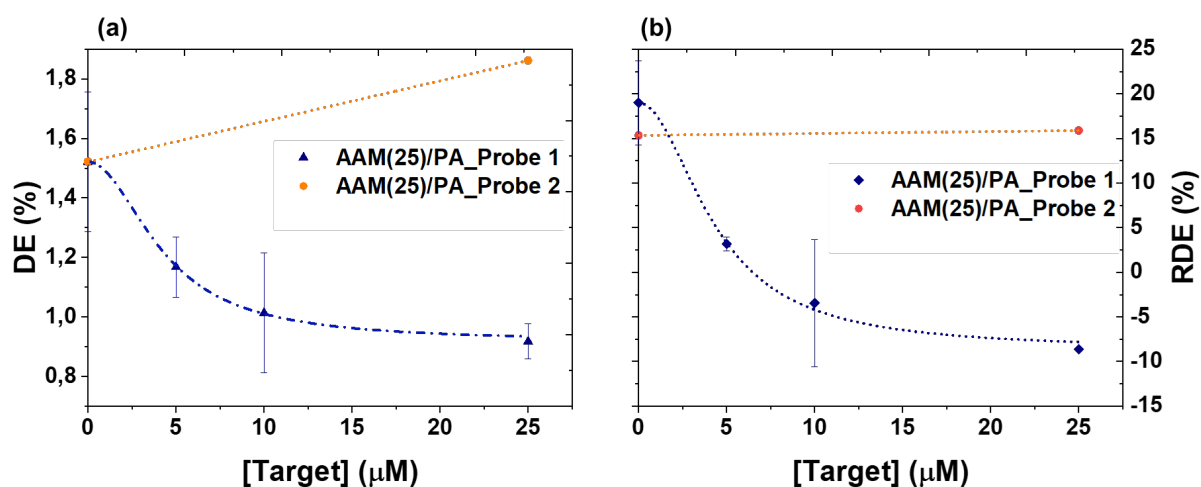
Figure 5. Change in the diffraction efficiency of SRG made of Probe-functionalized hydrogels after hybridization with Target 1. Left, Diffraction efficiency (DE) measured at λ=532 nm and, right, Relative diffraction efficiency of SRG functionalized with Probe 1 (blue) and Probe 2 (orange) hybridized with increasing concentrations of Target 1 (complementary to Probe 1). The DE changes with the amount of Target hybridized only for the SRG hydrogels functionalized with the complementary strand.

Therefore, the label-free biosensing assay using unlabeled probes, performed for (AM(25)/PA) hydrogels with the surface micropattern, showed excellent preliminary results. The LOD of DNA in our system is higher than most of the hydrogel-based systems described in the literature [41]. However, most of the approaches are based on labels or/ and elaborate DNA architectures. DNA hybridization with hydrogel has also been explored for actuators and other purposes [42] but poor consideration of the analytical performance is contemplated in these studies. Baba and coworkers have reported the use of diffraction gratings for the label-free detection of DNA with very low LOD but the DNA was amplified during the analysis [43]. Our results are very promising, but the diffraction efficiency calculated for the obtained hydrogel surface-micropattern is not high. Hence, further improvements in the micropattern fabrication can be realized to increase the initial DE% and, accordingly, the sensitivity for the analyte detection. These improvements involve the fabrication of thinner surface relief gratings, as well as the replication with lower period PET masters. Although fabrication of these gratings can be challenging, technologies such as two-photon polymerization can be used for fabricating 2D/3D microstructures with high accuracy [44, 45]. Also, quicker data acquisition and automatization of hydrogel SRGs will allow to increase the number of replicates, lowering the experimental error. Despite those facts, it was possible to directly detect the analyte with good selectivity and sensitivity, being this the first time that surface micro-patterned hydrogels are used to directly detect hybridization events.

4.5 Conclusions and Future Outlook

Optical biosensors are emerging for point-of-care testing (POCT), as they present some advantages such as increased sensitivity and suitability for being integrated into compact device with the purpose of being utilized out-of-the-lab. Overall, line-like periodic microstructures were successfully fabricated on bioresponsive hydrogel surface and employed as transducers for converting the analyte-bioreceptor binding into a measurable optical signal. The planned approach for the covalent immobilization of the bioreceptor probes had notable outcomes.

Furthermore, different bioreceptors with thiol terminal groups could be used, depending on the analyte to be detected. Accordingly, the developed biosensor can sense multiple analytes. Results obtained from the label-free biorecognition assay have shown a direct correlation between the diffraction efficiency measured and the target concentration. The label-free biosensor as designed could significantly contribute to direct and accurate analysis in medical diagnosis, being cheap, easy to fabricate and working without the need of further reagents. To fully achieve this, further aspects should be considered, such as the minimization of biofouling of hydrogels when they are immersed in real fluids. This can be achieved by tunning the composition of hydrogels, for instance using polyacrylamide copolymers or zwitterionic moieties [46].

Conflicts of Interest: The authors declare no conflict of interest.

4.6 References

1. Ahmed, M.U.; Saaem, I.; Wu, P.C.; Brown, A.S. Personalized diagnostics and biosensors: A review of the biology and technology needed for personalized medicine. Crit. Rev. Biotechnol. 2014, 34, 180–196.

2. Yang, J. Blood glucose monitoring with smartphone as glucometer. Electrophoresis 2019, 40, 1144–1147.

3. Sri, S.; Dhand, C.; Rathee, J.; Ramakrishna, S.; Solanki, P.R. Microfluidic Based Biosensors as Point of Care Devices for Infectious Diseases Management. Sens. Lett. 2018, 17, 4–16.

4. Shafiee, H.; Wang, S.; Inci, F.; Toy, M.; Henrich, T.J.; Kuritzkes, D.R.; Demirci, U. Emerging Technologies for Point-of-Care Management of HIV Infection. Annu. Rev. Med. 2015, 66, 387–405.

5. Li, F.; Li, H.; Wang, Z.; Wu, J.; Wang, W.; Zhou, L.; Xiao, Q.; Pu, Q. Mobile phone mediated point-of-care testing of HIV p24 antigen through plastic micro-pit array chips. Sens. Actuators B Chem. 2018, 271, 189–194.

6. Nava, G.; Zanchetta, G.; Giavazzi, F.; Buscaglia, M. Label-free optical biosensors in the pandemic era. Nanophotonics 2022, 11, 4159–4181.

7. Samuel, V.R.; Rao, K. A review on label free biosensors. Biosens. Bioelectron. X 2022, 11, 100216.

8. Long, F.; Zhu, A.; Shi, H. Recent Advances in Optical Biosensors for Environmental Monitoring and Early Warning. Sensors 2013, 13, 13928–13948.

9. Khansili, N.; Rattu, G.; Krishna, P.M. Label-free optical biosensors for food and biological sensor applications. Sens. Actuators B: Chem. 2018, 265, 35–49.

10. Yetisen, A.K.; Naydenova, I.; da Cruz Vasconcellos, F.; Blyth, J.; Lowe, C.R. Holographic Sensors: Three-Dimensional AnalyteSensitive Nanostructures and Their Applications. Chem. Rev. 2014, 114, 10654–10696.

11. Lucío, M.I.; Cubells-Gómez, A.; Maquieira, Á.; Bañuls, M.-J. Hydrogel-based holographic sensors and biosensors: Past, present, and future. Anal. Bioanal. Chem. 2022, 414, 993–1014.

12. Ullah, F.; Othman, M.B.H.; Javed, F.; Ahmad, Z.; Akil, H.M. Classification, processing and application of hydrogels: A review. Mater. Sci. Eng. C 2015, 57, 414–433.

13. Pardeshi, S.; Damiri, F.; Zehravi, M.; Joshi, R.; Kapare, H.; Prajapati, M.K.; Munot, N.; Berrada, M.; Giram, P.S.; Rojekar, S.; et al. Functional Thermoresponsive Hydrogel Molecule to Material Design for Biomedical Applications. Polymers 2022, 14, 3126.

14. Chen, M.; Wang, Y.; Zhang, J.; Peng, Y.; Li, S.; Han, D.; Ren, S.; Qin, K.; Li, S.; Gao, Z. Stimuli-responsive DNA-based hydrogels for biosensing applications. J. Nanobiotechnol. 2022, 20, 40.

15. Mateescu, A.; Wang, Y.; Dostalek, J.; Jonas, U. Thin Hydrogel Films for Optical Biosensor Applications. Membranes 2012, 2, 40–69.

16. Di, Y.; Wang, P.; Li, C.; Xu, S.; Tian, Q.; Wu, T.; Tian, Y.; Gao, L. Design, Bioanalytical, and Biomedical Applications of AptamerBased Hydrogels. Front. Med. 2020, 7, 456.

17. Makhsin, S.R.; Goddard, N.J.; Gupta, R.; Gardner, P.; Scully, P.J. Optimization Synthesis and Biosensing Performance of an Acrylate-Based Hydrogel as an Optical Waveguiding Sensing Film. Anal. Chem. 2020, 92, 14907–14914.

18. Rebelo, R.; Barbosa, A.I.; Caballero, D.; Kwon, I.K.; Oliveira, J.M.; Kundu, S.C.; Reis, R.L.; Correlo, V.M. 3D biosensors in advanced medical diagnostics of high mortality diseases. Biosens. Bioelectron. 2019, 130, 20–39.

19. Tavakoli, J.; Tang, Y. Hydrogel Based Sensors for Biomedical Applications: An Updated Review. Polymers 2017, 9, 364.

20. Du, X.; Zhai, J.; Li, X.; Zhang, Y.; Li, N.; Xie, X. Hydrogel-Based Optical Ion Sensors: Principles and Challenges for Point-of-Care Testing and Environmental Monitoring. ACS Sens. 2021, 6, 1990–2001.

21. Lin, X.; Fang, M.; Yi, C.; Jiang, Y.; Zhang, C.; Pan, X.; Luo, Z. Functional hydrogel for fast, precise and inhibition-free point-of-care bacteria analysis in crude food samples. Biomaterials 2022, 280, 121278.

22. Chin, L.K.; Li, H.; Choi, J.-H.; Iwamoto, Y.; Oh, J.; Min, J.; Beak, S.K.; Yoo, D.; Castro, C.M.; Lee, D.; et al. Hydrogel Stamping for Rapid, Multiplexed, Point-of-Care Immunostaining of Cells and Tissues. ACS Appl. Mater. Interfaces 2022, 14, 27613–27622.

23. Park, C.H.; Kim, T.; Lee, G.H.; Ku, K.H.; Kim, S.-H.; Kim, B.J. Fluorescent Polymer-MoS2 -Embedded Microgels for Photothermal Heating and Colorimetric Monitoring. ACS Appl. Mater. Interfaces 2020, 12, 35415–35423.

24. Chen, W.; Tian, R.; Xu, C.; Yung, B.C.; Wang, G.; Liu, Y.; Ni, Q.; Zhang, F.; Zhou, Z.; Wang, J.; et al. Microneedle-array patches loaded with dual mineralized protein/peptide particles for type 2 diabetes therapy. Nat. Commun. 2017, 8, 1777.

25. He, R.; Niu, Y.; Li, Z.; Li, A.; Yang, H.; Xu, F.; Li, F. A Hydrogel Microneedle Patch for Point-of-Care Testing Based on Skin Interstitial Fluid. Adv. Heal. Mater. 2020, 9, e1901201.

26. Liu, D.; Jia, S.; Zhang, H.; Ma, Y.; Guan, Z.; Li, J.; Zhu, Z.; Ji, T.; Yang, C.J. Integrating Target-Responsive Hydrogel with Pressuremeter Readout Enables Simple, Sensitive, User-Friendly, Quantitative Point-of-Care Testing. ACS Appl. Mater. Interfaces 2017, 9, 22252–22258.

27. Gao, N.; You, H. Recent Applications of Point-of-Care Devices for Glucose Detection on the Basis of Stimuli-Responsive Volume Phase Transition of Hydrogel. BioChip J. 2021, 15, 23–41.

28. Choi, N.W.; Kim, J.; Chapin, S.C.; Duong, T.; Donohue, E.; Pandey, P.; Broom, W.; Hill, W.A.; Doyle, P.S. Multiplexed Detection of mRNA Using Porosity-Tuned Hydrogel Microparticles. Anal. Chem. 2012, 84, 9370–9378.

29. Sola, D.; Alamri, S.; Lasagni, A.F.; Artal, P. Fabrication and characterization of diffraction gratings in ophthalmic polymers by using UV direct laser interference patterning. Appl. Surf. Sci. 2019, 476, 128–135.

30. Zezza, P.; Lucío, M.I.; Maquieira, A.; Bañuls, M.-J. DNA -based hydrogels for high-performance optical biosensing application. Talanta 2022, 244, 123427.

31. Resetco, C.; Hendriks, B.; Badi, N.; Du Prez, F. Thiol–ene chemistry for polymer coatings and surface modification—building in sustainability and performance. Mater. Horizons 2017, 4, 1041–1053.

32. Lucío, M.I.; Montoto, A.H.; Fernández, E.; Alamri, S.; Kunze, T.; Bañuls, M.-J.; Maquieira, A. Label-free detection of C-Reactive protein using bioresponsive hydrogel-based surface relief diffraction gratings. Biosens. Bioelectron. 2021, 193, 113561.

33. Bañuls, M.-J.; González-Martínez, M.; Sabek, J.; García-Rupérez, J.; Maquieira, Á. Thiol-click photochemistry for surface functionalization applied to optical biosensing. Anal. Chim. Acta 2019, 1060, 103–113.

34. Negrini, N.C.; Volponi, A.A.; Sharpe, P.T.; Celiz, A.D. Tunable Cross-Linking and Adhesion of Gelatin Hydrogels via Bioorthogonal Click Chemistry. ACS Biomater. Sci. Eng. 2021, 7, 4330–4346.

35. Lim, K.S.; Klotz, B.J.; Lindberg, G.C.J.; Melchels, F.P.W.; Hooper, G.J.; Malda, J.; Gawlitta, D.; Woodfield, T.B.F. Visible Light CrossLinking of Gelatin Hydrogels Offers an Enhanced Cell Microenvironment with Improved Light Penetration Depth. Macromol. Biosci. 2019, 19, e1900098.

36. Nguyen, A.K.; Goering, P.L.; Elespuru, R.K.; Das, S.S.; Narayan, R.J. The Photoinitiator Lithium Phenyl (2,4,6-Trimethylbenzoyl) Phosphinate with Exposure to 405 nm Light Is Cytotoxic to Mammalian Cells but Not Mutagenic in Bacterial Reverse Mutation Assays. Polymers 2020, 12, 1489.

37. Bilgic, M.B.; Kaya, K.; Orakdogen, N.; Yagci, Y. Light-induced synthesis and characterization of "Clickable" polyacrylamide hydrogels. Eur. Polym. J. 2022, 167, 111062.

38. Escorihuela, J.; Bañuls, M.-J.; Puchades, R.; Maquieira, Á. Site-specific immobilization of DNA on silicon surfaces by using the thiol–yne reaction. J. Mater. Chem. B 2014, 2, 8510–8517.

39. Nair, D.P.; Podgórski, M.; Chatani, S.; Gong, T.; Xi, W.; Fenoli, C.R.; Bowman, C.N. The Thiol-Michael Addition Click Reaction: A Powerful and Widely Used Tool in Materials Chemistry. Chem. Mater. 2014, 26, 724–744.

40. Khajouei, S.; Ravan, H.; Ebrahimi, A. DNA hydrogel-empowered biosensing. Adv. Colloid Interface Sci. 2020, 275, 102060.

41. Cangialosi, A.; Yoon, C.; Liu, J.; Huang, Q.; Guo, J.; Nguyen, T.D.; Gracias, D.H.; Schulman, R. DNA sequence–directed shape change of photopatterned hydrogels via high-degree swelling. Science 2017, 357, 1126–1130.

42. Yasui, T.; Ogawa, K.; Kaji, N.; Nilsson, M.; Ajiri, T.; Tokeshi, M.; Horiike, Y.; Baba, Y. Label-free detection of real-time DNA amplification using a nanofluidic diffraction grating. Sci. Rep. 2016, 6, 31642.

43. Wang, X.; Wei, Z.; Baysah, C.Z.; Zheng, M.; Xing, J. Biomaterial-based microstructures fabricated by two-photon polymerization microfabrication technology. RCS Adv. 2019, 9, 34472–34480.

44. Nekrasov, N.; Yakunina, N.; Nevolin, V.; Bobrinetskiy, I.; Vasilevsky, P.; Gerasimenko, A.Y. Two-Photon Polymerization of Albumin Hydrogel Nanowires Strengthened with Graphene Oxide. Biomimetics 2021, 6, 66.

45. Chan, D.; Chien, J.; Axpe, E.; Blankemeier, L.; Baker, S.W.; Swaminathan, S.; Piunova, V.A.; Zubarev, D.Y.; Maikawa, C.L.; Grosskopf, A.K.; et al. Combinatorial Polyacrylamide Hydrogels for Preventing Biofouling on Implantable Biosensors. Adv. Mater. 2022, 34, 210976.

4.7 Supplementary information

S-I   Nucleotide Sequence of Probes and Targets Used

Table S1. Nucleotide Sequence of Probes and Targets used.

Name	Sequence (5′ to 3′)	5′ end	3′end
Probe 1	CCCGATTGACCAGCTAGCATT	SH	None
Probe 2 (control probe)	ATCGACACCCCTATCACGATT	SH	None
Target 1	AATGCTAGCTGGTCAATCGGG	None	None
Target 2	AATGCTAGCTGGTCAATCGGG	Cy5	None

S-II   Scheme of Hydrogel Synthesis
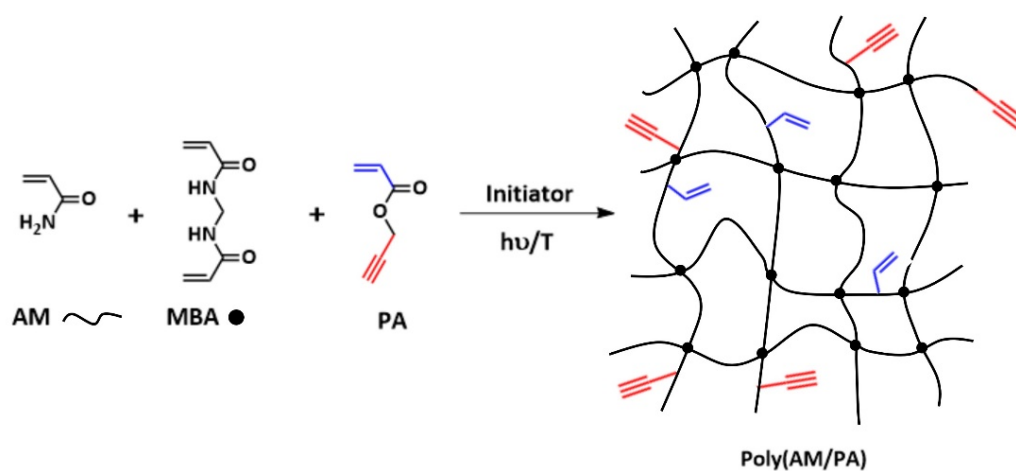
Scheme S1. Schematic representation of the hydrogel synthesis by free-radical polymerization (FRP). AM: Acrylamide, MBA: N, N'-methylenebis (acrylamide), PA: propargyl acrylate, Initiator=DMPA: 2,2-Dimethoxy-2-phenylacetophenone.
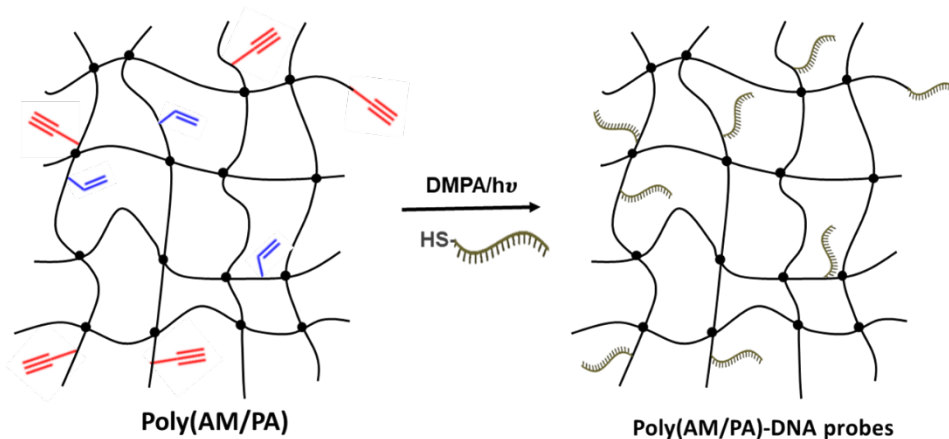
Scheme S2. Thiol probe immobilization by thiol-ene and thiol-yne click reaction of (AM/PA) hydrogels by UV light. AM: Acrylamide, PA: propargyl acrylate, Initiator=DMPA: 2,2-Dimethoxy-2-phenylacetophenone.

S-III   Hydrogel composition optimization

Table S2. Hydrogel compositions

Entry	Hydrogel	AM (% w/v)	MBA (% w/v)	PA (µL)	Consistency / Appearance
1	AM(8)_0.050	8	0.050	0	Soft
2	AM(8)_0.125	8	0.125	0	Soft
3	AM(8)_0.250=AM(8)	8	0.250	0	Adaptable
4	AM(8)/PA_0.050=AM(8)/PA	8	0.050	15	Soft
5	AM(8)/PA_0.125	8	0.050	15	Soft
6	AM(8)/PA_0.250	8	0.125	15	Adaptable
7	AM(25)_0.050=AM(25)	25	0.050	0	Adaptable
8	AM(25)_0.125	25	0.125	0	Adaptable
9	AM(25)_0.250	25	0.250	0	Brittle
10	AM(25)/PA_0.050=AM(25)/PA	25	0.050	15	Adaptable
11	AM(25)/PA_0.125	25	0.125	15	Brittle
12	AM(25)/PA_0.250	25	0.250	15	Brittle
13	AM(32)_0.050	32	0.050	0	Adaptable
14	AM(32)_0.125	32	0.125	0	Brittle
15	AM(32)_0.250	32	0.250	0	Brittle
16	AM(32)/PA_0.050	32	0.050	15	Brittle
17	AM(8)/PA_0.125	32	0.125	15	Brittle
18	AM(32)/PA_0.250	32	0.250	15	Brittle
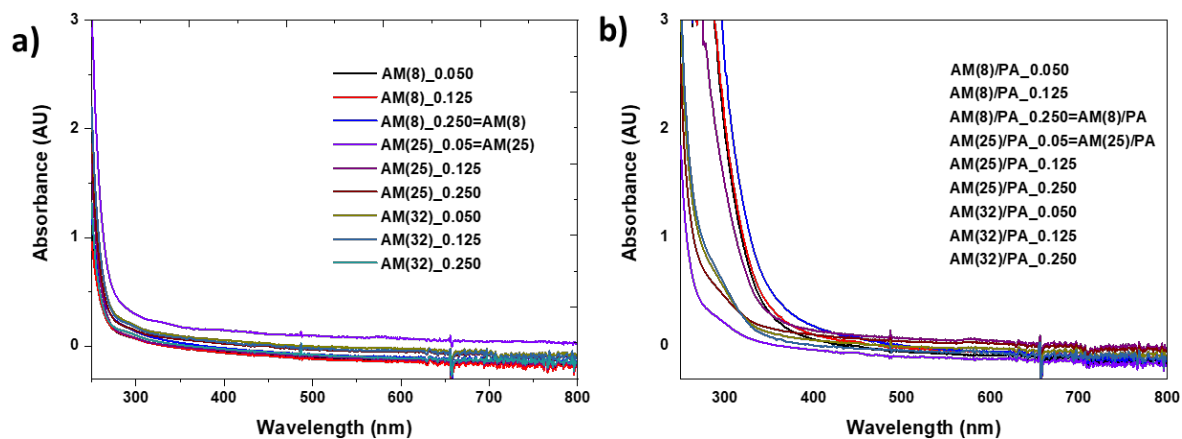
Figure S1. UV-Visible spectra of hydrogels with different compositions a) without PA and b) with PA.

Figure S2. Digital images of hydrogels pieces with different compositions and consistency AM(8)/PA_0.050, soft; b), b) AM(8)/PA_0.250, adaptable and c) AM(32)/PA_0.250, brittle.

Figure S3. Digital images of selected hydrogels pieces with different compositions a) AM(8)_0.250, b) AM(25)/PA_0.050 c) AM(8)/PA_0.250, and d) AM(25)_0.250.
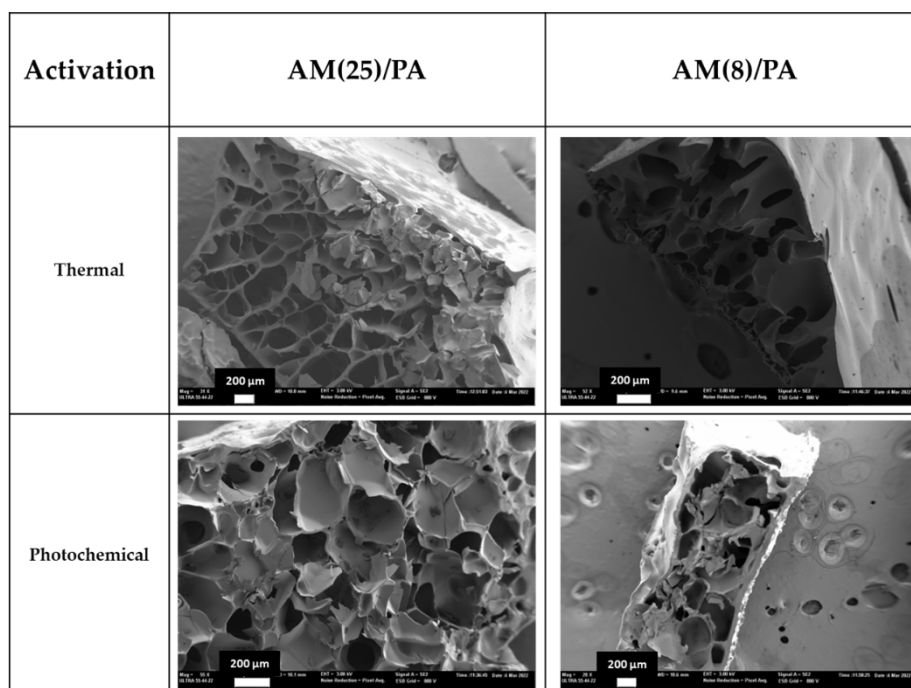
Figure S4. Porosity observed by SEM for selected hydrogel compositions (AM(25)/PA_0.050) and (AM(8)/PA_0.250) prepared by thermal and photochemical activation.

S-IV   Swelling Degree of Hydrogel
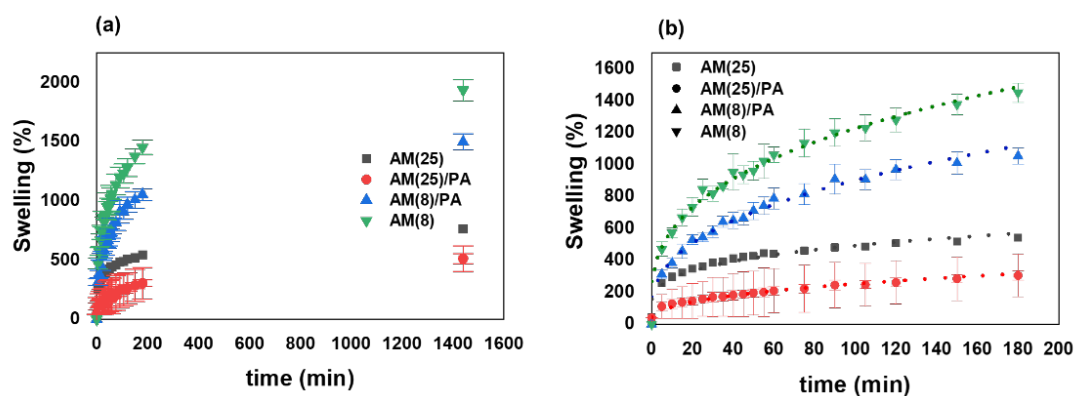
Figure S5. Swelling kinetic studies for (AM(25)/PA), (AM(8)/PA), AM(25) and AM(8) hydrogels soaked in PSB-T (obtained by thermal activation). b Enlargement of the first part of the graph (from 0 to 200 min).

S-V   ATR-FTIR spectrum of AM(25) hydrogel
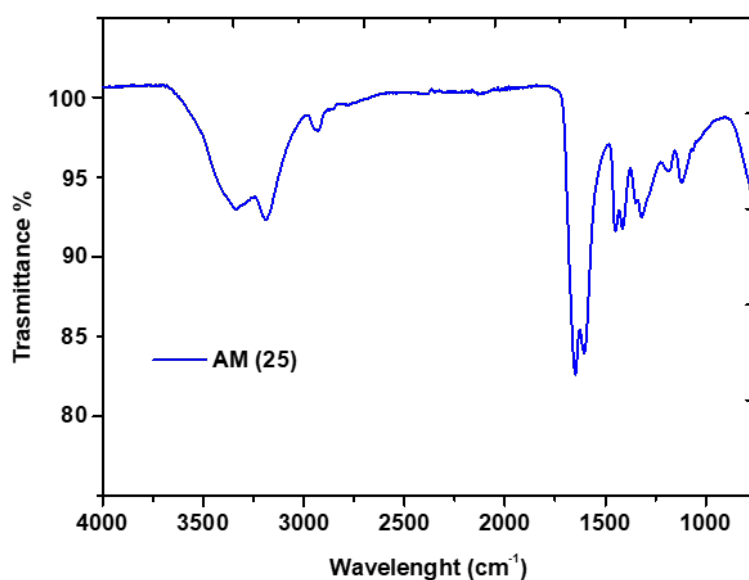
Figure S6. ATR-FTIR spectrum of AM(25) hydrogel.

S-VI   Details of Fluorescence Signals
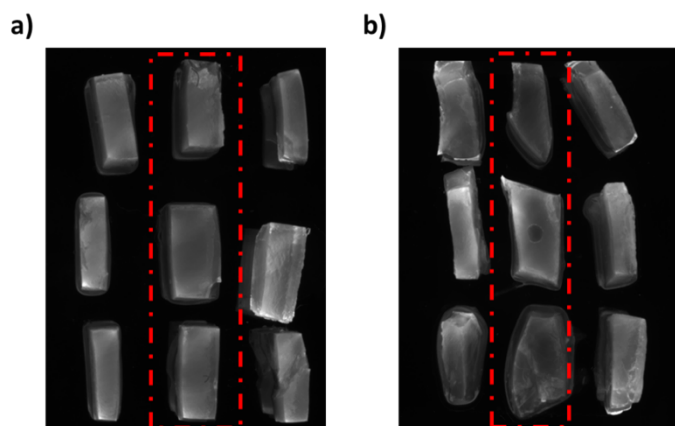
Figure S7. Fluorescence signals obtained for probe-functionalized a)(AM(8)/PA) hydrogel and b) (AM(25)/PA) after hybridization with Target 2 for 1h at 37°C (λex = 633 nm, λem = 670 nm). Firstly, hydrogels of were functionalized during the synthesis, using the first strategy (one-pot, photochemical) with 1 µM of the thiolated probes: Probe 1. After overnight washing with PBS-T, they were hybridized with 1 µM of fluorescent-labeled Target 2. Hydrogels were cutted in three pieces and the central piece was flipped prior to analysis to observe the signals of the cross-section profile. Fluorescence signals were collected after hybridization. Experiment was carried out in triplicate (three rows of the images). The fluorescence signal is visible in all three pieces for both hydrogels.

Label	(AM(25)/PA) + Probe 2	(AM(25)/PA) + Probe 1	AM(25) + Probe 1
After 2 hours washing			
After overnight washing			
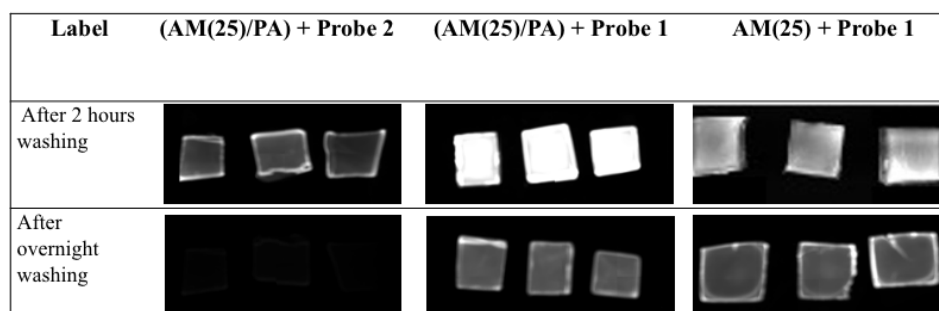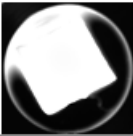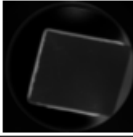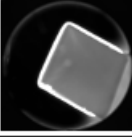
Figure S8. Fluorescence signals obtained for probe-functionalized (AM(25)/PA) hydrogel after hybridization with Target 2 (λex = 633 nm, λem = 670 nm). Firstly, hydrogels were functionalized during the synthesis, using the first strategy (one-pot, photochemical) with 1 µM of the thiolated probes: Probe 1 and, as a control, Probe 2. After overnight washing with PBS-T, they were hybridized with 1 µM of fluorescent-labeled Target 2. Fluorescence signals were collected after hybridization and 2 hours washing and after overnight washing with SSC1x. The fluorescence signal remained only in the case of Probe 1, complementary to the Target.

Label	AM(25) + Probe 1	AM(25)/PA + Probe 2	AM(25)/PA + Probe 1
Before washing			
After overnight washing			
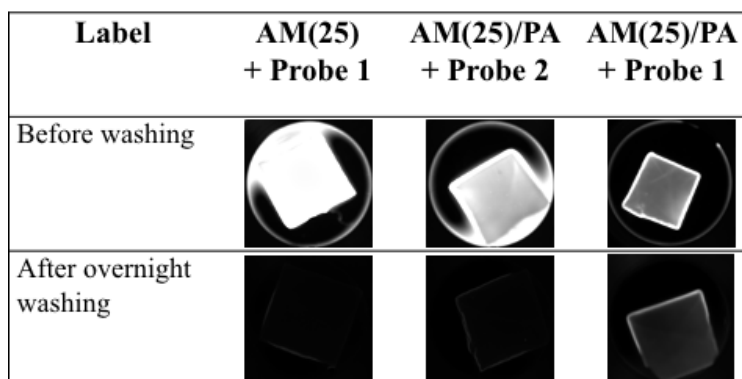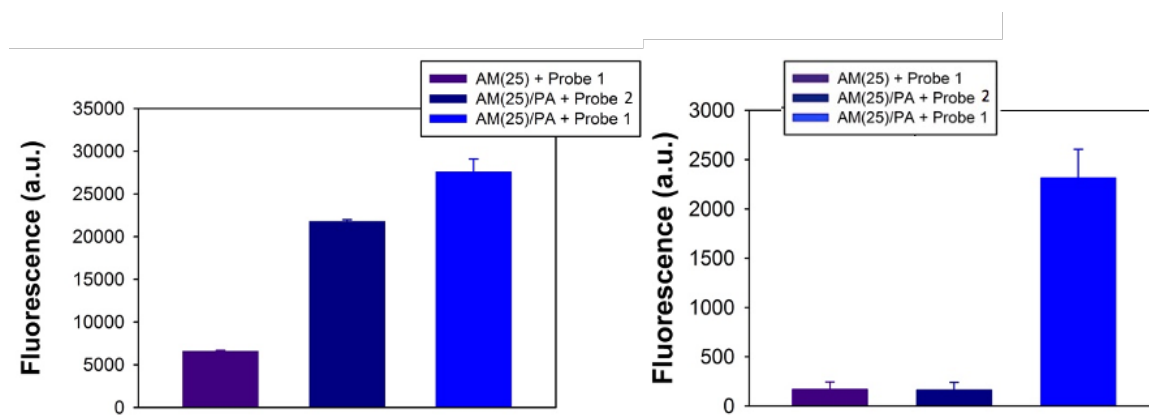
Figure S9. Fluorescence signals obtained for AM(25) and (AM(25)/PA) hydrogels through hybridization assay with Target 2 (λex = 633 nm, λem = 670 nm) . Firstly, hydrogels were biofunctionalized with thiolated probes (Probe 1 and Probe 2) at 1 µM after the polymerization. In the first bar chart, fluorescence signals were registered just after the hybridization assay with 0.5 µM of Target 2. In the second bar chart, the fluorescence was registered after overnight washing with SSC1x in order to wash away all the non-specific binding.

Figure S10. Fluorescence signals obtained for (AM(8)/PA) hydrogel through hybridization assay with Target 2 (λex = 633 nm, λem = 670 nm). Firstly, hydrogels were functionalized with thiolated probes (Probe 1 and the control probe Probe 2) at 1 µM during the synthesis, using the one-pot synthesis strategy. After overnight washing with PBS-T, they were hybridized with 1 µM of the Target 2. Fluorescence signals, after hybridization, were collected after overnight washing with SSC1x. The experiment was conducted in triplicate.
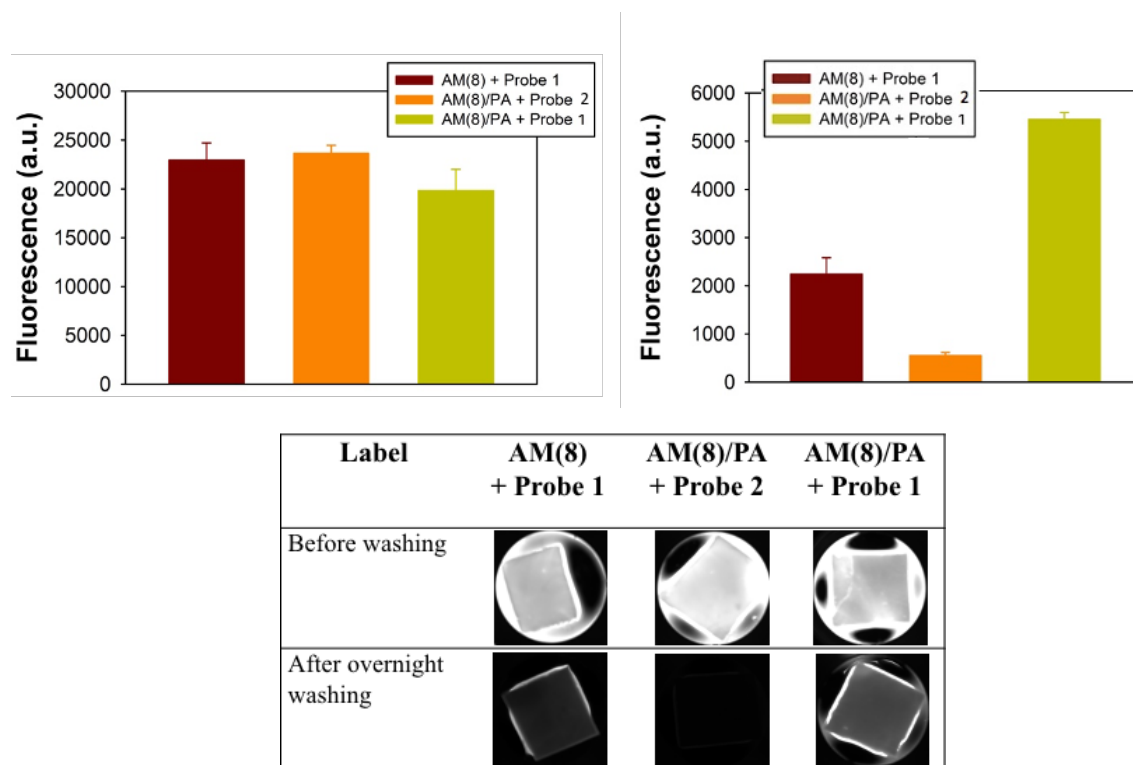
Figure S11. Fluorescence signals obtained for AM(8) and (AM(8)/PA) hydrogels through hybridization assay with Target 2 (λex = 633 nm, λem = 670 nm). Firstly, hydrogels were functionalized with thiolated probes (Probe 1 and, as control probe, Probe 2) at 1 μM after the synthesis, using the two-step strategy. In the first bar chart, fluorescence signals were registered just after the hybridization assay with 1 μM of the Target 2. In the second bar chart, the fluorescence was registered after overnight washing with SSC 1x in order to wash away all the non-covalent probe binding.

S-VII Diffraction Efficiency Measurements
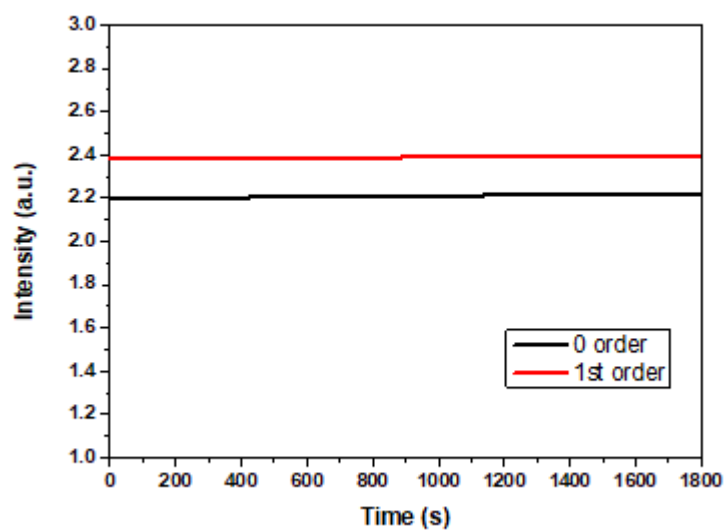
Figure S12. Stability of the measured signals with the optical setup over night: Intensities of the zero and first diffraction orders generated by the AM(25)/PA hydrogel immersed in SSC1X withing the wells of the plate were registered with the photodiodes after illumination with the laser beam (λ=532 nm).

5- Chapter 5

Holographic Recording of Unslanted Volume Transmission Gratings in Acrylamide/Propargyl Acrylate Hydrogel Layers:

Towards Nucleic Acids Biosensing

5- Chapter 5. Holographic Recording of Unslanted Volume Transmission Gratings in Acrylamide/Propargyl Acrylate Hydrogel Layers: Towards Nucleic Acids Biosensing

Following the research line described in the previous two chapters, an optimization process for the recording of volume holographic gratings within the hydrogel layer previously developed was performed. This work focused on improving the design of a volume holographic grating to act as an optical transducer. Our hypothesis is that by designing a grating with higher diffraction efficiency the performance of the biosensor can be increased. The challenge has been to investigate the best conditions for recording unslanted volume transmission gratings within analyte-sensitive hydrogel layers. For the first time, to our knowledge, volume transmission gratings were directly recorded in Acrylamide/propargyl acrylate hydrogel thin layers. After the recording process, the gratings were fully characterized by measuring their angular Bragg selectivity curves. Additionally, the stability in water of the recorded volume grating was studied in view of their potential use with biological analytes. Finally, oligonucleotide probes were anchored, after the hydrogel synthesis and recording of the volume holographic gratings, by covalent immobilization using thiol-yne coupling click-chemistry. The success of functionalisation and the specific response to hybridisation were demonstrated by fluorescent labelling.
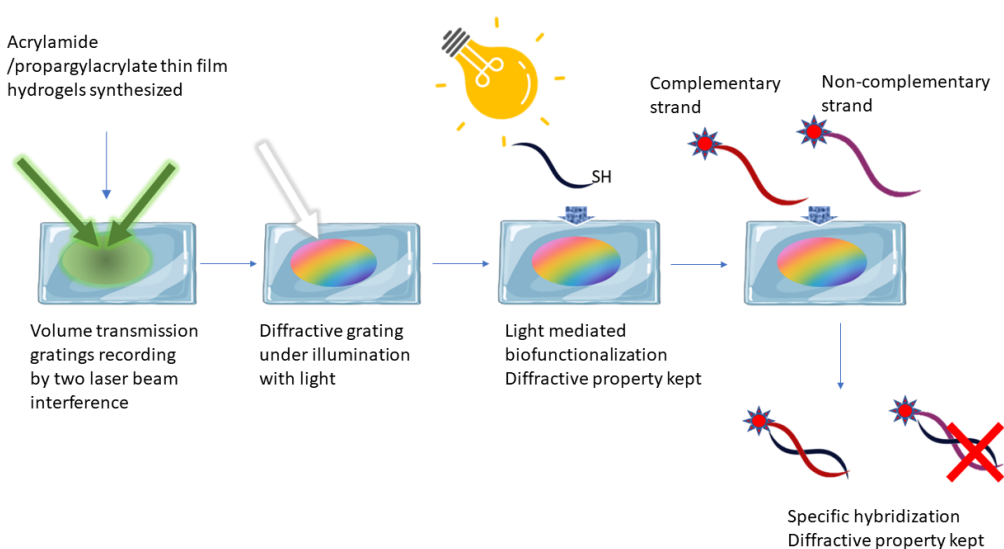
Summary figure. Overview of chapter 5

Holographic Recording of Unslanted Volume Transmission Gratings in Acrylamide/Propargyl Acrylate Hydrogel Layers: Towards Nucleic Acids Biosensing

Paola Zezza[1,2,3], María Isabel Lucío[1], Izabela Naydenova[2,3], María-José Bañuls[1,4,*] , Ángel Maquieira[1,4]

[1] *Instituto Interuniversitario de Investigación de Reconocimiento Molecular y Desarrollo Tecnológico (IDM), Universitat Politécnica de Valéncia, Universitat de València, Camino de Vera s/n, 46022 Valencia, Spain; pzezza@doctor.upv.es (P.Z.); malube@upv.es (M.I.L.); amaquieira@qim.upv.es (Á.M.)*

[2] *School of Physics and Clinical and Optometric Sciences, Technological University Dublin, City Center Campus, Central Quad, Grangegorman Lower, D07 ADY7 Dublin, Ireland; izabela.naydenova@tudublin.ie*

[3] *Centre for Industrial and Engineering Optics, Technological University Dublin, 13 Camden Row, D08 CKP1 Dublin, Ireland*

[4] *Departamento de Química, Universitat Politècnica de València, Camino de Vera s/n, 46022 Valencia, Spain*

* Correspondence: mbpolo@upv.es

5.1 Abstract

The role of volume hydrogel holographic gratings as optical transducers in sensor devices for point-of-care applications is increasing due to their ability to be functionalized for achieving enhanced selectivity. The first step in the development of these transducers is the optimization of the holographic recording process. The optimization aims at achieving gratings with reproducible diffraction efficiency, which remains stable after reiterative washings, typically required when working with analytes of a biological nature or several step tests. The recording process of volume phase transmission gratings within Acrylamide/Propargyl Acrylate hydrogel layers reported in this work was successfully performed, and the obtained diffraction gratings were optically characterized. Unslanted volume transmission gratings were recorded in the hydrogel layers diffraction efficiencies; up to 80% were achieved. Additionally, the recorded gratings demonstrated stability in water after multiple washing steps. The hydrogels, after functionalization with oligonucleotide probes, yields a specific hybridization response, recognizing the complementary strand as demonstrated by fluorescence. Analyte-sensitive hydrogel layers with holographic structures are a promising candidate for the next generation of in vitro diagnostic tests.

5.2 Introduction

Holographic biosensors are emerging as a new technology for the development of portable analytical devices for label-free detection applications [1]. Holograms offer a direct transduction method with several advantages, such as fast response and high sensitivity. Typically, holograms are recorded in various photosensitive materials, such as silver halide films, dichromated gelatins or photopolymers [2]. Self-processing materials, such as photopolymers, are the most used in recent years, since they have excellent holographic characteristics and low cost [3].

Recently, hydrogels have attracted attention for holographic sensing applications [4]. These materials are made of three-dimensional polymeric networks of hydrophilic polymers with a high water-absorbing capacity [5]. Moreover, their composition can be fine-tuned in order to obtain appropriate chemical, mechanical and biological characteristics, enabling the incorporation of specific probes, such as oligonucleotides, proteins and others [6 –8]. Hydrogels as support matrices for biosensing allow for the high incorporation of recognition elements in three dimensions and the provision of an aqueous and biocompatible microenvironment. For the fabrication of holographic gratings in hydrogels, it is important to obtain a transparent layer with good optical quality and high permeability. Holographic recording in light-sensitive materials is based on the process of photoinduced polymerization [9]. The fabrication method of volume holographic gratings consists of sensitizing the recording layer with a light-absorbing material and exposing it to laser light with periodically varying intensity. Normally, a mixture of monomers, a crosslinker, a free radical generator and a dye photosensitizer are required for the recording of volume transmission gratings [10]. Photopolymers are typically formed by a polymeric binder and other components that allow for the fabrication of dry layers, but the use of hydrogels as holographic matrices is strongly appealing for obtaining materials stable in aqueous environment [11,12]. On exposure to light, the photosensitizer dye reacts through electron transfer to generate free radicals so that polymerization can begin. Hence, the components of the recording material are spatially redistributed when illuminated by an optical interference pattern, resulting in a holographic volume grating. The formation of the grating involves a spatial variation in the density of the polymeric layer due to diffusion driven by the concentration gradient of monomer molecules, from non-irradiated to irradiated areas [13]. The overall refractive index is higher in the polymerized region than in the unpolymerized one due to the higher density of polymer when compared to monomer (VTG recording, Figure S1, Supporting Information). The achieved diffraction efficiency of the recorded hologram depends on many factors, such as the parameters used during recording, such as exposure time and laser intensity, as well as the chemical composition and thickness of the recording layer [14]. Holographic sensor, and biosensors in particular, are still at an early stage of development.

In fact, most common applications focus on physical and chemical sensing (humidity, pH, gases and solvents), but very few are focused on biosensing [15]. The principle of the detection of holographic biosensors is based on the alteration of the diffraction efficiency when an interaction with the target biomolecule (e.g., DNA strand) occurs. Alternatively, a change in the period of the recorded grating can occur due to the material swelling or shrinkage, leading to a different position of the angle of the Bragg peak. Light-sensitive hydrogels functionalized with analyte-sensitive units represent an unexplored opportunity for the fabrication of holographic biosensors. To date, relatively few holographic gratings have been obtained in hydrogels and used as transducers for biosensing. But this sensing technique is of great interest and potential for monitoring different targets. Notably, the transduction of the detector signal into a simple optical readout by holographic gratings can be useful for point-of-care diagnostic devices. A significant advantage of holographic gratings based on hydrogel biosensors is that they can enable the detection of analytes without labelling, thus eliminating the need for additional labels or reagents. Another beneficial aspect of hydrogel-based biosensors is that their composition can be tuned, and they can be easily functionalized with recognition molecules, including enzymes, antibodies, nucleic acids and aptamers, using conventional bio-conjugation techniques. However, there are still some challenges to overcome for the use of this methodology for applications as label-free biosensors. To achieve good analytical performance of holographic hydrogel-based biosensors, the immobilized recognition element plays a crucial role, and additional labelling and signal amplification strategies are often required. Alternatively, the performance of the hydrogel-based holographic grating can be further improved by optimizing the diffractive grating design. Another challenge is to obtain quantitative and repeatable results, due to the difficulty of controlling the quality of the gratings, especially in soft materials, such as hydrogels. A holography-based transduction method has been successfully demonstrated for the detection of biomolecules, volatile organic compounds and metal ions [15]. For example, volume holographic gratings (VHGs) based on hydrogels as sensing platforms have been widely employed for the measure of pH [16], humidity and temperature [17,18], metal ions [19,20], and glucose [21,22]. However, to our knowledge, the direct detection of oligonucleotides has not yet been performed by holographic sensing.

This means that there are no biosensors based on this technology that can detect DNA or RNA. This work focused on the optimization of the recording process of unslanted volume transmission gratings (VTGs) in Acrylamide/Propargyl Acrylate (AM/PA) hydrogel layers. The composition of the hydrogel had already been optimized in a previous work, in which hydrogels were surface micropatterned and utilized as biosensors [23]. By using this hydrogel composition, the bioreceptor elements (thiol-modified DNA probes) can be covalently immobilized via thiol-yne click reaction both before and after the fabrication of the volume grating. The aim of this work is to record holographic gratings in hydrogel layers with high diffraction efficiencies, for achieving an improved sensitivity of the designed holographic biosensor. In fact, phase holograms recorded in the volume of the layer offer the advantage of achieving a diffraction efficiency of nearly 100%, which is much higher than sinusoidal surface gratings with diffraction efficiencies of around 30% [16]. Herein, unslanted volume transmission gratings (VTGs) were recorded directly in (AM/PA) hydrogel layers, to the best of our knowledge, for the first time. Also, their capability to be biofunctionalized with an covalently attached oligonucleotide probe and to perform specific hybridization, thereby keeping their diffractive property, is demonstrated. Initially, (AM/PA) hydrogel layers were prepared by thermal activation. Afterwards, to carry out the recording of unslanted VTGs, the hydrogel layers were incubated in the dark with the incubation solution. This solution contains an aqueous mixture of acrylamide monomers; N, N-methylene bisacrylamide as a crosslinker; triethanolamine (TEA) as an initiator; and erythrosine B (EB) as a dye. To optimize the recording process, different concentrations of the incubation solution and recording parameters were tested. After incubation time, the hydrogels were used in holographic recording, which was observed in real time. At the end of the recording process, the gratings angular Bragg selectivity curves were characterized. Finally, the stability in water of VTGs obtained within hydrogel layers was examined in view of their potential use in biosensing.

5.3 Results and Discussions

Thin films of hydrogels composed of AA, MBA and PA were prepared by adapting the described protocol [12,23]. AA and MBA acted as the skeletal monomer and crosslinker, respectively. PA is an additional monomer that provides the hydrogel with alkyne groups that are available to be functionalized with thiolated moieties by photo-click chemistry. We have previously optimized the relationship between monomers and crosslinkers (i.e., the crosslinking degree) needed to generate transparent and moldable hydrogels [23]. In addition, in the same study, we also fabricated hydrogels by photochemical and thermal activation. Thermal activation (i.e., using KPS as activator) yielded hydrogels with more homogenous and porous networks. Accordingly, for this work, we have chosen the previously optimized (see materials and methods section) and characterized composition and activator [23]. Once synthesized, the morphology of the lyophilized (AM/PA) hydrogel was characterized by SEM microscopy (Figure 1a). The typical porous structure of MBA-AA hydrogels of a low crosslinking degree can be observed. The ability of the hydrogel layer to swell is important to ensure that it is sufficiently permeable to facilitate the diffusion of the incubation solution. Figure 1b shows the degree of swelling of the lyophilized layers over time. These hydrogels reached approximately 500% swelling at 24 h, which is associated with the porosity of the hydrogel layer. In order to achieve a reproducible holographic recording in hydrogel layers, two different compositions of the incubation solution (Table 3) and then different recording parameters were initially tested. The hydrogel layers (AM/PA) placed on top of the microscopic slides were covered with 200 μL of incubation solution and stored inside Petri dishes in the dark at room temperature. Thus, the components of the incubation solution can penetrate the layer and thus participate in the photopolymerization. The holographic recording begins with the absorption of laser light by the sensitizing dye (erythrosine B), which is promoted to its an excited stated. It reacts then with TEA (the electron donor), producing TEA free radicals. These free radicals react with the monomer (AA) and crosslinker (MBA) to initiate free-radical polymerization.

Therefore, the optical sensitivity of the hydrogel to the wavelength of the recording beam is influenced by the concentration of the components in the incubation solution. The most important aspect observed for holographic recoding in hydrogels is that is essential that the hydrogel layer reaches complete swelling in water prior to the incubation phase. In fact, no effective holographic recording was achieved for non-hydrated (AM/PA) hydrogel layers using these volumes of incubation solution. In contrast, high diffraction efficiencies were obtained for the hydrogel layers after 24 h of complete swelling in distilled water.
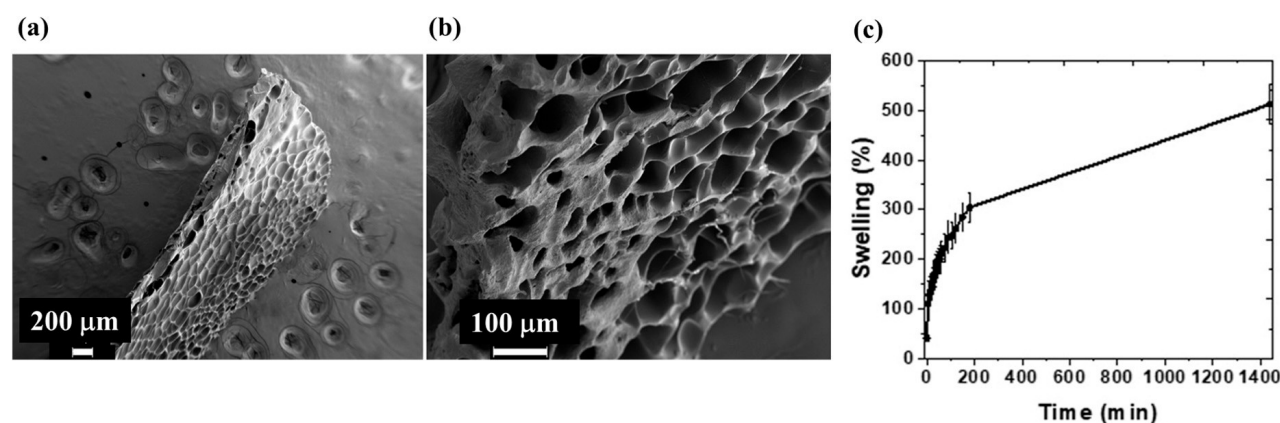
Figure 1. (a,b) show SEM images of the cross section of the hydrogel films at different magnifications, fully hydrated and then lyophilized, and (c) shows the swelling kinetic study of (AM/PA) hydrogel in PBS-T, using synthesized samples with a size of 1 cm^3.

**Table 1.** Characterization of unslanted volume grating obtained after delivering 200 µL of incubation solution A and evaluating different incubation times.

| Incubation Time (Days)	Layer Thickness (µm)	Recording Beams Intensity (mW/cm2)	Recording Exposure Time (s)	Maximum DE Achieved (%)
1	300	7.5	100	40
2	300	7.5	100	80
3	300	7.5	100	50

Two different incubation solutions, A and B (B solution having two-fold amount of AM and MBA than A solution), were tested for the recording process. For this experiment, incubation was carried out for 1 day. The DE was monitored in real time. Better results were observed with incubation solution A. In the case of solution B, it was observed that the real-time growth curve of the diffraction efficiency initially increases and then suddenly starts decreasing (Figure 2).

To achieve better final DE, VTG were recorded again with incubation solution B, but the laser exposure of the sample was stopped by the shutter when the diffraction efficiency started to decrease (Figure S2a). As expected, a higher DE was obtained when the exposition time was decreased (Figure S2b). The diffraction efficiency of VTG measured after the recording in the Bragg curve, where varying the incidence angle of the DE was recorded, was higher than that observed in real time during the recording process. The decrease in diffraction efficiency observed in real time (Figure 2) is most probably associated with the shrinkage of the hydrogel VTG that occurred during recording. In addition, an increased scattering of the diffraction produced by VTGs recorded with incubation solution B was observed. This behavior is due to the high concentration of monomer and crosslinker, which leads to the formation of a much harder and crosslinked VTG with a slight white color due to the increased scattering. However, it worth noting that this effect was not observed in the layers incubated with solution A. Thus, the use of incubation solution A was decided, as maintaining the same recording parameters used with solution B resulted in holographic gratings with a higher diffraction efficiency. Furthermore, it was possible to record VTGs of different dimensions: first, spots of 1.45 cm^2 were recorded, and later, considering their further expansion in water, smaller spots of 0.84 cm^2 were recorded (Figure 3). This parameter is important in view of using the holograms for biosensing. For example, for the functionalization with the DNA receptor, less probe material will be required compared to the complete functionalization of the VTG area.
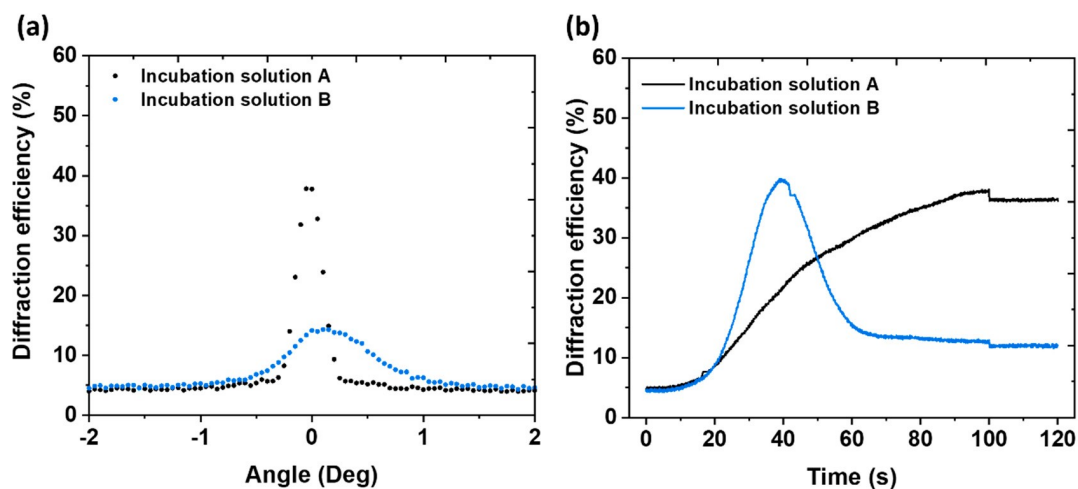
Figure 2. (**a**) Variation of the DE during the recording process. The real-time growth of DE in (AM/PA) hydrogel incubated with incubation solution A and B can be observed, and (**b**) variation of the DE with the incidence angle (Bragg curves) of the recorded VTGs.
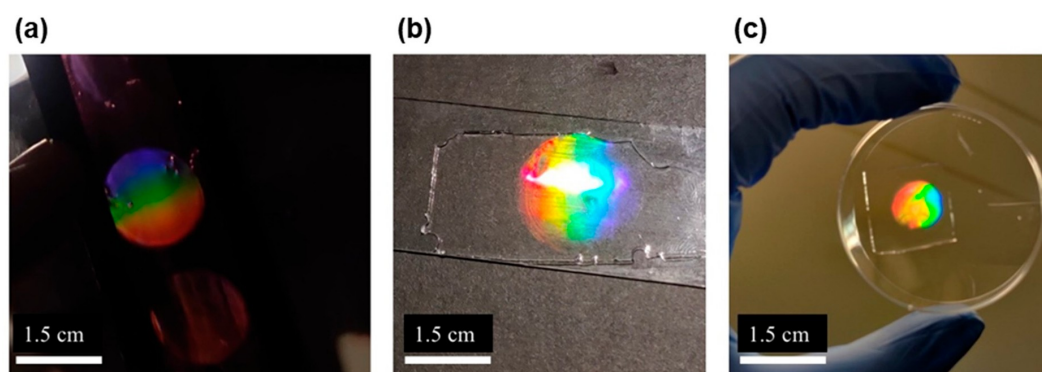
Figure 3. Digital photos of the transmission phase volume gratings recorded in (AM/PA) hydrogel layers: recorded spots of (**a**) 1.45 cm^2 after recording and (**b**) 2.72 cm^2 after first wash with distilled water; (**c**) smaller recorded spots of 0.84 cm^2, which (image not shown), after the first washing with distilled water, reached a size of 1.56 cm^2.

Further, using real-time monitoring of the recording process, different incubation times were tested with incubation solution A: one, two and three days of incubation. DE was monitored in real-time, and Bragg curves were obtained after the recording (Figure 4, Table 1).

The hydrogel layers were exposed for up to 100 s during holographic recording; it was observed that, after exposure, the diffraction efficiency continues to be stable. As it can be seen from the results, the dynamic linear range increases with increasing incubation days from one to two, obtaining a DE of 80% in the latter. Interestingly, the curve of hydrogels incubated for three days showed a significant inhibition time, the hydrogel layers incubated for three days start recording the transmission gratings after 40 s of laser light exposure, whereas the hydrogels incubated for one and two days show a faster response by starting the recording process within the first 20 s of exposure. After 100 s the DE was 50% for hydrogels incubated for three days, which is lower than the DE in layers incubated for two days. The behavior of the real-time diffraction efficiency is associated with the diffusion of the incubation solution within the hydrogel, which gradually decreases over time as the hydrogel layer begins to dry out. Two days of incubation allowed for the complete absorption of the incubation solution while ensuring optimal and reproducible holographic recording with high diffraction efficiency.
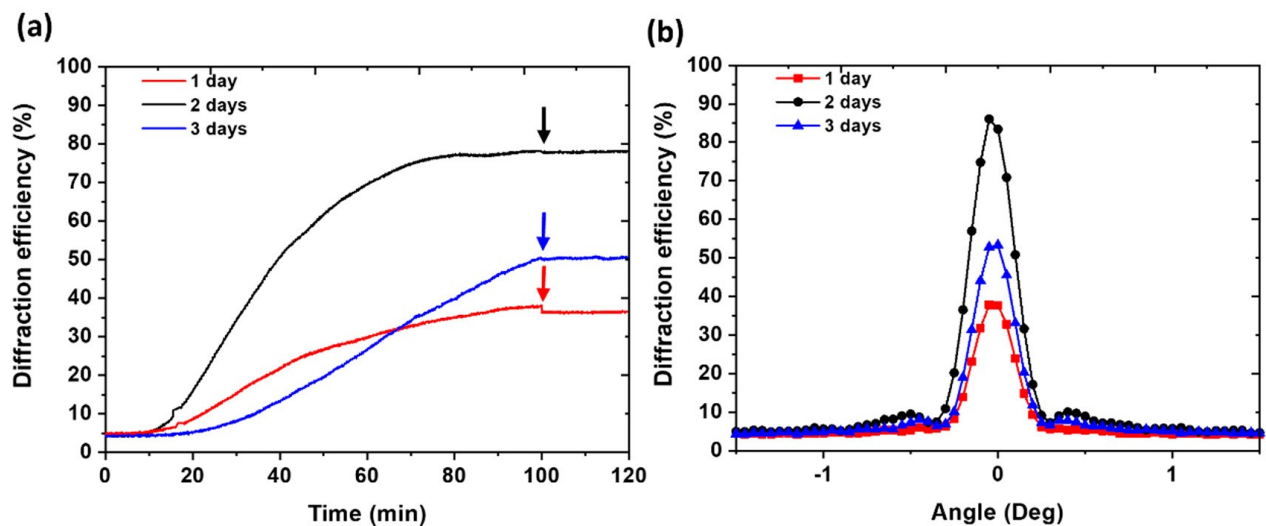

Figure 4. (**a**) Real-time growth curve of DE% and (**b**) the corresponding Bragg curves after one, two and three days of incubation with incubation solution A.

To study the VTG hydrogel stability, Bragg selectivity curves were measured just after recording of hydrogels incubated for 1 day with incubation solution A and after multiple overnight washing step with distilled water (Figure 5). After the first washing step, the components that did not react during the formation of the volume transmission gratings were washed away, which is reflected in a slight change in diffraction efficiency around 10%.

The observed broadening of the Bragg selectivity curve after the washing step can be explained by the dimensional change of the layer due to the swelling of the hydrogel grating. Thus, the recorded hydrogel grating swells and expands, resulting in a slight increase in fringe spacing. The hydrogels are generally soft and elastic, and the stable and interconnected 3D crosslinked structure of the optimized hydrogel (AM/PA) allows for stable volumetric diffractive structures.

To obtain the thickness and refractive index modulation of the recorded gratings, Bragg's angular selectivity curves were fitted using Kogelnik's coupled-wave theory [24]. An initial simulation was performed on a VTG with 35% diffraction efficiency (Figure S3, Supporting Information). Then, the theoretical fitting was performed on the Bragg curve obtained under the optimized conditions 80% DE (Figure S4, Supporting Information). Both Bragg curves obtained from the simulation are in good agreement with the respective experimental curves. The simulation results are summarized in Table 2.
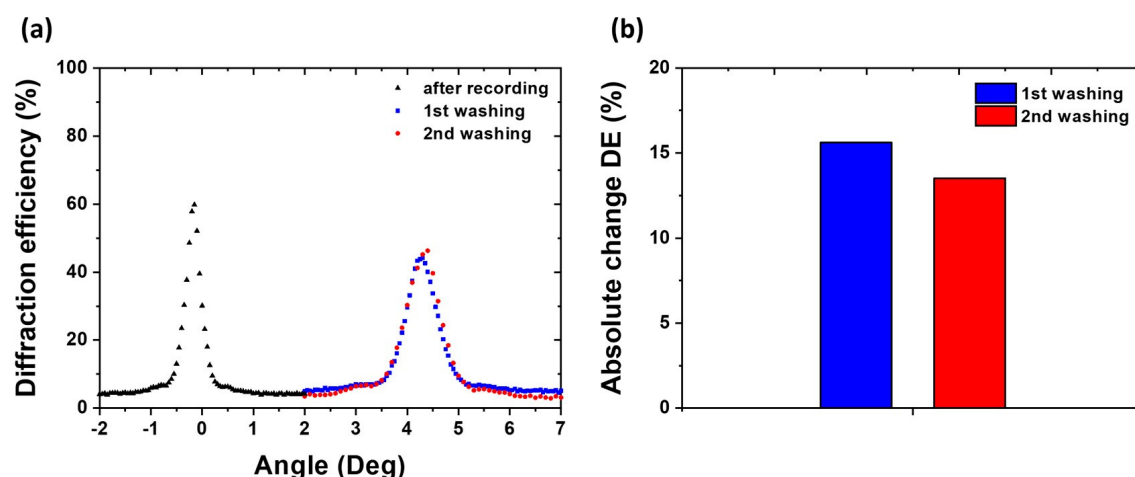
Figure 5. (**a**) Bragg selectivity curves of (AM/PA) hydrogel layers obtained after recording with 60% DE and after two overnight washes with approximately 44–46% DE. (**b**) Histogram of absolute DE% change after the washing steps.

Table 2. Results obtained by fitting Bragg selectivity curves.

	VTG Thickness (µm)	Refractive Index Modulation (RIM)
After recording	190	0.0010
First washing	60	0.0015
Second washing	62	0.0017

Furthermore, the Bragg curve of the optimized volume gratings was characterized over time to test how the diffraction efficiency and/or the fringe spacing are affected when the hydrogel starts drying (Figure 6). In this experiment, the Bragg curves of the (AM/PA) hydrogel layers were obtained at controlled times and temperature and the relative humidity conditions were also monitored. The fringe spacing (Λ) was calculated with Equation (1):

$$\Lambda = \frac{\lambda}{2\sin\left[\frac{(\text{peak}\theta1 - \text{peak}\theta2)}{2}\right]} \tag{1}$$

where λ is the wavelength of the probe beam, and (peak θ_1–peak θ_2) is the angle calculated in the Bragg curve between the two Bragg peaks. From the results, it was possible to observe a gradual decrease in diffraction efficiency already after one hour of sample drying at RT, while the fringe spacing did not change significantly during time. It can be observed that even when the hydrogel is dry, about 30% of the initial DE% is retained. At the same time, it can also be seen that the change in the VTG period as the hydrogel dries over time is about 1%.

(a)

Time (min)	DE (%)
30	64.98
60	58.31
120	38.36
180	31.38
240	19.40

(b)

(c)

(d)
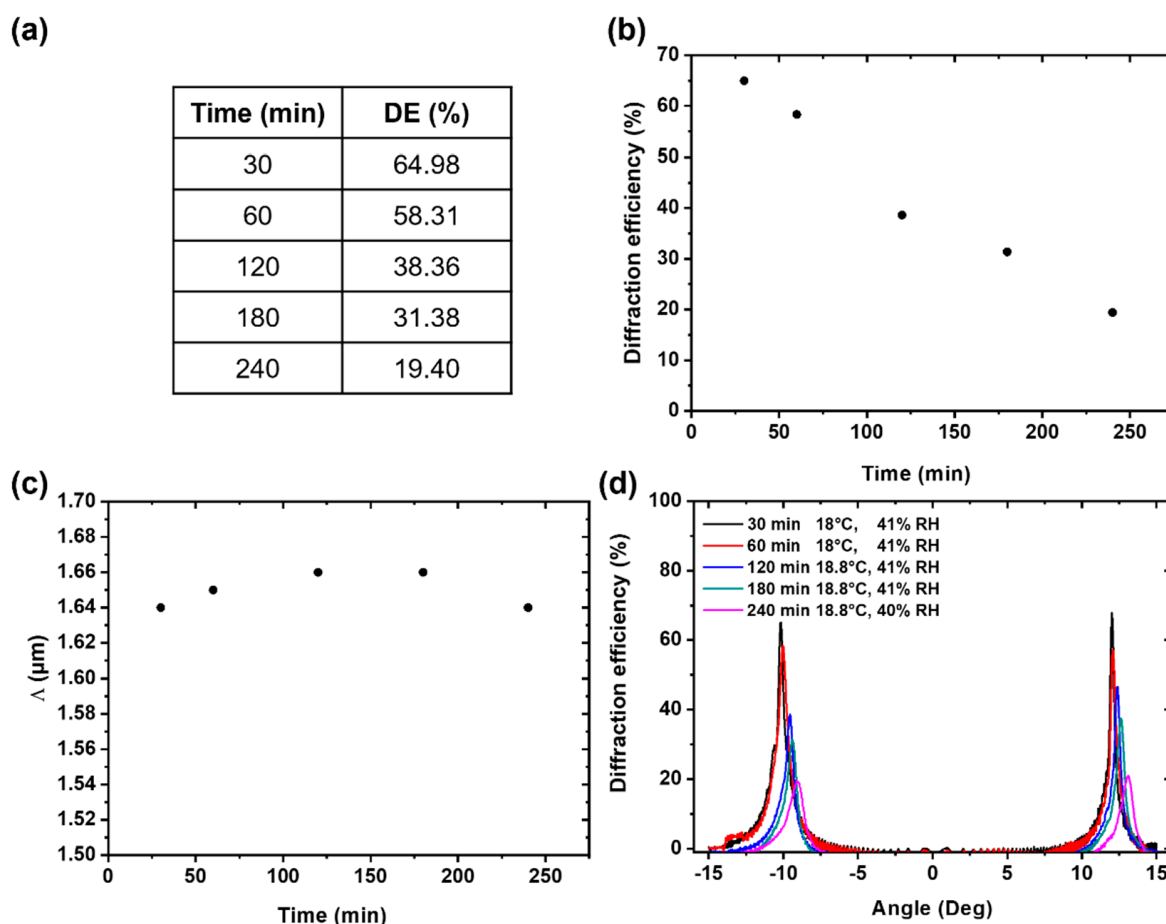
Figure 6. (**a**) Data of the hydration state study and (**b**) diffraction efficiency change over time. (**c**) Fringe spacing versus time and (**d**) Bragg selectivity curves of (AM/PA) hydrogel layer while drying over time.

Biofunctionalization of VTGs and Hybridization Assays by Fluorescence Detection

Some of the hydrogels recorded with volume gratings were subjected to the analysis of hybridization ability with complementary strands using fluorescence detection. For that, starting from a VTG with a DE of 20% in water, they were conditioned in SSC1x, and their diffraction diminished to one half. Then, VTGs conditioned in SSC1x were incubated with 5 μM solution of an oligonucleotide probe bearing a thiol group in THF/Ac-TCEP 1:1, and irradiated for 30 min, according to the protocol described for biofunctionalization [24]. After washing with SSC1x for several hours, the diffraction efficiency decreased further by 40%.

Then, the VTG hydrogel was submitted to serial incubations with increasing concentrations of Cy5-labeled oligonucleotides (0.2; 0.5; 1 and 2 µM), with the complementary sequence of the immobilized probe for 1 h. Each condition was assayed by triplicate. After each incubation, the VTG was washed with SSC1x for 1 h, and the fluorescence was recorded. The same experiment was carried out with a biofunctionalized VTG but using a non-complementary sequence for the hybridization, as a control of the specificity in the target biorecognition.

As it can be observed in Figure 7, the fluorescence increased with the concentration of complementary strand, while in the case of hybridization with the non-complementary target, only residual fluorescence remained inside the VTG hydrogel. Thus, it was concluded that the probe was successfully immobilized inside the VTG, keeping its bioavailability to hybridize in a specific manner. Furthermore, VTG hybridized with the complementary target keeps their diffractive capacity (Figure S5, Supporting Information).
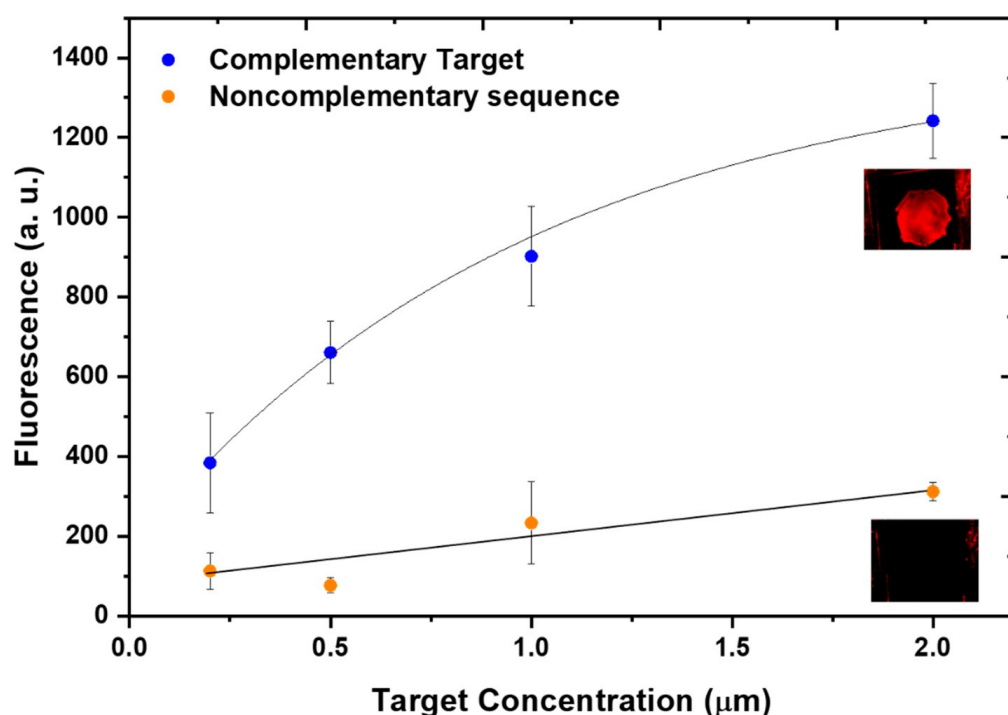
Figure 7. Fluorescence intensity of VTG hydrogels biofunctionalized with an oligonucleotide probe and incubated with increasing concentrations of labeled complementary target (blue) or labeled non-complementary sequence (orange) washed with SSC1x for 1h.

To characterize the prepared hydrogels, and to demonstrate their robustness, the reusability of the biofunctionalized hydrogels was tested. For that, a biofunctionalized VTG hybridized with the complementary labeled oligonucleotide was subjected to different dehybridization conditions, and the dehybridization was monitored by fluorescence (Figure 8a). As expected, the initial fluorescence (target incubation) decreased consider- ably after SSC1x washing. Then, it slightly decreased after dehybridization with water washing, and even more when the temperature was increased, however, a residual fluorescence still remained inside the VTG hydrogel. This indicated that the hydrogel was not fully dehybridized. The complete dehybridization was achieved when 50% formamide in SSC1x was used, as in this case, and the fluorescence signal disappeared totally. The VTG hydrogel, fully dehybridized, was submitted to another hybridization cycle, and the corresponding control, with a non-complementary target was carried out. Figure 8b shows the fluorescence signal after washing with SSC1x. After the dehybridization, specific hybridization was again achieved, demonstrating the reusability of the bioresponsive hydrogel. Although one-shot assay is typically used in biosensing protocols, the reusability test gives a characterization of the material robustness.
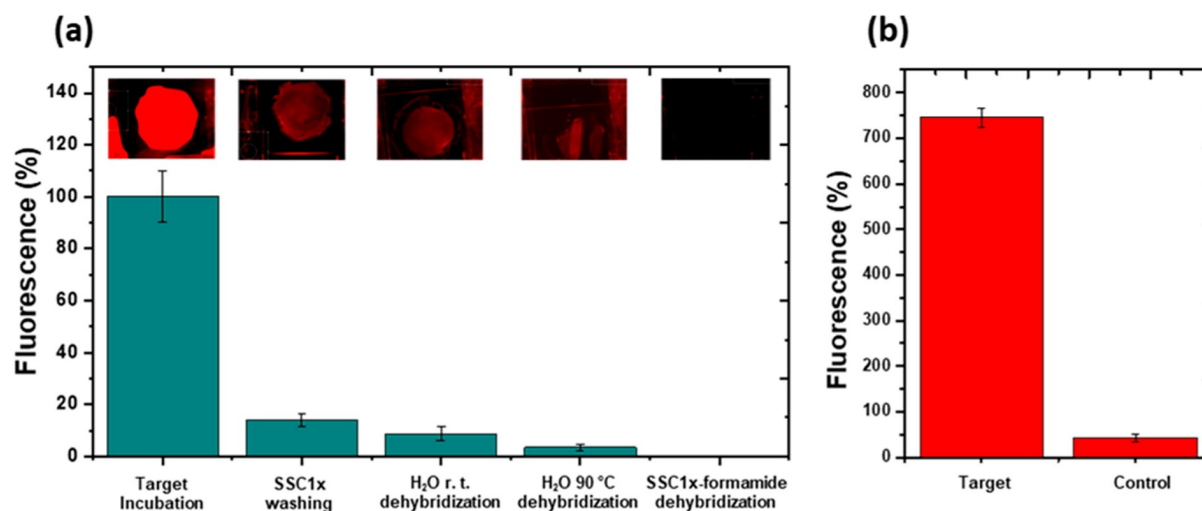
Figure 8. (**a**) Fluorescence (%) measured after target hybridization, washing with SSC1x, and after the several dehybridization steps carried out at different conditions. All fluorescence images were capture using the same acquisition conditions (gain and exposition time). Fluorescence was normalized to the maximum signal (target incubation). (**b**) Fluorescence of the VTG hydrogel dehybridized with SSC1x-formamide after a second cycle of hybridization with a complementary target and a non-complementary target control labeled with Cy5. Incubation was carried out for 1h in SSC1x and washing was performed for 1h in SSC1x.

5.4 Conclusions

Unslanted volume transmission gratings (VTGs) were recorded in an Acrylamide/ Propargyl Acrylate hydrogel layer with good reproducibility and good optical quality. The conditions of the incubation and recording processes were successfully optimized and VTG hydrogels were optically characterized. Furthermore, the volume hydrogel gratings were found to be stable in water, maintaining their diffraction efficiency even after successive washes. The optimized holographic recording process performed in hydrogel layers can be useful for the design of potential holographic biosensors. The hydrogel VTGs can be biofunctionalized with an oligonucleotide probe, which can act as a bioresponsive material, hybridizing only with the complementary strand target and retaining their diffractive properties.

The reusability of the bioresponsive hydrogel for several hybridization cycles has been also demonstrated. Thus, these three-dimensional hydrogel networks with embedded diffractive structures are promising candidates for the analysis of targets involved in diseases and health monitoring, as they are able to perform label-free detection, which can save cost and time and reduce assay complexity.

5.5 Materials and Methods

Materials

Acrylamide (AM) (98.5%, Molecular weight (MW)=71.08 g/mol), propargyl acrylate (PA) (98%, MW=110.11 g/mol), N, N'-methylenebisacrylamide (MBA) ($\geq$99.0%, MW=154.17 g/mol), potassium persulfate (KPS) ($\geq$99.0 %, 270.32 g/mol), triethanolamine (TEA) (98%, MW=149.19 g/mol), formamide ($\geq$99.0 %, MW=45.04 g/mol), 2,2-Dimethoxy-2-phenylacetophenone (DMPA) (99%, MW=256.30 g/mol), tris (2-carboxyethyl) phosphine hydrochloride (TCEP) ($\geq$99.0 %, MW=286.65 g/mol), sodium acetate ($\geq$99.0 %, MW=82.03 g/mol), tetrahydrofuran (THF) (99,9 %, MW=72.11 g/mol), sodium chloride (NaCl) ($\geq$99% MW=58.44 g/mol), sodium citrate dihydrate ($\geq$99.0%, MW=294.10 g/mol), ethylenediaminetetraacetic acid (EDTA) ($\geq$99.0%, MW=292.24g/mol), and erythrosine B (EB) dye ($\geq$95.0%, MW=835.89 g/mol) were all purchased from Sigma–Aldrich and used without any further purification. The Ac-TCEP buffer, pH 4.5, consists of 25 mM of TCEP, 0.15 M sodium acetate, 0.1 M EDTA, and 0.1 M NaCl in DI water and the saline-sodium citrate buffer (SSC1x, pH 7.4) consists of 0.15 M NaCl and 0.015 M sodium citrate. The oligonucleotides were supplied by Sumilab (Valencia, Spain), and the sequences used are listed in Table S1 (Supporting Information).

Hydrogel Layers Preparation

Hydrogel layer preparation was performed using an adapted protocol [12,23]. First, 25% (w/v) of AM, 0.05% (w/v) of MBA 75 µL of PA, and 1% (w/v) of KPS were mixed in 5 mL of distilled water. Then, (AM/PA) hydrogel layers were obtained by depositing 500 µL of the pre-polymer solution onto a well, made of a mould (5 cm × 1.4 cm × 340 µm) sticked to a levelled glass slide (7.5 cm × 2.5 cm) (Labbox Labware, S.L., SLIBG10-050, Premia de Dalt, Spain). The full well was covered with another glass slide and squeezed with two clamps. Hydrogels were synthesized by thermal activation for 30 minutes at 60 °C (Scheme 1). After the polymerization time, the top glass slide was removed, and hydrogels were soaked overnight in distilled water at RT. The calculated thickness of the hydrogel layer was approximately 300 ± 10 µm.
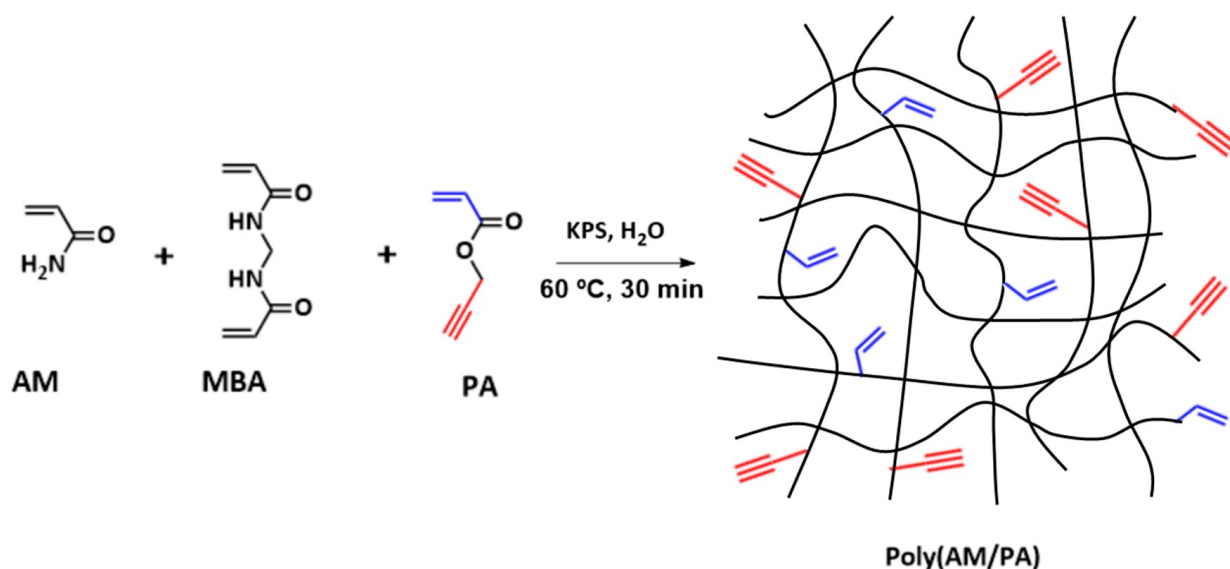
Scheme 1. Representation of the hydrogel synthesis by free-radical polymerization (FRP). AM: Acrylamide, MBA: N, N′-methylenebis (acrylamide), PA: propargyl acrylate, KPS: potassium persulfate. The highlighted functional (acryl in blue, and propargyl in red) groups are used for the bioreceptor incorporation. Figure adapted from [23].

Morphology Characterization

The morphological characterization of (AM/PA) hydrogel layers was performed using scanning electron microscopy (SEM, Gemini SEM 500 system, Zeiss, Oxford Instruments, Oxford, UK). First, hydrogels layers were immersed in distilled water to completely swell. Then, they were frozen at 20 ◦C prior to lyophilization overnight (Telstar Lyoquest freeze-drier, Azbil Telstar Technologies, S. L. U., Terrasa, Spain). The resultant dry aerogel samples were finally covered with a Au layer of about 15 nm using sputter-coating (BAL-TEC SCD 005 sputter coater, Leica microsystems, Wetzlar, Germany).

Swelling Behavior Studies

The swelling kinetics were obtained for the (AM/PA) hydrogel. Freeze-dried hydrogel samples of approximately 1 cm^3 were used for this study. The lyophilized samples were immersed in PBS-T (10 mL) at RT and their weight was recorded successively over time until a constant weight (total swelling) was reached. The degree of swelling (%) was calculated using Equation (2), where Wt is the weight of the hydrogel after being immersed in the buffer for a time 't' and W_0 is the weight of the lyophilized hydrogel before buffer immersion.

$$Swelling\ (\%) = \frac{Wt - Wo}{Wo} \cdot 100 \tag{2}$$

Incubation step before recording

Hydrogels layers were prepared for the holographic recording process. Two different incubation solutions were tested (A and B, Table 3). The incubation solutions contained an aqueous mixture of acrylamide; N, N-methylene bisacrylamide as a crosslinker; Tri-ethanolamine (TEA) as an initiator; and Erythrosine B (EB) as a dye. The Erythrosine B (EB) dye was previously dissolved in distilled water at 0.11% (w/v). A volume of 200 µL of incubation solution was deposited on the already polymerized hydrogel layers. The samples then were kept inside a Petri dish in the dark at room temperature until com- plete absorption of the compounds within the hydrogel matrix was achieved. Different incubation times were tested: 1 day, 2 days and 3 days.

Table 3. Composition of incubation solutions.

Incubation Solution	AM (g)	MBA (g)	TEA (mL)	EB (mL)
A	1	0.2	1	4
B	2	0.4	1	4

Holographic Recording and Probe Set-Up

The optical setup used (Figure 9) consists of a Nd:YVO$_4$ laser emitting at 532 nm for the recording and a He-Ne laser emitting at 633 nm for the reading (probe laser). Two collimated beams were obtained with equal intensity by splitting the laser light from the Nd:YVO$_4$ laser with a polarizing beam splitter (PBS). The intensity of the two beams was equalized with the help of a half-wave plate (HWP) positioned in front of the PBS, thus allowing for control over the state of polarization of the linearly polarized beam entering the PBS. After passing through the PBS the beam passed through a second half-waveplate. This was necessary to ensure that both recording beams have parallel polarizations for achieving maximum visibility of the interference pattern that is being recorded. Both recording beams were s-polarized. The total angle between the two recording beams of 24.6 degree was selected to create an interference pattern of a spatial frequency of 800 lines/mm (the grating period (Λ) was 1.25 µm). To ensure that the recording process was carried out properly, a He-Ne laser beam of 633 nm wavelength was used, as a probe beam, to fully characterize the holograms. The hydrogel samples were placed on a computer-controlled rotational stage (RS) (Newport ESP300). To acquire real-time diffraction efficiency growth (η) and subsequently Bragg selectivity curves, the intensity of the first-order diffracted beam (I_d) was monitored with an optical power meter (Newport Model 840). The signal from the optical power meter was sent to an analogue-to-digital converter connected to a computer. A LabVIEW program was used to control the shutters, rotational stage, and the data acquisition. The volume transmission grating spot size was reduced from 1.45 cm^2 to 0.84 cm^2 using a diaphragm.
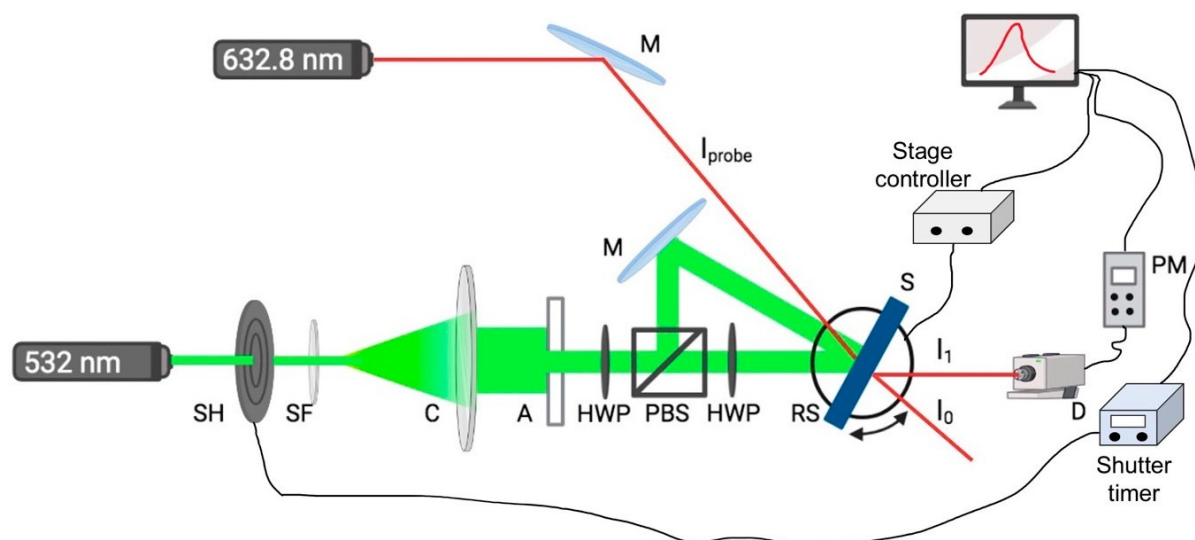
Figure 9. Experimental set-up for the recording of volume transmission gratings. The recording beam wavelength was 523 nm, and real-time monitoring was carried out with probe beam of 632.8 nm. M: Mirror, SH: shutter, SF: spatial filter, C: collimating lens, A: aperture, PBS: beam splitter, HWP: half wave plate; RS: rotational stage, S: sample, D: detector, PM: power meter.

Holographic Recording and Characterization of Hydrogel Layers

Holographic volume gratings were recorded within hydrogel layers using transmission geometry (Figure S1a). Specifically, phase holograms were recorded through the laser-light-induced photopolymerization process, which led to the modulation of the refractive index within the hydrogel layer. Volume transmission gratings (VTGs) were recorded directly on Acrylamide/Propargyl Acrylate hydrogel layers using the unslanted configuration, in which the two recording beams have equal angles of incidence. Recording parameters, such as green laser power and exposure time, were optimized for the recording process. The development of the hydrogel holographic gratings was monitored by measuring the diffraction efficiency (DE% or η) growth curves in real time with the probe beam (red). The diffraction efficiency of the recorded VTGs was calculated as the ratio of the diffracted beam intensity (I_d) to the incident beam intensity (I_{probe}) per cent.

To observe the dependence of the intensity of the diffracted light (I_d) on the angle of incidence of the probe beam, Bragg selectivity curves of hydrogel VTGs were obtained by rotating the sample holder placed on a high accuracy rotational stage (model Newport ESP300 with angular resolution of 0.001∘). After recording, hydrogels were immersed in distilled water and the diffraction efficiency was measured after several washes to verify the stability of the recorded VTGs. In addition, Kogelnik's coupled-wave theory was used to fit the Bragg angular selectivity curves of the gratings and thus extract the thickness of the layers and the refractive index modulation created during the recording process [24].

Biofuncionalization of VTGs and Hybridization/Dehybridization Experiments
For future biosensing applications, the VTG layers were covalently functionalized with a thiol-modified DNA probe via the thiol-ene/thiol-yne-coupling photo-click reaction [23]. A 1 mL solution of a 1:1 THF/Ac-TCEP mixture at 5 µM of functionalization probe was prepared, and 1% (*w/v*) DMPA photoinitiator was added. VTG hydrogels were placed inside circular containers with 300 µL of the prepared probe solution and irradiated at 365 nm in a UV photoreactor, LightOx PhotoReact (13 mW/cm^2 light power) (Sigma-Aldrich, Madrid, Spain) for 30 min. Then, biofunctionalized VTGs were washed overnight in SSC1x. DE was monitored before and after the biofunctionalization in SSC1x. Biofunctionalized VTGs were incubated with serial increasing concentrations of Cy5-labeled complementary or non-complementary sequence as a target (0.2; 0.5; 1 and 2 µM) for 1 h and washed for 1 h with SSC1x. The fluorescence signal was monitored after every washing step using a homemade surface fluorescence reader (SFR) equipped with a CCD camera ($\lambda = 647$ nm, exposure time = 10 s, gain = 1). Fluorescence image data processing was performed with the GenePix Pro 4.0 software from Molecular Devices, Inc. (Sunnyvale, CA, USA). The probe and targets used are listed in Table S1 (Supporting Information). Dehybridization of VTGs hybridized with 1 µM of labeled complementary target after their washing with SSC1x was carried out by different approximations: (a) the immersion of the VTGs in 5 mL of H_2O for 16 h at RT; (b) the immersion of the VTGs in 5 mL of H_2O for 1 h at 90 ∘C; and (c) the immersion in 5 mL SSC1x, 50% formamide. Fluorescence was registered after every step ($\lambda = 647$ nm, exposure time = 5 s, gain = 1).

A second hybridization step was carried out with the VTGs dehybridized with SSC1x, 50% formamide, with labeled complementary and not-complementary target at 5 µM, following the previously described protocol. Fluorescence was registered after washing with SSC1x ($\lambda = 647$ nm, exposure time = 5 s, gain = 1).

Supplementary Materials: The following supporting information can be downloaded at: https://www.mdpi.com/article/10.3390/gels9090710/s1, Figure S1: Recording and probing of a volume transmission holographic grating, and probe beam path inside the layer, θB Bragg angle; Table S1: Sequences of DNA used; Figure S2: Real-time growth curves of diffraction efficiency, and Bragg curves of (AM/PA) hydrogel incubated with incubation solution B; Figure S3: Theoretical and experimental angular selectivity curves for VTG recorded in hydrogel layers (AM/PA); Figure S4: Theoretical and experimental angular selectivity curves for the optimised conditions for VTG recorded in hydrogel layers (AM/PA); Figure S5: Diffraction pattern projected on a white screen of biofunctionalized VTG hydrogel.

5.6 References

1. Yetisen, A.K.; Naydenova, I.; Da Cruz Vasconcellos, F.; Blyth, J.; Lowe, C.R. Holographic Sensors: Three-Dimensional Analyte- Sensitive Nanostructures and Their Applications. *Chem. Rev.* 2014, *114*, 10654–10696. [CrossRef] [PubMed]

2. Blanche, P.A. Holographic Recording Media and Devices. *Encycl. Mod. Opt.* 2018, *4*, 87–101. [CrossRef]

3. Mihaylova, E.M. Water-Soluble Holographic Photopolymers for a Sustainable Future—A Review. *Coatings* 2022, *12*, 1765. [CrossRef]

4. Pal, A.K.; Labella, E.; Goddard, N.J.; Gupta, R. Photofunctionalizable Hydrogel for Fabricating Volume Optical Diffractive Sensors. *Macromol. Chem. Phys.* 2019, *220*, 1900228. [CrossRef]

5. Sun, X.; Agate, S.; Salem, K.S.; Lucia, L.; Pal, L. Hydrogel-Based Sensor Networks: Compositions, Properties, and Applications—A Review. *ACS Appl. Bio Mater.* 2021, *4*, 140–162. [CrossRef] [PubMed]

6. Madduma-Bandarage, U.S.K.; Madihally, S.V. Synthetic Hydrogels: Synthesis, Novel Trends, and Applications. *J. Appl. Polym. Sci.* 2021, *138*, 50376. [CrossRef]

7. Lu, J.; Chen, Y.; Ding, M.; Fan, X.; Hu, J.; Chen, Y.; Li, J.; Li, Z.; Liu, W. A 4arm-PEG Macromolecule Crosslinked Chitosan Hydrogels as Antibacterial Wound Dressing. *Carbohydr. Polym.* 2022, *277*, 118871. [CrossRef] [PubMed]

8. Lu, J.; Fan, X.; Hu, J.; Li, J.; Rong, J.; Wang, W.; Chen, Y.; Liu, W.; Chen, J.; Chen, Y. Construction and Function of Robust and Moist Bilayer Chitosan-Based Hydrogel Wound Dressing. *Mater. Des.* 2023, *226*, 111604. [CrossRef]

9. Fouassier, J.P.; Allonas, X.; Burget, D. Photopolymerization Reactions under Visible Lights: Principle, Mechanisms and Examples of Applications. *Prog. Org. Coat.* 2003, *47*, 16–36. [CrossRef]

10. Neipp, C.; Taleb, S.I.; Francés, J.; Fernández, R.; Puerto, D.; Calzado, E.M.; Gallego, S.; Beléndez, A. Analysis of the Imaging Characteristics of Holographic Waveguides Recorded in Photopolymers. *Polymers* 2020, *12*, 1485. [CrossRef]

11. Ramírez, M.G.; Lucío, M.I.; Morales-Vidal, M.; Beléndez, A.; Bañuls, M.J.; Maquieira, Á.; Pascual, I. Holographic Transmission Gratings Stored in a Hydrogel Matrix. *Photosensit. Mater. Their Appl.* 2020, *11367*, 22–29. [CrossRef]

12. Berramdane, K.; Ramírez, M.G.; Zezza, P.; Lucío, M.I.; Bañuls, M.J.; Maquieira, Á.; Morales-Vidal, M.; Beléndez, A.; Pascual, I. Processing of Holographic Hydrogels in Liquid Media: A Study by High-Performance Liquid Chromatography and Diffraction Efficiency. *Polymers* 2022, *14*, 2089. [CrossRef]

13. Jiang, N.; Davies, S.; Jiao, Y.; Blyth, J.; Butt, H.; Monteelongo, Y.; Yetisen, A.K. Doubly Photopolymerized Holographic Sensors. *ACS Sens.* 2021, *6*, 915–924. [CrossRef] [PubMed]

14. Gleeson, M.R.; Sheridan, J.T. A Review of the Modelling of Free-Radical Photopolymerization in the Formation of Holographic Gratings. *J. Opt. A Pure Appl. Opt.* 2009, *11*, 024008. [CrossRef]

15. Davies, S.; Hu, Y.; Jiang, N.; Blyth, J.; Kaminska, M.; Liu, Y.; Yetisen, A.K. Holographic Sensors in Biotechnology. *Adv. Funct. Mater.* 2021, *31*, 2105645. [CrossRef]

16. Marshall, A.J.; Young, D.S.; Blyth, J.; Kabilan, S.; Lowe, C.R. Metabolite-Sensitive Holographic Biosensors. *Anal. Chem.* 2004, *76*, 1518–1523. [CrossRef] [PubMed]

17. Lalisse, A.; Mohtar, A.A.; Nguyen, M.C.; Carminati, R.; Plain, J.; Tessier, G. Quantitative Temperature Measurements in Gold Nanorods Using Digital Holography. *ACS Appl. Mater. Interfaces* 2021, *13*, 10313–10320. [CrossRef] [PubMed]

18. Liu, H.; Yu, D.; Zhou, K.; Mao, D.; Liu, L.; Wang, H.; Wang, W.; Song, Q. Temperature-induced spectrum response of volume grating as an effective strategy for holographic sensing in acrylamide polymer part I: Sensing. *Appl. Opt.* 2016, *55*, 9907–9916. [CrossRef]

19. Bianco, G.; Ferrara, M.A.; Borbone, F.; Zuppardi, F.; Roviello, A.; Striano, V.; Coppola, G. Volume Holographic Gratings as Optical Sensor for Heavy Metal in Bathing Waters. *Opt. Sens.* 2015, *9506*, 95062B. [CrossRef]

20. Yetisen, A.K.; Qasim, M.M.; Nosheen, S.; Wilkinson, T.D.; Lowe, C.R. Pulsed Laser Writing of Holographic Nanosensors. *J. Mater. Chem. C* 2014, *2*, 3569–3576. [CrossRef]

21. Elsherif, M.; Hassan, M.U.; Yetisen, A.K.; Butt, H. Wearable Contact Lens Biosensors for Continuous Glucose Monitoring Using Smartphones. *ACS Nano* 2018, *12*, 5452–5462. [CrossRef] [PubMed]

22. Davies, S.; Hu, Y.; Blyth, J.; Jiang, N.; Yetisen, A.K. Reusable Dual-Photopolymerized Holographic Glucose Sensors. *Adv. Funct. Mater.* 2023, *33*, 2214197. [CrossRef]

23. Zezza, P.; Lucío, M.I.; Fernández, E.; Maquieira, Á.; Bañuls, M.J. Surface Micro-Patterned Biofunctionalized Hydrogel for Direct Nucleic Acid Hybridization Detection. *Biosensors* 2023, *13*, 312. [CrossRef] [PubMed]

24. Kogelnik, H. Coupled Wave Theory for Thick Hologram Gratings. *Bell Syst. Tech. J.* 1969, *48*, 2909–2947. [CrossRef]

25. Toal, V. *Introduction to Holography*, 2nd ed.; CRC Press: Boca Raton, FL, USA, 2022. [CrossRef]

5.7 Supplementary information

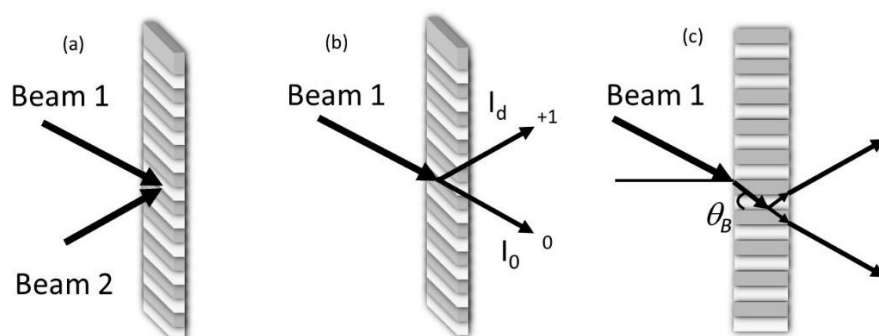*Volume transmission holographic gratings (VTG) recording*

Volume phase transmission holographic gratings can be recorded after illumination of the photosensitive material with an interference pattern created by two coherent light beams as shown in Figure S1a [25]. The spatially varying light intensity leads to a spatially varying refractive index and/or thickness of the photosensitive layer. Thus, when the layer is illuminated with one of the recording beams, the light is diffracted, and the second beam is reconstructed (Figure S1b). The grating can diffract light when illuminated with a probe beam of a different wavelength λp incident near Bragg angle. Maximum diffraction efficiency is observed when the recorded grating is illuminated at θB (Bragg angle, Figure S1c), which is fulfilling the Bragg condition (Equation (1)):

$$2\Lambda \sin \theta B = \lambda p, \tag{1}$$

Where Λ is the grating period, λp is the wavelength inside the layer.
The diffraction efficiency of the grating h is defined as the ratio of the diffracted beam intensity I_d and the probe beam intensity I_0, (Equation (2)):

$$\eta = Id/Io, \tag{2}$$

Figure S1. (a) recording and (b) probing of a volume transmission holographic grating. (c) Probe beam path inside the layer, θB Bragg angle.

Any deviation from Bragg angle corresponding to the specific probe wavelength will lead to a decrease of the measured diffraction efficiency. The curve presenting the dependence of the diffraction efficiency of the holographic grating on the probe beam incident angle is called angular Bragg selectivity curve. It is often used to characterise the recorded structure and any dimensional and refractive index changes occurring in response to the presence of the analyte can be observed as changes in height and/or position of the Bragg angular selectivity curve.

Table S1. Sequence of DNA used for biofunctionalization of the VTGs and biosensing assays.

| Name	Sequence (5′ to 3′)	5′ end	3′end
Functionalization Probe	CCCGATTGACCAGCTAGCATT	SH	None
Complementary target	AATGCTAGCTGGTCAATCGGG	Cy5	None
Non-complementary target (negative control)	CCCGATTGACCAGCTAGCATT	Cy5	None
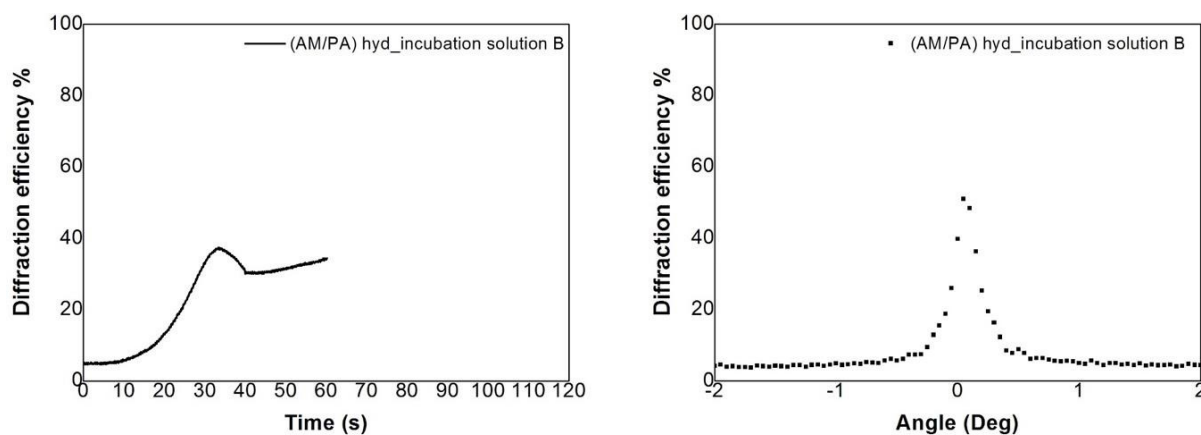
Figure S2. On the left, real-time growth curves of diffraction efficiency of (AM/PA) hydrogel incubated with incubation solution B (the laser exposure of the sample was stopped by the shutter when the diffraction efficiency started to decrease). On the right, the corresponding Bragg curves registered after recording.
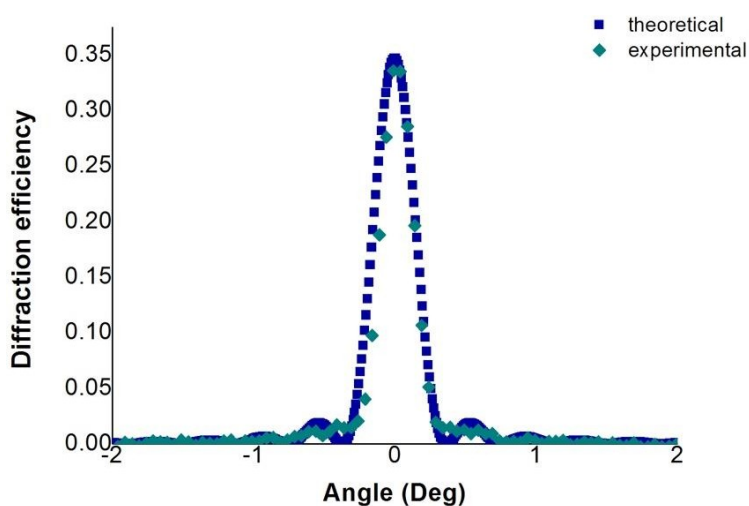
Figure S3. Theoretical and experimental angular selectivity curves for VTG recorded in hydrogel layers (AM/PA). The two curves are in good agreement. The theoretical fit is obtained according to Kogelnik's coupled wave theory for volume phase gratings [24] resulting in a hydrogel thickness of 190 μm and a refractive index modulation (RIM) of 0.000517.
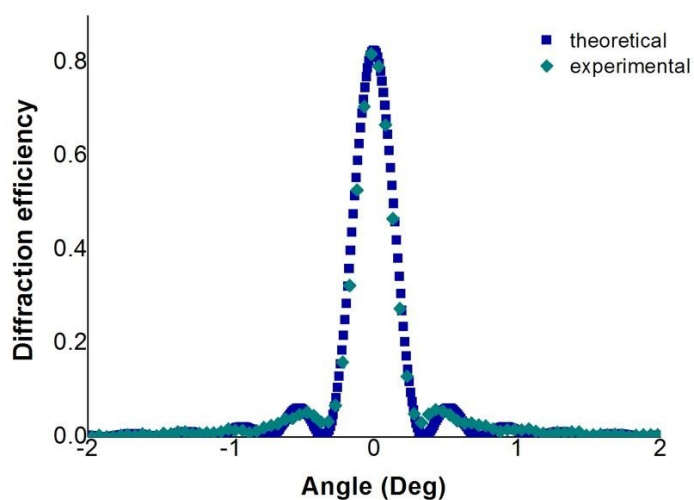
Figure S4. Theoretical and experimental angular selectivity curves for the optimised conditions for VTG recorded in hydrogel layers (AM/PA). The results show a good fit between the two curves. Fitting results showed a hydrogel thickness of 190 µm and a refractive index modulation (RIM) of 0.000963.

Figure S5. Diffraction pattern projected on a white screen of biofunctionalized VTG hydrogel functionalized with the thiolated probe after its hybridization with 2 µM of the complementary target and washing with SSC1x. VTG was surrounded by SSC1x and illuminated with the probe laser beam at 633 nm.

References (in manuscript text):

[24] Kogelnik, H. Coupled Wave Theory for Thick Hologram Gratings. Bell Syst. Tech. J. 1969, 48, 2909–2947.

[25] Toal, V. Introduction to Holography, 2nd ed.; CRC Press: Boca Raton, FL, USA, 2022. https://doi.org/10.1201/9781003155416.

6- Chapter 6

CONCLUSIONS
AND PERSPECTIVES

6- Chapter 6
CONCLUSIONS AND PERSPECTIVES

In the thesis work, bioresponsive hydrogel gratings were obtained using simple and rapid fabrication procedures. The diffractive structures obtained, composed of oligonucleotide probes, demonstrated interesting biosensing capabilities.

The first study of this thesis identifies and resolves an important requirement for the development of a hydrogel-based biosensor, which is related to the biofunctionalisation strategy that must preserve the activity of DNA probes during bio-recognition (Chapter 3). The results of this investigation reveal that covalent immobilisation of biomolecules and incorporation into a 3D network leads to an increase in sensitivity. Approaches based on fluorescent detection in the microarray format were used to demonstrate the performance of biofunctionalised hydrogels, achieving a target DNA quantification of 2.36 pmol cm-2 for an immobilised probe concentration of 5 μM. Furthermore, the compositions of the optimised hydrogels showed great abilities to be patterned into surface relief gratings (SRG) by soft lithography. From a broader perspective, this work establishes the basis for fabricating diffractive structures and emphasises their potential application in the quantification of DNA hybridisation.

In Chapter 4, the SRG-based DNA biosensor discussed showed a LOD of 2.4 μM for the detection of unlabelled DNA hybridisation. Compared to previous work, the LOD reported in this thesis work is higher than that of other unlabelled optical biosensors. Although the LOD obtained is insufficient to achieve the required sensitivity for diagnostic purposes, the results are encouraging. This is due to the fact that the biosensor is based on inexpensive materials compatible with large-scale industrial production, and also that the diffractive grating was fabricated using soft lithography, which is competitive in terms of cost and complexity. In light of all these findings, SRGs have proven to be a powerful and challenging alternative to standard nanofabrication techniques. Its simplicity, cost-effectiveness and versatility are a great advantage when it comes to fabricating diffractive structures in a wide range of configurations and substrates.

However, SRGs replicated with soft lithography still have some inherent limitations, such as thermal-only polymerisation, poor reproducibility of the obtained patterns and high thicknesses that limit their sensitivity. In fact, the diffraction efficiency obtained for hydrogel-based SRGs is low, ranging between 1 and 12%. Therefore, further efforts are needed to improve the engineering of these biosensors and, consequently, their applicability as portable sensing devices.

The third research in this thesis (Chapter 5) reports a direct photopatterning method to fabricate volumetric transmission gratings (VTGs) in hydrogels, based on holographic recording. Characterisation results show that these VTGs hydrogels can be obtained with good reproducibility. These VTGs proved to be excellent diffractive transducers achieving up to 80% diffraction efficiency. Compared to SRGs, this photopatterning method has a major improvement in terms of homogeneity, reproducibility and fabrication time. Large areas (1.45 cm2) of homogeneous volumetric gratings can be obtained in less than 100 seconds, whereas SRGs require longer times (15 minutes for inking and 90 minutes for moulding). As far as the sensitivity of biosensors is concerned, the two methods of fabricating diffractive gratings perform differently. In fact, volume phase transmission gratings (VTG) can achieve 100% diffraction efficiency and thus have a high dynamic range.

In addition to all the advantages mentioned above, the developed diffractive biosensor opens up new avenues for further investigations that extend its scope and exploit its potential for biosensing. For instance, the developed biosensor can be easily adapted to other bioreceptors (other proteins, IgG, DNA, etc.) and photochemical immobilisation reactions, depending on the target of interest. In addition, to get closer to the final goal, the proposed experiments will have to be extended to more complex samples, such as real ones, which generally contain large amounts of interfering substances. In this way, it will be possible to better define their analytical performance in terms of selectivity.

Furthermore, taking into account that holographic biosensors are still in the early stages of transition to mass production, some drawbacks still need to be overcome and the support material and transducer need to be carefully designed. In this context, this thesis sought to contribute to this field by designing new strategies to obtain holographic analyte-reactive devices based on hydrogels.

Despite advances in holographic sensor applications, the design of a holographic biosensor for nucleic acid detection is a less explored field. In summary, the results of this thesis provide an in-depth study of the fabrication of diffractive gratings in hydrogels, investigating alternative fabrication and immobilisation strategies to those existing in the state of the art, and extend the scope of these systems by reporting for the first time direct monitoring of DNA hybridisation. In addition to the results presented here, this thesis also establishes new perspectives for improving the performance of hydrogel-based diffractive biosensors. Finally, these results point towards new holographic diagnostic devices to offer new solutions for point-of-care analysis for in vitro diagnostics.